2018-07-01

The Clinical Significance of HPRT as a Diagnostic and Therapeutic Biomarker for Hematological and Solid Malignancies

Michelle Hannah Townsend
Brigham Young University

The Clinical Significance of HPRT as a Diagnostic and Therapeutic Biomarker for Hematological and Solid Malignancies

Michelle Hannah Townsend

A dissertation submitted to the faculty of
Brigham Young University
in partial fulfillment of the requirements for the degree of

Doctor of Philosophy

Kim L. O'Neill, Chair
Richard A. Robison
K. Scott Weber
Steven Johnson
Stephen R. Piccolo

Department of Microbiology and Molecular Biology

Brigham Young University

ABSTRACT

The Clinical Significance of HPRT as a Diagnostic and Therapeutic Biomarker for Hematological and Solid Malignancies

Michelle Hannah Townsend
Department of Microbiology and Molecular Biology, BYU
Doctor of Philosophy

An estimated 1,735,350 new cancer diagnosis and 609,640 cancer related deaths are predicted to occur in the United States in 2018. To improve patient prognosis, biomarkers are needed to identify cancer in early stages. When diagnosed at an early stage, cancer is more likely to respond to treatments and patients have a higher survival rate. Consequently, there is an ever-present need to identify biomarkers that can aid in the detection of cancer. Additionally, there is a paradigm shift in the field of cancer treatment towards immunotherapy. Traditional cancer treatments include chemotherapy, radiation, and hormone therapy and are not cancer-specific, which leads to bystander effects on the patient's normal organs that often harm the patient and create unnecessary hardship. To alleviate this, immunotherapy utilizes a patient's own immune cells to attack and destroy cancer cells via cancer-specific biomarkers. These biomarkers are ideally on the surface of cancer cells and absent from the patient's normal cells to avoid healthy tissue destruction. With this new therapy, there is a recent push to find surface antigens for immunotherapy techniques.

This dissertation describes the characterization of HPRT as a diagnostic and therapeutic biomarker for the detection and possible treatment of hematological and solid malignancies. We describe the general upregulation of HPRT upon malignancy and show that this elevation in protein expression is independent of stage, which indicates that it would be useful as an early stage diagnostic companion tool. We have preliminarily linked the elevation in HPRT to a mutation in one of its prime transcription factors, p53. Specific mutation in p53 called Gain of Function mutations have shown to influence salvage pathway enzyme expression, and we have shown that mutations in p53 are relevant to the elevated levels of HPRT within several cancer types. In addition, we also found that HPRT associates significantly with the membrane of several cancer cell lines as well as patient samples. We found that HPRT has insignificant expression on normal cells, which suggests it may be useful as a targetable biomarker for immunotherapy. Throughout our analysis, we also determined that HPRT might have a role in immune regulation as an elevation of the protein correlates to the decrease of several pro-inflammatory genes involved in immune activation. The knowledge gained from the data presented in this dissertation have opened up new functions for HPRT outside of simple nucleotide production and have confirmed that HPRT has a unique role in cancer that has not been previously reported.

Keywords: Hypoxanthine Guanine Phosphoribosyltransferase, HPRT1 or HGPRT, cancer biomarker, salvage enzyme

ACKNOWLEDGMENTS

I would like to thank my mentor, Dr. O'Neill for his support and belief in me. He accepted me into his lab with very limited experience and I am so appreciative of the chance he took on me because it has truly changed my life. I have developed such a love for research in his lab, which all stemmed from that initial chance he took. I would also like to thank the other members of my graduate committee: Dr. Robison, Dr. Weber, Dr. Johnson, Dr. Piccolo, and Dr. Alder, for their advice and feedback in guiding my research. The mentorship of my entire committee has made me a better scientist and influenced me to think outside of the mold and develop, sometimes crazy, ideas. In addition, I would also like to thank my lab members who have provided me with not only research assistance but also comic relief. I would especially like to acknowledge and thank the support and friendship of Abigail Felsted and Rachel Brog; these women are incredible scientists and have inspired me so much to become a better scientist and person.

I would like to thank my parents David and Valeri Passey for their constant encouragement of my academic endeavors and for their sacrifice on my behalf. I am so fortunate to have parents who were willing to support me in the development of my talents and interests no matter how grand they seemed at the time. I would also like to thank my siblings for planning and arranging events and activities that have provided me with the support I needed to get through my PhD.

Finally, I would like to dedicate this work to my husband, Thomas, and my two daughters, Aubrey and Emma. Thomas has always provided me with so much drive as I see his work ethic and his passion for his field, it makes me want to work harder to achieve my goals. He has been so influential in pushing me to do my very best and has backed that up with support at home whether that manifests as doing the dishes or watching our children while I am at a

conference. He has always been a proponent of my academic endeavors and I so appreciate his example and love. I want to thank my beautiful girls as well because they provide me so much happiness, love, and motivation. I am more productive and utilize my time better because I know that I am working for them. They provide so much unconditional love and all I want to do is show them an example of academic dedication and ultimately create a better life for them.

TABLE OF CONTENTS

LIST OF TABLES

LIST OF FIGURES

ABBREVIATIONS

APRT- Adenine Phosphoribosyltransferase

DCK- Deoxycytidine Kinase

HPRT- Hypoxanthine Guanine Phosphoribosyltransferase

BSE- Back Scatter Electron

EDAX- Energy-Dispersive Analysis X-ray

GSE- Gaseous Side Electron

LSM- Lymphocyte Separation Medium

SEM- Scanning Electron Microscopy

PBS- Phosphate-Buffered Saline

ALL- Acute Lympoblastic Leukemia

GAPDH- Glyceraldehyde 3-Phosphoate Dehydrogenase

TCGA- The Cancer Genome Atlas

HRP- Horseradish Peroxidase

TBST- Tris Buffered Saline-Tween20

BSA- Bovine Serum Albumin

PI- Propidium Iodide

FITC- Fluorescein

APC- Allophycocyanin

FBS- Fetal Bovine Serum

TPS- Think Pair Share

GOF- Gain of Function

TME- Tumor Microenvironment

CD19- Cluster of Differentiation 19

Her2- Human Epidermal Growth Factor Receptor 2

PSCA- Prostate Stem Cell Antigen

CEA- Carcinoembryonic antigen

CD33- Siglec-3

GAP- Ganglioside G2

CD5- Cluster of differentiation 5

PSMA- Prostate specific membrane antigen

ROR1- Receptor Tyrosine Kinase like Orphan Receptor 1

CD70- Cluster of differentiation 70

CD38- Cluster of differentiation 38

BCMA- B cell maturation antigen

MUC1- Mucin 1

EphA2- Ephrin type-A receptor 2 precursor

EGFRvIII- Epidermal growth factor receptor variant III

IL13Rα2- Interleukin 13 receptor, alpha 2

CD133- Prominin-1

GPC3- Glypican 3

EpCam- Epithelial cell adhesion molecule precursor

FAP- Fibroblast activation protein alpha

TK1- Thymidine Kinase I

TAG-72- Tumor associated glycoprotein-72

GUCY2C- Guanylyl cyclase C

CT antigens- Cancer/testis

SUMMARY OF CHAPTERS/APPENDICES

Summary of Introduction Chapter

Chapter 1 contains two publications that outline the purpose of my research. The first publication provides background information of HPRT and its relation to health and disease. The second publication provides a comprehensive look into the current biomarkers in clinical trials for CAR T cell therapy. These two publications provide insights into why we are analyzing HPRT as a possible biomarker for immunotherapy. Published paper in Medical Oncology (DOI: 10.1007/212032-018-1144-1) and published paper in the Journal of Experimental and Clinical Cancer Research (DOI: 10.1186/s13046-018-0817-0).

Summary of Research Chapters

Chapter 2 describes the initial project I completed upon entering the lab, which focused on the carcinogenicity of a common herbicide, Glyphosate. There has been substantial debate recently into the safety of using glyphosate as an herbicide in agriculture. With this in mind, we wanted to evaluate the DNA damaging effects of various levels of glyphosate to determine whether there was a significant increase in DNA damage, and at what concentration level this damage occurred. We showed that at physiological levels within the body, glyphosate had no increase in DNA damage on human cancer cell lines, but at levels above 100mM there was significant increases in DNA damage. We also determined that for mid-level concentration of 1mM the cells showed significant repair and following 2 hours of incubation, the cells were able to fully recover. We showed that glyphosate poses little threat to DNA at physiologic concentrations and cells are able to recover subsequent damage caused by the chemical when initial damage occurs. Paper published in Regulatory Toxicology and Pharmacology (DOI: 10.1016/j.yrtph.2017.02.002).

Chapter 3 evaluates the changes in IL-10 and TGF-β expression between primary tumors and metastatic tumors to determine if there is an increase level of anti-inflammatory cytokines that aid in a cancer cells ability to colonize other organ sites and avoid immune surveillance. We found no significant changes in TGF-β expression within malignant tumors compared to normal controls but did find that IL-10 exhibited variability among the various patients, with a higher percentage of metastatic patients showing elevated IL-10. These results suggest that IL-10 may play a role in metastatic potential of the cancer cells and that tumors with an immunosuppressive microenvironment may be more successful at invading other tissue. Paper published in Cancer Biology and Therapy (DOI: 10.1080/15384047.2017.1360453).

In Chapter 4 we conducted a pedagogical study to evaluate whether student performance and concept mastery increased utilizing think pair share quizzes over traditional multiple-choice quizzes in class in response to a Teaching Enhancement Grant Funding proposal. We found that TPS questions are easily implemented into lecture-style classrooms and promote student communication and group learning, which then corresponds to a better understanding of the material being taught. Based on test scores and student feedback, TPS quizzes were preferred over standard quizzes and showed a clear improvement in classroom atmosphere and fostered a collaborative environment. Paper under review.

Chapter 5 explores the expression of HPRT on the cell surface of two non-small cell lung cancer cell lines: NCI-H460 and A549. In addition, we also evaluated the upregulation of the protein in lung cancer tissue. We showed that HPRT has a significant localization to the membrane of both NCI-H460 cells and, to a lesser extent, A549 cells. We also found that YHPRT was significantly elevated in approximately 50% of lung cancer patients. These data suggest that HPRT could be used as not only a therapeutic biomarker due to its surface

expression on malignant cells, but also as a diagnostic biomarker of developing malignancy. Paper published in OncoTargets and Therapy (DOI: https://doi.org/10.2147/OTT.S128416).

Chapter 6 evaluates the expression of HPRT on the surface of cancer cell lines (SW480, SW620, Colo205 and HT-29), normal colon tissue, and malignant patient tissue. We found that SW480, SW620, and HT-29 cells all had significant expression of HPRT on the cell surface, while Colo205 cells had insignificant expression. In patients, we found that normal colon samples had no significant presence on the cell surface, but 1 of the 2 malignant samples analyzed had surface presentation of HPRT. To confirm the variable nature of HPRT upregulation and surface presentation, we found that 59% of patients had an upregulation of HPRT in their tumors when compared to normal colon samples. These data show that HPRT surface expression is not restricted to cancer cell lines as it is present in patient samples. Additionally, data presented in this publication show the variable nature of HPRT presentation and expression as not all of the colon cancer cell lines or patients evaluated had surface expression. Paper published in Molecular and Cellular Oncology (DOI: https://doi.org/10.1080/23723556.2018.1481810).

Chapter 7 thoroughly analyzes the expression of HPRT in patient tissue to determine whether it could be used as a diagnostic biomarker for early stage detection of malignancy. We found that in lung, breast, colon, and prostate tissue, HPRT was elevated in 35%-55% of patients analyzed. In addition, we also found the same variability in RNA-sequencing data from TCGA as HPRT experienced a general trend of increased expression in cancer patients. The upregulation of the protein within malignant tissue was independent of cancer stage, which indicate that the cause of the upregulation is most likely mutational in nature. The stage independence also shows that HPRT could be used as an early stage diagnostic biomarker. Paper published in Cancer and Clinical Oncology (DOI: https://doi.org/10.5539/cco.v6n2p19).

Chapter 8 describes an investigation into the use of HPRT as a standard endogenous control for cancer-related studies. We had observed and published that HPRT was upregulated in a majority of malignant tissue, yet it is widely used as a normalization control for gene expression analysis. The purpose of this project was to show that HPRT should not be used as a control and provide sufficient evidence to suggest its removal from use as a standard control. We found that on the level of RNA, protein, and tissue the expression of HPRT is too variable to be utilized as a standard. Paper under review.

Chapter 9 elaborates on the surface expression of HPRT in B cell malignancies in addition to determining possible molecular mechanisms behind the elevation of HPRT within malignant samples. We found that HPRT is found on the surface of both Raji cells and in seven of the nine ALL patient samples we analyzed. Following this, we also ranked every B cell line according to their HPRT expression and found that genes with a positive correlation to HPRT expression were involved in DNA replication/repair and proliferation, but half of the genes with a negative correlation to HPRT expression were pro-inflammatory cytokines. This suggests that HPRT may have an influence on the immune system by downregulating pro-inflammatory cytokine production. Paper under review.

Chapter 10 explores the expression of four target genes in endometrial cancer to determine if they would be valuable as diagnostic and therapeutic biomarkers. We found that all four genes, JAG2, AURKA, PGK1, and HPRT1, had elevated expression in malignant tissue when compared to normal tissue. In addition, PGK1 and HPRT1 had a stage dependence. In addition, we also found that HPRT1 and AURKA expression had the most significant impact on patient survival with higher expressing patients showing a lower overall survival. Subsequently, we evaluated the drugs that had the highest impact on the gene expression of all target genes and found that MEK and Topo I inhibitors had the best impact on reducing HPRT1 expression, while

drugs that had an impact on AURKA elevation were inhibitors of microtubule function. Paper under review.

Summary of Appendices

Appendix 1 describes the presence of HPRT on the surface of some prostate cancer cells and determines a preliminary association between HPRT expression and a gain of function mutation in p53. We found that HPRT is not universally localized to the surface of cancer cells and determine that DU145 cells have surface presentation while PC3 cancer cells do not. As PC3 cells are null for p53 expression and DU145 cells have a mutated form of p53 we determined that there is differential expression of HPRT in several cancers with mutations in the p53 transcription factor. Paper in preparation.

Appendix 2 describes the initial association HPRT has with the immune system. We determined that HPRT elevation corresponds significantly with the downregulation of several cytokines and both pro-inflammatory and anti-inflammatory genes. We also determined that HPRT has a significant impact on the survival of several cancer types. This may be a result of decreased tumor infiltration by immune cells in high expressing patients that we observed in several cancer types. We hypothesized the effects that elevated HPRT has on immune cells is directly caused by an increase in guanosine production upon HPRT elevation. To test this we treated different immune cell subsets with guanosine and adenosine and measured their activation. We found that in T cells there was no influence with guanosine treatment, while B cells showed a reduction in activation similar to adenosine treatment. This data indicates that HPRT may be elevated in the tumor microenvironment as a method to control immune invasion and afford protection for the tumor. Paper in preparation.

General Overview

We have found that HPRT expression is variable between cancer patients and has a significant elevation in several malignancies. This overexpression is also manifest as surface localization of the protein as HPRT expresses on the cell membrane of several cancer types. We hypothesize this surface expression to be directly caused by a GOF mutation in p53, but this is still under investigation. In addition, we have also shown that HPRT has an impact on immune regulation and acts to downregulate several immune-regulatory cytokines. We have preliminarily linked this role to the over-production of guanosine, which has been shown to have immunomodulatory functions in the CNS. All together the data presented in this dissertation implicate HPRT as a significant contributor to the tumor microenvironment and also as a potential target for immunotherapy.

CHAPTER 1

The Biology and Clinical use of HPRT as a Biomarker for Immunotherapy

A Review of HPRT and its Emerging Role in Cancer

Michelle H. Townsend, Richard A. Robison, and Kim L. O'Neill

Citation: Townsend, M.T., Robison, R.A., O'Neill K.L., A Review of HPRT and its Emerging Role in Cancer. Medical Oncology. 2018. DOI: 10.1007/212032-018-1144-1

The following is taken from an article published in the Journal of Cancer Research and Clinical Oncology. All content and figures have been formatted for this dissertation.

Abstract

Hypoxanthine Guanine Phosphoribosyltransferase (HPRT) is a common salvage housekeeping gene with a historically important role in cancer as a mutational biomarker. As an established and well known human reporter gene for the evaluation of mutational frequency corresponding to cancer development, HPRT is most commonly used to evaluate cancer risk within individuals and determine potential carcinogens. In addition to its use as a reporter gene, HPRT also has important functionality in the body in relation to purine regulation as demonstrated by Lesch-Nyhan patients whose lack of functional HPRT leads to significant purine overproduction and further neural complications. This regulatory role, in addition to an established connection between other salvage enzymes and cancer development, points to HPRT as an emerging influence in cancer. Recent work has shown that not only is the enzyme up-regulated within malignant tumors, it also has significant surface localization within some cancer cells. With this is mind, HPRT has the potential to become a significant biomarker not only for the characterization of cancer, but also for its potential treatment.

Nucleotide Synthesis Pathways

Nucleotides are an integral component of cellular life due to their versatility and abundance[1]. Their functional flexibility is demonstrated as ATP and GTP are utilized in both DNA and RNA synthesis and maintenance, while simultaneously act as energy sources for the cell[2,3]. Because the cell is reliant on their correct synthesis, the processes that regulate nucleotide production are tightly structured and controlled[4]. These mechanisms are responsible for maintaining adequate nucleotide levels at all times within the cell, which elevate as high as 5 to 10 fold increases during G1 and S phases of the cell cycle[5].

There are two distinct biological pathways eukaryotic cells utilize to synthesize nucleotides: de novo synthesis and the salvage pathway. De novo synthesis is an energetically expensive 15 step process that requires up to 28 enzymes to synthesize nucleotides from raw materials within the cell[6]. The enzymes involved specifically in purine biosynthesis are responsible for converting organic glucose into phosphoribosyl pyrophosphate (PRPP), which can then be converted into GTP and ATP[7]. Because it requires extensive energy, this anabolic pathway is primarily used when the demand for nucleotides is the most prominent: during G1 and S phase[8]. Although complex in nature, this process is highly conserved between organisms, suggesting that it is ancient in origin[9].

The second mechanism, the salvage pathway, has several derived mechanisms that synthesize nucleotides from used materials within the cell[9]. While de novo synthesis creates the components of nucleotides, the salvage pathway utilizes a clever approach that 'recycles' parts from old nucleotides and pieces them together to form complete nucleotides. Due to the recycling nature of the salvage pathway, it is the chosen nucleotide synthesis mechanism throughout the cell cycle for both purines and pyrimidines as it aids in conserving valuable energy. Specifically, for purine synthesis, it is estimated that 90% of free purines in humans are

recycled[10]. Therefore, the enzymes involved in this process are responsible for providing necessary purine nucleotides for DNA synthesis and maintenance.

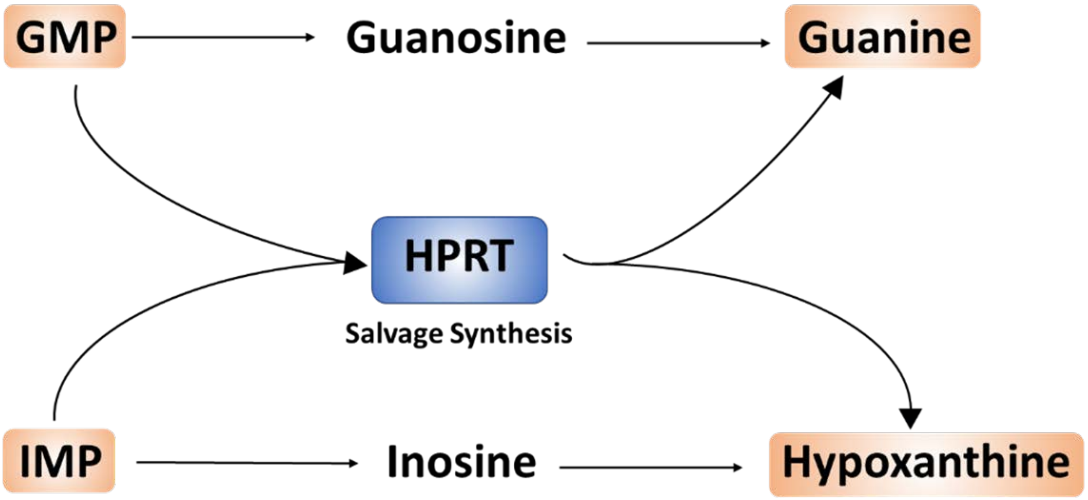

Figure 1-1A. *An Overview of the HPRT enzyme function*. HPRT is responsible for the transfer of a ribose monophosphate from PRPP to hypoxanthine and guanine to form inosine monophosphate (IMP) and guanine monophosphate (GMP), respectively. Pyrophosphate is the byproduct from this reaction. After IMP and GMP are synthesized they are converted to functional nucleotides used in DNA synthesis and repair

Hypoxanthine Guanine Phosphoribosyltransferase (HPRT) is a salvage pathway enzyme responsible for the formation of IMP and GMP from precursors within the cell to eventually form Inosine and Guanine, respectively (Figure 1-1A)[11]. HPRT transfers phosphoribose from PRPP to hypoxanthine and guanine bases[10,12]. The enzyme is composed of ten beta strands and six alpha helices with residues 37-189 forming the core of the enzyme[13]. Depending on the pH of the surrounding tissue, the protein can exist as either a dimer or a tetramer with identical subunits[13–15]. The molecular weight of each of the protein subunits is 48.9 kDa and the molecule has an instability index of 21.69, classifying the protein as stable. The functional homo tetramer contains four subunits labeled A, A', B, and B' (Figure 1-2A)[13].

The HPRT enzyme consists of several regions that each have distinct functions in substrate recognition and reactivity. The carboxy terminal end of the central beta sheet is primarily involved in substrate recognition. The core region of the protein contains twisted parallel beta sheets with five beta strands that are surrounded by four alpha helices. Residues 65-74 form the most flexible portion of the protein as they create a loop that will bind pyrophosphate. The residues of the enzyme that will bind PRPP substrate are 129-140, which are located on the floor of the active site. In order for enzymatic activity in the active site to be successful the metal ion Mg2+ is required[13,15].

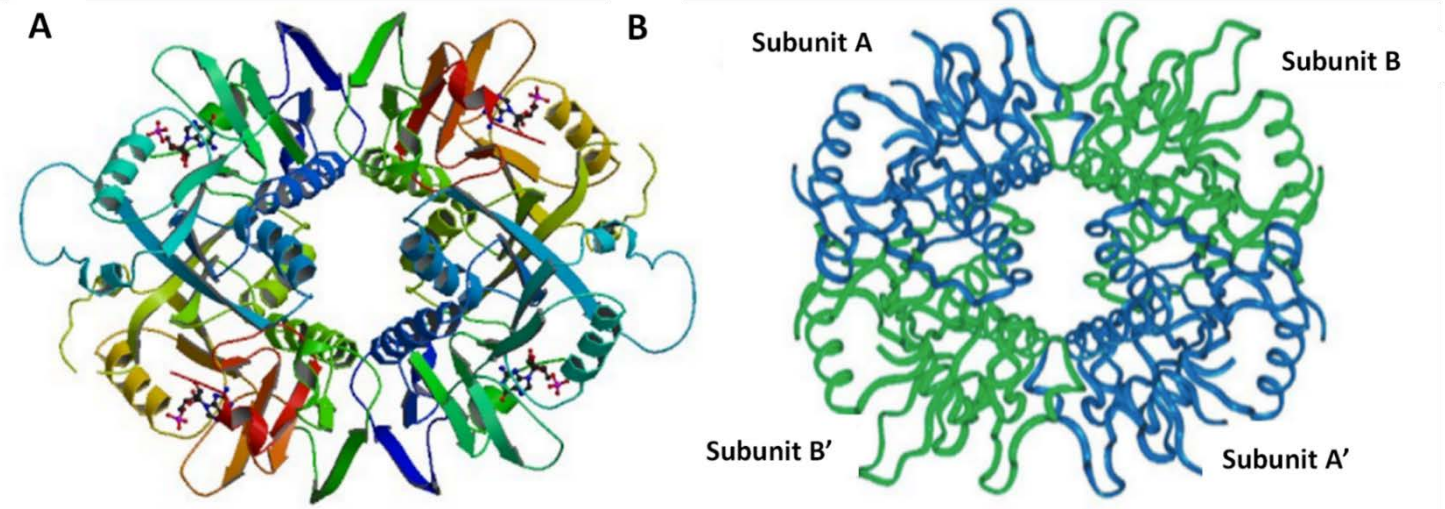

Figure 1-2A. *HPRT Protein Structure.* The homo tetramer structure of human HPRT. The homo tetramer structure of human HPRT. A) The protein consists of only 27% alpha helices and 27% beta sheets, which indicates that the remaining 46% of the enzyme consists of beta turns and random coils. B) Individual subunit labeling is indicated by the altering colors. Each subunit is identical and is translated from the same mRNA message.

The hprt locus

The *hprt* gene is 47,827bp and resides on the long arm of the X chromosome (Figure 1-3A). The gene is relatively large, especially considering that only a small portion of the transcribed DNA is eventually translated. There are 9 exons that code for a 217 amino acid protein, which represents only 1.3% of the original genomic message [10,16,17]. Because the final protein product is involved in cellular maintenance, the control sequences upstream of the *hprt*

gene contain the hallmarks of a mammalian housekeeping gene; there is an absence of 5' transcriptional sequences including the TATA and CAAT boxes and there are exceptionally GC-rich sequences with many GC hexanucleotide motifs along the 5' end of the gene[18]. As a housekeeping gene, *hprt* is found in all somatic tissue in low levels[19]. In a majority of human cells *hprt* mRNA transcripts comprise only 0.005 to 0.01% of the total mRNA within the cell[20]. The only exception is in central nervous tissue where there is an unusually elevated level of HPRT expression ranging from 0.02 to 0.04% of the total mRNA, which is a 4 fold increase in comparison to other somatic tissue[20,21]. This elevated expression is not fully understood because cells in the central nervous system (CNS) are not stimulated to divide and would therefore require less machinery for nucleotide synthesis. In addition, the human genome contains non-functional HPRT homologous regions in the autosomal DNA of chromosomes 5, 11, and 13[16]. These DNA sequences are not known to be transcribed and are most likely pseudogenes, but their exact origin and expression is not well understood[22].

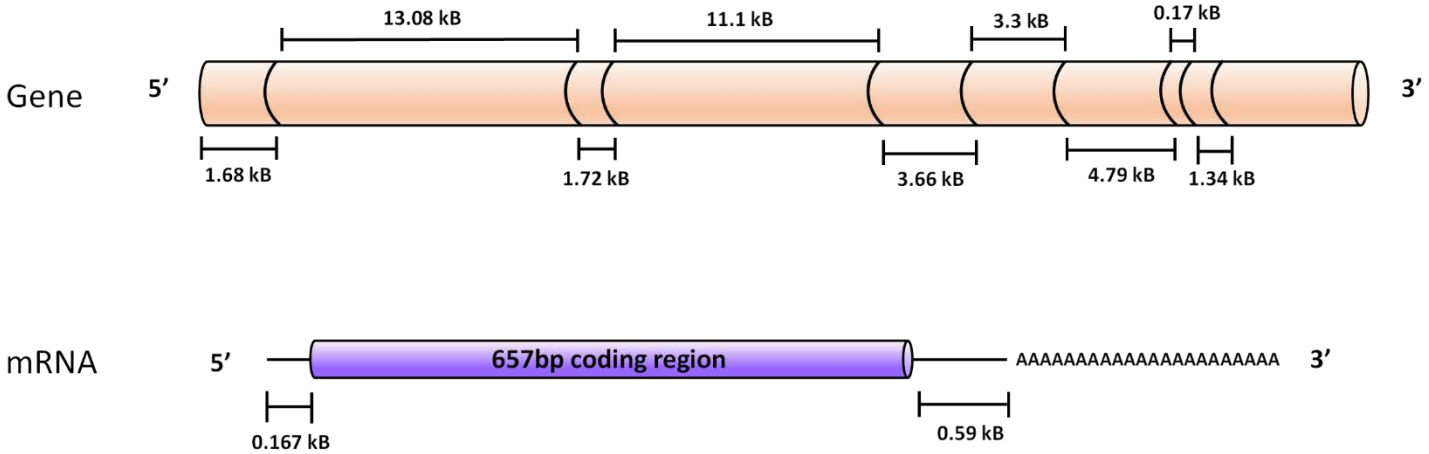

Figure 1- 3A. *The HPRT locus.* The HPRT gene contains 9 exons coding for a 657bp coding mRNA and a resulting 217 amino acid protein.

HPRT regulatory role: Examples from Lesch-Nyhan Syndrome

As an essential housekeeping protein, a deficiency of HPRT results in a spectrum of diseases that directly correspond with the availability of the protein. Individuals with a complete lack of functional HPRT develop Lesch-Nyhan syndrome, while individuals with a partial deficiency develop gout-like symptoms characteristic of Kelley-Seegmiller syndrome[21]. Because the gene is located on the X chromosome, it is an X-linked recessive condition that predominantly affects males of diseased families. A common thread that connects these distinct diseases is the presence of hyperuricemia in patients. The excess of uric acid within the plasma, usually ranging between 9 and 12 grams per liter, contributes to many of the underlying symptoms typical of HPRT deficiency[22]. These symptoms are not present in individuals who are deficient in any of the other salvage pathway enzymes despite having the same function in nucleotide synthesis.

Lesch-Nyhan syndrome is primarily characterized by severe neurological illnesses. Patients suffer from dystonia, choreoathetosis, twisting and writhing, akathisia, akinesia, and several other motor neuron disorders that make successful voluntary motion incredibly difficult and frequently impossible. Along with motor neuron dysfunction, patients also suffer from severe self-injurious behavior that can lead to self-mutilation[22–28]. Along with improper neural development, Lesch-Nyhan patients also show significant purine overproduction. This overproduction indicates that HPRT is crucial in not only the synthesis of purines, but also the regulation of their production[21].

When patients have a reduced level of HPRT rather than a complete deficiency they develop gout-like manifestations and eventual gouty arthritis, distinctive of Kelley-Seegmiller syndrome[21]. Partial HPRT deficiency usually develops from a point mutation resulting in a single amino acid substitution within the protein[22]. Many such mutants have been characterized and are

often present in the amino-terminal domain of the protein[27]. These mutations generally stay within family lineages, and it is rare that two separate families share the same mutation. Symptoms are directly related to, and caused by, the excess production of uric acid within the body. Diseased individuals pass large amounts of urate crystals into the urine for a majority of their early life, and after approximately 20 years of chronic hyperuricemia an inflammatory response develops that leads to arthritis[17]. In Lesch-Nyhan Syndrome and Kelley-Seegmiller syndrome the regulatory nature of HPRT is demonstrated as the lack of the protein results in an over-production of purines. We suggest a possible negative feedback loop controlling purine production that may be regulated by the availability of HPRT within the cell: as cells have sufficient purines, HPRT is utilized to halt further purine synthesis.

Relationship between other salvage pathway enzymes and cancer

Involved in the same salvage pathway nucleotide synthesis pathway as HPRT, Thymidine Kinase 1 (TK1), previously known as fetal TK, is an enzyme that controls pyrimidine synthesis of thymine. TK1 catalyzes the conversion of thymidine to deoxythymidine monophosphate (dTMP)[29]. Due to its presence in the serum of cancer patients, TK1 is known as a proliferative biomarker in cancer development and as a biomarker to monitor recurrence[30–35]. The serum detection of TK1 is an early step in cancer growth and has been used as an early detection system for cancer prevention as elevated serum levels have been shown to correspond with tumor aggressiveness[30,36–38]. It has also been suggested that TK1 could be used to distinguish between slowly growing tumors and more aggressive, fast growing tumors[39]. In addition, TK1 has been established as a cancer biomarker for multiple cancers including leukemia, colorectal cancer, lung cancer, breast cancer, and prostate cancers[37,40]. As an established biomarker for cancer development, TK1 demonstrates the relationship between cancer proliferation and the control of salvage enzymes.

HPRT as a reporter gene

The role HPRT has played within the realm of cancer has been largely limited to its use as an established human reporter gene. The *hprt* gene is currently used to assess somatic mutations and mutagenesis in *in vitro* and *in vivo* studies evaluating potential carcinogens and cancer therapies[41–45]. As the first human somatic gene mutation assay developed, the HPRT assay has been thoroughly used to identify and select mutant cells by taking advantage of the biochemical pathways used to synthesize DNA within cells[46–48]. Mutations in the *hprt* locus are carefully monitored in studies of individuals exposed to both potential mutagens and carcinogenic agents to determine the effects of exposure to DNA integrity and resulting cancer risk[49–53] Using this mutational biomarker, researchers have found significant correlations between HPRT mutations and increased cancer risk[45,50,52–58]. Gladd and Tindall used the *hprt* locus to determine the mutation rate of various cancer cell lines with mismatch repair-gene defects[59]. While Branda et al. utilized the *hprt* locus to monitor the DNA mutation rate of women with breast cancer treated with tamoxifen, radiotherapy, or chemotherapy[54]. As such as influential biomarker for cancer development, the utilization of *hprt* has led to significant contributions to the cancer community.

Emerging role in cancer

Recently, new evidence has indicated an emerging role for HPRT within cancer. Researchers have found that HPRT has elevated expression specifically within cancer cells. Muller et al., using quantitative PCR, found that HPRT was present in breast cancer cell lines (MDA-MB-231), primary tumors, and tumor-infiltrated lungs of SCID mice injected with MDA-MB-231 breast cancer cells. Yet, they found no detectable amount of the enzyme in normal lungs from healthy mice counterparts. Additionally, Muller et al. found that the mRNA levels of *hprt* directly correlated with the tumor load of the tested mouse, indicating that the level of HPRT

within the mouse was related to the size of the tumor[60]. Furthermore, evaluation of HPRT expression in cancer patients via immunohistochemistry shows significant variability between cancer patients[61]. Overall, HPRT is generally over-expressed within cancer patients as data from both tissue and RNA-seq shows significant increases in protein levels within malignant samples[61]. While there is an overall increase in malignancy, HPRT over-expression is not a consistent trend within all patients, and only a cohort of cancer patients experience an up-regulation[61]. This indicates that the regulation of HPRT synthesis is compromised within those patients. As previously discussed, HPRT has a regulatory function within the cell that may contribute to this apparent lack of transcriptional control within malignant cells. As a protein with differential expression, HPRT has the potential to be used as a characterization tool when assessing patient tumors and evaluating treatment options.

In addition to showing unique expression profiles within malignant tumors, HPRT also has been implicated as a possible surface biomarker. Recent work has shown that HPRT co-localizes with the plasma membrane of certain cancer cell lines[62]. As a potential cancer-associated antigen, HPRT could become a target for emerging immunotherapies designed to attack cancer cells displaying unique surface proteins. As the expression of the enzyme is generally consistent and extremely low within normal cells, HPRT could become a useful tool for those patients who experience an upregulation. We propose that HPRT is involved in some regulatory pathway monitoring and controlling nucleotide synthesis and protein production and within a malignant environment this regulation is lost and HPRT becomes over-expressed allowing cancer cells to bypass pathways controlled or regulated by strict HPRT production. Further work is required to solidify HPRT as a significant biomarker for cancer identification, characterization, and possible targeting, but the enzyme has recently shown significant promise as not only a mutational reporter gene, but also a cancer biomarker and neoantigen.

The expansion of targetable biomarkers for CAR T cell therapy

Michelle H. Townsend, Gaju Shrestha, Richard A. Robison, and Kim L. O'Neill

Citation: Townsend, M.T., Shrestha, G., Robison, R.A., O'Neill K.L., The expansion of targetable biomarkers for CAR T cell therapy. DOI: 10.1186/s13046-018-0817-0

The following is taken from an article published in the Journal of Experimental and Clinical Cancer Research with slight modifications. All content and figures have been formatted for this dissertation.

Abstract

Biomarkers are an integral part of cancer management due to their use in risk assessment, screening, differential diagnosis, prognosis, prediction of response to treatment, and monitoring progress of disease. Recently, with the advent of Chimeric Antigen Receptor (CAR) T cell therapy, a new category of targetable biomarkers has emerged. These biomarkers are associated with the surface of malignant cells and serve as targets for directing cytotoxic T cells. The first biomarker target used for CAR T cell therapy was CD19, a B cell marker expressed highly on malignant B cells. With the success of CD19, the last decade has shown an explosion of new targetable biomarkers on a range of human malignancies. These surface targets have made it possible to provide directed, specific therapy that reduces healthy tissue destruction and preserves the patient's immune system during treatment. As of May 2018, there are over 100 clinical trials underway that target over 25 different surface biomarkers in almost every human tissue. This expansion has led to not only promising results in terms of patient outcome, but has also led to an exponential growth in the investigation of new biomarkers that could potentially be utilized in CAR T cell therapy for treating patients. In this review, we discuss the biomarkers currently under investigation and point out several promising biomarkers in the preclinical stage of development that may be useful as targets.

Background

As the new paradigm shift in cancer treatment, immunotherapy is the epitome of personalized medicine, as a patient's immune system is enlisted to fight their own cancer. Originally manifest as monoclonal antibody therapy, immunotherapy now has a broadened definition that encompasses tumor vaccines, checkpoint blockades, bispecific antibodies, tumor infiltrating lymphocytes (TILs), and most recently, chimeric antigen receptor (CAR) T cell therapy. T cells are a critical component of the adaptive immune system as they not only orchestrate cytotoxic effects, but also provide long term cellular 'memory' of specific antigens[63]. Commonly, a patient will have TILs specific for their tumor but these cells are often retrained by the tumor microenvironment to become anergic and nonfunctional[64]. T cells endogenously require the interaction between MHC displayed peptides and their TCR to activate[65], but CAR T cells have been engineered to activate via an antibody fragment towards a tumor-associated or tumor-specific antigen (TAA and TSA, respectively). CAR T cells are a "living drug" comprised of a single chain variable fragment (scFv) fused to the signaling domain of a T cell. Upon recognition and binding to the scFv target, the T cell activates and subsequent target cell killing is initiated. CAR T cell therapy has been revolutionary in the treatment of hematological malignancies with the targets CD19 and CD20 but has been unable to translate effectively to solid tumors. A major drawback for CAR therapy in solid malignancies is the lack of cancer-specific tumor targets. While hematological malignancies do not necessarily require antigen

target specificity towards cancer cells, solid tumor targets do, and the specific biomarker cannot be expressed on normal tissue.

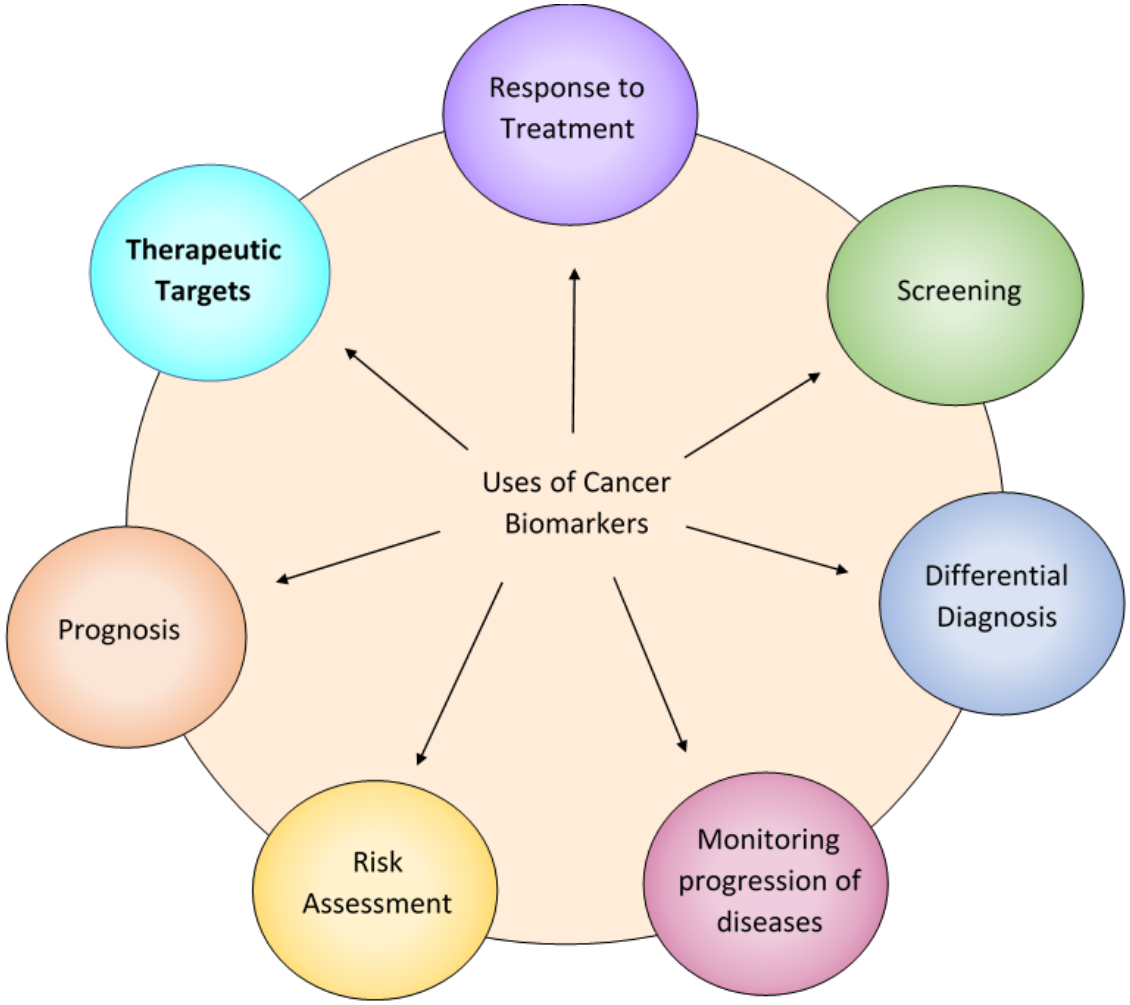

Figure 1-1B. *Uses of Cancer Biomarkers.* Cancer biomarkers have had a historically proven useful for several different aspects of cancer patient care. With the advent of immunotherapy, surface cancer biomarkers are being utilized as therapeutic targets to direct and orchestrate an immune response in a cancer-specific fashion.

With over 300 CAR T cell therapy clinical trials ongoing in CAR therapy as of May 2018, there has been an equally impressive effort to identify and characterize TAA or TSA surface biomarkers in solid tumors. Biomarkers have been an integral component of cancer for several decades, and with the expansion of CAR T cell therapy, a new category of therapeutic biomarkers has arisen. These markers can be used to direct CAR T cells to malignant target cells (Figure 1-1B). The effort to identify and characterize these therapeutic biomarkers has been substantial and has increased exponentially over the last decade. As a result, 18 surface

biomarkers are currently being evaluated in clinical trials (Figure 1-2B). In addition, there is also a significant number of pre-clinical biomarkers that have shown promise as targets for CAR therapy due to their unique expression on cancer cells. Here, we summarize the biomarkers currently under investigation in clinical trials for both hematological and solid malignancies, along with those that may prove useful in future CAR therapies for solid tumors.

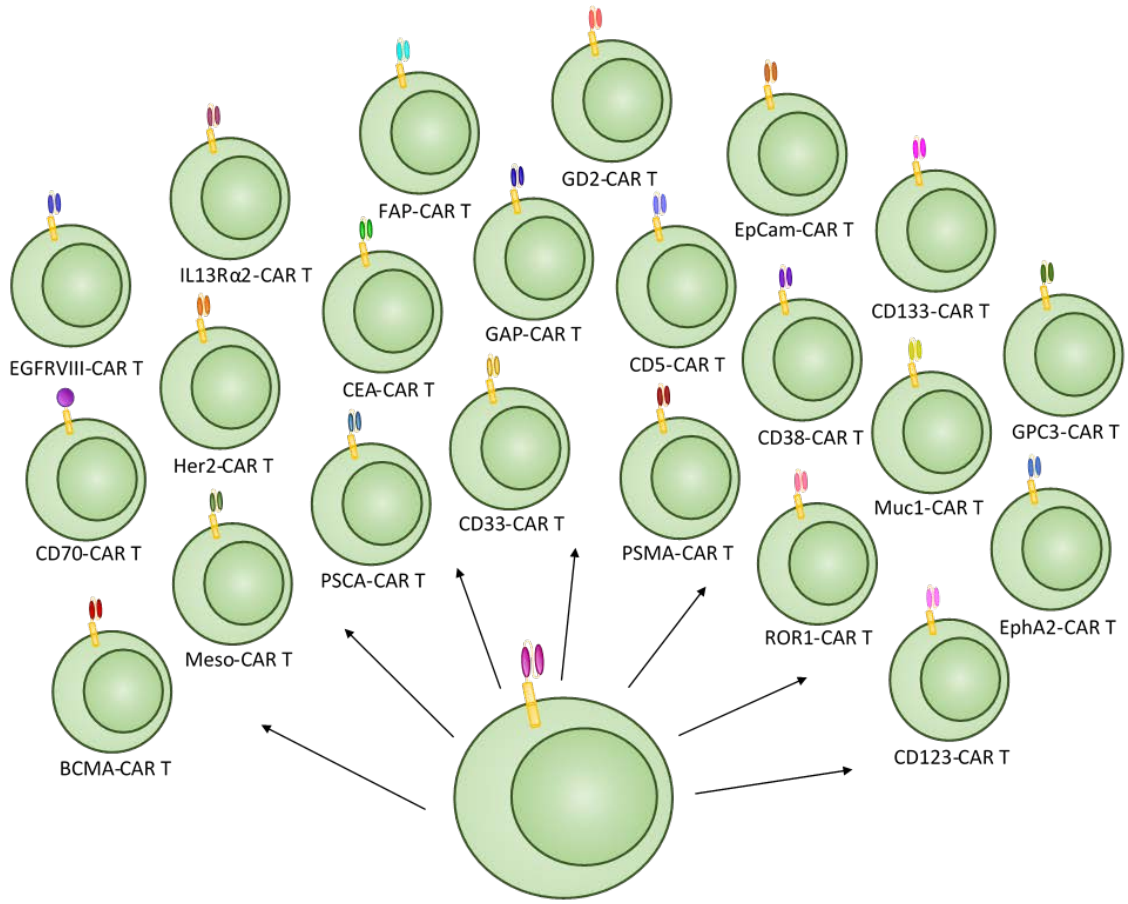

Figure 1-2B. *Current CAR T cells in clinical trials*. From the initial success of CD-19 CAR T cell therapy, several new biomarker targets have emerged and are being tested in clinical trials. This expansion of targets has expanded CAR T cell therapy to the treatment of not just hematological malignancies, but also to solid tumors as well.

Surface Biomarkers have expanded significantly over the last decade

CAR T cell therapy was initially conceptualized in 1989[66] and was recognized as an effective therapeutic after targeting CD19 for the treatment of lymphomas and leukemias [67–69].

This led to an exponential growth in CAR therapy and as a direct consequence, in surface biomarker discovery (Figure 1-3B). In 2012, there were a total of 5 clinical trials, four targeting CD19 and one targeting Mesothelin. This number has continued to grow and the number of biomarkers tested in a clinical setting has also expanded from 2 to 25. The year 2017 saw more clinical trials than any previous year with 111 initiated, targeting 17 different biomarkers (Table 1-1B). This growth demonstrates not only the efficacy of CAR T cell therapy, but also the huge push in immunotherapy to find new and better targets.

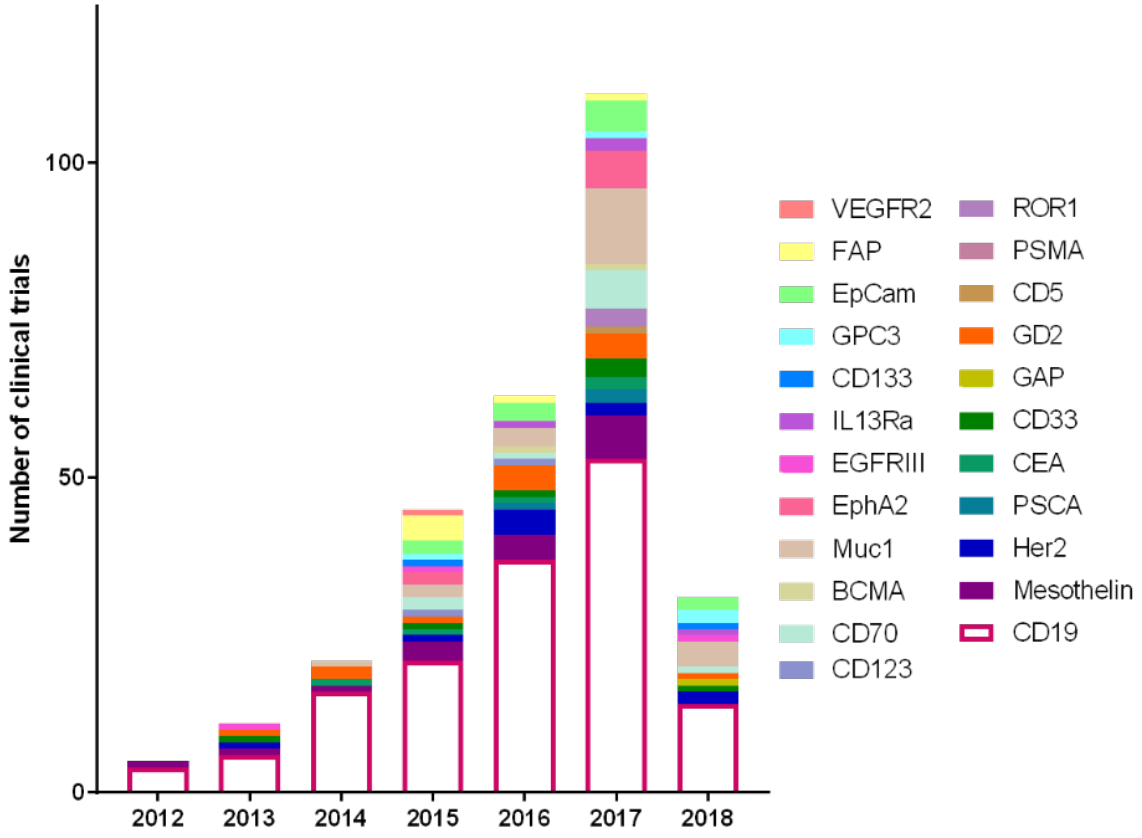

Figure 1-3B. *Clinical trial Biomarkers as of May 2018 by year.* The expansion of CAR targets is shown as the diversity and number of clinical trials has exponentially increased from 2012. Not only are there more clinical trials utilizing CAR T cell therapy, there are also more targets being evaluated.

Table 1-1B. Current Clinical Trials (as of April 2018)

Target	Name	Function	Disease	Clinical Trials in 2018
CD19	Cluster of Differentiation 19	Dominant signaling component on mature B cells	ALL, B cell lymphoma, leukemia, Non-Hodgkin lymphoma,	NCT03366350*, NCT03366324*, NCT02546739*, NCT03448393*, NCT03467256*, NCT03488160*, NCT03016377*, NCT03468153*, NCT03483688*, NCT03398967*, NCT03229876*, NCT03455972*, NCT03423706*, NCT03497533*
Mesothelin		exact function of mesothelin in these normal mesothelial cells is unclear.	Pancreatic cancer, Cervical Cancer, Ovarian Cancer, Lung Cancer, Peritoneal carcinoma, Fallopian tube cancer, Colorectal Cancer, Breast Cancer	NCT02930993+, NCT03182803+, NCT03030001+, NCT02706782+, NCT01583686+, NCT03356795+, NCT03054298+, NCT03267173+, NCT02792114+, NCT02959151+, NCT02580747+, NCT02414269+, NCT02465983+, NCT03323944+,
Her2	Human Epidermal Growth Factor Receptor 2	Activate intracellular signaling pathways in response to extracellular signals.	CNS tumor, Breast Cancer, Ovarian Cancer, Lung Cancer, Gastric Cancer, Colorectal Cancer, Glioma, Pancreatic Cancer, Glioblastoma	NCT03500991*, NCT03423992*, NCT02713984+, NCT03267173+, NCT02792114+, NCT02442297+, NCT00889954+, NCT03423992+, NCT01109095+, NCT02706392+, NCT00902044+, NCT03389230+,
PSCA	Prostate Stem Cell Antigen	Not well understood	Pancreatic cancer, lung cancer	CT03198052+, NCT02744287+, NCT03267173+
CEA	Carcinoembryonic antigen	Cell adhesion	Liver metastases, lung cancer, colorectal cancer, gastric cancer, breast cancer, pancreatic cancer,	NCT02850536+, NCT02349724+, NCT03267173+, NCT02959151,
CD33	Siglec-3	Transmembrane receptor on myeloid lineage	Myeloid leukemia,	NCT03473457*, NCT02958397+, NCT03126864+, NCT03222674+,
GAP	GTPase-activating protein	Terminating G protein signaling	Solid tumors	NCT02932956*
GD2	Ganglioside G2		Glioma, Cervical cancer, sarcoma, neuroblastoma,	NCT03423992*, NCT03356795+, NCT02992210+, NCT01953900+, NCT02761915, NCT03373097+, NCT02765243+, NCT03423992+, NCT03294954+, NCT03356782+, NCT02919046+,
CD5	Cluster of differentiation 5	TCR inhibitory molecule	T cell acute lymphoblastic lymphoma, T-non-Hodgkin lymphoma,	NCT03081910+,
PSMA (PSMA/TGFβ)	Prostate specific membrane antigen	Transmembrane protein	Cervical cancer, Prostate cancer, Bladder cancer	NCT03356795+, NCT03089203+ (-TGFβ), NCT03185468+, NCT01140373+
ROR1	Receptor Tyrosine Kinase like Orphan Receptor 1	Modulates neurite growth in the CNS	Breast cancer, lung cancer, lymphoblastic leukemia,	NCT02706392+,
CD123	IL-3RA	Involved in hematopoietic progenitor cell differentiation and proliferation	AML, Leukemia,	NCT03473457*, NCT03125577+, NCT02937103+, NCT03114670+, NCT02159495+, NCT03098355+,

				NCT03222674+, NCT03203369+, NCT03190278+,
CD70	Cluster of differentiation 70	Induces proliferation of costimulated T cells	B cell malignancies, pancreatic cancer, renal cell cancer, breast cancer, melanoma, ovarian cancer	NCT03125577+, NCT02830724+,
CD38	Cluster of differentiation 38	Cell adhesion, signal transduction, and calcium signaling	Myeloma,	NCT03464916*, NCT03473496*, NCT03473457*, NCT03125577+, NCT03222674+, NCT03271632+,
BCMA	B cell maturation antigen	Mediates the survival of plasma cells	Myeloma	NCT03448978*, NCT03473496*, NCT03430011*, NCT03455972*, NCT02954445+, NCT03322735+, NCT03338972+, NCT03318861+, NCT02215967+, NCT03093168+, NCT03274219+, NCT03302403+, NCT03492268+, NCT03288493+, NCT03070327+, NCT03196414+, NCT03448978+, NCT02958410+, NCT03287804+, NCT03473496+, NCT03380039+, NCT03430011+, NCT03361748+, NCT03455972+, NCT02546167+, NCT03271632+
Muc1	Mucin 1	Mucous barrier formation on epithelial surfaces	Sarcoma, Leukemia, Pancreatic cancer, cervical cancer, lung cancer, hepatocellular carcinoma, breast cancer, glioma, colorectal cancer, gastric cancer	NCT03179007+, NCT02587689+, NCT02617134+, NCT03198052+, NCT03356795+, NCT03267173+, NCT03222674+, NCT03356782+
EphA2	Ephrin type-A receptor 2 precursor	Eph-ephrin bidirectional signaling pathway of mammalian cells	Glioma	NCT03423992*
EGFRVIII	Epidermal growth factor receptor variant III	Cell differentiation and proliferation	Glioblastoma	NCT03283631*
IL13Ra2	Interleukin 13 receptor, alpha 2	Signal processing via Jak-STAT	Glioma	NCT02208362+
CD133	Prominin-1	unknown	Glioma, AML, Liver Cancer, Pancreatic Cancer, Ovarian Tumor, Colorectal Cancer, Breast Cancer	NCT03473457*, NCT03356782+, NCT03423992*
GPC3	Glypican 3	Regulate cell growth, division, and survival	Heptocellular carcinoma, lung cancer, Lymphoma, Leukemia, Pancreatic Cancer, Colorectal Cancer	NCT02905188*, NCT02932956*, NCT02715362+, NCT03130712+, NCT02395250+, NCT02876978+, NCT03198546+, NCT02723942+, NCT03084380+, NCT03302403+, NCT03146234+, NCT02959151+,
EpCam	Epithelial cell adhesion molecule precursor	Embryonic stem cell proliferation and differentiation	Breast Cancer, Colon Cancer, Pancreatic Cancer, Esophageal Carcinoma, Gastric Cancer, Prostate Cancer, Hepatic Carcinoma, Lymphoma, Leukemia	NCT02915445+, NCT03013712+, NCT02729493+, NCT02725125+, NCT02728882+, NCT02735291+
FAP	Fibroblast activation protein alpha	Neuropeptide regulation. hFGF21 inactivation	Pleural Mesothelioma	NCT01722149+

Note. +; indicate trials ongoing/active, *; indicate trials that started in 2018

Current Clinical Targets for Hematological Malignancies

As the most studied and researched target for CAR therapy, CD19 has shown impressive success in clinical settings to treat Acute Lymphoblastic Leukemia (ALL), Non-Hodgkin Lymphoma (NHL), and Chronic Lymphocytic Leukemia (CLL)[70]. Despite the high levels of complete response rates in patients, relapse from CD19 CAR therapy can occur via a suppressive tumor microenvironment or antigen escape[71–73]. With this in mind, new targets are being identified and evaluated to treat hematological malignancies. Among these new targets are CD5, CD123, CD33, CD70, CD38, and BCMA. These same targets have already shown promise using drug-conjugated antibodies, and several have been FDA approved for treatment (Figure 1-4B). These biomarkers are now being evaluated as targets for adoptive T cell CAR therapy to treat hematological malignancies.

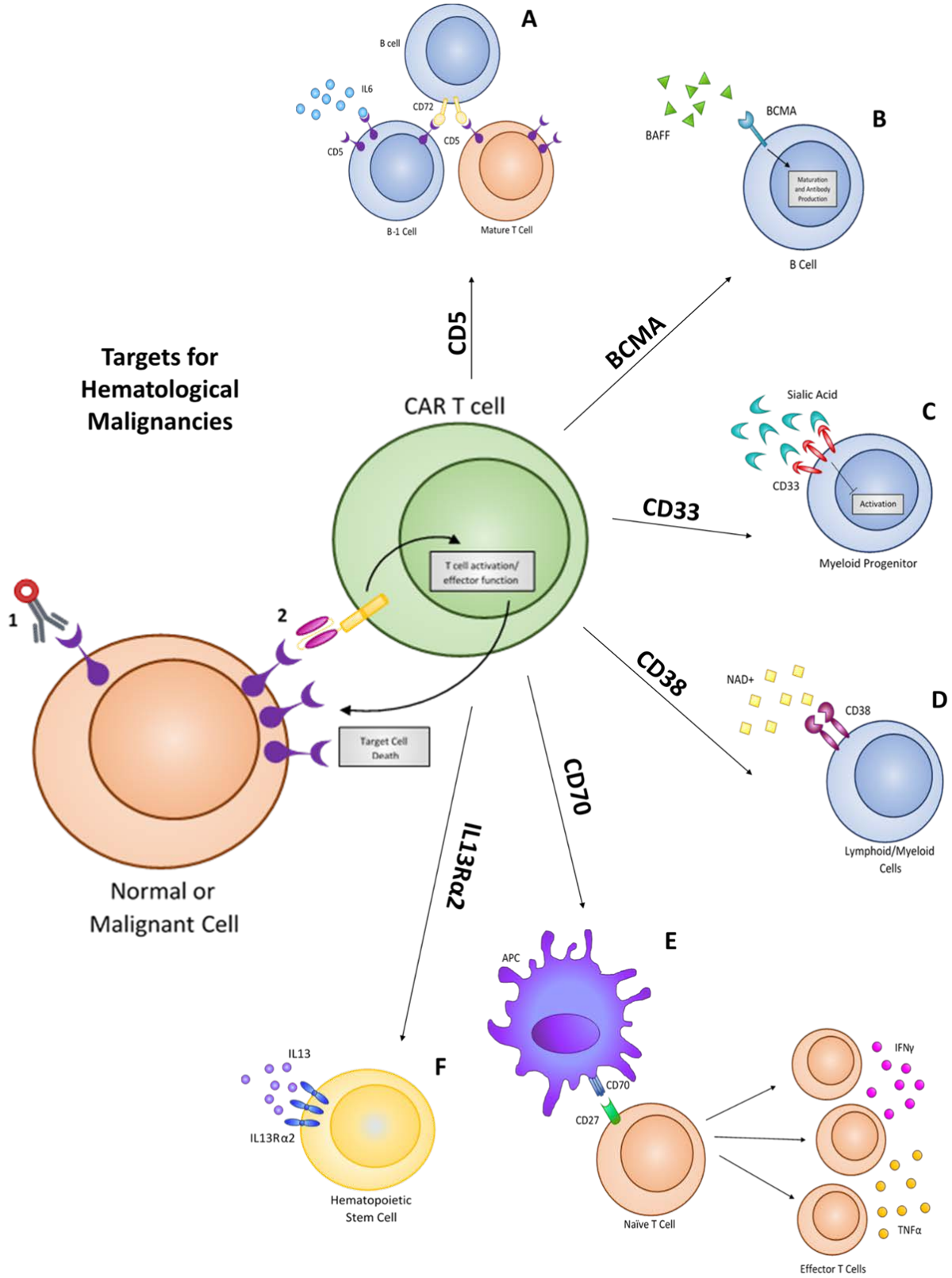

Figure 1-4B. *Biomarker targets for hematological malignancies.* The endogenous function of each of A) CD5, B) BCMA, C) CD33. D) CD38, E) CD70, and F) IL13Rα2 are shown. These targets are all being utilized to treat hematological malignancies in clinical trials. They are not cancer-specific and do have expression on normal cells but have an elevation within cancer that is being used for targeting.

CD5

CD5 is a negative regulator of TCR signaling and is expressed on the surface of most T cells and on a specific subpopulation of B cells (B-1) found most commonly in fetal cells[74] (Figure 1-4A-B). CD5 has high expression in approximately 80% of T-cell acute lymphoblastic leukemia (T-ALL) and T cell lymphomas along and also has significant expression on B-cell lymphomas[75]. CD5 was first utilized as an immunotherapy treatment via immunotoxin-conjugated antibodies[76–82] that aided in the depletion of malignant T cell populations in treated patients. More recently, CD5 has been utilized as a CAR target to treat T cell malignancies directly. As CD5 is not cancer specific, this treatment results in T cell aplasia[83,84]. While this is not ideal for long term patient immune functionality, the therapy is effective in eliminating malignant T cell populations and prolonging patient survival.

IL13Rα2

Interleukin-3 receptor alpha chain (IL13Rα2 or CD123) is a surface receptor found overexpressed in several hematological malignancies including blastic plasmacytoid dendritic cell neoplasm (BPDCN)[85], hairy cell leukemia[86,87], B-cell acute lymphocytic leukemia (B-ALL) [86,88], and Acute myeloblastic leukemia (AML)[89,90]. As the receptor expression is limited on hematopoietic stem cells, the receptor has promising use as a targetable biomarker for CAR therapy[90,91] (Figure 1-4F-B). Initial targeting of IL13Rα2 was conducted utilizing the natural ligand, IL-3, but CAR T cell approaches are now being utilized to further target this receptor to treat primarily AML patients. Initial trials with CD123 CAR cells showed potent cytotoxicity against AML cells within mice[92–95] and in human patients[96]. This preliminary success has led to its further testing in clinical trials, evaluating this therapy for both safety and efficacy against AML. IL13Rα2, like CD5, is not cancer specific, and the consequence of CD5 CAR T cells is severe myeloablation[97].

CD33

CD33 is a transmembrane receptor that binds sialic acid and causes inhibition of activation. The protein is expressed on AML blasts and normal myeloid progenitors[98–102] (Figure 1-4C-B). Because CD33 is absent in adult pluripotent hematopoietic stem cells and has elevated expression on approximately 85-90% of AML patients, the antigen has gained clinical significance as a TAA[103–105]. In initial trials testing the efficacy of CD33 CAR T cells, patients showed signs of an inflammatory reaction in response to infused CAR T cells: chills, fever, and elevated cytokine levels. This resulted in reduced blasts within the bone marrow following two weeks of therapy[106]. Following these preliminary tests, clinical trials are ongoing to determine if CD33 is a safe and effective treatment for myeloid leukemia.

CD70

CD70 is a target that is being utilized to treat both hematological malignancies as well as solid tumors (Table 1-1B). CD70 is the membrane-bound ligand of the CD27 receptor (TNF superfamily)[107–109] (Figure 1-4E-B). Expression of CD70 is limited to diffuse large B-cell and follicular lymphomas, as well as Hogkins lymphoma, multiple myeloma, and EBV-associated malignancies[110–114]. Additionally, CD70 is also expressed on other malignancies such as glioma[115–118], breast cancer[119,120], renal cell carcinoma[110,121–123], ovarian cancer[124–126], and pancreatic cancer[124,127]. Targeting this antigen is feasible as CD70/CD27 signaling is not essential for the development of a functional immune system as $CD27^{-/-}$ mice recover from infection in a similar time frame as $CD27^{WT}$ mice[128,129]. Targeting was first performed using monoclonal antibodies against CD70, and this showed promise in animal models[110,130,131]. CD70 CAR T cell treatments are unique because an antibody fragment against CD70 is not being utilized; instead, the CAR signaling domain is attached to the human CD27 protein, the natural binding partner of CD70, which functions with similar specificity as an scFv[107].

CD38

CD38 is a glycoprotein associated within lipid rafts and is specific to cell surface receptors that function to regulate calcium flux and mediate signal transduction in both lymphoid and myeloid cells[132–134]. While CD38 is expressed consistently on myeloma cells[132,135], it's expression is limited on normal lymphoid and myeloid cells[136] (Figure 1-4D-B). As a TAA, CD38 has been used as a target via monoclonal antibody treatment (Daratumumab)[132], which was approved by the FDA in 2015 for patients with multiple myeloma[137]. Daratumumab showed an overall response rate of 31%, which demonstrates the success of utilizing CD38 as a target. CD38 CAR T cells have shown similar efficacy against double-hit lymphoma cells (MYC rearrangement along with BCL2 or BCL6 rearrangement)[138]. With promising data, CD38 CAR T cells are currently in phase I trials against myeloma to test safety and dosing.

BCMA

B cell maturation antigen (BCMA) is a TNF receptor that binds B-cell activating factor (BAFF) and is universally expressed on myeloma cells but has insignificant expression on major adult organs[139] (Figure 1-4B-B). BCMA is exclusively expressed in B-cell lineage cells, and is expressed during plasma cell differentiation[140]. In preclinical models, anti-BCMA CAR T cells have shown effective killing of myeloma cells both *in vitro* and *in vivo*[141,142]. Following Phase I safety studies, some patients experienced neurotoxicity and cytokine release syndrome, which are common side effects of CAR T cell treatment[143]. Other side effects of targeting BCMA are similar to those of other hematological malignancies, as patients suffer from partial or complete B cell aplasia.

Current clinical targets for solid tumors

While CAR T cell therapy has been very successful against hematological malignancies, it has been challenging to apply this technology to solid tumors. This challenge has resulted in a strong effort to discover biomarkers for solid malignancies. As such, there are 17 biomarkers currently in clinical trials for solid tumors (Figure 1-5B).

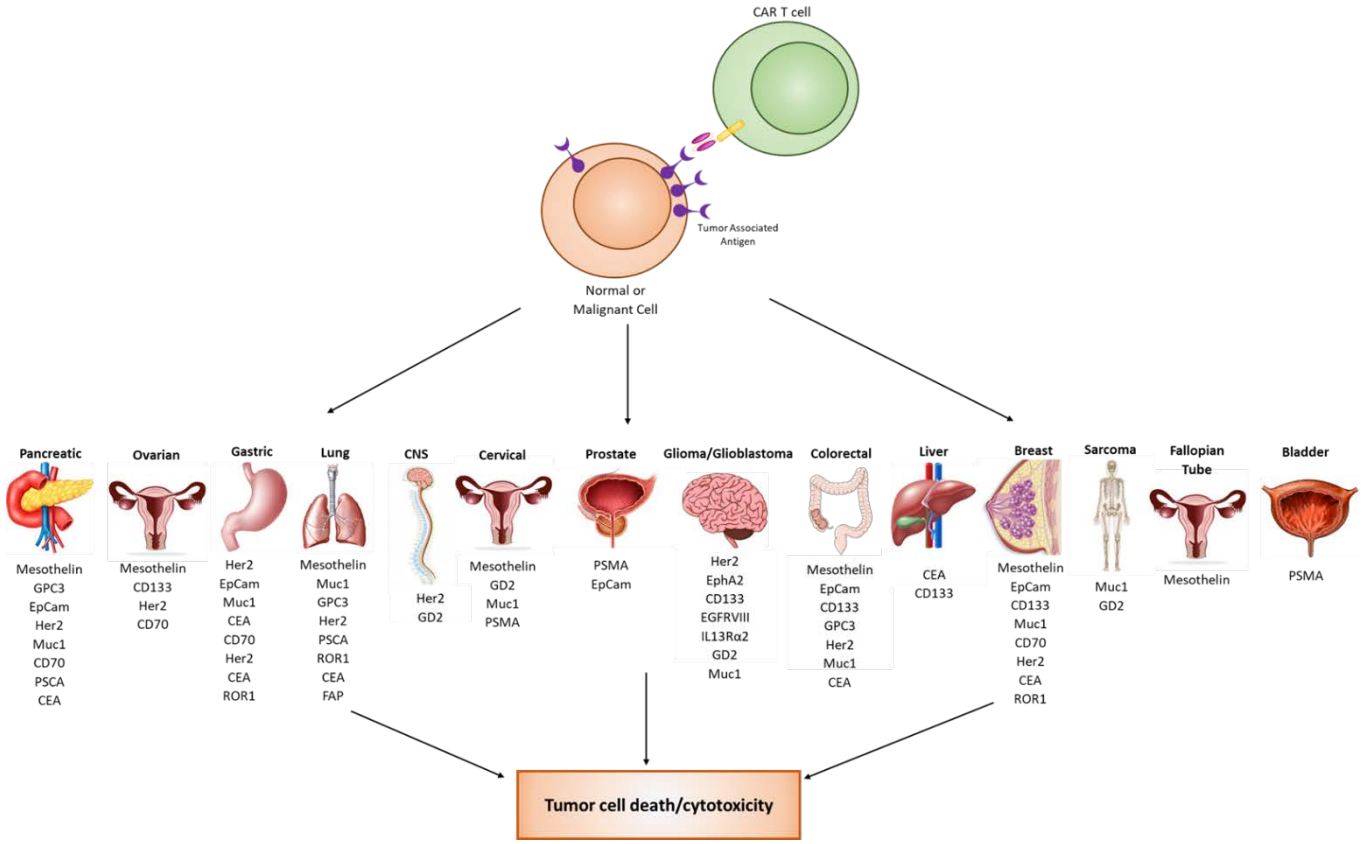

Figure 1-5B. *Biomarker targets for solid malignancies.* Over 14 different organ types are currently being targeted using a variety of different biomarkers. Many biomarker targets have expression in several different cancer types.

Mesothelin

Mesothelin (MSLN), the second most frequently targeted biomarker after CD19, has emerged as an attractive target for cancer immunotherapy. MSLN is a cell-surface glycoprotein with presence in the sera of cancer patients as soluble MSLN-related peptide (SMRP). Within normal tissue, the expression of MSLN is restricted to mesothelial cells lining the pericardium, peritoneum, and pleura. Yet, in cancer cells, MSLN is overexpressed on nearly a third of human

malignancies[144]. Elevated levels of MSLN have been reported on ovarian cancers[145,146], non-small-cell lung cancers[147,148], breast cancers[149,150], esophageal cancers[151], colon and gastric cancers[152], and pancreatic cancers[153]. In addition, Lamberts et al. reported MSLN expression in other solid tumors such as thyroid cancer, renal cancer, and synovial sarcoma[154]. The biological function of MSLN is nonessential given that MSLN$^{-/-}$ mice do not show any phenotypic abnormalities[155]. However, the overexpression of MSLN has been associated with cancer cell proliferation, increased local invasion and metastasis, and resistance to apoptosis induced by cytotoxic agents[150,156–158]. MSLN-CAR T cells have been created and tested against ovarian cancer, and lung cancer[156]. These CAR T cells have shown significant increases in T cell proliferation, T cell redistribution to metastatic sites, reduction in tumor burden, and increased overall survival. This promising pre-clinical data has led to several Phase I clinical trials to test the safety and efficacy of MSLN CAR T cell therapy against several tumors (Table 1-2B). Initial Phase I clinical trials have shown transient expression of the MSLN-CAR T cells and minimal cytokine release syndrome or on-target, off-tumor effects (NCT01355965, NCTO 02159716 & NCTO01897415). A single infusion of MSLN-CAR T cells resulted in decreased tumor burden and patients had no signs of long-term toxicities 1-2 months post infusion[159].

Table 1-2B. Mesothelin CAR T cell clinical trials (as of April 2018)

	Title	Recruitment	Conditions	Phases	NCT number
1	Anti-mesothelin CAR T Cells for Patients with Recurrent or Metastatic Malignant Tumors	Recruiting	Mesothelin Positive Tumors	Phase 1	NCT02930993
2	PD-1 Antibody Expressing CAR T Cells for Mesothelin Positive Advanced Malignancies	Recruiting	Advanced Solid Tumor	Phase 1, Phase 2	NCT03030001
3	A Study of Mesothelin Redirected Autologous T Cells for Advanced Pancreatic Carcinoma	Recruiting	Pancreatic Cancer	Phase 1	NCT02706782

4	CTLA-4 and PD-1 Antibodies Expressing Mesothelin-CAR-T Cells for Mesothelin Positive Advanced Solid Tumor	Recruiting	Advanced Solid Tumor	Phase 1, Phase 2	NCT03182803
5	Pilot Study of Autologous T-cells in Patients with Metastatic Pancreatic Cancer	Completed	Pancreatic Cancer	Phase 1	NCT02465983
6	Intervention of CAR-T Against Cervical Cancer	Recruiting	Cervical Cancer	Phase 1, Phase 2	NCT03356795
7	Autologous Redirected RNA Meso CAR T Cells for Pancreatic Cancer	Completed	Metastatic Pancreatic Ductal Adenocarcinoma (PDA)	Phase 1	NCT01897415
8	Evaluate the Safety and Efficacy of CAR-T in the Treatment of Pancreatic Cancer.	Recruiting	Pancreatic Cancer	Early Phase 1	NCT03267173
9	CART-meso in Mesothelin Expressing Cancers	Completed	Metastatic Pancreatic (Ductal) Adenocarcinoma, Epithelial Ovarian Cancer, Malignant Epithelial Pleural, Mesothelioma	Phase 1	NCT02159716
10	CAR T Cells in Mesothelin Expressing Cancers	Active, not recruiting	Lung Adenocarcinoma, Ovarian Cancer, Peritoneal Carcinoma, Fallopian Tube Cancer, Mesotheliomas Pleural, Mesothelioma Peritoneum	Phase 1	NCT03054298
11	Treatment of Relapsed and/or Chemotherapy Refractory Advanced Malignancies by CART-meso	Recruiting	Malignant Mesothelioma, Pancreatic Cancer, Ovarian Tumor, Triple Negative Breast Cancer, Endometrial Cancer, Other Mesothelin Positive Tumors	Phase 1	NCT02580747
12	Autologous CARTmeso/19 Against Pancreatic Cancer	Active, not recruiting	Pancreatic Cancer	Early Phase 1	NCT03497819
13	Malignant Pleural Disease Treated with Autologous T Cells Genetically Engineered to	Recruiting	Malignant Pleural Disease, Mesothelioma, Lung Cancer, Breast Cancer	Phase 1	NCT02414269

	Target the Cancer-Cell Surface Antigen Mesothelin				
14	A Study of Chimeric Antigen Receptor T Cells Combined with Interventional Therapy in Advanced Liver Malignancy	Recruiting	Hepatocellular Carcinoma, Metastatic Pancreatic Cancer Metastatic Colorectal Cancer	Phase 1, Phase 2	NCT02959151
15	CAR T Cell Receptor Immunotherapy Targeting Mesothelin for Patients with Metastatic Cancer	Recruiting	Cervical Cancer, Pancreatic Cancer, Ovarian Cancer, Mesothelioma, Lung Cancer	Phase 1, Phase 2	NCT01583686
16	CAR T Cell Immunotherapy for Pancreatic Cancer	Active, not recruiting	Pancreatic Cancer	Phase 1	NCT03323944
17	Autologous Redirected RNA Meso-CIR T Cells	Completed	Malignant Pleural Mesothelioma	Phase 1	NCT01355965
18	T-Cell Therapy for Advanced Breast Cancer	Recruiting	Breast Cancer, Metastatic HER2-negative Breast	Phase 1	NCT02792114

Her2

HER2 (Human epidermal growth factor 2) is a transmembrane tyrosine kinase in the ERBB family. The HER2 receptor plays an important role in normal cell growth and differentiation, activating PI3K/Akt and RAS/Raf/MEK/MAPK pathways[160]. Studies have reported HER2 protein overexpression, gene amplification, and mutation in many cancers including breast, lung, colorectal, brain, ovarian, and pancreas[161]. Overexpression of HER2 has been found to be associated with increased tumor cell proliferation and invasion[162], decreased response to hormonal treatment[163], and resistance to apoptosis[164]. HER2 has been targeted utilizing DNA vaccines, peptide vaccines, and dendritic vaccines which have shown promising results in both preclinical and early clinical studies[165,166]. Trastuzumab, a humanized monoclonal antibody developed to target overexpressed HER2 receptor, has also shown success as an immunotherapy treatment. Transtuzumab, along with chemotherapy, has increased overall survival and risk of recurrence compared to chemotherapy alone in HER2 overexpressing breast

cancer patients[167]. Several groups have reported the anti-tumor activity, persistence, and application feasibility of HER2 CAR T cells preclinically in HER2 overexpressing cancer as an alternative targeted therapy[168–170]. The success of preclinical experiments of HER2 CAR T cell has led to the initiation of several clinical trials for the treatment of various cancers (Table 1-3B)[171–173].

Table 1-3B. *HER2 CAR T cell clinical trials (As of April 2018).*

	Title	Recruitment	Conditions	Phases	NCT Number
1	HER2-specific CAR T Cell Locoregional Immunotherapy for HER2-positive Recurrent/Refractory Pediatric CNS Tumors	Not yet recruiting	Central Nervous System Tumor	Phase 1	NCT03500991
2	A Clinical Research of CAR T Cells Targeting HER2 Positive Cancer	Recruiting	Breast Cancer, Ovarian Cancer, Lung Cancer, Gastric Cancer, Colorectal Cancer, Glioma, Pancreatic Cancer	Phase 1, Phase 2	NCT02713984
3	Chimeric Antigen Receptor-Modified T Cells for Breast Cancer	Completed	Breast Cancer	Phase 1, Phase 2	NCT02547961
4	T Cells Expressing HER2-specific Chimeric Antigen Receptors(CAR) for Patients with Glioblastoma	Recruiting	Glioblastoma	Phase 1	NCT02442297
5	Memory-Enriched T Cells in Treating Patients with Recurrent or Refractory Grade III-IV Glioma	Not yet recruiting	Glioblastoma, Malignant Glioma	Phase 1	NCT03389230
7	Evaluate the Safety and Efficacy of CAR-T in the Treatment of Pancreatic Cancer.	Recruiting	Pancreatic Cancer	Early Phase 1	NCT03267173
8	Her2 Chimeric Antigen Receptor Expressing T Cells in Advanced Sarcoma	Recruiting	Sarcoma	Phase 1	NCT00902044
9	CMV-specific Cytotoxic T Lymphocytes Expressing CAR Targeting HER2 in Patients With GBM	Active, not recruiting	Glioblastoma Multiforme (GBM)	Phase 1	NCT01109095
10	T-Cell Therapy for Advanced Breast Cancer	Recruiting	Breast Cancer, Metastatic HER2-negative Breast	Phase 1	NCT02792114
11	Personalized Chimeric Antigen Receptor T Cell Immunotherapy for Patients with Recurrent Malignant Gliomas	Recruiting	Malignant Glioma of Brain	Phase 1	NCT03423992
12	Treatment of Chemotherapy Refractory Human Epidermalgrowth Factor	Unknown status	Advanced HER-2 Positive Solid Tumors	Phase 1, Phase 2	NCT01935843

	Receptor-2(HER-2) Positive Advanced Solid Tumors				
13	Her2 and TGFβ CTLs in Treatment of Her2 Positive Malignancy	Active, not recruiting	HER2 Positive Malignancies	Phase 1	NCT00889954
14	Genetically Modified T-Cell Therapy in Treating Patients with Advanced ROR1+ Malignancies	Recruiting	Recurrent Adult Acute Lymphoblastic Leukemia, Recurrent Mantle Cell Lymphoma, Refractory Chronic Lymphocytic Leukemia, Non-Small Cell Lung Cancer, Triple-Negative Breast Carcinoma	Phase 1	NCT02706392

GD2

GD2 is a ganglioside antigen that is expressed on the surface of several malignancies including neuroblastoma[174], glioma, cervical cancer, and sarcoma[175,176]. The normal expression of the protein is limited to neurons, melanocytes, and peripheral nerve fibers[176–178]. One of the most successful trial reports for CARs in solid tumors has been using GD2 as a target for neuroblastoma[179–182]. Not only did GD-2 CAR T cells induce a response in 30% of patients, including a complete remission in 3 patients, but researchers found long term persistence of the CAR T cells post treatment, which subsequently reduced tumor recurrence/progression [182]. Meanwhile, GD2 monoclonal antibodies (Dinutuximab) have been effective for the control of neuroblastoma[176,183–185] and this product is currently FDA approved for that application. There have been some observed cytotoxicities associated with targeting GD2, such as sensorimotor demyelinating polyneuropathy caused by anti-GD2 biding to peripheral myelin in the posterior pituitary[177]. In preclinical models, severe lethal CNS toxicity caused by CAR T cell infiltration and proliferation within the brain resulted in neuronal destruction[186]. Therefore, although there

has been success utilizing CAR therapy in patients, necessary precautions need to be taken to avoid neurotoxicity as GD2 has expression in normal neural cells. GD2, as of May 2018, has 10 ongoing clinical CAR T cell trials targeting primarily neuroblastoma (Table 1-4B). A majority of these clinical trials are in phase I status to determine the safety of the treatment. One of the clinical trials (NCT02765243) is testing the incorporation of a kill switch, which is an engineered suicide gene (iCasp9) to help avoid neurotoxicity.

Table 1-4B. *GD2 CAR T cell clinical trials (as of April 2018)*

	Title	Recruitment	Conditions	Phases	NCT Number
1	Anti-GD2 CAR T Cells in Pediatric Patients Affected by High Risk and/or Relapsed/Refractory Neuroblastoma	Recruiting	Neuroblastoma	Phase 1, Phase 2	NCT03373097
2	Anti-GD2 4th Generation CART Cells Targeting Refractory and/or Recurrent Neuroblastoma	Recruiting	Neuroblastoma	Phase 2	NCT02765243
3	A Phase I Trial of T Cells Expressing an Anti-GD2 Chimeric Antigen Receptor in Children and Young Adults with GD2+ Solid Tumors	Completed	Sarcoma, Osteosarcoma, Neuroblastoma , Melanoma	Phase 1	NCT02107963
4	CAR-T Cell Immunotherapy for GD2 Positive Glioma Patients	Completed	GD2 Positive Glioma	Phase 1, Phase 2	NCT03252171
5	Study Evaluating the Efficacy and Safety With CAR-T for Relapsed or Refractory Neuroblastoma in Children	Recruiting	Relapsed or Refractory Neuroblastoma	Not Applicable	NCT02919046
6	A Cancer Research UK Trial of Anti-GD2 T-cells (1RG-CART)	Recruiting	Relapsed or Refractory Neuroblastoma	Phase 1	NCT02761915
7	Study on GD2 Positive Solid Tumors by 4SCAR-GD2	Recruiting	Solid Tumor	Phase 1, Phase 2	NCT02992210
8	Intervention of CAR-T Against Cervical Cancer	Recruiting	Cervical Cancer	Phase 1, Phase 2	NCT03356795
9	Safety and Efficacy Evaluation of 4th Generation Safety-engineered CAR T Cells Targeting Sarcomas	Recruiting	Sarcoma, Osteoid Sarcoma, Ewing Sarcoma	Phase 1, Phase 2	NCT03356782
10	iC9-GD2-CAR-VZV-CTLs/Refractory or Metastatic GD2-positive Sarcoma/VEGAS	Active, not recruiting	Sarcomas	Phase 1	NCT01953900

MUC1

MUC1 is a large transmembrane glycoprotein that is transcriptionally upregulated in breast and ovarian tumors[187,188]. MUC1 expression is confined to normal luminal epithelium, and the expression is lost upon transformation[189–193]. MUC1 has recently become an interesting target in cancer immunotherapy because of the overexpression of aberrantly glycosylated MUC1 in most solid tumors and several hematological malignancies. This is in addition to the role of MUC1 in cancer progression, invasion, metastasis, angiogenesis, and chemoresistance. Although expressed significantly on malignant cells, MUC1 targeting presents some complications as MUC1 is shed and may inhibit tumor antibody binding/recognition[194]. MUC1 also has the ability to inhibit T cell function and thereby promotes an anti-inflammatory TME[195]. CAR T-cell therapy targeting MUC1 has been beset with several challenges such as steric hindrance and glycosylation-related epitope heterogeneity[196]. Following CAR optimization with tripartite endodomains and high affinity screening for effective ScFv fragments, MUC1-CAR T cells showed significant delays in tumor growth in mouse xenograft models[197]. MUC1-CAR T cells also show enhanced proliferation, increased IFN-ϒ secretion, and enhanced anti-tumor efficacy when compared to control CAR T cells in vitro[198]. Based on the success of these preclinical MUC1-CAR T cells, several clinical trialstargeting MUC1 in several cancer types have begun (Table 1-5B). Early phase 1 clinical trials revealed no initial adverse side-effects and patient cytokine levels increased, indicating a positive response as tumor necrosis was observed[199].

Table 1-5B. *MUC1 CAR T cell clinical trials (as of April 2018)*

	Title	Recruitment	Conditions	Phases	NCT Number
1	Phase I/II Study of Anti-Mucin1 (MUC1) CAR T Cells for Patients with MUC1+ Advanced Refractory Solid Tumor	Recruiting	Hepatocellular Carcinoma, Non-small Cell Lung Cancer, Pancreatic Carcinoma, Triple-Negative Invasive Breast Carcinoma	Phase 1, Phase 2	NCT02587689

2	Anti-MUC1 CAR T Cells and PD-1 Knockout Engineered T Cells for NSCLC	Recruiting	Lung Neoplasm Malignant, Non-small Cell Lung Cancer	Phase 1, Phase 2	NCT03525782
3	CTLA-4 and PD-1 Antibodies Expressing MUC1-CAR-T Cells for MUC1 Positive Advanced Solid Tumor	Recruiting	Advanced Solid Tumor	Phase 1, Phase 2	NCT03179007
4	CAR-T Cell Immunotherapy in MUC1 Positive Solid Tumor	Recruiting	Malignant Glioma of Brain, Colorectal Carcinoma, Gastric Carcinoma	Phase 1, Phase 2	NCT02617134
5	PSCA/MUC1/PD-L1/CD80/86-CAR-T Cells Immunotherapy Against Cancers	Recruiting	Lung Cancer	Phase 1	NCT03198052
6	Multi-CAR T Cell Therapy for Acute Myeloid Leukemia	Recruiting	Acute Myeloid Leukemia	Phase 1, Phase 2	NCT03222674
7	Intervention of CAR-T Against Cervical Cancer	Recruiting	Cervical Cancer	Phase 1, Phase 2	NCT03356795
8	Evaluate the Safety and Efficacy of CAR-T in the Treatment of Pancreatic Cancer.	Recruiting	Pancreatic Cancer	Early Phase 1	NCT03267173
9	Safety and Efficacy Evaluation of 4th Generation Safety-engineered CAR T Cells Targeting Sarcomas	Recruiting	Sarcoma, Osteoid Sarcoma, |Ewing Sarcoma	Phase1, Phase 2	NCT03356782

GPC3

Glypican-3 (GPC3) is a GPI bound sulfate proteoglycan involved in cellular growth, differentiation, and migration[200,201]. GPC3 shows elevated expression in approximately 75% of hepatocellular carcinoma samples, but had no expression in corresponding normal tissue[202,203]. GPC3 is also elevated within breast cancer[204], melanoma[205], and pancreatic cancer[206,207] demonstrating its use across a wide variety of cancer types. GPC3 CAR T cells showed promising preclinical results targeting tumors in mouse xenograft models[208]. In human trials there was minimal toxicity and all patients tolerated the treatment (NCT02395250)[209]. Further clinical trials targeting lung cancer, pancreatic cancer, and colorectal cancer are ongoing.

IL13Rα2

There are currently two clinical trials, one initiated in 2015 and one in 2018, testing the efficacy and safety of IL13Rα2 directed CAR T cells against glioma patients. IL-13 is a T helper 2 (TH2) derived cytokine involved in immune regulation. IL13Rα2 is an IL-13 receptor that acts as a decoy by directly competing with the IL13Rα1 receptor to elicit downstream STAT signaling[210,211]. IL13Rα2 receptors are upregulated in approximately 50% of glioma patients and have a strong correlation with poor survival[212]. As a gene that is highly expressed in tumor infiltrating macrophages (TIM) and tumor-associated macrophages (TAM), but shows minimal expression in normal brain tissue, IL13Rα2 has been previously studied as a cancer vaccine, and more recently as a direct target for CAR therapy. Initially, IL13Rα2 CAR T cells were developed utilizing a membrane-tethered IL13 ligand mutated at residue 13 (E→Y)[212] as the antigen recognition domain. Unfortunately, it was determined that these domains also recognized IL13Rα1 receptors as well, which raised significant safety concerns. New CAR T cell constructs targeting IL13Rα2 therapy rely on scFv-based targeting. With this modification in antigen specificity, scFv-based IL13Rα2 CARs induce tumor regression in mouse xenograft models of glioma and show insignificant recognition of IL13Rα1 receptors[213].

PSCA

Prostate stem cell antigen (PSCA) is a serine protease[214,215] expressed in the basal cells of normal prostate cells [216] and is overexpressed in approximately 80% of prostate cancers[217–220]. In addition, PSCA expression increases with both high gleason score, and metastasis[219]. The expression of PSCA is limited to the basal cell epithelium in the prostatic epithelium[217]. As a protein attached to the cell surface via a GPI-anchor, it serves as an ideal target for prostate cancer and further metastatic sites[219]. PSCA has also been found expressed on other cancer types such as gastric cancer, gallbladder adenocarcinoma[221–223], non-small-cell lung cancer[216,224], ad

pancreatic cancer[225]. In humanized mouse models, CAR T cells targeting PSCA induced significant antitumor activity in pancreatic cancer[225]. Although initial results have been promising, preclinical reports have shown that tumors can escape PSCA-CAR T cells and while treatment does prolong survival, it does not necessarily eradicate PSCA-expressing tumors[226,227].

VEGFR2

Vascular endothelial growth factor receptor 2 (VEGFR2) is an important mediator of tumor angiogenesis[228,229]. VEGFR2 is involved in microvascular permeability, endothelial cell proliferation, invasion, migration, and survival[230]. Overexpression of VEGFR2 has been associated with increased metastasis in several malignancies[231,232], and VEGFR2 expression has also been shown on squamous cell carcinomas of the head and neck[233], colorectal cancer[234,235], breast cancer[236,237], and NSCLC[238–240]. While overexpressed in cancer, the expression of VEGFR2 in normal tissue is restricted to endothelia and mesothelial[241]. Initial targeting of VEGFR2 with monoclonal antibodies has resulted in growth inhibition and decreased micro vessel density while simultaneously inducing tumor cell apoptosis and necrosis[242,243]. These preclinical results have been shown in NSCLC, renal carcinoma, hepatocellular carcinoma, melanoma, ovarian cancer, and colorectal cancer[231,244–248]. To date, only one clinical trial has been enrolled utilizing CAR T cells against VEGFR2 (NCT01218867)[249].

CEA

Carcinoembryonic antigen (CEA) is a glycoprotein on the surface of several carcinomas[250]. The most studied use for CEA as a surface biomarker has been in liver metastasis, especially originating from colorectal cancer[251–253]. CEA is also significantly expressed on the surface of gastric cancer, pancreatic cancer, ovarian cancer, and lung cancers[254]. While CEA is expressed on the surface of some normal cells, including epithelial cells in the pulmonary tract

and in the gastrointestinal tract, these normal sites of expression are invisible to immune detection as CEA is restricted to the apical surface of the epithelial cells that face the lumen in normal adults[255,256]. As the cells are 'invisible' to immune detection it renders CEA an attractive target with limited bystander cytotoxicity. Following cancer development, epithelial cells lose apical polarity, which subsequently results in CEA gaining access to the blood stream and into the serum of the patient[257]. This renders CEA a useful diagnostic biomarker, as serum detection can serve to identify cancer development for several cancer types including breast[258–260], skin cancer[261], NSCLC[262–264], gastric[259,265–268], and pancreatic cancer[259,269–272]. Preclinical testing with CEA-CAR T cells has shown that lymphodepletion or myeloablation prior to infusion is required to induce a response in mice with CEA+ tumors[255]. Initially, CEA was targeted utilizing engineered TCRs, but trials were halted as patients developed severe colitis as a result of off target killing of normal epithelial cells[273]. These same results have yet to be observed with CAR T cell therapy targeting CEA, but patients are treated with caution to avoid on-target, off-tumor cytotoxicity.

PSMA

Prostate specific membrane antigen (PSMA), or Glutamate carboxypeptidase II (GCPII)[215], is a glycoprotein[274] with three known activities including folate hydrolase[275], NAALADase[276], and dipeptidyl peptidase[274]. While PSMA is expressed in normal prostate epithelium[274], it has been shown in 90% of human prostate tumors including their respective metastatic sites[215,277,278]. PSMA has also been expressed in low levels in salivary glands, brain, and kidneys[279–281]. In initial pre-clinical models, anti-PSMA CAR T cells were able to effectively target and eliminate 60% of tumors in treated animals while significantly improving overall survival *in vivo*[282]. Following Phase I clinical trials, no anti-PSMA toxicities were noted and 40% of patients achieved clinical partial responses (PR)[283]. More recently, PSMA CAR T cells

have been designed to resist TGFβ suppression, which is commonly found in prostate cancers, via a negative TGFβ receptor II [284].

ROR1

Receptor tyrosine kinase like orphan receptor 1 (ROR1) is a Wnt5a surface receptor expressed during embryonic development, but generally absent from adult tissue with the exception of adipocytes, gut, pancreas, and parathyroid glands[285–287]. In the case of cancer, ROR1 has shown high levels in several solid malignancies: pancreatic[288,289], ovarian[288,290–292], breast[288,293–295], lung[288,296,297], gastric cancer[298], and colorectal cancer[299]. High levels of ROR1 have shown strong correlation to poor patient outcome and also to developing metastasis[292,300]. There has been some conflicting preclinical studies where CAR T cells targeting ROR1 have demonstrated severe cytotoxicity as the cells accumulated within the lungs[301]. Meanwhile, other studies have shown great success in targeting ROR1, which may be a direct cause of the specificity of the antibody utilized for the scFv[302,303]. Currently, ROR1 is being used in clinical trials to target breast and lung cancers.

FAP

Fibroblast activation protein (FAP) is a transmembrane serine protease with high expression on cancer-associated stromal cells (CASC) in epithelial cancers[304–306]. In pancreatic tumors, FAP shows significant elevation and is correlated with worse clinical outcome[307]. In colorectal cancer, patients with high levels of FAP were more likely to develop metastasis, recurrence, and aggressive disease progression[308]. FAP does not have this same expression within normal cells, as most stromal cells have insignificant levels of the protein[309–311]. As a therapeutic target, FAP has been utilized as a useful cancer vaccine in inhibiting tumor growth and increasing cytotoxicity[304,312,313]. As the biomarker has shown success as a targeting agent,

CAR T cells targeting FAP have been developed. These FAP CAR T cells show conflicting results as some groups report limited antitumor efficacy[314], while others report significant tumor cytotoxicity with minimal off-tumor killing[315] along with prolonged survival[316]. While the use of FAP CAR T cells may extend to many different organ sites, current clinical trials are designed to treat pleural mesothelioma.

EpCAM

Epithelial cell adhesion molecule (EpCAM or CD326) is a transmembrane glycoprotein that functions to abrogate E-cadherin-mediated cell adhesion, and functions within transcriptional complexes inducing c-myc and cycline A & E expression[317,318]. EpCAM has shown overexpression in a range of tumors including colon adenocarcinoma, stomach adenocarcinoma, pancreatic adenocarcinoma, lung adenocarcinoma, ovarian adenocarcinoma, and breast adenocarcinoma[319,320]. The protein is found at the basolateral cell membrane of normal adult tissue [321]. EpCAM has shown significance as a biomarker for early cancer development [322]. Like several other biomarker targets described, monoclonal antibody therapy targeting EpCAM (Catumaxomab) has been used in patients to treat peritoneal carcinomatosis (PC) which resulted in a slight increase in survival[323]. Further clinical trials with Catumaxomab have been used to target bladder cancer[324], head and neck cancer[325], ovarian cancer[326], and metastatic disease[327]. These trials resulted in an increase in overall patient survival. EpCAM specific CAR T cells have been developed to treat prostate, breast, and peritoneal cancers and have shown suppressed tumor progression/delayed disease as well as CAR T cell trafficking into the tumor site[328–331].

EGFRvIII

Epidermal growth factor receptor variant III (EGFRvIII) is a gain of function mutated EGFR that arises from the genomic deletion of exons 2-7. The deletion of these exons leads to a ligand-independent receptor that endows cells with a significant growth advantage over normal cells[332]. EGFRVIII is commonly found within glioblastoma patients, especially in CD133+ glioblastoma cancer stem cells[333]. As a tumor-specific antigen, EGFRvIII has been targeted utilizing FDA approved cancer vaccines (Rindopepimut), which result in significant improved survival[334]. Due to its success as a cancer vaccine, CAR T cells have been developed to directly target malignant cells expressing EGFRvIII. These CAR T cell therapies have shown delayed tumor growth, elimination of EGFRVIII+ tumor cells, and increased pro-inflammatory cytokine release in an antigen dependent manner[335–338]. A first-in-human study of intravenous delivery of a single dose of autologous EGFRvIII-CAR T cells (NCT02209376) had reported that the infusion of cells was feasible and safe, with no off-tumor toxicity or cytokine release syndrome. In this study, 10 patients with recurrent glioblastoma (GBM) were treated with EGFRvIII-CAR T cells. At least one patient achieved stable disease for over 18 months with a single infusion of CAR T cells. The median overall survival was about 8 months in all patients. The study, however, found that tumor microenvironment increased the expression of inhibitory molecules and infiltration by regulatory T cells which suppressed effector CAR T cell functions[339]. While there are promising results using this target, there may be suppressive factors that limit its efficacy in patients. There are nine clinical trials ongoing (as of May 2018) targeting a variety of tumor types (Table 1-6B).

Table 1-6B. *EGFRvIII CAR T cell clinical trials (as of April 2018)*

	Title	Recruitment	Conditions	Phases	NCT Number
1	EGFRvIII CAR T Cells for Newly-Diagnosed WHO Grade IV Malignant Glioma	Recruiting	Glioblastoma, Gliosarcoma	Phase 1	NCT02664363
2	Pilot Study of Autologous Anti-EGFRvIII CAR T Cells in Recurrent Glioblastoma Multiforme	Recruiting	Glioblastoma Multiforme	Phase 1	NCT02844062
3	Intracerebral EGFR-vIII CAR-T Cells for Recurrent GBM	Not yet recruiting	Recurrent Glioblastoma Multiforme, Recurrent Brain Tumor	Phase 1	NCT03283631
4	4SCAR-IgT Against Glioblastoma Multiform	Enrolling by invitation	Glioblastoma Multiforme	Phase 1, Phase 2	NCT03170141
5	CAR T Cell Receptor Immunotherapy Targeting EGFRvIII for Patients with Malignant Gliomas Expressing EGFRvIII	Recruiting	Malignant Glioma, Glioblastoma, Gliosarcoma	Phase 1, Phase 2	NCT01454596
6	Evaluate the Safety and Efficacy of CAR-T in the Treatment of Pancreatic Cancer.	Recruiting	Pancreatic Cancer	Early Phase 1	NCT03267173
7	Autologous T Cells Redirected to EGFRVIII-With a Chimeric Antigen Receptor in Patients With EGFRVIII+ Glioblastoma	Active, not recruiting	Patients with Residual or Reccurent EGFRvIII+ Glioma	Not Applicable	NCT02209376
8	Personalized Chimeric Antigen Receptor T Cell Immunotherapy for Patients with Recurrent Malignant Gliomas	Recruiting	Malignant Glioma of Brain	Phase 1	NCT03423992
9	Long-term Follow-up of Subjects Exposed to Lentiviral-based CART-EGFRvIII Gene-modified Cellular Therapy Products in Cancer Studies	Enrolling by invitation	A long-term follow-up study of CART-EGFRvIII Infusion		NCT02666248

EphA2

Ephrin type A receptor (EphA2) is a receptor tyrosine kinase that plays a key role in the development of cancer disease. EphA2 enhances tumorigenesis and progression via interactions with other cell-surface receptors such as EGFR and HER2/ErbB2, which in turn amplify MAPK, Akt, and Rho family GTPase activities[340–342]. EphA2 has shown expression in normal brain, skin, bone marrow, lung, thymus, spleen, liver, small intestine, colon, bladder, kidney, uterus, testis and prostate at low levels[343,344]. Overexpression of EphA2 has been observed in malignant tissue

which has been linked to poor clinical prognosis[345–347]. EphA2 has been targeted through a variety of avenues including viral vectors, RNA interference, small molecule inhibitors, recombinant proteins, and immunotherapy. Small molecule inhibitors (FDA approved-Dasatinib) of EphA2 have significantly reduced tumor growth in several cancer types, and have shown anti-tumor efficacy via the reduction of EphA2 expression and kinase activity upon treatment [348,349]. On the heels of the success of these methods, CAR T cells have been developed to target EphA2 in Lung cancer[350], glioma[351], and glioblastoma[352] which have all demonstrated cytotoxic effects both *in vitro* and *in vivo*[353].

Combination therapy with multiple biomarker targets

To aid in providing both specificity and longevitiy of CAR T cells, efforts have been made to combine different biomarker targets to elicit T cell responses. These CARs are termed "tandem CARs" and are designed to express two antigen binding domains. Following binding of both scFv fragments, CAR T cells are able to send an activation signal and elicit target cell death, but are unable to do this if only one scFv binds[354]. BCMA CAR T cells have been linked to CS1-CAR T cells and designed to express both CAR molecules on the cell surface. They found that this combination elicited potent and specific anti-tumor activity through both antigens *in vitro* and *in vivo*[355]. HER2/IL-13RA2 CAR T cells have been designed and showed additive T cell activation when both receptors were engaged, resulting in superior sustained activity[356]. In addition, these tandem CARs avoided antigen escape, which is the primary drawback from CAR therapy as cancer evolves to sequester target antigen expression. CD20/CD19 tandem CARs have also been developed, but showed no difference between tandem CAR killing and single antigen specificity CARs in this context[357]. This demonstrates that only certain combinations of biomarker targets are effective in a tandem CAR design. CD19 has also been combined with Her2 and showed the engineered cells could preserve the cytolytic activity of T cells[358]. This is

an ongoing worthwhile pursuit to develop CARs that have specific killing with minimal cytotoxic effects to healthy tissue. By activating upon two ScFv signals, bystander organ killing could be reduced as different antigen combinations can decrease on-target, off-tumor killing.

In an effort to increase CAR–tumor specificity and reduce off-tumor toxicity inhibitory chimeric antigen receptors (iCARs) have been developed to ensure healthy tissue is not targeted by CAR T cells. iCAR cells are designed with an ingrained override signal. When in contact with only the tumor antigen, CAR T cells elicit a cytotoxic response to the target cell, but when in contact with normal tissue antigens, the T cells are effectively turned 'off' via anti-inflammatory co-stimulation. This new technique may provide a way for biomarkers to be used in combination to elicit extremely specific effects within cancer and avoid healthy tissue toxicity[359,360].

Up and coming biomarkers

As CAR therapy expands, so does the need for discovering new cancer-specific biomarkers that can serve as targets. We show some biomarkers with preliminary preclinical data that may be useful as future CAR targets.

CT antigens

Cancer/testis (CT) antigens have normal expression limited to adult testicular germ cells, but have shown expression in various tumor cells such as ovarian cancer, lung cancer, melanoma, breast cancer, glioma, and colon cancer[361–368]. Because male germ cells are unable to present antigens to T cells, CT antigens can be targeted with minimal cytotoxicity to normal tissue. While current efforts to target CT antigens are primarily focused on modified high specific TCR regions[369], there is an opportunity to target these antigens using CAR T cells as well.

GUCY2C

Guanylyl cyclase C (GUCY2C) is a membrane-bound protein found on the apical surfaces of intestinal epithelial cells, but is also a cancer mucosa antigen that is overexpressed in both primary and metastatic colorectal cancers as well as esophageal and gastric cancers[370–375]. It has been determined that CD8+ T cell responses are expanded when cells are vaccinated against GUCY2C. These cells are effective at eliminating metastatic colorectal tumors[376,377]. Initial GUCY2C targeting with CAR T cells has shown promising specificity and demonstrated reduced tumor number and increased survival in mice with GUCY2C+ tumors. This target shows potential for the possible CAR T cell treatment of colorectal tumors in human patients.

TAG-72

Tumor associated glycoprotein-72 (TAG-72) is a pancarcinoma antigen that shows expression in ovarian cancer[378], colorectal cancer[379], breast cancer[380–382], and prostate cancer[383,384]. While TAG-72 is present in the normal female reproductive tract, the expression is limited and generally weaker than that seen in cancer[385]. While 91% of endometrial adenocarcinoma samples showed TAG-72 expression, the expression of TAG-72 in normal tissue appears to be hormone (estrogen and progesterone) dependent, which can be utilized to prevent expression in normal patient tissue during treatment[386]. As such, TAG-72 may have potential as a possible biomarker for the treatment of some cancer types.

HPRT1/TK1

Salvage enzymes Thymidine Kinase 1 (TK1) and Hypoxanthine guanine phosphoribosyltransferase (HPRT1) have recently shown potential as surface antigens for CAR T cell therapy. HPRT1 is a salvage pathway enzyme that synthesizes guanine and inosine throughout the cell cycle[10]. The protein is a housekeeping protein that is found within all normal

somatic cells in low levels[19]. There is an upregulation of HPRT1 in certain cancer types, making it a promising biomarker for the treatment of these cancers[61,387]. In addition, the protein has also been shown to have significant surface localization on certain malignancies such as lung and colorectal cancer[62,388]. As HPRT1 expression is limited to the cytosol within normal cells, the unique surface localization of the protein makes it promising as a targetable biomarker. TK1 is another salvage enzyme responsible for the synthesis of thymidine in the cell cycle and has been used as a serum biomarker for cancer detection and recurrence[29,32,34,36]. Recently, there has been evidence that shows that TK1 may also be upregulated within some malignancies and displayed on the surface of the cell[389]. As proteins normally restricted intracellularly, TK1 and HPRT could be used as surface antigens for CAR therapy with minimal bystander cytotoxicity.

Conclusions

As CAR T cell therapy expands, so does the search for new biomarker targets for both hematological and solid malignancies. We have provided an analysis of the biomarker targets currently under investigation in clinical trials, in addition to those that may show clinical significance in the future upon further development. Immunotherapy is becoming the new standard in patient care and has experienced huge growth and expansion over the last decade. As CAR T cells become more sophisticated and as new biomarkers are discovered to expand treatment to numerous cancer types, the field of immunotherapy will reach more patients and aid in the improvement of care.

CHAPTER 2

Evaluation of various glyphosate concentrations on DNA damage in human Raji cells and its impact on cytotoxicity

Michelle Townsend, Connor Peck, Matthew Heaton, Richard Robison, and Kim O'Neill

Citation: Michelle Townsend, Connor Peck, Wei Meng, Matthew Heaton, Richard Robison, and Kim O'Neill. Evaluation of various glyphosate concentrations on DNA damage in human Raji cells and its impact on cytotoxicity. Regulatory Toxicology and Pharmacology. 85 (2017) 79-85. DOI: 10.1016/j.yrtph.2017.02.002

The following chapter is taken from an article published in Regulatory Toxicology and Pharmacology. All content and figures have been formatted for this dissertation.

Abstract

Glyphosate is a highly used active compound in agriculturally based pesticides. The literature regarding the toxicity of glyphosate to human cells has been highly inconsistent. We studied the resulting DNA damage and cytotoxicity of various glyphosate concentrations on human cells to evaluate DNA damaging potential. Utilizing human Raji cells, DNA damage was quantified using the comet assay, while cyto- toxicity was further analyzed using MTT viability assays. Several glyphosate concentrations were assessed, ranging from 15 mM to 0.1 mM. We found that glyphosate treatment is lethal to Raji cells at concentrations above 10 mM, yet has no cytotoxic effects at concentrations at or below 100 mM. Treatment concentrations of 1 mM and 5 mM induce statistically significant DNA damage to Raji cells following 30e60 min of treatment, however, cells show a slow recovery from initial damage and cell viability is unaffected after 2 h. At these same concentrations, cells treated with additional compound did not recover and maintained high levels of DNA damage. While the cytotoxicity of glyphosate appears to be minimal for physiologically relevant concentrations, the compound has a definitive cytotoxic nature in human cells at high concentrations. Our data also suggests a mammalian metabolic pathway for the degradation of glyphosate may be present.

Introduction

Since their inception in 1939 by the Swiss chemist Paul Muller, pesticides have become a global phenomenon and a standard approach to pest prevention[390]. The use of pesticides increased exponentially from 196 million pounds in 1960 to 632 million pounds in 1981, and in 2008 an estimated 516 million pounds were being used yearly[391]. It is estimated that if pesticides were banned for a year, the year-ending supplies of corn, wheat, and soybeans would decrease by 73%[392,393]. As a result, the use of these herbicides has become an integral part of the world- wide economy[392].

A critical component in the majority of pesticides and weed killers is the non-selective herbicide glyphosate. This chemical targets the shikimate pathway, which is crucial to the development and growth of plants[394]. Glyphosate interrupts the function of the enzyme 5-enolpyruvylshikimate 3-phosphate synthase, which is responsible for catalyzing the reversible formation of 5-enolpyruvylshikimate 3-phosphate and inorganic phosphate from the organic molecules shikimate 3-phosphate and phosphoenolpyruvate[395,396]. By doing so, glyphosate halts the synthesis of the aromatic amino acids required for protein synthesis, thereby inhibiting plant growth.

Recently, there has been substantial debate regarding the non- toxic nature of glyphosate in humans[397–399]. Glyphosate was labeled as a "probable carcinogen" by the IARC, and various studies have shown it to be cytotoxic at high concentrations[399,400]. These potential side effects are concerning due to glyphosate's extensive agricultural use worldwide.

Despite being a topical treatment, there is evidence that glyphosate is absorbed into the soil and water, which causes great concern for consumer health[401–403]. This concern has led to multiple studies of glyphosate cytotoxicity and carcinogenicity.

In vitro studies have yielded inconsistent results regarding glyphosate's cytotoxic properties. In a study conducted by Gasnier et al., toxicity to HepG2 cells appeared at glyphosate concentrations as low as 5 ppm during a 24 h incubation period, and concentrations of 120 nM induced DNA damage after 24 h exposure[399]. Koller et al. found that in TR146 cell lines, treatment with Roundup induced lower cell viability, while treatment with the active ingredient in Roundup, glyphosate, did not induce any significant change in cell viability[404]. Li et al. found that at concentrations of 15 mM, 25 mM, and 50 mM, glyphosate did not decrease cell viability in epithelial cell lines RWEP-1, pRNA-1-1, and in normal cells[405]. Manas et al. (2009) determined that in Hep-2 cells there was "no statistically significant clastogenic effects quantitatively detected in any glyphosate treatments." The extensive variation among the literature has made it difficult to accurately assess the health risk of glyphosate. Recently in 2015, the International Agency for Research on Cancer (IARC) concluded glyphosate induced significant genotoxic effects for both Glyphosate and its metabolite aminomethylphosphonic acid (AMPA). Although the Expert Panel reviewed the data and concluded glyphosate did not induce oxidative stress characteristic of carcinogenicity, there remains a substantial level of confusion with regards to the 'safe' nature of glyphosate [406]. Due to its high use in agricultural and consumer settings, continued research is important to ensure the protection of individuals exposed to the compound[407,408].

The purpose of this study was to investigate the concentration- dependent nature of glyphosate DNA damaging potential in Burkitt's B Cell Lymphoma (Raji) cells using the comet assay and MTT viability assays[400,409–412]. We treated cells with concentrations of glyphosate ranging from 0.1 mM to 15 mM and measured resulting DNA damage and loss of cell viability after various lengths of exposure. We hypothesized that the discrepancies in past results may be, in part, due to the utilization of different treatment conditions across protocols. The use of a

broad range of concentrations and incubation times allowed us to gain a more complete understanding of glyphosate's cytotoxic and carcinogenic effects in Raji human cells.

Materials and Methods

Chemicals and reagents

Low melting agarose, Glyphosate (95% purity), MTT cell viability assay, and Propidium Iodide were purchased from Sigma-Aldrich, Inc. (Milwaukee, WI). Hydrogen Peroxide and L-glutamine was purchased from Fisher Scientific (Pittsburg, PA). Fetal Bovine Serum was purchased from Hyclone (Logan, UT). RPMI 1640 was purchased from Mediatech, Inc. (Manassas, VA).

Equipment

A Zeiss Axioscope fluorescence microscope was used to image all Comet experiments. TriTek CometScore Freeware v1.5 software was utilized to determine tail moment values.

Cell culture

Burkitt's Lymphoma (Raji) cells (ATCC CCL-86) were obtained from American Type Culture Collection (ATCC) and cultured ac- cording to ATCC recommendations at 37 °C and 5% CO_2. Cells were cultured in RPMI 1640 (Mediatech, Inc. Manassas, VA) and supplemented with 10% FBS and 2 mM L-glutamine (Fisher Scientific, Pittsburg, PA). Media was replaced every 48 h. Cells utilized for experimentation were placed in exponential growth and had a minimum viability of 95% as determined by Trypan blue cell staining. Cells were authenticated by the University of Arizona Genetics Core in May 2016. Raji cells were utilized for this analysis because the replication time is 18 h long and allowed the assays to cover the entire cell cycle.

Compound preparation

Glyphosate was dissolved initially to a 50 mM stock concentration in PBS. This solution was then diluted further to create stocks of 25 mM, 15 mM, and 10 mM. These aliquots were diluted in PBS to the concentrations tested (5 mM, 1 mM, 100 mM, 10 mm, 1 mM, and 0.1 mM). Aliquots were stored in 15 mL conical vials at 4 °C. For use in MTT viability assays, glyphosate was diluted in cell culture RPMI media to the final test concentrations and stored at 4 °C.

Alkaline comet assay

Raji cells were incubated with either hydrogen peroxide, PBS, or glyphosate. The concentration and time points varied depending on the experimental run. Time intervals tested included 10, 20, 30, 40, 50, 60, 75, 90, 105, and 120 min. Concentrations of 0.1 mM, 1 mM, 10 mM, 100 mM, 1 mM, 5 mM, 10 mM, and 15 mM were tested at each of the time points. Cells were suspended at a concentration of 200,000 cells per 100 mL treatment. Once treated, cells were washed twice in 4 °C PBS, and then suspended at 200,000 cells per 100 mL of PBS. The cells were then prepared for the comet assay. Glyphosate treatment was conducted at 37 °C in a water bath.

Samples were prepared for comet analysis by following the methods described by Xiao et al. (2014). with slight modifications. In brief, samples were mixed with low melting point agarose and layered on double frosted microscope slides [413]. The slides were placed in alkaline lysis buffer for 60 min, rinsed with ddH_2O and then placed in alkaline electrophoresis buffer for 20 min. They were then electrophoresed for 30 min at 24 V and 400 mA. Following electrophoresis, slides were allowed to rest in ddH_2O for 15 min, then fixed in 20 °C 100% ethanol for 5 min and allowed to dry overnight. Slides were then stained with propidium iodide for 15 min, rinsed with ddH_2O, and imaged. All comets were scored using TriTek CometScore Freeware v1.5. Every experimental run tested a single concentration for multiple time points.

Each time point contained a minimum of two slides as replicas. Approximately 50 comets were analyzed per slide, totaling 100 comets per time point per treatment concentration. Each concentration was replicated multiple times in order to ensure consistency. Comet Assay results are reported in terms of tail moment. Tail moment is defined as the product of the tail length and the percentage of DNA in the tail. These values are given as part of the output by the CometScore software and are widely reported for Comet analysis (Olive et al., 1990).

A similar protocol was utilized to test the effects of secondary glyphosate exposure at 1 mM and 5 mM concentrations. In these experiments, 200 mL additional glyphosate was added to the cells after 60 min of initial treatment, while 200 mL of PBS was added to the negative control.

Cell viability assay

Samples were prepared for the MTT cell viability assay by the methods described by Hamid et al. (2004). with slight modifications. Glyphosate treatments were diluted in Raji cell growth media to their final test concentrations. Raji cells were incubated in this prepared growth media for 24 h in a 96-well plate at 37 °C and 5% CO_2. The 24 h time period was chosen because Raji cells divide every 18 h, which ensures the entire cell cycle was taken into account. After incubation, 10 mL of kit provided MTT reagent at a concentration of 5 mg/mL was added to each well. Following 3 h of incubation, 100 mL of DMSO detergent was added to each well. The plate was then incubated on a shaker at 4 °C for 2 h and evaluated at a 570 nm absorbance.

Statistical analysis

Relationships between exposure time and tail moment were modeled statistically using a natural spline to account for nonlinearity (Parang et al., 2000). The number of knots was selected based on Akaike Information Criteria (AIC) and parameters were estimated using least squares. P-Values <0.05 were considered statistically significant.

Results

Cell death at high concentrations of glyphosate

Glyphosate rapidly induced DNA damage and cell death in Raji cells following treatment at concentrations of 10 mM and 15 mM after only 30 min of treatment. Cells exposed at these concentrations quickly adopted an apoptotic profile characterized by the lack of a clear head and the appearance of a long, rounded tail, as shown in Fig. 2-1. Tail moments were significant after just 10 min of glyphosate exposure. After 30 min, the damage was so extensive that comet analysis was unfeasible due to software restraints.

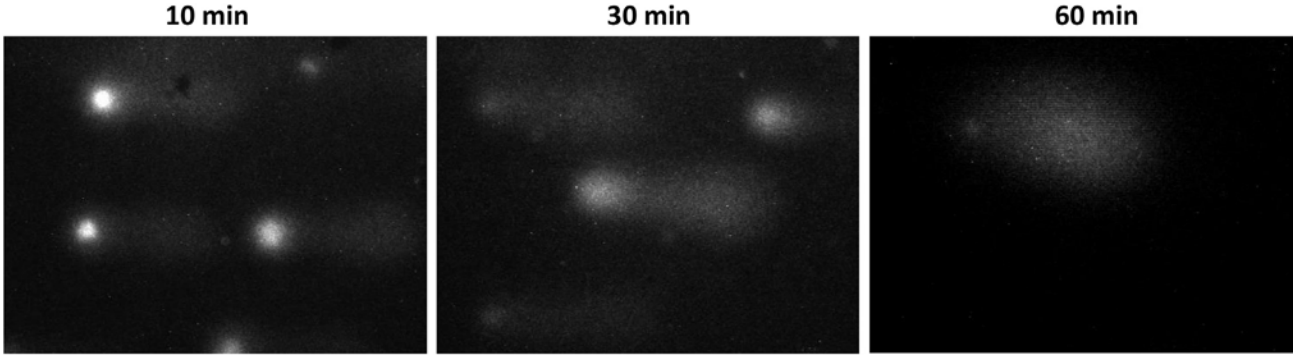

Figure 2-1. *Comet assay analysis of Raji cells exposed to 10 mM glyphosate.* Cells at 10 mM and 15 mM concentrations underwent severe DNA damage and cell death soon after exposure. Dead cells were characterized by a loss of a defined comet head and a large, fragmented DNA tail. The extensive amount of damage at later time points made analysis impractical due to software restraints.

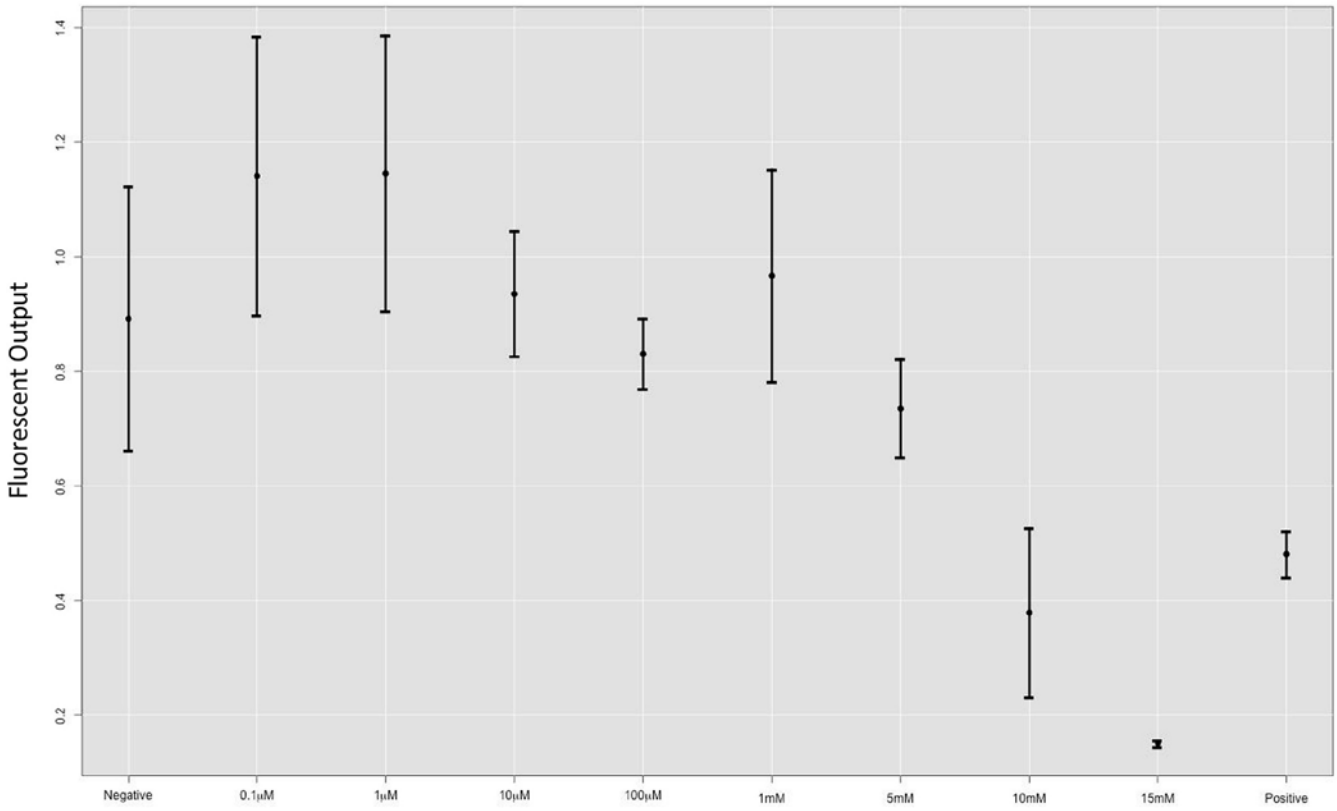

Figure 2- 2. *MTT analysis of Raji cells exposed to various glyphosate concentrations.* Hydrogen Peroxide (positive) was utilized as a control to measure thorough cell death, and cells suspended in cell growth media (negative) was utilized as a control for standard cell death as a result of treatment conditions. Following 24 h of incubation with glyphosate, there was a significant loss of cell viability following treatment with 10 mM and 15 mM glyphosate. Concentrations of 5 mM and lower did not have a significant loss of viability when compared to the negative control. This indicates the damage to Raji cells at 15 mM and 10 mM glyphosate was enough to sustain complete cell death, while concentrations at or below 5 mM sustained cell viability.

To confirm that cell death had occurred, cell viability was quantified using MTT viability assays. Results, shown in Fig. 2-2, indicate a significant loss of cell viability after 24 h treatments with 10 mM and 15 mM concentrations of glyphosate. A comparison shown in Fig. 2-4 outlines the difference in appearance of cells that maintain viability to those who undertake severe DNA damage characteristic of cell death.

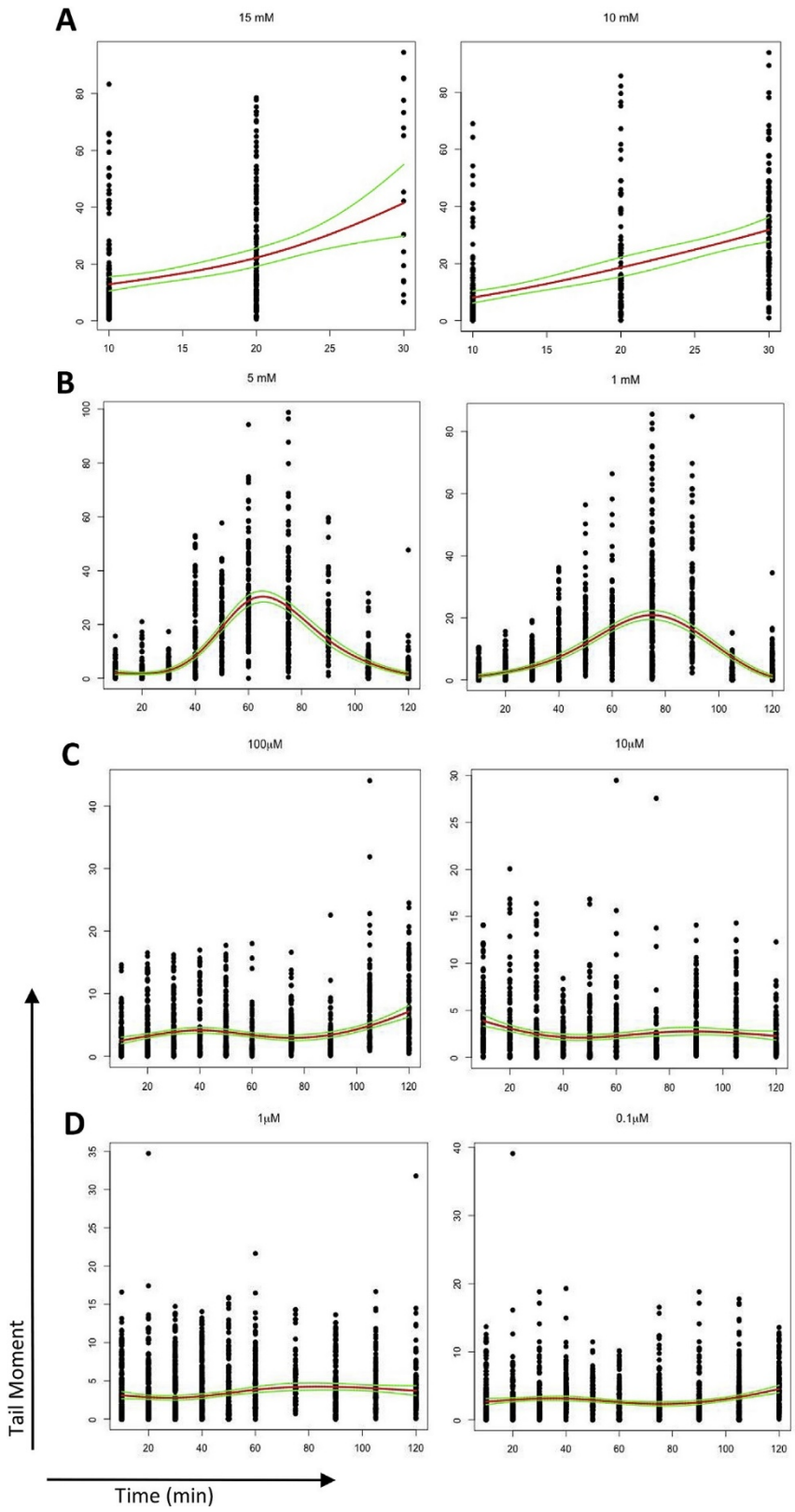

Figure 2-3. *Tail moment values of cells treated with various concentrations of glyphosate across 2 h of treatment.* Tail moment values (quantifiable measure of DNA damage) are listed on the y-axis (scale varies at different concentrations), and treatment times are labeled on the x-axis. Each concentration was individually evaluated and assigned a 95% confidence interval, which is displayed in green, while the mean value is shown in red. A, Cells exposed to glyphosate concentrations of 15 mM and 10 mM sustained severe DNA damage with tail moments above 25, which was indicative of cell death. Within 30 min of treatment, all cells had adopted the characteristic profile of a dead cell (Fig. 2-1). B, Raji cells exposed to glyphosate concentrations of 5 mM and 1 mM had statistically significant DNA damage after 60e75 min of treatment. This damage was not present in later time points and cells were able to recover full viability after 120 min of treatment. C, Cells treated with 100 mM and 10 mM of glyphosate did not show statistically significant DNA damage, and cells retained full viability throughout the full 120-min treatment. D, Physiologically relevant concentrations of glyphosate were exposed to Raji cells over a 120 min period and did not experience any significant DNA damage.

Minimal cytotoxicity at low, physiologically relevant concentrations of glyphosate

For concentrations of glyphosate at or below 100 mM, tail mo- ments were not statistically significant at any time point as shown in Fig. 2-3. MTT analysis in Fig. 2-2 likewise showed no decrease of cell viability following glyphosate treatment at these concentrations. These findings indicate a lack of cytotoxicity to Raji cells at low treatment concentrations, suggesting that the risk of glyphosate exposure at standard physiological levels may be negligible.

DNA damage and cellular recovery at 1 mM and 5 mM concentrations

Cells exposed to 1 mM and 5 mM concentrations of glyphosate had significant tail moments after 40 min of glyphosate incubation. Tail moments reached a maximum following 60 min and 80 min of treatment for 5 mM and 1 mM concentrations of glyphosate, respectively. Interestingly, as shown in Fig. 2-3, a steady decrease in tail moment was observed in later time points and after 2 h of treatment, the DNA damage was no longer significant.

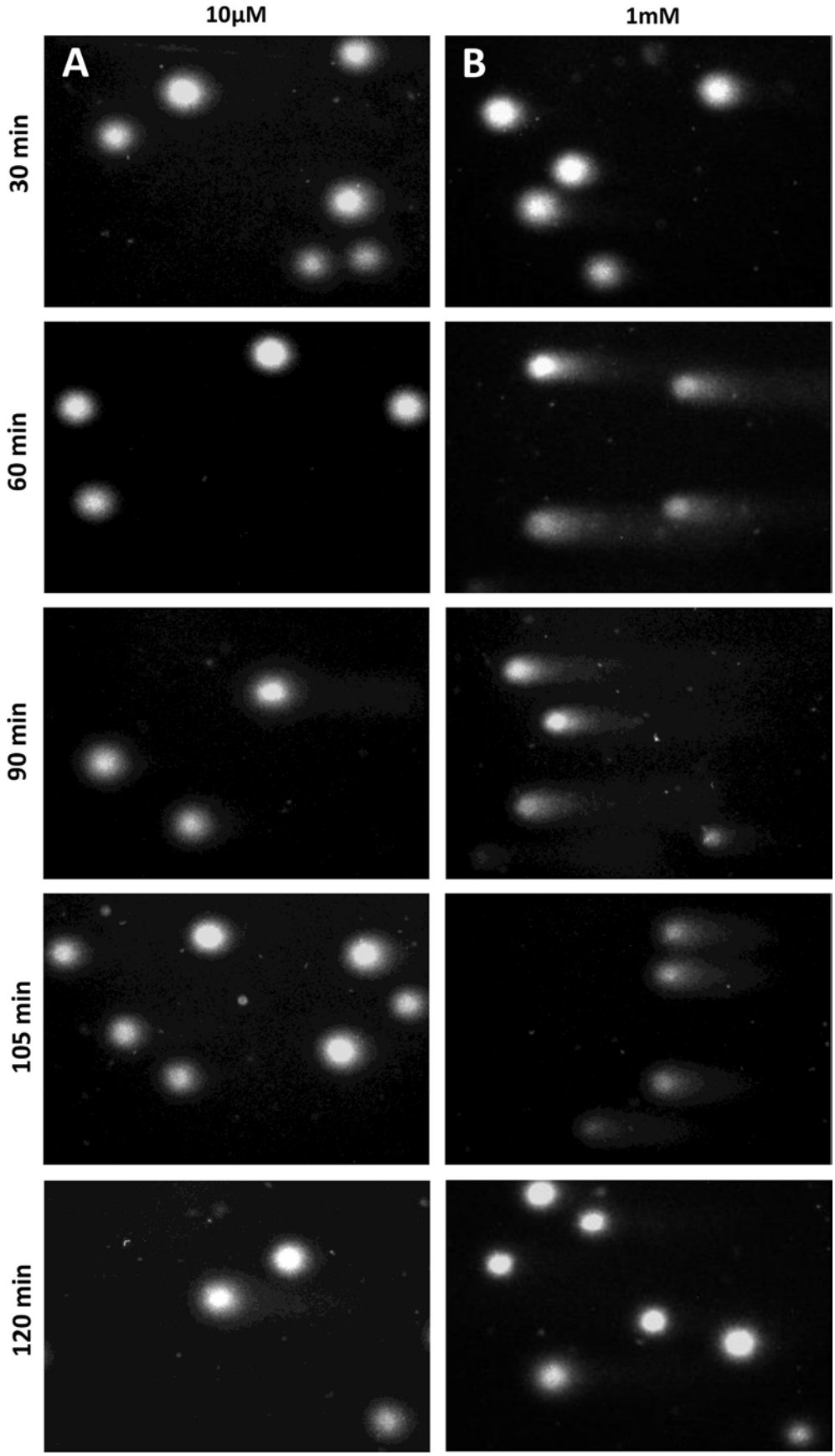

Figure 2-4. *Raji cells treated with 1 mM and10 mM glyphosate concentrations experience different damaging events.* A, Following treatment with 10 mM glyphosate, Raji cells showed no signs of DNA damage and the 'head' of the cells stayed intact throughout the 2 h treatment time. B, After exposure to 1 mM glyphosate, cells started to show signs of damage after 60 min of treatment that subsided after 2 h. At the end of the 2 h incubation, cells were fully viable with no signs of severe DNA damage.

The decrease in tail moment may suggest that the induced DNA damage was insufficient to trigger cell death, and that cells were able to recover from the damaging event. MTT analysis supported this hypothesis, showing no significant loss of cell viability after 24 h incubations at either concentration.

In order to further elucidate the comet analysis results at 1 mM and 5 mM, cells were treated again with glyphosate at these concentrations 1 h after initial treatment. There was a significant difference between cells receiving only primary treatment and cells receiving the additional treatment (Fig. 2-5). Raji cells exposed to the compound twice did not show the same pattern of recovery, with tail moments reaching levels above 20 for 1 mM and 25 for 5 mM glyphosate treatment. Meanwhile, cells with only primary expo- sure to the compound showed a decrease in DNA damage, with tail moments dropping from 15 to 5.8 for 1 mM and 23.67 to 6.74 for 5 mM treatments of glyphosate.

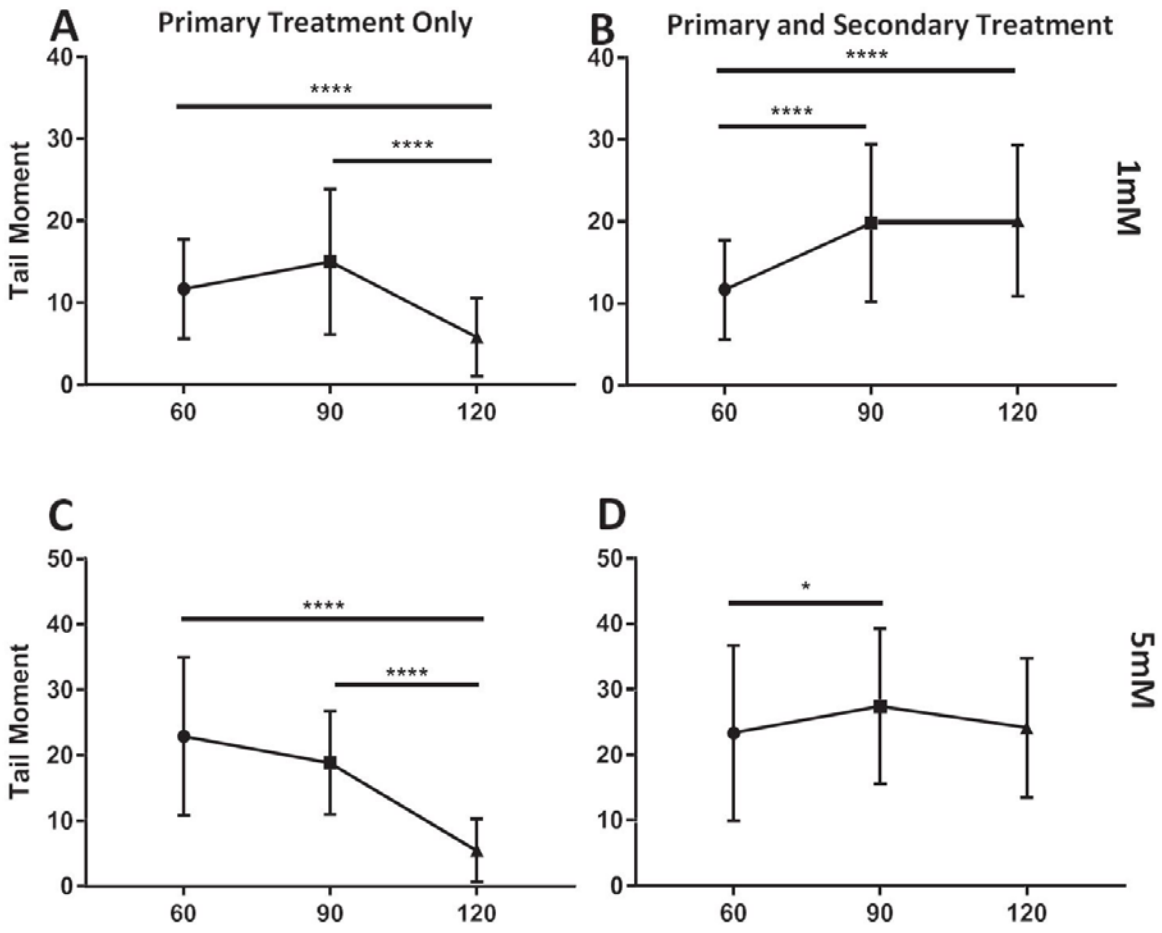

Figure 2-5. Tail moments of Raji cells incubated with 1 mM and 5 mM glyphosate concentrations after primary and secondary exposure to the compound. A, Raji cells were evaluated after initial treatment with 1 mM glyphosate. Following the same pattern as previously reported, the cells underwent a damaging event (tail moment 15.01) that was later recovered. At the end of the 2 h incubation, cells had gained viability and maintained a low tail moment value of 5.82. B, Raji cells receiving both primary and secondary treatment of 1 mM glyphosate did not experience the same recovery as those only treated with primary glyphosate. At 60 min, Raji cells were again incubated with 1 mM glyphosate. Tail moments in this case were increased slightly and do not show the same decrease as primary only treated cells and maintained high tail moment values above 20. C, Cells treated with primary 5 mM glyphosate only showed a pattern of recovery in cell viability with tail moments dropping from 23.67 to 6.74. D, When Raji cells were incubated with 5 mM glyphosate primary and secondary treatment, there was no recovery observed and the tail moment increased from 23.67 to 28.03. These data suggest that after primary treatment, Raji cells may be metabolizing the compound and breaking it down to its less toxic metabolites.

Discussion

These results show that the DNA damaging and cytotoxic potential of glyphosate is related to exposure length and treatment concentration, suggesting a dose-dependent relationship for glyphosate's cytotoxic effects. These data show that glyphosate induced significant DNA damage only when cells are exposed to concentrations several orders of magnitude larger than those attainable *in vivo*. Our data support the established evidence that glyphosate is "not genotoxic" in human cells at physiologically relevant concentrations[414]. While these data ultimately support glyphosate's classification as a potential carcinogen, they suggest that its effects are negligible when exposure is minimal. Our results do implicate the need for further studies of the physiological uptake and bioavailability of glyphosate for agricultural workers, who may be subject to extended exposure and are thus at higher risk. Further- more, our studies at 1 mM and 5 mM suggest that cells initially damaged by glyphosate may have the ability to repair and regain viability if repeated exposure is not experienced.

Another important consideration obtained from this study is the utility of multiple time points in the comet assay. This aspect of the experimental design allowed for accurate assessment of the DNA- damaging event that took place. Our results show that incubation times used in the comet assay can affect results dramatically; the extent of DNA damage changed drastically across different incubation time points. The 1 mM concentration at 1 h, for example, showed that severe DNA damage occurred. Yet, at 2 h with the same treatment, no DNA damage was evident. If cells had only been evaluated at this time, results would suggest that there was no cytotoxic activity and the initial DNA damaging event would be missed. Cytotoxic activity might also be underestimated by standard viability assay in which the DNA damage is insufficient to induce cell death. Because of our analysis across multiple time points, we were able to observe both the DNA damaging event as well as the ensuing recovery. We recommend that in future

utilizations of the comet assay or related assays measuring mutagenic or clastogenic events, incubation times be considered and evaluated.

Conclusion

Human cell exposure to glyphosate has minimal cytotoxicity and DNA damage at concentrations at or below 100 mM.

CHAPTER 3

Metastatic colon adenocarcinoma has a significantly elevated expression of IL-10 compared to primary colon adenocarcinoma tumors

Michelle H. Townsend, Abigail M. Felsted, Stephen R. Piccolo, Richard A. Robison, and Kim L. O'Neill

Citation: Michelle H. Townsend, Abigail M. Felsted, Stephen R. Piccolo, Richard A. Robison, and Kim L. O'Neill. Metastatic colon adenocarcinoma has a significantly elevated expression of IL-10 compared to primary colon adenocarcinoma tumors. Cancer Biology & Therapy. 2017. DOI: 10.1080/15384047.2017.1360453

The following chapter is taken from an article published in Cancer Biology and Therapy. All content and figures have been formatted for this dissertation.

Abstract

Classical anti-inflammatory cytokines are known to play a role in both cancer progression as well as cancer elimination. We evaluated the anti-inflammatory cytokines IL-10 and TGF-β in patients with colon adenocarcinoma and metastatic colon adenocarcinoma utilizing immunohistochemical assays to determine the expression of the cytokines between various malignant tissues. We found tissues stained with TGF-β showed no significant upregulation within malignant tumors when compared to normal tissue controls. We observed high levels of TGF-β presence in most tissues similar to GAPDH expression. Within both colon adenocarcinoma and metastatic carcinomas there was a significant variability among patients in the expression of IL-10. While some patients experienced insignificant increases in the cytokine compared to controls, other patients had a clear upregulation of the protein within their tissue. In addition, there was an increase in the number of patients positive for IL-10 upregulation within metastatic tumors when compared to primary tumors. These data indicate that there is substantial variability between patients in regards to IL-10 expression, which may further aid in characterizing tumors and evaluating metastatic potential.

Introduction

Globally, colorectal cancer (CRC) is the third most prevalent cancer and comprises approximately 10% of diagnosed cancers [415]. The majority of individuals at high risk for CRC development are over 50 years of age, as incidence rates increase 50 fold in patients ages 60-79 when compared to patients younger than 40 [416]. While there has been noteworthy improvements in early screening and combinatorial treatment development, in the United States 49,190 individuals died of the disease in 2016 [417]. As colon cancer grows, mutates, and evolves within patients, it is important to understand the unique environment surrounding tumor growth and development, and its ability to evade immune detection [418,419].

As the primary form of communication between cells, cytokines have a powerful impact on regulating both proliferation and immune responses in the tumor microenvironment [420,421]. Cytokine profiles can induce anti-tumor responses, which often lead to a favorable prognosis, but can also result in supporting malignancy in conditions of chronic inflammation [422]. These cytokine profiles are assessed by measuring the concentration of both pro- and anti-inflammatory cytokines and evaluating their expression within malignant cells [423]. Cytokines within the tumor microenvironment are produced by both cancer cells and immune cells that are recruited to the malignant site [424]. Tumors will often skew cytokine profiles to support growth and proliferation by influencing surrounding cells to secrete potent pro-inflammatory cytokines such as TNF-α, IL-8, IL-6, and IL-1β [424–426]. Cancer cells rely on a pro-inflammatory environment to activate signaling pathways, such as NF-κB and Ap-1, responsible for supporting cell survival [426]. In order to combat this, several anti-inflammatory drugs have been tested for efficacy in preventing or treating CRC, such as nonsteroidal anti-inflammatory drugs (NSAIDs), to reduce inflammation at the tumor site [424–427].

Known to be widely expressed within a majority of somatic tissue, transforming growth factor beta (TGF-β) is a cytokine known for its induction of peripheral tolerance and anti-inflammatory responses. TGF-β is shown to have a tumor suppressive role within cancers, as it functions to inhibit cell proliferation, induce apoptosis, and inhibit cell immortalization [428]. Yet, as cancer progresses within some patients, there is an increase in TGF-β levels which leads to the inhibition of cell adhesion and promotion of angiogenesis, supporting immunosuppression in the tumor microenvironment, and the degradation of the extracellular matrix [428,429]. These factors contribute to the success of a tumor to metastasize [430]. As a result, TGF-β has been implicated as a factor involved in promoting metastasis. To further clarify the role of TGF-β in colon adenocarcinoma we investigated its levels within primary tumors and metastatic tumors to determine whether cancer had an increased ability to metastasize when TGF-β was highly expressed.

Interleukin-10 (IL-10) is a potent anti-inflammatory cytokine secreted primarily from Th2 cells. While inhibiting antigen presenting cells, IL-10 is also responsible for suppressing the production of pro-inflammatory cytokines [420]. It has been shown that upon transferring the IL-10 gene into tumors, there was an observed decrease in metastatic ability and an increase in protective immunity against the tumor [431–433]. Yet, other sources claim that secreting IL-10 promotes the suppression of antitumor immune responses and protects the tumor against immune attack within CRC cells [432]. These conflicting results exemplify the pleiotropic nature of IL-10, especially within the tumor microenvironment, and the alternative roles it can play within cancer progression.

While there has been extensive investigation into the nature of pro-inflammatory cytokines within tumor tissue, the expression of these anti-inflammatory cytokines within CRC tumors is not as well characterized. Specifically, there remains a need to determine anti-

inflammatory cytokine production within metastatic CRC tumors to evaluate whether cells undergo transcriptional changes in cytokine gene expression when relocating to an alternative environment within the body. The purpose of this study is to evaluate both IL-10 and TGF-β expression within CRC patients with both colon adenocarcinoma as well as metastatic colon adenocarcinoma to investigate variability of these anti-inflammatory cytokines within CRC tumors.

Results

IL-10 has a significant upregulation in 20% of patients with colon adenocarcinoma

When tissues were stained for IL-10, there was a significant upregulation of the cytokine that occurred within a fifth of the patients when compared to normal controls (Fig 3-1). To aid in distinguishing this variability, tissues were separated into 'Adenocarcinoma IL-10 Low', representing patients with insignificant IL-10 expression, and 'Adenocarcinoma IL-10 High', representing patients with significant IL-10 expression (Fig 3-2). On average, the gray staining intensity of IL-10 in Adenocarcinoma IL-10 Low patients was 125.51, while the average staining intensity in Adenocarcinoma IL-10 High patients was 111.46 (Fig 3-1A). As lower gray values indicated more antigen binding, this difference was statistically significant ($p<0.0001$) and

showed that there was a clear divide among patients in regards to the presence of IL-10 within their tumors.

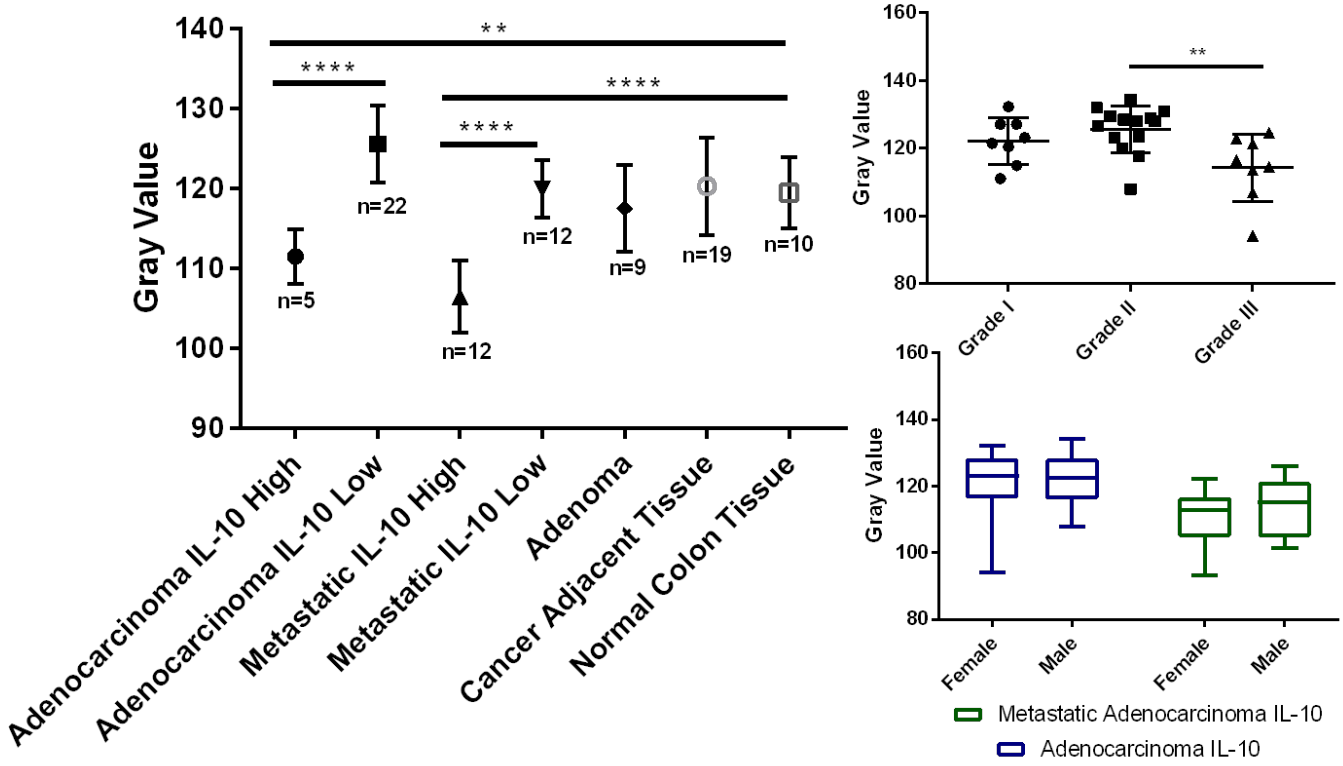

Figure 3-1. *Statistical analysis of IL-10 expression within colon cancer tissue*. (A) Expression of IL-10 within all tissue types shows statistically significant increases in the cytokine within cancer tissue when compared to controls. 'Adenocarcinoma IL-10 High' tissue indicates tissues who had significant Il-10 expression and 'Adenocarcinoma IL-10 Low' tissue indicates tissue who had insignificant IL-10 expression. This same nomenclature is applied to the metastatic tissues. (B) All tissues [Adenocarcinoma IL-10 Low and Adenocarcinoma Il-10 High] were combined to determine the overall IL-10 expression within cancer grades. Overall, IL-10 expression had a significant increase in expression in Grade III tissue. (C) We found no statistically significant changes in IL-10 production between genders.

Further analysis revealed there was a significant increase (p=0.0049) in IL-10 expression within Grade III tumors when compared to Grade II tumors (Fig 3-1B). These data indicate IL-10 expression may be linked to the differentiation of the cancer cell, as cells that are poorly differentiated have an increased expression of IL-10. We also evaluated the differences between

sexes and found no statistically significant (p =0.8778) relationship between IL-10 production and sex (Fig 3-1C).

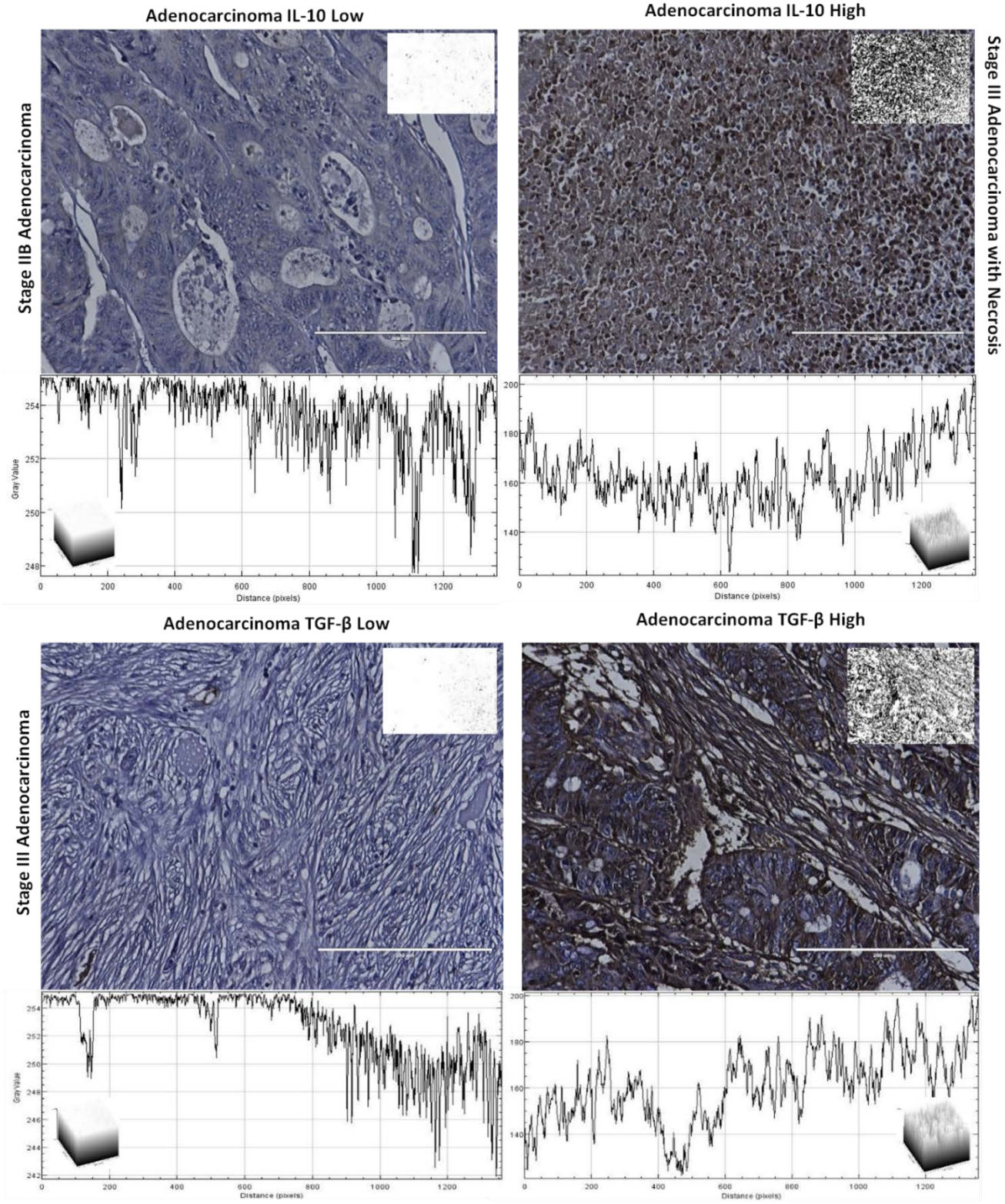

Figure 3-2. *IL-10 and TGF-β staining of colon adenocarcinoma tissue.* Each tissue is displayed with the gray scale image, with an applied threshold, in the top right corner of the image. Below each image is the intensity map of the tissue with the gray values on the Y-axis. Within each of the intensity maps is a graphical representation of the level of gray staining. The scale bar indicates a magnification of 200. (A) Tissue from a 66-year-old female with Stage IIB colon adenocarcinoma who showed minimal levels of IL-10 expression characteristic of approximately 80% of patients. (B) Tissue from a 78-year-old female with stage III adenocarcinoma who experienced a significant upregulation of IL-10 within her tumor, which was characteristic of approximately 20% of the patients. (C) Tissue from a 64-year old male with stage III adenocarcinoma. This individual was rare among the samples analyzed as he had no visible staining of TGF-β. (D) Tissue from a 71-year old male with stage IIB adenocarcinoma, who had significant levels of TGF-β characteristic of only 13% of the tissues.

Patients with metastatic colorectal adenocarcinoma have an increased proportion of IL-10 upregulation

As with colon adenocarcinomas, metastatic cancer samples had a similar divide between patients that experienced a significant expression of IL-10 and those that did not. This difference between patients was skewed in the opposite direction of colon adenocarcinoma tissue: instead of having a majority of patients with no significant IL-10 expression, a majority of metastatic samples were positive for IL-10. While 20% of patients with colon adenocarcinoma were positive for expression, 53% of patients with metastatic adenocarcinoma had elevated levels of IL-10 (Fig 3-3B). These results indicate that IL-10 may be an important factor contributing to metastasis and the ability of a metastatic cell to survive.

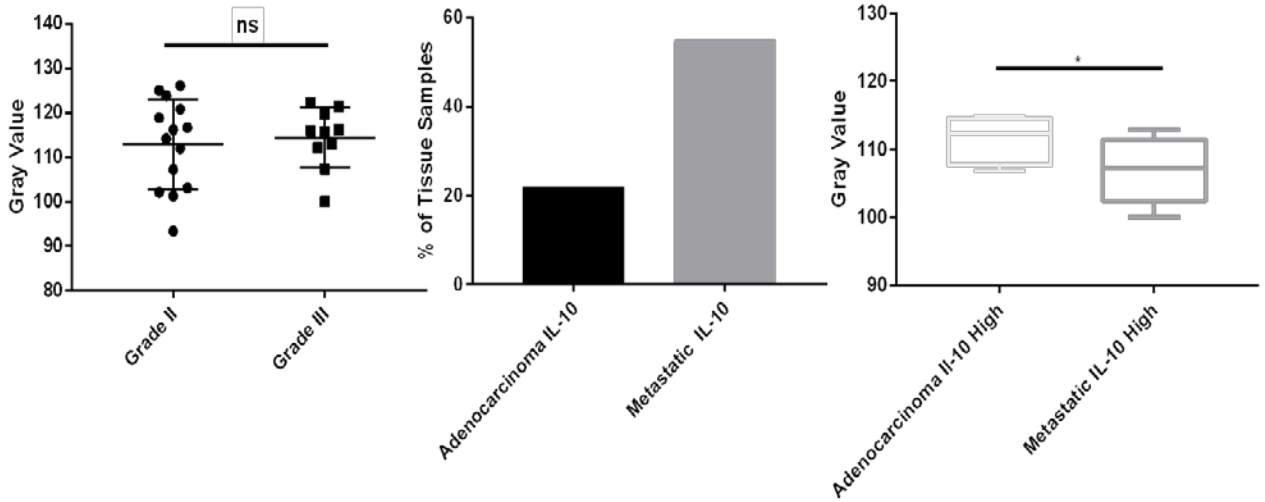

Figure 3-3. *Statistical analysis of IL-10 expression within metastatic adenocarcinoma*. (A) Within metastatic tissue there was no statistically significant increase in IL-10 presence with changes in grade. (B) While there were positive tissues within both adenocarcinoma and metastatic adenocarcinoma, patients with metastatic adenocarcinoma had a more prevalent presence of IL-10. (C) Along with an increase in the amount of patients with elevated IL-10 expression, the average stain intensity of patients with metastatic adenocarcinoma was significantly higher than patients with primary adenocarcinoma.

Tissue samples were similarly split into 'Metastatic IL-10 Low' and 'Metastatic IL-10 High' samples (Fig 3-4). The average staining intensity of Metastatic IL-10 Low samples was 119.95, while the average staining of Metastatic IL-10 High samples was 106.42 (Fig 3-1A). This difference was statistically significant ($p<0.0001$) and indicates a clear divide between patients regarding IL-10 production, as lower values indicate more IL-10 within the tissue. In addition, the average intensity of Metastatic IL-10 High samples was significantly darker than Adenocarcinoma IL-10 High ($p=0.027$), indicating a higher expression of IL-10 within metastatic malignant cells (Fig 3-3C).

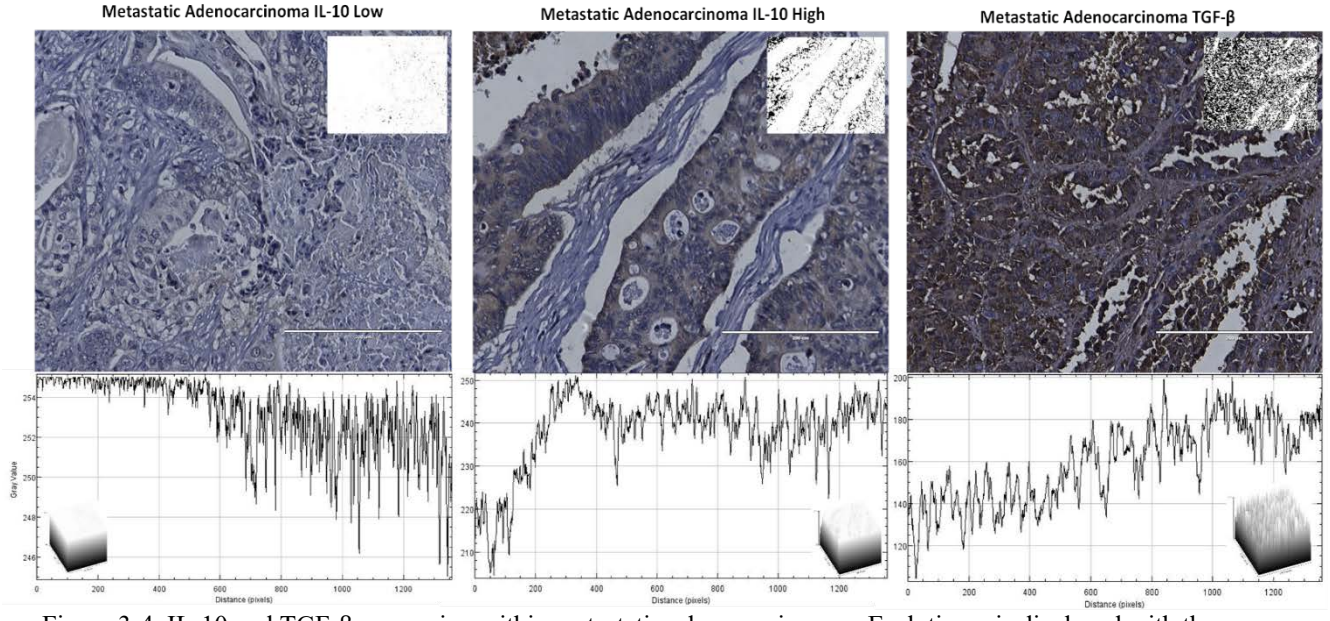

Figure 3-4. IL-10 and TGF-β expression within metastatic adenocarcinomas. Each tissue is displayed with the gray scale image, with an applied threshold, in the top right corner of the image. Below each image is the intensity map of the tissue with the gray values on the Y-axis. Within each of the intensity maps is a graphical representation of the level of gray staining. The scale bar indicates a magnification of 200. (A) Tissue from a 43-year-old male with grade 2 metastatic adenocarcinoma from the colon had minimal levels of IL-10 expression representative of 44% of

patients. (B) Tissue from a 51-year-old female with metastatic adenocarcinoma who had significantly upregulated expression of IL-10 representative of 55% of tissue evaluated. (C) Tissue from a 58-year-old male with metastatic adenocarcinoma stained with TGF-β. All metastatic tissues exhibited this same level of TGF-β staining. This level of staining was consistent through all of the tissue types.

While there was a statistically significant difference within colon adenocarcinoma samples in regards to grade, there was no statistically significant change in IL-10 expression within metastatic adenocarcinomas when considering grade (Fig 3-3A). As metastatic tumors are very commonly poorly differentiated, we expected to see no clear divide between any determined grades.

To determine whether the observed IL-10 increase in metastatic tumors was also seen within individual patients upon metastasis we examined a small cohort (n = 13) of individuals with expression data from both primary tumor sites and matching metastatic tumor sites. Within this small cohort there was no statistically significant difference in overall IL-10 expression between primary tumors and metastatic tumors. However, one patient had a significantly elevated expression of IL-10 within their metastatic tumor when compared to their primary tumor (Fig 3-5B). Additionally, we analyzed IL-10 expression data in a larger set of metastatic tumors to determine the general distribution of the cytokine within metastasis. We found that there were generally low levels of the cytokine as observed within tissue. However, the expression profile showed a right skewed pattern with a small fraction of patients showing considerably highly elevation of IL-10, and several other patients who had a general upregulation (Fig 3-5A). For patients who experience this upregulation, it may be beneficial to target IL-10 to reduce metastatic potential.

TGF-β expression is generally consistent throughout all patient tissue

While IL-10 showed variable expression within tumors when compared to normal controls, there was no significant changes in expression within tissue stained for TGF-β. Four

patients experienced very low levels of TGF-β uncharacteristic of any other tissue samples (Fig 3-5B & 3-2C). These patients had an average staining intensity of 110.95, which is significant ($p<0.0001$) when compared to both cancerous tissue and normal tissue, which had an average staining intensity of 87.82 (Fig 3-5A). These patients represented a fraction of the samples, and the unusual lack of expression may be used as an additional tool for characterizing individual tumors and mutations within patients.

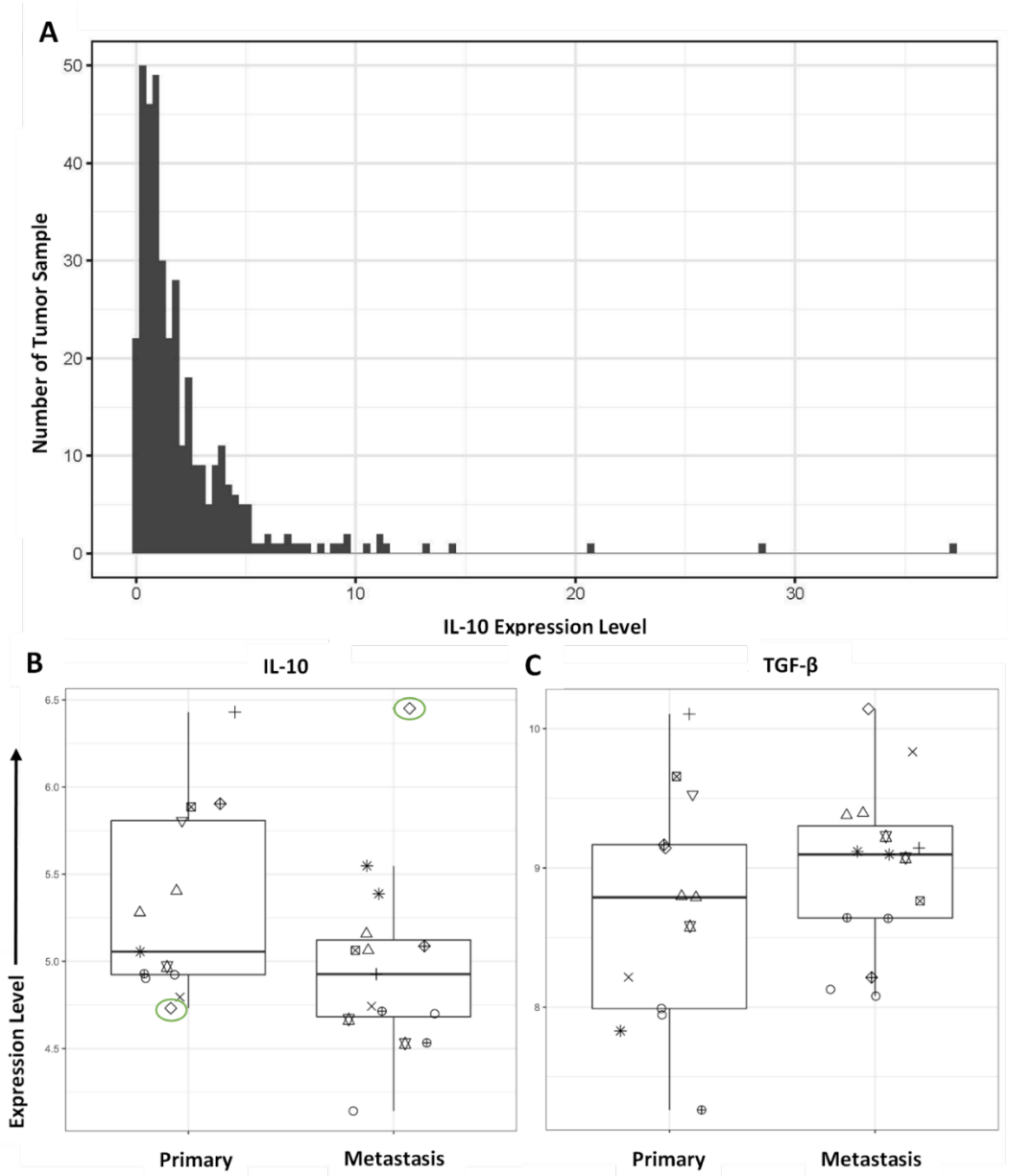

Figure 3-5. *IL-10 and TGF-β expression profiles in patients from TCGA.* (A) 396 metastatic tumors were analyzed for IL-10 expression. The number of patients is plotted against the Expression profile in transcripts per million. (B) IL-10 expression within primary and metastatic tumors was plotted to show differences within the same individual.

On patient experienced significantly elevated IL-10 and is shown in green. This same cohort was utilized to also evaluate (C) TGF-β expression between primary and metastatic tumors.

The expression of TGF-β did not experience any changes in staining intensity between metastatic adenocarcinomas or colon adenocarcinomas. (Fig 3-2D & 3-4C) In addition, while analyzing a small cohort of patients with both primary tumor and metastatic tumor samples, there was no statistically significant difference between the two sites in regards to TGF-β expression (Figure 3-5C).

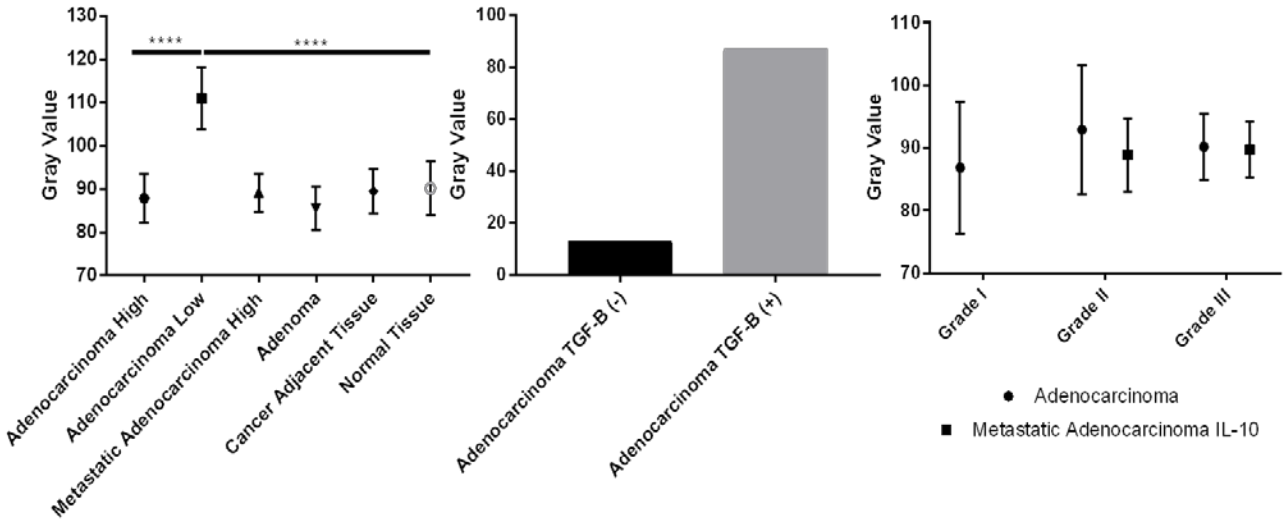

Figure 3-6. *Statistical analysis of TGF-β expression within colon cancer tissue*. (A) TGF-β showed a consistent level of expression across all tissue types, including normal tissue, with the exception of 4 patients who had insignificant levels of TGF-β expression. (B) Number of patients with positive expression of TGF-β and negative levels of TGF-β. There was a small proportion of patients that had no TGF-β expression. (C) There was no significant difference in TGF-β expression between tissue grades in colon adenocarcinoma samples or metastatic adenocarcinoma samples.

Discussion

These results show that immunosuppressive cytokine levels of IL-10 have variable expression within different colon adenocarcinoma tumors and may provide insights into the strategies tumors utilize in order to avoid immune detection. Both anti-inflammatory cytokines as well as pro-inflammatory cytokines are known to be involved in contributing to positive and negative patient outcome and help to establish the complexity of the tumor microenvironment.

The complexity of the tumor microenvironment is supported by the cytokines secreted within the tumor site and is often protective for cancer cells and provides an atmosphere optimal for cancer cell growth. This supportive environment is no longer present as individual metastatic cancer cells break off from the primary tumor to invade other tissue. Instead of being nurtured by a very well organized, structured tumor site, metastatic cells are faced with several challenges where they often have to alter gene expression in order to survive.

A critical target for IL-10 is the inhibition of antigen presenting cells. IL-10 functions to down-regulated MHC expression and co-stimulatory molecules critical for the activation of effector T cells [434–436]. In addition, IL-10 contributes to the expression of Foxp3 and TGF-β, which sustain Treg populations [434,437]. Tregs are influential in the success of a tumor to metastasize as they aid in tumor cell survival within the circulation. Because cancer cells are escaping from a well-established environment, a vast majority of cells released do not successfully establish metastatic sites. Those cells that successfully avoid destruction within circulation make changes to the transcriptional control of genes to promote an environment that supports immune evasion [438]. These transcriptional changes often involve increasing levels of IL-10 in order to elevate the number of Tregs within the surrounding environment. By increasing Treg differentiation, metastatic cells can increase their chance of survival when breaking away from the primary tumor. Our results show that within metastatic tumors there is a significant increase in the number of patients with elevated IL-10 when compared to primary tumors. This indicates that IL-10 may play a role in promoting metastasis and controlling the immune environment to support metastatic tumor cell escape.

Within the primary tumor site, IL-10 production can both support and interfere with cancer cell survival, which may explain why the levels of IL-10 are so variable between CRC patients. IL-10 can function to stimulate the immune system by increasing the frequency of

cytotoxic CD8+ T cells and natural killer cells depending on the other cytokines present within the tumor microenvironment (IL-2 for T cell activation and IL-19 for Natural killer cell activation) [439,440]. The anti-tumor effects of IL-10 are also demonstrated as IL-10 modifies and efficiently regulates the quality of antigen presentation [434]. The effects of IL-10 within the primary tumor are modulated by the surrounding cytokine profile and expression of the protein can provide insights into approaches the tumor takes to skew the immune response to either anti-inflammatory or pro-inflammatory.

We did not find a significant increase in TGF-β when comparing metastatic tumors to endogenous tumors. Our results show that the levels of TGF-β do not vary significantly between normal colon tissue and malignant colon tissue, indicating its role within cellular maintenance is essential for all tissue. Yet, we did observe tissue from 4 patients with insignificant levels of TGF-β which may provide physicians with a targeted treatment for those individuals who lack the protein, as this phenomenon was only experienced within patients with malignant tissue.

Classical anti-inflammatory cytokines exhibit complex effects on tumor growth and development. The presence of these cytokines within malignant tissue can provide key insights into strategies elicited by the tumor to promote growth. Within each individual patient there is a unique cytokine profile which determines the microenvironment surrounding the tumor and the strategies tumors utilize in order to survive and adapt. We have shown that IL-10 is extremely variable among patients and could provide physicians with additional tools for characterizing individual patient tumors.

While this study examines IL-10 and TGF-β levels within a small cohort of individuals, there is need for an analysis within an extrinsic dataset with more patients. Further investigation will need to be conducted in the future to determine the source of IL-10 and TGF-β within these tumors. Understanding the composition of cells that secrete these cytokines will provide

additional insights into ways to potentially reduce their expression within the tumor microenvironment.

Materials and Methods

Chemicals

DIVA antigen retrieval solution, Background Sniper blocking agent, Universal negative, Mach 4 HRP antibodies, DAB Peroxidase, and Hematoxylin were all purchased from Biocare Medical. IL-10 and TGF-β antibodies were purchased from Thermo Fisher Scientific. GAPDH polyclonal antibody was purchased from cell signaling.

Patients

Colorectal Adenocarcinoma Tissue Microarrays were obtained from Biomax. Each microarray contains 30 cases of colon adenocarcinoma (grade 1-3), 30 cases of Metastatic adenocarcinoma from the colon (grade 2-3), 10 cases of tubular adenoma, 20 samples of cancer adjacent normal tissue, and 10 samples from normal colon tissue. Adenocarcinoma tissue was assessed for TMN grading and stage. Patient ages ranged from 29 -81 for malignant samples. Sex was also variable between samples (Table 3-1).

All procedures performed in studies involving human participants were in accordance with the ethical standards of the institutional and/or national research committee and with the 1964 Helsinki declaration and its later amendments or comparable ethical standards.

Table 3-1. *Distribution of malignant colon tissue and controls*

Tissue Type	Number of Patients	Grade Range	Age Range	M/F	GV: IL-10/TGF-β
Adenocarcinoma	30	1-3	31-79	14/16	121.66 / 90.52
Metastatic Adenocarcinoma from the colon	30	2-3	30-79	17/13	112.66 / 89.61
Tubular Adenoma	10	-	31-69	6/4	117.5 / 85.57
Cancer Adjacent Normal Colon Tissue	20	-	32-81	16/4	120.26 / 89.46
Normal Colon Tissue	10	-	29-42	10/0	119.88 / 90.15

Immunohistochemistry

Tissues were incubated in Histoclear and rehydrated with a series of ethanol washes. Tissues were incubated with a DIVA solution for 30 minutes before treatment with a Background Sniper block. Block was administered for 30 minutes before tissues were washed and treated with primary antibodies at a 1:100 dilution. Following primary antibody treatment overnight at 4°C, tissues were washed and treated with Mach 4 HRP antibodies for 20 minutes at room temperature. After several washes, a DAB Peroxidase solution is added to the tissues. Areas of antibody binding will convert the colorless substrate to a brown product to highlight regions of antibody binding. Then, tissues are treated with a hematoxylin solution to show cell nuclei. Along with IL-10 and TGF-β treatment, GAPDH was utilized as a positive control and a universal negative was utilized as a negative control for expression.

Tissue Quantification

Following tissue imaging, all tissue was analyzed utilizing ImageJ software. Briefly, tissue images were each placed under an 'IHC toolbox' program with a selected "more DAB" option to discard areas of the sample without sufficient DAB staining. Following this, tissue images were converted to a gray scale and then placed under a threshold. In order to avoid incorporating bias from negative space within the image, a threshold was applied to the image to measure only areas of staining. The threshold applied for these samples was 50-150 and was determined utilizing GAPDH and the universal negative samples as guides. Samples with an average gray intensity of less than 115 were considered positive for cytokine expression ("High") and samples with an average gray intensity above 115 were considered negative for cytokine expression ("Low"). Once the threshold was applied to all images, they were assessed for average gray intensity. Low gray values are indicative of darkly stained tissue, and high gray

values are indicative of not staining. Following this evaluation, the images were also analyzed utilizing plot surfaces to quantify the levels of gray intensity throughout the sample.

Bioinformatic Analysis

We evaluated differences in expression levels of the IL-10 and TGF-β1 genes between primary tumors (n = 13) and metastases (n = 15) in datqa published by Vignot, et at.[28] These data had been generated using one-color Agilent microarrays. We preprocessed and normalized the data using the limma software package (v.3.30.13), using settings recommended in the limma User's Guide. To plot the data, we used the ggplot2 package (v.2.2.1). These software packages are implemented for the R statistical software.

Next we evaluated RNA-Sequencing data from The Cancer Genome Atlas (TCGA) for metastatic melanoma patients (n = 367). These data had previously been prepared using the featureCounts algorithm and summarized to transcripts-per-million values. We used the ggplot2 package (v.2.2.1) to plot these data.

Statistical analysis

Comparison between tissue samples was conducted utilizing ANOVA statistical analysis with the multiple comparison method. In addition, two-way ANOVA tests were performed to compare the mean expression of each antibody between colon adenocarcinoma and metastatic carcinoma tissues. Finally, t tests were utilized in conjunction to confirm statistical significance. All statistical analysis was evaluated using GraphPad Prism 7 software. Differences were considered significant when the p value was < 0.05.

Funding Details

This work was funded by the Simmons Center for Cancer Research at Brigham Young University.

Supplementary Figure 3-1

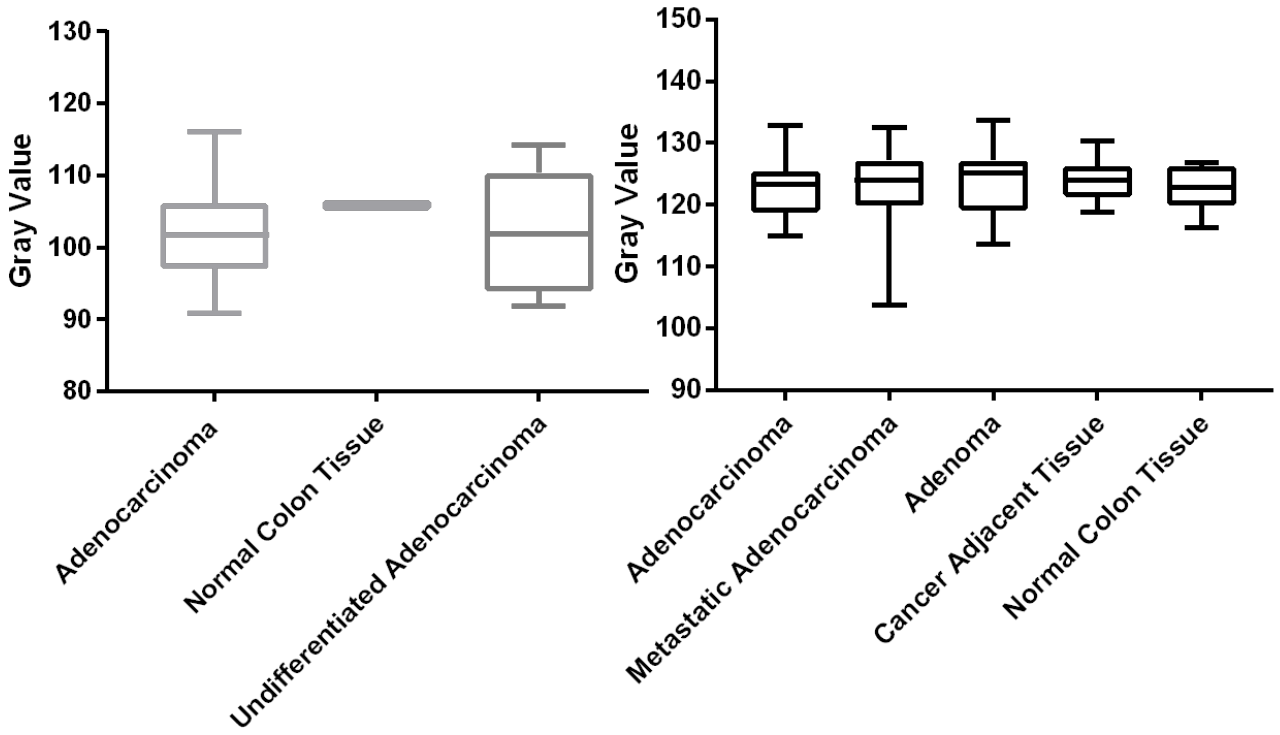

Isotype negative and GAPDH positive controls for tissue quantification.

CHAPTER 4

The Implementation of Think Pair Share Quizzes in undergraduate courses encourages collaborative learning and enhances critical thinking

Michelle H. Townsend, Tanner McGuire, and Kim L O'Neill

Citation: Michelle H. Townsend, Tanner McGuire, and Kim L. O'Neill. (under review). The implementation of think pair share quizzes in undergraduate courses encourages collaborative learning and enhances critical thinking. The Canadian Journal of the Scholarship of Teaching and Learning.

The following chapter is taken from an article in Review in the Canadian Journal of the Scholarship of Teaching and Learning. All content and figures have been formatted for this dissertation.

Abstract

Critical thinking and interactive learning, while essential to a student's success, are difficult to implement in college lectures of over 200 students. We designed this study to determine whether Think Pair Share (TPS) was an effective strategy to integrate in college courses to enhance student collaboration and critical thinking. The implementation of interactive learning strategies are often costly and require substantial effort by the professor. Thus, there is a need to find simple strategies to incorporate into college courses to improve student collaboration, while cultivating positive classroom environments. TPS is a teaching strategy with the potential to replace standard quizzes. Given a difficult, thought provoking question students are prompted to answer the question independently, in pairs, and then within groups. The aim of this study is to determine whether replacing standard quizzes with TPS questions improves student learning and concept mastery within college classrooms. Our results indicate that students preferred TPS quizzes over standard quizzes and a majority of students indicated that they felt more comfortable and challenged when given TPS quizzes over standard quizzes. This is a teaching technique that can easily be introduced to any higher education environment with limited cost and time to both administrators and educators.

Introduction

In college courses it is often difficult to implement standard teaching strategies frequently utilized to optimize learning in high school classrooms. Instructors are tasked to teach classes of 100-300 students while also covering a significant amount of content within the span of a few short months. As a result, students often have a difficult time with the transition from high school to a college lecture format [441].

As of 2013, the average high school classroom size was 15.9 individuals [442]. As these same students enter college they are required to change their method of learning as the classroom sizes are often over 200 students and the instructor is not easily available. College instructors estimate 42% of their freshman students were not adequately prepared by their prior education for the expectations of a college-level course [441]. The same frustration experienced by professors due to this lack of preparation also plagues students as they deal with the frustrations of re-learning how to learn.

College classes are often restricted to a lecture-style format. While this form of instruction is the most efficient way to communicate large amounts of information in the shortest amount of time, it is not ideal for inducing effective student learning and understanding [443,444]. It has been suggested that college students begin to have difficulty providing their full attention to lecturers after 15 minutes of instruction [445]. This is enhanced by the ever-increasing distractions that students are exposed to in the current digital society [446]. As a result, students start to fall behind on content and develop a disinterest in the course.

In previous courses we have observed a bimodal curve in which a certain percentage of the class has significant struggles and a resulting failing score. This curve demonstrates in part the negative effects of lecturing as some students are 'lost' in the process. To combat this, professors will often try and engage students in order to keep their attention and interest [447–449].

Frequently this presents as short quizzes during class to ensure students are studying the material and not falling behind [450,451]. We have integrated this strategy in previous courses but have seen minimal changes in student performance.

Think-Pair-Share (TPS) is an interactive learning strategy that can be easily implemented in large college classrooms where students can solve problems independently, in pairs, and in groups. Upon given a difficult question, students first answer with their own knowledge [452,453]. After individual thought, students are given the opportunity to communicate with another student and compare answers. This is followed by a group discussion and consensus on an answer to the question. Each of these steps is concluded with students providing their answers. This method utilizes student's own knowledge and resources to not only review and learn the material, but also provides students the opportunity to critically think and teach one another. By encouraging student communication TPS transforms the classroom from a static environment of content review to a collaborative classroom that encourages critical thinking and inspires discussion and debate between classmates[452,454]. Collaborative learning enables professors to enter a facilitating role as students engage in conversation while teaching one another[455]. Because college classrooms, particularly general education courses, are often composed of a melting pot of different fields, majors, and backgrounds some students are more familiar with concepts than others. By collaborating, the gap between student knowledge is lessened as those who are more competent in the material can instruct and lift those not as proficient[455]. This not only helps the student who is teaching master the content, but also helps the less proficient student view the material through a different perspective as they receive one-on-one training. This type of learning also provides a 'safe' environment for less proficient students to ask questions they may feel uncomfortable voicing to the entire class.

The use of peer instruction (PI) has been widely used in several classrooms and has shown merit in improving test performance and critical thinking[456–458]. Yet, the use of the full PI technique is often difficult for higher education professors to implement in large class sizes, especially teaching a subject with a high content load, such as molecular biology[459]. In comprehensive survey of PI use, approximately 9% of instructors responded that "the quantity of material to cover in a semester often made it difficult to devote class time to ConcepTests"[460]. TPS is a shorter, modified version of PI that can be easily implemented into a college course without significant changes to the educator's time constraints in order to ensure the full content of the lectures are still covered.

The aim of this study was to investigate the advantages of think pair share questions over traditional quizzes. We evaluated both the outcome of student performance along with student opinions of their learning experience and evaluations of student collaboration. Utilizing the same course including: lectures, tests, assignments, and readings, we compared a course with traditional quiz questions with a course utilizing the TPS technique. In addition to this assessment, we also evaluated the demand and difficulty for the professor to implement TPS within a college setting.

Methods

Experimental Course

We performed this experiment at an internationally recognized and attended university and utilized a freshman level introductory General Biology course. This class was chosen because it is designed to be one of the first courses freshman students take for a general education biology requirement. The course is called MMBio121 and is named "General Biology: Health and Disease" and covers the basics of biological concepts with a focus on how they influence human diseases. The course was separated into 10 different units (supplementary Table

4-1 &4 -2) covering a wide range of biological concepts. An example of the learning outcomes within every unit is given in supplementary Table 4-2. The book used in this course is called 'How Life Works' and is published by MacMillan. The book also includes a subscription to a Launchpad website with resources for students to utilize. This course was taught in the Fall of 2015, Winter of 2016, and Fall of 2016. The course is 15-weeks long and includes 2 midterm tests and a comprehensive final. Weekly quizzes were held every Friday, excluding test weeks, and there were bi-weekly Launchpad online learning assignments. Additionally, three small one-page research reports were assigned to allow students to research controversial topics to increase their interest in the coursework. The course was taught Monday, Wednesday, and Friday from 10am to 11am. The relative abundance of freshman is displayed in Figure 4-1. These numbers are not completely accurate as several 'true' Freshman students are considered Sophomores due

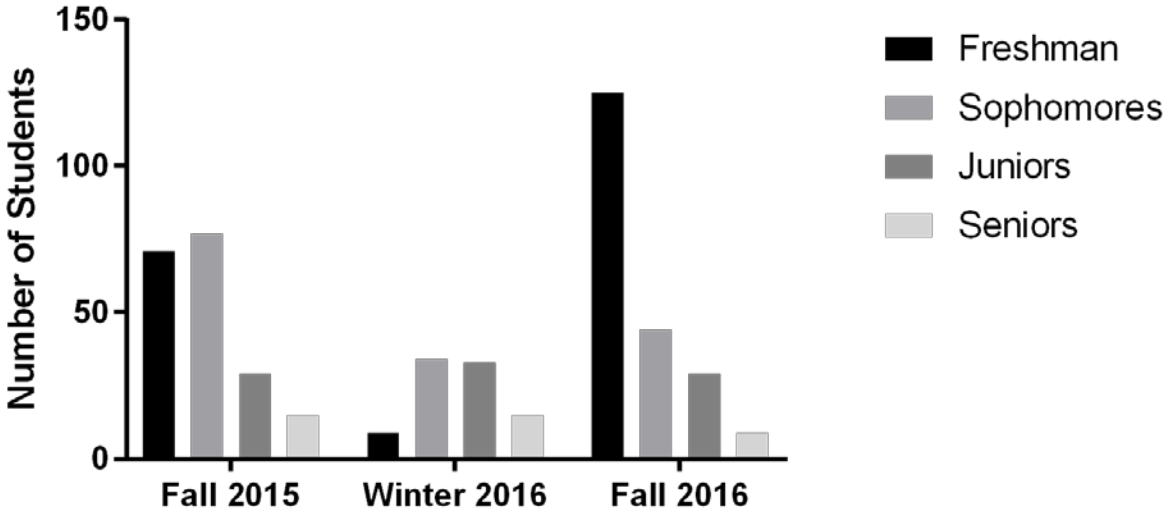

to AP credit received in high school.

Figure 4-1. *Class Age Distribution.* Each of the semesters evaluated was assessed for the relative Freshman and Sophomore abundance.

TPS questions were developed utilizing the most difficult learning outcomes from the previous control semesters (Table 14-A). The assigned learning outcome for each quiz is shown in Table 4-2.

Table 4-1. *Student test performance according to learning outcome*

	Learning Outcome	Description	Question(s)	Student Success (%)
Fall 2015				
Test 1	1.13	Create a mRNA strand from a DNA template.	9	15
	1.18	Create an amino acid chain using codon chart and mRNA strand	43	20
	1.19	Explore different protein structure and how they contribute to functionality	24	27
			35	25
	1.9	Explain the experiments that determined DNA was the genetic material	17	37
	1.8	Describe the difference between DNA and RNA	16	45
Test 2	3.2	Label and describe photosynthesis	30	20
	3.4	Describe cellular respiration and its location	30	20
	4.3	Explain cellular signals	21	39
	5.4	Identify and explain haploid, diploid, and polyploidy	11	39
	3.1	Analyze converting chemical energy to usable energy	19	51
Final	3.2	Label and describe photosynthesis	27	22
	7.6	Describe X-linked and Y-Linked Traits	29	24
	8.13	Explain mitochondrial DNA inheritance	53	26
	9.9	Create a diagram of primary and secondary infection	46	30
	6.1	Define a genome	33	15
Winter 2016				
Test 1	1.13	Create a mRNA strand from a DNA template	8	27
	1.14	Understand how mRNA is processed and why it is important for protein diversity in Eukaryotic organisms	9	50
			44	57
	1.15	Label and explain the process of translation including where it takes place, the proteins involved, the organelles involved, and the final products.	29	62
			48	69
			49	44
	1.16	Compare and contrast the differences and similarities between prokaryotic and eukaryotic translation.	14	56
			39	63
	1.19	Explore the different protein structures and understand how those specific structure contributes to the function.	22	19
			37	67
Test 2	3.2	Label and describe photosynthesis and the process by which light energy is used to convert carbon dioxide to glucose.	30	20
			20	41
	3.4	Describe the process of cellular respiration and explain its location within the cell, the organelles and molecules involved, and the importance of oxidative phosphorylation	35	24
			40	66
			2	65
	4.1	Draw an example of a general signaling between cells	9	38
	3.1	Analyze how cells take energy from glucose.	19	43
Final	6.1	Define a genome.	33	21
	8.13	Explain how mitochondrial DNA is passed on to offspring.	53	24
	3.2	Label and describe photosynthesis	27	29
	6.9	Explain why mitochondria have their own genome	18	7
	5.4	Identify and explain the differences between haploid, diploid, and polyploidy.	11	33
			52	67

Fall 2016				
	Learning Outcome	Description	Question(s)	Student Success (%)
Test 1	1.19	Explore different protein structure and how they contribute to functionality	22	28
	1.14	Understand how mRNA is processed and why it is important for protein diversity in Eukaryotic organisms	9	30
			44	56
	1.13	Create a mRNA strand from a DNA template.	8	33
	1.2	Describe organisms whose determination of life is not yet decided	34	35
	1.8	Describe the differences between RNA and DNA	15	40
Test 2	3.1	Analyze converting chemical energy to usable energy	19	40
	3.2	Label and describe photosynthesis	1	66
			14	67
			20	52
			30	22
	4.1	Draw an example of a general signaling between cells	9	47
	5.3	Explain the difference between chromosomes, homologous chromosomes, and sister chromatids. Understand which chromosome doesn't have a homologous pair.	49	51
	10.7/10.8	Describe viral infections and their symptoms	4	56
Final	6.1	Define a genome	33	17
	6.9	Explain why mitochondria and chloroplasts have their own genome	18	19
	3.2	Label and describe photosynthesis and the process by which light energy is used to convert carbon dioxide to glucose	27	23
	8.13	Explain how mitochondrial DNA is passed on to offspring.	53	23
	5.4	Identify and explain the differences between haploid, diploid, and polyploidy. Give examples of cells with both haploid and diploid chromosomes.	11	27

Note. Each test for the control semesters with standard quizzes was evaluated for the concepts most difficult for students. Each question along with the student success rate and the assigned learning outcome is listed for each test. The tests for the TPS course were also evaluated using the same techniques and the resulting learning outcomes are listed.

Quizzed Course (QC)

Every Friday a five question quiz was given to the students. The quiz was scored for 10pts with each correct question response worth 2 pts. These quizzes were given in complete silence without student access to materials. Each question had 30-45 seconds of allotted time for students to provide their answer. iClicker technology was utilized to acquire student answers. Because students were being graded for correct responses, the quizzes given were less difficult to maintain adequate student grades.

Table 4-2. *Quiz topic associated learning outcome.*

Think Pair Share Quiz Number	Tested Learning Outcome	Learning Outcome Description
1	1.1	Identify and Describe the various qualifications for life
2	1.9	Explain the experiments that determined that DNA was the genetic material
3	1.13, 1.18	Create a mRNA strand from a DNA template strand; Create a chain of amino acids using the codon chart and an mRNA strand
4	3.2	Label and describe photosynthesis and the process by which light energy is used to convert carbon dioxide to glucose.
5	3.4	Describe the process of cellular respiration and explain its location within the cell, the organelles and molecules involved, and the importance of oxidative phosphorylation
6	4.3, 4.5	Explain each of the following types of cellular signals: a. Paracrine b. Endocrine c. Juxtacrine d. Autocrine
7	5.4	Identify and explain the differences between haploid, diploid, and polyploidy. Give examples of cells with both haploid and diploid chromosomes.
8	7.6	Describe X-Linked Traits and Y-Linked Traits. Compare and contrast the differences between the two and explain their expression within individuals.
9	3.2	Label and describe photosynthesis and the process by which light energy is used to convert carbon dioxide to glucose.

Note. Each quiz number is shown with the learning outcome that was tested. The questions generated for the TPS using the learning outcomes as the topic were designed to be difficult and test student problem solving.

TPS Course (TPSC)

Every Friday a single TPS question was given to students. These questions were designed to be very difficult to inspire critical thinking. We prepared the topics for the TPS based on the lowest scoring learning outcomes from previous courses. Students were given approximately 2 minutes to answer the question on their own without any access to material, and would input their response. Students were then allowed approximately 2 minutes to discuss with a partner, and would input their response. Finally, students could discuss within groups the answer to the question. The final student answers were recorded followed by the true answer reveal. Following the answer reveal, we would explain the reasoning behind the correct answer. These quizzes were not graded based on correct responses, however, students were given participation points for responses.

Student Feedback

At the end of the TPSC students were given a five-question survey with inquiries about their experience utilizing the TPS technique in class. Additionally, we also provided an additional question where students could write their own thoughts, which was the source of the quotes throughout the paper. This survey was assigned points to ensure that we obtained a comprehensive overview of students thought on their TPS experience and to reduce sampling bias. All survey results were anonymous to ensure students shared their true feelings without the worry of repercussion. This research utilized educational tests and survey procedures along with general public observations and is exempt from IRB approval as there was no identifying links to the participating subjects.

Results

Quiz results show the stepwise change in answers as the class discusses the problem

As students answered individually, in pairs, and in groups there was a significant shift in the responses towards the correct answer in most the quizzes (Figure 4-2). A clear example of this shift is in Quiz 5 where a third of students had obtained the right answer when responding individually, but the majority of the class was evenly spread through the other incorrect responses. As the students thought in pairs the number of individuals with the correct answer increased, and when those pairs collaborated in groups the number of students with the correct answer again increased to half of the students. This type of progress was very common throughout the quizzes, and indicates that students are being influenced by their peers in a

constructive fashion as many of the students switched from an incorrect answer to the correct answer.

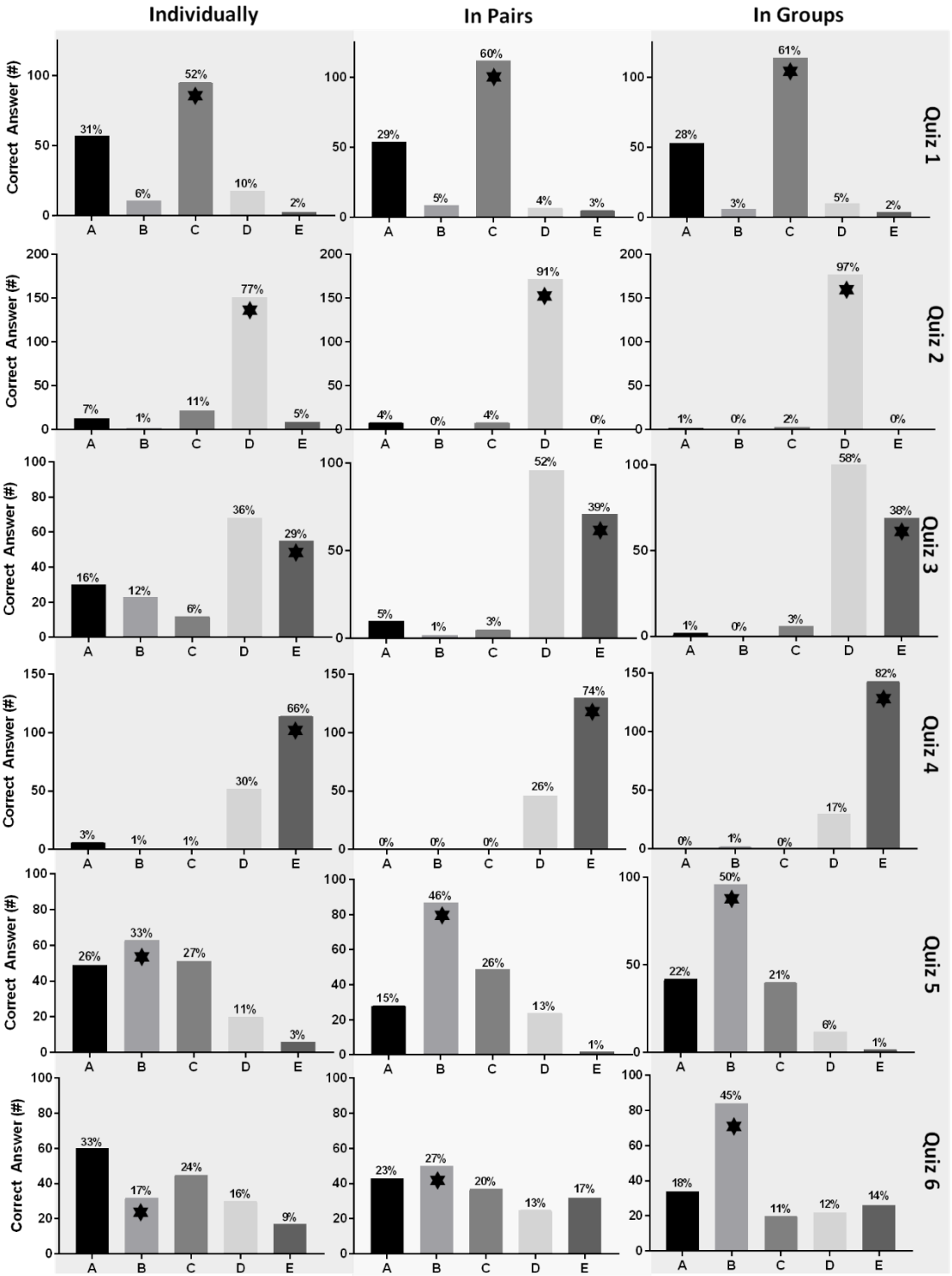

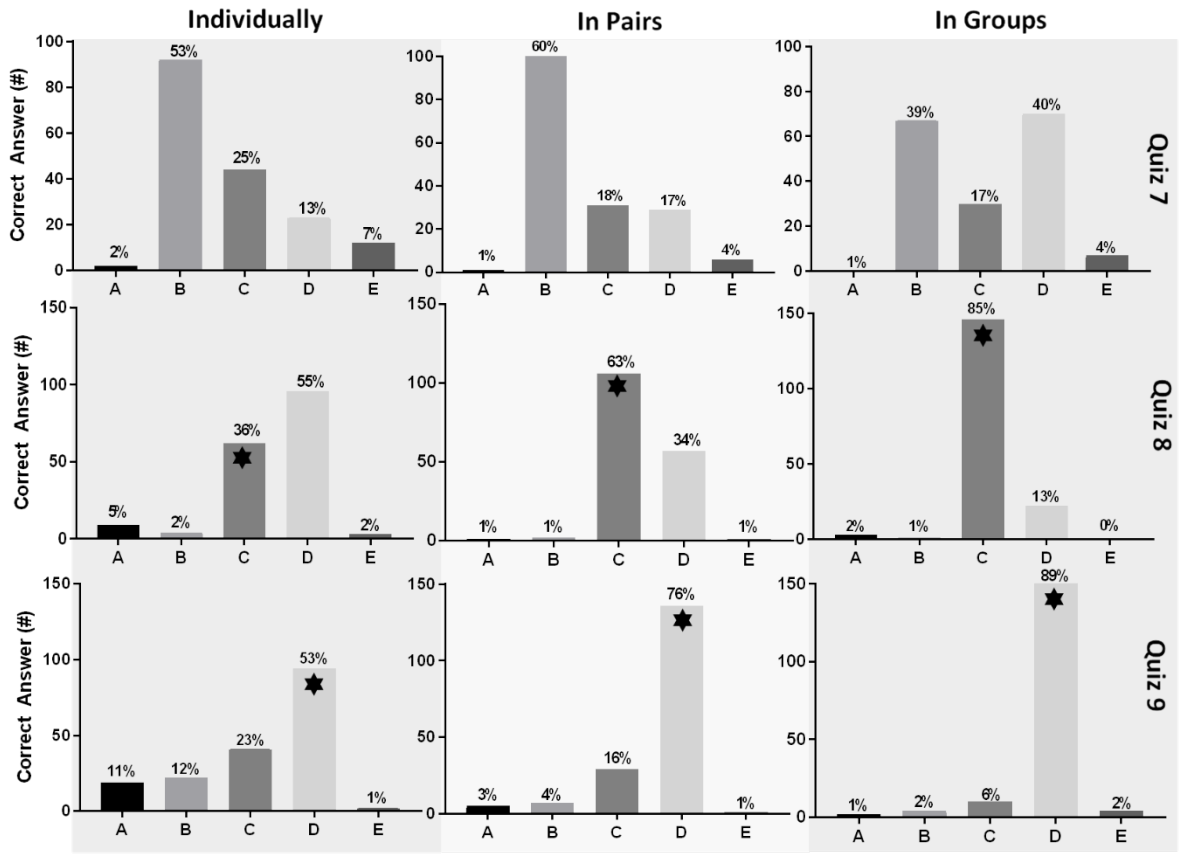

Figure 4-2. *Quiz results for TPS questions.* Quiz responses from the students for the 9 quizzes are listed here to analyze the success of student cooperation while discussion the question posed. Graphs labelled "individually" show the results of student responses after answering using their own knowledge. Graphs labeled "in pairs" shows student responses after collaborating with a partner, and graph "in groups" visualizes student final responses after group discussion. Each quiz is listed on the right-handed side and the relative abundance of each answer is displayed above the answer choice.

In addition, these quiz results also demonstrate the influence and importance of having all three steps in the TPS process. Several quizzes experienced a shift in the classroom responses towards the correct answer only after the class had collaborated within groups. Quiz 6 is the best example of this process as the students were still divided almost equally among all the answers until group discussion where a definitive answer emerged. This shows that all three steps are crucial in the TPS process as different learning is nurtured within each step. There were also scenarios such as with Quiz 8, where a clear majority of the students preferred an incorrect answer, but over the course of the discussion there was a turn in the class and the correct answer

ended up being the leading majority. These examples show that the collaboration between students influenced the resulting answers each student provided as students with a clearer understanding of the concepts are able to explain themselves to other less-confident students.

There was a significant improvement in the overall classroom environment as students felt safe to answer questions

When students in the TPSC were given the opportunity to interact with one another, there was a distinguishable change in the overall environment during the course. Students were clearly more vocal and engaged in the lectures. This was a substantial change in comparison to the QC where the professor consistently had difficulties engaging the course as students were not responsive to humor or questioning. The TPSC over the semester became more light-hearted which enabled better discussion and a safer environment for inquiry.

Over 90% of the students in the TPSC "strongly agreed" or "agreed" that the TPS questions improved the atmosphere of the class. This overwhelming majority shows that students believed the TPS questions gave them an important opportunity to interact with their peers.

> "This process helps students in the class to get to know each other a little better and feel more comfortable in asking for help later on"
>
> "I think it made the class become a safer place for questions, discussions, and mistakes"
>
> "This experience creates a sense of togetherness, or communal effort, enhancing the classroom connection between students by giving them an opportunity to work together and apply what they have been taught"

These are some of the comments students said in regarding the improved atmosphere within the classroom. As one student pointed out, the questions provided an opportunity for

people to work together that is not often found in college courses of this size. Many people reported an increase in friendships and several students experienced less caution when asking other students for help later on in the course. In addition, because there was a collaborative environment, many students felt the classroom a safer place to ask questions. This safe environment also fostered the idea that making mistakes increases learning. All of these factors in conjunction made this class very responsive and interactive within the learning process.

Students felt an increased mastery of the concepts presented in class by learning from their peers

As questions were presented throughout the semester, the students increased their communication with one another. During quizzes students are actively discussing, turning their bodies around to interact with groups behind them or pointing to the question making an argument for their answer. This collaboration aided in expanding students understanding of difficult concepts. Over 92% of the students in the TPSC "Agreeing" or "Strongly Agreeing" that student collaboration was important to gain new perspectives of challenging concepts (Figure 4-3).

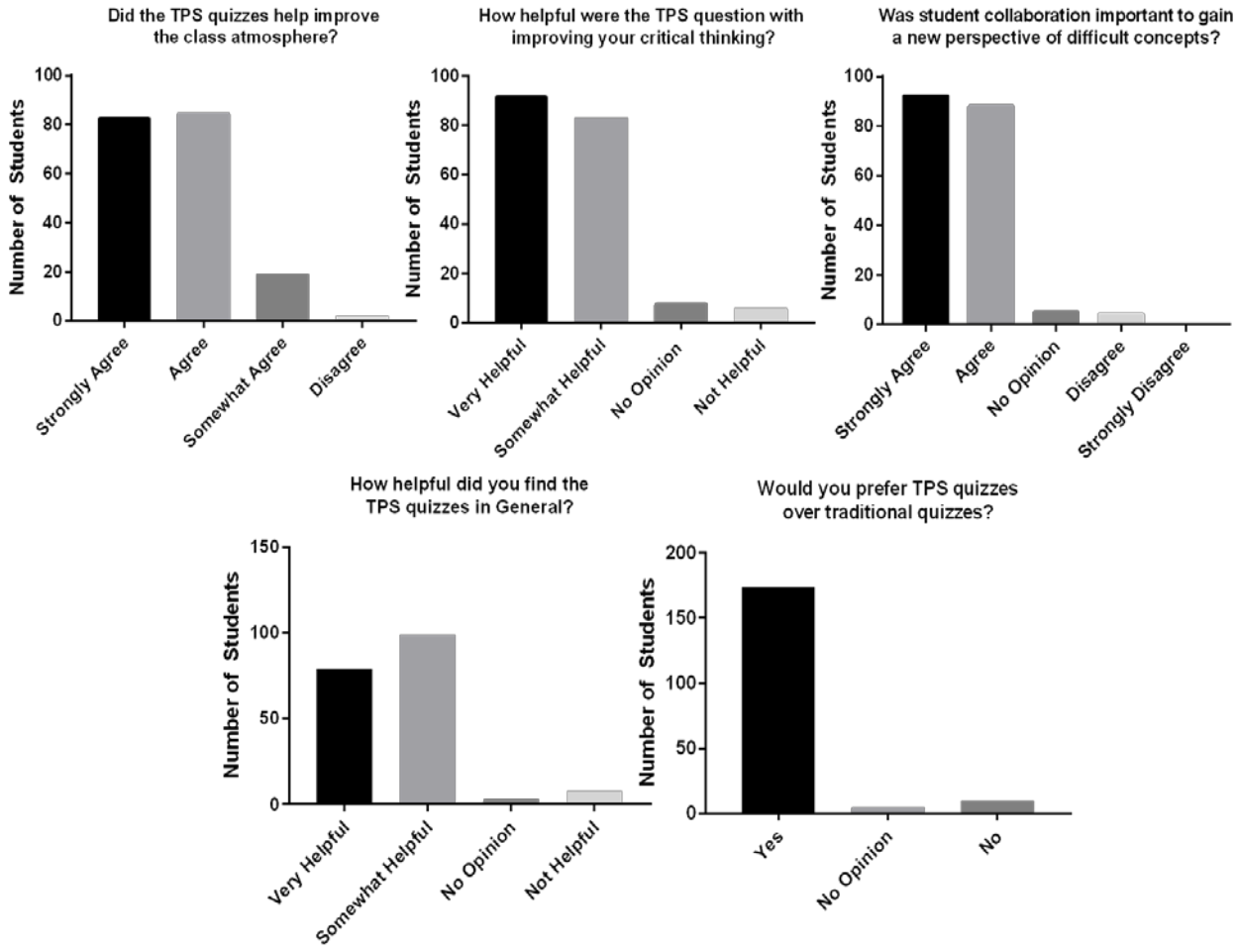

Figure 4-3. *The following questions were given to the students to evaluate their opinion of the TPS quiz format.* The question posed to the student is given above the graph displaying the results. The relative number of students with each answer is displayed.

By learning from their peers, several students were able to obtain a new perspective of the material by receiving explanations through different viewpoints than the professor. This type of teaching is especially important for students that have different learning languages from that of the professor. By sharing the responsibility of teaching, individuals who would have otherwise had a difficult time understanding the teaching style of the professor are able to grasp the concepts through the explanations of their fellow classmates.

"(TPS questions) Helps me to understand the concepts better when I can ask someone to explain something to me that I don't get the first time the professor explains it"

"Provided an opportunity for me to not only apply my knowledge but gain insight and perspective from my peers. It helped me to understand concepts that would be otherwise very hard to grasp."

"It is really helpful seeing different ways to solve the problem and the different ways people think"

"I found the think pair share quizzes to be extremely helpful because I realized I was thinking about the problems wrong, so when someone else explained it to me I understood the concept better and actually kept remembering it as I studied and listened to lecture"

"Teaching and discussing with a small group of your peers goes a LONG way to help introduce and retain information"

Additionally, this format of questioning provided students the opportunity to teach. As one of the most effective ways to retain and master concepts, teaching helped solidify material and retain knowledge. Since the questions covered a large array of information, every student had the opportunity to teach as each concept is learned differently by every individual. Students felt this was extremely helpful during their mastery of the course content.

"I felt way more involved in the concepts and I was enabled to learn more through either teaching other students or using other students to teach me"

> "They (TPS questions) gave me an opportunity to teach what I know about the question to my peers quickly, which helps me determine how much I actually know about the subject and what I need to refine with my studying"

Finally, several students expressed their satisfaction with verbally expressing their thoughts. Many times, a student may think through a question and come up with logical conclusions in their mind, but the act of verbalizing those thoughts in an effective way to communicate their reasoning to other students requires completely different skills and a very thorough understanding of the question. This articulation and the discussion/argument between students evoked a deeper investigation into the underlying concepts behind each question as students had to make logical arguments for their answer.

> "By talking through the question with someone else or with a group of people, I am able to understand the concept more clearly because it forces me to describe my answers vocally with precision"

> "I felt like I understood the material better when I was able to explain it to someone else and change their opinion"

Students felt less pressure and anxiety during quizzes, which enhanced their ability to critically think and test their understanding

With the freedom to ask extremely difficult questions, the professor was able to challenge students. This stimulating environment is usually not possible using traditional quizzes because students are too concerned with grading, and experience frustration and anxiety when a question is beyond their understanding. A large majority of the class preferred TPS questions (92%) over traditional quizzes (Figure 4-3). By providing a question that is designed and known to be very

challenging, students feel less pressure to get the "right" answer and can instead focus on where their understanding is lacking.

> "I liked the TPS quizzes because they weren't as stressful as traditional quizzes and gave me a chance to ask other people questions"
>
> "I liked that it was graded on participation, so there was low pressure and we could explore more difficult questions"
>
> "My favourite part is that it was okay if we got the quiz questions wrong because that places more emphasis on learning something new and takes the stress off of making sure the answer is correct"
>
> "It was a non-stressful way to push our critical thinking and problem-solving skills"

Because students were not required to have a correct answer for their grade, freedom was given to ask questions to test student's ability to critically think about the concepts discussed in class. As a result, 93% of the students in the TPSC reported the Think Pair Share questions to be "Helpful" or "Very Helpful" in improving their critical thinking (Figure 4-3). This suggests that the students knew they experienced an improvement in their critical thinking and problem solving skills as they applied their knowledge to practical scenarios.

> "I feel that collaborative thinking helped broaden my understanding of difficult topics"
>
> "They (TPS questions) demanded more of an understanding of the material rather than mere memorization, which can often be more challenging as it differs from the typical high school mind-set. By letting us work in groups, it makes the transition a lot smoother and easier"

There was an increase in student performance on TPS quizzed learning outcomes

Table 4-1 show the differential success of students between the TPSC and QC courses on tests based on learning outcome. The most difficult learning outcomes for both control QC semesters were 1.13 for test 1 and 3.2 for test 2. Yet, in the TPSC student performance significantly increased for these learning outcomes. In addition, several learning outcomes in the QC that students had poor performance had a significantly better outcome within the TPSC. There was a decrease in the slight bimodal curve experienced in the QC courses as overall student performance increased, and less students were 'lost' during the semester (Figure 4-4).

Figure 4-4. *Listed is the test performance for all the evaluated semesters.* The test given is displayed above (there were a total of 3 tests during the semester) and the semester the test was given is shown on the right. Each histogram of student performance shows distinguishing differences between the semesters and between overall student performance.

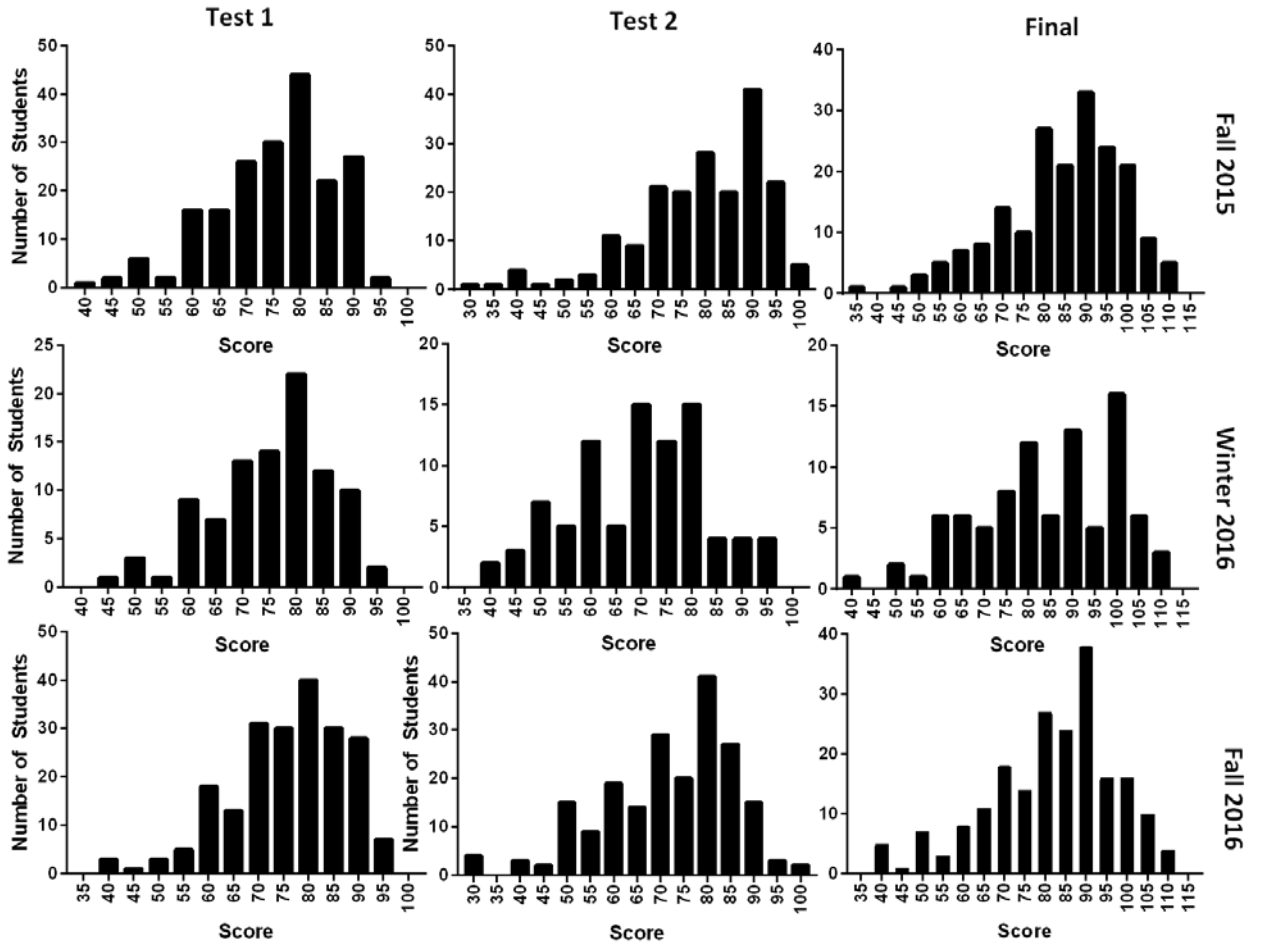

An instructor view of the TPSC in comparison to the QC

Often it is difficult to entertain and keep a class of over 200 students engaged within a 50-minute lecture. Yet, when given TPS questions, this challenge was considerably diminished as students provided the necessary energy and enthusiasm to maintain high levels of class participation and thought-provoking inquiries. This made teaching easier as the instructor can gauge student understanding through proposed questions. Meanwhile, students would also aid in suggestions and provide their own insights into the material, which helped invoke constructive discussions on applications of the concepts being addressed.

We have also found that TPS questions are as easy to implement within a college classroom as a standard quiz. Both quiz formats utilize an iClicker system to record grades, which is often already implanted into the course for other purposes. TPS questions also only require the creation of one quiz question, which may lighten the work load of the instructor as they are not required to create multiple questions. Finally, the time requirement for TPS quizzes is very similar to the time required to take a standard quiz. As such, the transition between the formats is relatively simple and TPS quizzes are easy to integrate into a standard lecture.

Implications of this technique in a general classroom

The think pair share strategy has shown to be valuable in a college setting to enhance both student critical thinking and classroom atmosphere. This strategy can easily be implemented in any college classroom across the world to enhance student learning as it only requires the instructor to prepare a challenging question on the material taught. In addition, because students are collaborating with each other, we suggest that this technique is helpful when teaching a mosaic of students from different ethnic backgrounds. Because students can choose those in which they sit next to, they can converse with those who they prefer. This provides extra

opportunities for second language learners, who struggle with content and language barriers, as they collaborate with other second language learners to explain difficult concepts. We performed this experiment within a science course because the content is generally difficult for students to grasp, but this technique can be applied to any subject to provide opportunities for students to collaborate and solve problems.

Conclusions

The results of this study emphasize the importance of collaborative learning within a college classroom, especially within a subject that is historically difficult. We found that students who successfully engaged in conversation and discussion with their fellow classmates were able to master the concepts being discussed in lecture. By increasing cooperation between students and encouraging discussion, students increased performance on evaluations compared to students who were given standard quizzes and were not given the opportunity to engage with one another in class. When challenged with questions designed to inspire critical thought, students performed significantly better upon discussion within peer groups [461]. This demonstrates the superiority and effectiveness of Think Pair Share quizzes compared to traditional quizzes within college courses.

While the scope of this study was limited to one course, our findings also report that the implementation of these quizzes within classrooms does not take substantial effort on the part of the educator. As such, this technique provides a relatively simple step for educators to bring collaboration into their large courses. The results of this study highlight the importance of providing opportunities for collaborative learning in college lecture-style courses for student concept mastery in addition to providing a strategy that can provide this within courses.

Funding Details

The work for this manuscript was supported by a Teaching Enhancement Grant

Supplementary Tables

Supplementary Table 4-1. Course Content Outline.

Unit: Title	Concepts	Description
Unit One: Information Transfers Necessary for Life	Life: Chemical, Cellular, and Evolutionary Foundations	Life works according to fundamental principles of chemistry and physics. The fundamental unit of life is the cell.
	The Molecules of Life	Carbon is the backbone of organic molecules. Organic molecules include proteins, nucleic acids, carbohydrates, and lipids, each of which is built from simpler units.
	Nucleic Acids and Transcription	DNA stores and transmits genetic information. Transcription is the process by which RNA is synthesized from DNA.
	Translation and Protein Structure	Translation is the process where mRNA specifies the order of amino acids in a newly synthesized protein
Unit 2: Lipids, Membranes, and Energy Acquisition	Lipids, Membranes, and Cell Compartments	Cell membranes are composed of lipids, proteins, and carbohydrates
	Making Life Work: Capturing and Using energy	Chemical reactions involve the breaking and forming of bonds
Unit 3: Cellular Respiration and Photosynthesis	Cellular Respiration: Harvesting Energy from Carbohydrates and Other Fuel Molecules	Cellular respiration is a series of catabolic reactions that convert the energy in fuel molecules into ATP
	Photosynthesis: Using Sunlight to Build Carbohydrates	Photosynthesis is the major pathway by which energy and carbon are incorporated into carbohydrates
Unit 4: Cell Communication, Structure, and Function	Cell Signaling	Cells communicate primarily by sending and receiving chemical signals
	Cell and Tissue Architecture	Tissues and organs are communities of cells that perform special functions
Unit 5: Cell Division and Replication	Cell Division	During cell division, a single parental cell divides into two daughter cells
	DNA Replication and Manipulation	A single parental molecules of DNA produces two daughter molecules
Unit 6: Genomes and DNA Techniques	Genomes	A genome is the genetic material of a cell
Unit 7: Mutation and Repair	Mutation and DNA Repair	DNA can be damaged but most DNA damage is repaired
	Genetic Variation	Genetic variation describes common genetic differences among individuals in a population
	Mendelian Inheritance, Inheritance of Sex	Genetic inheritance provides the framework for an individual and several diseases are related to sex-linked traits.
Unit 8: Evolution	Evolution: How Genotypes and Phenotypes Change Over Time	Evolution is the change in the frequency of alleles or genotypes over time
Unit 9: Immunology	Natural Defense Against Pathogens	Study of the body's natural defense against disease
Unit 10: Health and Disease	Epidemiology	Study of the occurrence of disease within populations and the variables affecting that.
	Bacterial and Viral Diseases	Diseases associated to bacterial or viral infections
	Soil Borne Bacterial Diseases	Diseases from soil residing bacteria that affect human health
	Water Borne Bacterial Diseases	Diseases from water residing bacteria that affect human health
	Eukaryotic Pathogens	Eukaryotic organisms that have an influence on human health

Note. Displayed is the content covered throughout the course. Each unit is separated according key concepts.

Supplementary Table 4-2. Course Content Outline.

Objective	Description
1.1	Identify and describe the various qualifications for life
1.2	Describe organisms whose determination of life is not yet decided and give evidence for and against those organisms being classified as living or nonliving
1.3	Draw the structure of an element including: protons, neutrons, and electrons
1.4	Describe the various chemical bonds and how they are important in molecular stability
1,5	Describe lipids, proteins, nucleic acids, and carbohydrates and explain how they are important in maintaining organism life and functionality
1.6	Identify various amino acids by their structure.
1.7	Label and explain the individual components of DNA including the nitrogenous bases (Adenine, Thymine, Guanine, and Cytosine), the sugar-phosphate backbone, the sugar, and the antiparallel nature of DNA
1.8	Describe the differences between RNA and DNA
1.9	Explain the experiments that determined that DNA was the genetic material
1.10	Identify and provide the function of the proteins associated with DNA replication:
1.11	Compare and Contrast the differences and similarities between Prokaryotic Transcription and Eukaryotic Transcription
1.12	Describe various proteins associated with Transcription
1.13	Create a mRNA strand from a DNA template strand
1.14	Understand how mRNA is processed and why it is important for protein diversity in Eukaryotic organisms
1.15	Label and explain the process of translation including where it takes place, the proteins involved, the organelles involved, and the final products.
1.16	Compare and contrast the differences and similarities between prokaryotic and eukaryotic translation and the resulting consequences of their differences.
1.17	Relate how mistakes in translation can lead to serious problems in the cell in regards to the protein product.
1.18	Create a chain of amino acids using the codon chart and an mRNA strand
1.19	Explore the different protein structures and understand how those specific structure contributes to the protein's functionality and purpose in the cell.
1.20	Explain the scientific method and how it has contributed to our understanding of scientific principles.

Note. The following is a table of the learning outcomes that were evaluated for Unit 1 to provide an example of the expectations for the remainder of the units. Each unit had similar learning outcomes that were used to evaluate the concepts that were most difficult for students to comprehend. These learning outcomes became the focus of the TPS questions created.

CHAPTER 5

Non-small-cell lung cancer cell lines A549 and NCI-H460 express hypoxanthine guanine phosphoribosyltransferase on the plasma membrane

Michelle H Townsend, Michael D Anderson, Evita G Weagel, Edwin J Velazquez, K Scott Weber, Richard A Robison, and Kim L O'Neill

Citation: Michelle H. Townsend, Michael D. Anderson, Evita G. Weagel, Edwin J. Velazquez, K. Scott Weber, Richard A. Robison, and Kim L. O'Neill. Non-small-cell lung cancer cell lines A549 and NCI-H460 express hypoxanthine guanine phosphoribosyltransferase on the plasma membrane. OncoTargets and Therapy. 2017: 10 1921-1932. DOI: https://doi.org/10.2147/OTT.S128416

The following chapter is taken from an article published in OncoTargets and Therapy. All content and figures have been formatted for this dissertation.

Abstract

In both males and females, lung cancer is one of the most lethal cancers worldwide and accounts for .30% of cancer-related deaths. Despite advances in biomarker analysis and tumor characterization, there remains a need to find suitable biomarker antigen targets for treatment in late-stage lung cancer. Previous research on the salvage pathway enzyme TK1 shows a unique relationship with cancer patients as serum levels are raised according to cancer grade. To expand this analysis, the other salvage pathway enzymes were evaluated for possible upregulation within lung cancer. Adenine phosphoribosyltransferase, deoxycytidine kinase, and hypoxanthine guanine phosphoribosyltransferase (HPRT) were assessed for their presentation on two non-small-cell lung cancer cell lines NCI-H460 and A549. In the present study, we show that deoxycytidine kinase and adenine phosphoribosyltransferase have no significant relationship with the membrane of NCI-H460 cells. However, we found significant localization of HPRT to the membrane of NCI-H460 and A549 cells. When treated with anti-HPRT antibodies, the average fluorescence of the cell population increased by 24.3% and 12.9% in NCI-H460 and A549 cells, respectively, in comparison with controls. To ensure that expression was not attributed to cytoplasmic HPRT, confocal microscopy was performed to visualize HPRT binding on the plasma membrane. After staining NCI-H460 cells treated with both fluorescent antibodies and a membrane-specific dye, we observed direct overlap between HPRT and the membrane of the cancer cells. Additionally, gold-conjugated antibodies were used to label and quantify the amount of HPRT on the cell surface using scanning electron microscopy and energy-dispersive analysis X-ray. Further confirming HPRT presence, the gold weight percentage of the sample increased significantly when NCI-H460 cells were exposed to HPRT antibody ($P=0.012$) in comparison with isotype controls. Our results show that HPRT is localized on the surface of these non-small-cell lung cancer cell lines.

Introduction

Lung cancer is one of the leading causes of cancer-related deaths in both males and females worldwide. In 2015, 221,200 individuals in the US were diagnosed with lung cancer, while another 158,040 individuals were killed by the disease [462]. Approximately 85% of lung cancer cases are diagnosed as non-small-cell lung cancer, which encompasses squamous cell carcinoma, adenocarcinoma, and large cell carcinoma [463]. Despite advances in combinatorial therapy using both chemotherapy and radiotherapy, patient outcome has not improved at a satisfactory rate [464]. Currently, the 1-year survival rate for lung cancer patients is 44%, and the 5-year survival is only 17%. Low survival is largely attributed to late-stage diagnoses. Approximately 57% of patients are diagnosed at a late stage, leading to reduced treatment options and increased mortality. When diagnosed at a late stage, the survival rates are reduced to 26% and 6% for 1-year and 5-year survival, respectively [462].

Because early detection of lung cancer is integral to patient survival and outcome, substantial efforts have been made to develop noninvasive tests that identify non-small-cell lung cancers, allowing physicians to diagnose the disease at an earlier stage [465,466]. Although profiling cancer tissues to find circulating biomarkers can aid in identifying tumor-derived proteins, these methods are extremely invasive. As a result, researchers have developed techniques to identify cancer biomarkers in the sputum of patients. These tests utilize DNA-based assays to detect methylated gene promoter regions that are commonly found in tumors and lead to the loss of tumor suppressor function [467,468]. RARβ is a chief candidate for this type of analysis because it is involved in cellular signaling during embryonic morphogenesis, cell growth, and differentiation [469]. Studies show that 95% of the cancer tissue has upregulated methylation of the RARβ promoter compared to controls, demonstrating its use as an effective biomarker for lung cancer detection [469]. The p16 tumor suppressor gene has also been used in early detection through

evaluation of hypermethylation at its locus [470–472]. This methylation change is often detected in precursor lesions of tumors and serves as an early event in cancer development and progression [473]. In addition, recent advancements have allowed physicians to detect cancer using breath samples from patients by analyzing volatile organic compounds. By evaluating panels of patients, cancer profiles are established that can later be used as references to aid physicians in early lung cancer detection [474,475].While these methods are promising for the early recognition of lung cancer, they are not suitable for the treatment of patients.

Once lung cancer is detected and diagnosed, a majority of patients are treated with surgery, chemotherapy, radiation therapy, and targeted therapy. For patients suffering with non-small-cell lung cancer, the most common treatment is chemotherapy combined with targeted drugs. Although many patients go into remission after initial treatment, a large percentage eventually relapse, and chemotherapy regimens offer little advantage over other treatments for advanced non-small-cell lung cancer [476]. New therapies utilize cancer antigens to target tumors, which enables physicians to personalize treatments. Treatment efficacy is enhanced with tumor biopsies, which classify the individual mutations in a tumor to help determine the best course of treatment [477]. Because of these biopsies, multiple genes have been assessed and shown as biomarkers for lung cancer due to their upregulation in comparison with normal tissue. CBLC, CYP24A1, S100P, and ALDH3A1 all have 5- to 10-fold increases in the level of expression in both adenocarcinoma and squamous cell carcinoma samples in comparison with normal tissue [478]. This information leads to personalized treatment and aids physicians in determining effective drug regimens. For example, ~10% of patients with non-small-cell lung cancer have a mutation in the epidermal growth factor receptor (EGFR) that renders them sensitive to tyrosine kinase inhibitor drugs [479–482]. Although personalizing treatment based on tumor characteristics can be

effective and lead to increased survival rates for small subsets of patients, the current targeted treatments lack specificity and can often lead to unwanted off-target effects [483].

The purpose of this study was to find a lung cancer biomarker on the surface of non-small-cell lung cancer cells. Due to the proliferative capacity of cancer cells and the need for necessary nucleotide production to support rapid division, the salvage pathway enzymes deoxycytidine kinase (DCK), adenine phosphoribosyltransferase (APRT), and hypoxanthine guanine phosphoribosyltransferase (HPRT) were evaluated for potential expression on non-small-cell lung cancer cell lines. DCK functions by transferring a phosphate group to deoxycytidine in the production of cytosine bases. APRT catalyzes the transfer of a phosphoribosyl group from phosphoribosyl pyrophosphate (PRPP) to adenine, forming adenine monophosphate in the production of adenine bases. HPRT is a crucial enzyme for the large-scale production of guanine and inosine bases. HPRT functions by transferring phosphoribose from PRPP to hypoxanthine or guanine bases to form inosine monophosphate (IMP) and Guanine monophosphate (GMP), respectively [10,12]. We designed this study to evaluate the potential of these salvage pathway enzymes as possible biomarker targets for the treatment of non-small-cell lung cancer.

We utilized a variety of methods, including flow cytometry, confocal microscopy, and scanning electron microscopy, to determine whether DCK, APRT, or HPRT had any significant relationship with the surface of H460 and A549 cells. In addition, we also evaluated HPRT expression within patient tissue to determine whether there was a unique elevation in patients with lung carcinoma. Although we found no significant relationship between DCK and APRT with H460 non-small-cell lung cancer cells, HPRT had a significant colocalization with the membrane of both A549 and H460 cancer cells.

Materials and Methods

Chemicals

Mouse-antihuman HPRT monoclonal antibody clone 1F8D11 (Thermo Fischer Scientific, Waltham, MA, USA) was aliquoted and stored at −20°C. DCK antibody clone 2243C2 (Santa Cruz Biotechnology Inc., Dallas, TX, USA) and APRT antibody lot 10196 (Abnova, Taipei City, Taiwan) were stored at −20°C. Mouse-FITC and rabbit-FITC antibody (Sigma Aldrich, St Louis, MO, USA) were stored at 4°C and were used in minimal light conditions. Bovine serum albumin (BSA, Sigma Aldrich) and sodium thiolsulfate (Macron Fine Chemicals, Center Valley, PA, USA) were dissolved in phosphate-buffered saline (PBS) at a 1% concentration and stored at 4°C. A 50% glutaraldehyde stock solution (Electron Microscopy Sciences, Hatfield, PA, USA) was stored at −20°C, and workable solutions were diluted to 0.25% in PBS and stored at 4°C. Glycine (Thermo Fischer Scientific) was diluted to 0.2 mM in PBS and stored at 4°C. NF-κB polyclonal antibody (Bioss Antibodies, Woodburn, MA, USA) was stored at −20°C. CD44 monoclonal antibody (One World Lab, San Diego, CA, USA) was stored at −20°C.

Cell culture conditions

The human non-small-cell lung cancer cell lines H460 and A549 were obtained from the American Type Culture Collection (Rockville, MD, USA). H460 cells were grown in RPMI 1640 medium supplemented with 10% fetal bovine serum and 2 mM L-glutamine (all from Hyclone, Logan, UT, USA). A549 cells were grown in DMEM/F12 medium supplemented with 10% fetal bovine serum and 4 mM L-glutamine (all from Hyclone). The cell media were replaced every 48 hours, and cells were trypsinized and reduced once 90% confluence was obtained. Cells were treated with Accutase (Stemcell Technologies, Vancouver, Canada) when

utilized for flow cytometry, and when plated for all other applications. All cells were grown at 37°C and 5% CO_2. Cell lines were authenticated in May 2016 by the University of Arizona Genetics Core.

Flow cytometry

The expressions of HPRT, DCK, and APRT in cultured cells were evaluated by measuring the levels of fluorescence in cells treated with each salvage pathway enzyme antibody. All samples were analyzed on a Blue/Red Attune (Applied Biosystems, Foster City, CA, USA), which recorded 25,000–50,000 events per sample. Briefly, 250,000 cells were incubated with 200 µL of PBS containing 1 µg of antibody to DCK, APRT, and HPRT for 15 minutes on ice. Cells were then labeled with FITC-conjugated secondary (mouse or rabbit) antibody for 15 minutes on ice. Isotypic IgG and unstained cells served as negative controls. The forward/side-scatter plots were used to gate out cell doublets and dead cells. Resulting data were analyzed and plotted using FlowJo Software (FlowJo Enterprise, Ashland, OR, USA). CD44 was utilized as a positive control (Figures 5-S1 and 5-S2), and NF-κB was utilized as a negative control.

Confocal microscopy

Fluorescently stained cells were examined under an epifluorescence microscope (Olympus, Tokyo, Japan) equipped with a laser confocal system (Bio-Rad Laboratories, Hercules, CA, USA) using a 15 mW Krypton/argon laser. Image processing was carried out with Laser Sharp Computer Software (Bio-Rad Laboratories). After accutase treatment, cells were plated at a concentration of 4×105 cells/mL on glass coverslips. Following 1 day of growth, cells were incubated in 500 µL of PBS containing 2.5 µg of anti-HPRT antibody for 15 minutes on a shaker at 4°C. Cells were then labeled with 2.5 µg of FITC-conjugated secondary antibody for

15 minutes on a shaker at 4°C. Then, cells were incubated at 37°C for 10 minutes with a 1:1,000 dilution of a Cell Mask Deep Red plasma membrane dye (Fisher Scientific, Waltham, MA, USA).

Scanning electron microscopy

After acutase treatment, cells were plated at a concentration of 400,000 cells/mL on glass coverslips. After 1 day of growth, cells were placed in 6-well plates and washed three times with PBS followed by a 1% BSA in PBS wash, a 1% sodium thiolsulfate in PBS wash, and a 1% sodium azide wash for 5 minutes each at 4°C. Cells were then incubated with 5 µg of primary antibody conjugated to Biotin for 15 minutes on a shaker at 4°C. After primary incubation, cells were washed with 1% BSA followed by two washes with PBS. Then, cells were washed with 1% PBS–BSA and 1% sodium thiolsulfate for 5 minutes on a shaker at 4°C. Cells were then incubated with 2.5 µg of a streptavidin–gold conjugate (Nanoprobes, Yaphank, NY, USA) for 15 minutes on a shaker at 4°C. This was followed by a 1% BSA wash and three PBS washes. Cells were then fixed via incubation in a 0.25% glutaraldehyde solution diluted in PBS for 5 minutes. The reaction was extinguished by adding a 0.2 mM glycine diluted in PBS solution and incubating for 10 minutes until the solution turned to a slight yellow color. Cells were then washed three times with ddH_2O. Solutions A and B from the Nanoprobes gold enhancement kit were incubated together for 5 minutes. Solutions C and D were then added, vortexed, and 40 µL of the gold enhancement solution was added to each sample and incubated for 5 minutes. Each sample treated with gold enhancement is coated in a solution of 2 nm gold particles, but only gold already present via secondary antibody binding will be enhanced to form a definitive particle. Each sample was subsequently put through a series of dehydrations with 70%, 80%, 90%, and 100% EtOH before analysis. Gold-labeled samples were examined under a Phillips XL-30 ESEM using a 15 kV electron stream under low vacuum conditions at 0.8 Torr. A

gaseous side electron (GSE) detector was utilized to image the cell morphology and topography. A back scatter electron (BSE) detector was utilized to visualize gold particles on the cell surface. Once images for the cells were obtained, the elemental composition was evaluated using energy-dispersive analysis X-ray (EDAX). Because of gold enhancement, the elemental gold percentage of the background levels of gold was ~8%.

Immunohistochemistry

Lung carcinoma tissue arrays were obtained from Cybrdi (Frederick, MD, USA). These tissues contain various stages of cancer along with corresponding benign and normal tissues from 35 different patients. HPRT levels were assessed utilizing standard immunohistochemistry staining. Tissues were rehydrated in a series of ethanol washes before treatment with a DIVA decloaker solution to retrieve antigen. Tissues were then incubated with a background sniper solution to reduce nonspecific antibody binding. Following blocking, a primary antibody is added to the tissue at a concentration of 1:100 to 1:200 and incubated overnight at 4°C. Following primary staining, tissues were washed and then treated with secondary antibody conjugated to a horse radish perioxidase polymer and incubated for an hour. Following washing, a DAB (3,3′ diaminobenzidine) peroxidase solution is incubated with the tissues. Areas of antibody binding will convert the colorless substrate to a brown product, effectively highlighting the target protein. Tissues were treated with hematoxylin to stain the nucleus of the cells. Along with HPRT treatment, a universal negative antibody was used as a negative control.

Tissues were quantified utilizing ImageJ software. All images were evaluated using the IHC toolbox ImageJ plugin. The DAB option is chosen, and the tissue image is then removed of all other staining except for DAB. Following this analysis, the image is then converted to a gray scale and a threshold is applied in order to eliminate areas of white inherit in the tissue. Once the

threshold is applied, the average gray value of the tissue is collected. The same threshold is applied to all tissue samples in order to ensure consistency.

Statistical analysis

Analysis of variance (ANOVA) statistical analysis with the multiple comparison method was used to determine the differential surface expression of various treatments for flow cytometry data on both A549 and H460 cells. In addition, two-way ANOVA tests were performed to compare the mean values of HPRT expression between A549 and H460 cells. EDAX data were analyzed using ANOVA with the multiple comparison method in addition to unpaired t-tests to determine significance between samples. All statistical analyses were performed using GraphPad Prism
7 software. Differences were considered significant when the P-value was ,0.05.

Results

DCK and APRT are not found on the surface of non-small-cell lung cancer H460 cells

Flow cytometry utilizing FITC fluorescent antibodies was used to quantify the DCK and APRT surface antigens. Figure 5-1A and B shows the relative binding of DCK and APRT protein on the surface of H460 cells, while Figure 5-1C shows the binding of HPRT. In the presence of anti-DCK and anti-APRT antibody, there was no significant increase in the fluorescent intensity of treated samples and no resulting shift in the cell population. Further statistical analysis revealed that DCK and APRT were not significantly different than the secondary IgG antibody controls. These data show no relevant binding of specific antibodies to the cell surface and suggest that the therapeutic potential of DCK and APRT is minimal for non-small-cell lung cancers.

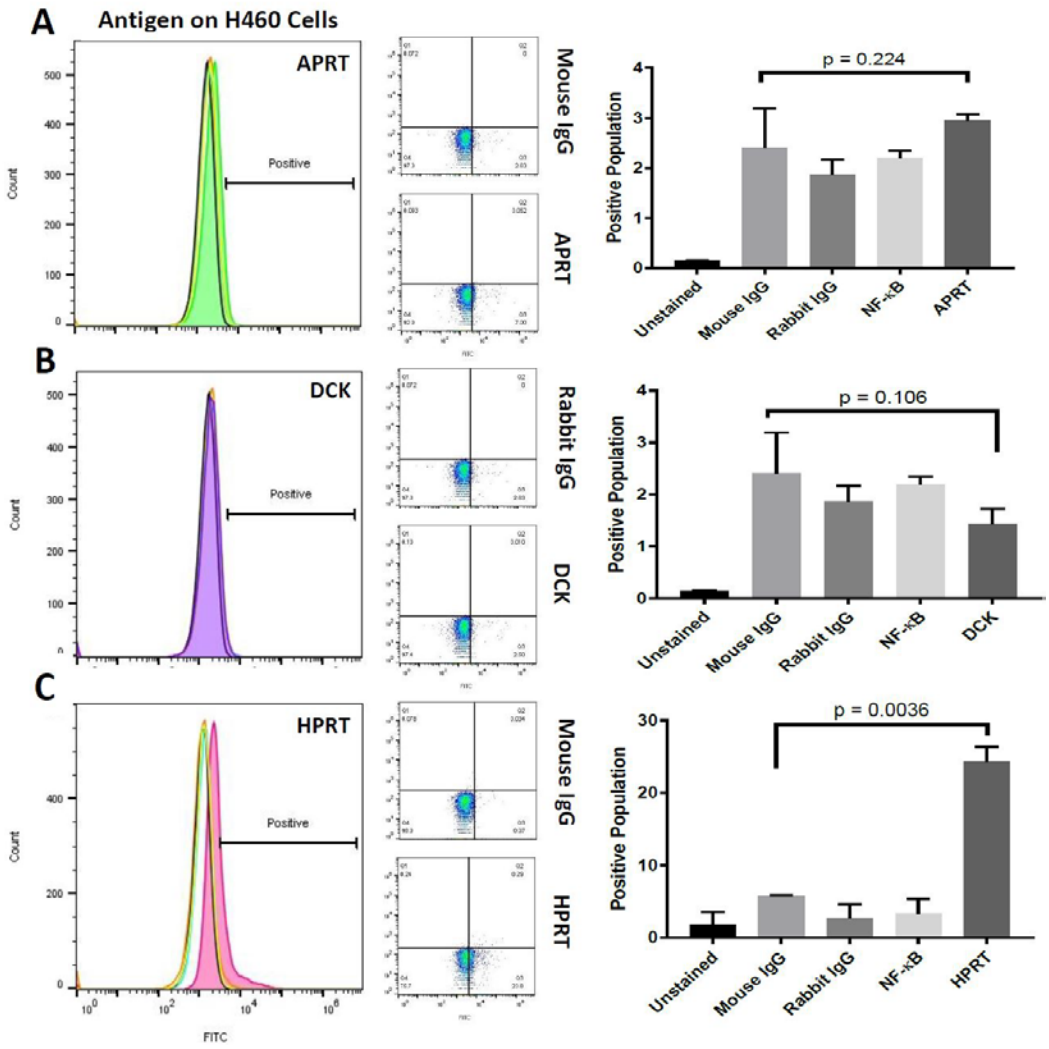

Figure 5-1. *Flow cytometry analysis of the salvage pathway enzymes in H460 cells.* Notes: The following samples were utilized in order to evaluate the expression of APRT, DCK, and HPRT on the surface of H460 cells: unstained (autofluorescence control), mouse IgG (nonspecific binding control), rabbit IgG (isotype control), NF-κB (cytosolic protein control), and CD44 (positive surface antigen). (A) When anti-APRT antibody (green) was used to treat cells, a resulting insignificant shift in the population was observed upon comparing the histogram diagrams to controls. This insignificant shift is also shown in the lack of movement from Q3 in isotype controls to Q3 in APRT-treated cells (equaling only 4%). Cells treated with APRT have an insignificant level of binding compared to isotype controls (P=0.224). (B) Cells treated with anti-DCK antibody (purple) had an even smaller shift in the fluorescent population compared to APRT. No cells from Q3 in the mouse IgG control moved to Q3 in the DCK-treated cells, indicating a complete lack of the DCK antigen on the surface of H460 cells. Statistical analysis reveals no presence of DCK on the surface of H460 cells (P=0.106). (C) When treated with anti-HPRT antibody (pink), the histogram representation of the cell population showed a definitive shift in the population toward a higher fluorescence. This was confirmed when .20% of the population from Q3 in the mouse IgG control shifted to Q4 upon HPRT treatment.

Of the three salvage pathway enzymes evaluated, only HPRT had a significant movement of the cell population toward a higher fluorescence, indicating the presence of HPRT on the surface of H460 cells. Statistical analysis shows significant HPRT binding on the surface of H460 cells (P=0.0036).

Abbreviations: APRT, adenine phosphoribosyltransferase; DCK, deoxycytidine kinase; HPRT, hypoxanthine guanine phosphoribosyltransferase.

Flow cytometry shows significant HPRT expression on the surface of A549 and H460 cells

When treated with anti-HPRT fluorescent antibodies, both A549 and H460 cancer cells had an increase in the fluorescent population (Figures 5-1C and 5-2). A 28% shift in the population is observed in H460 cells (Figure 5-1C), while a 12% shift is observed in A549 cells (Figure 5-3). Statistical analysis comparing anti-HPRT-treated cells with isotype IgG controls showed a statistically significant difference in H460 and A549 cells (Figures 5-1C and 5-2C). Thus, these data show a significant association between HPRT and the surface of non-small-cell lung cancer cells. This analysis also revealed a significantly higher HPRT surface expression in H460 cells when compared to A549 (Figure 5-3).

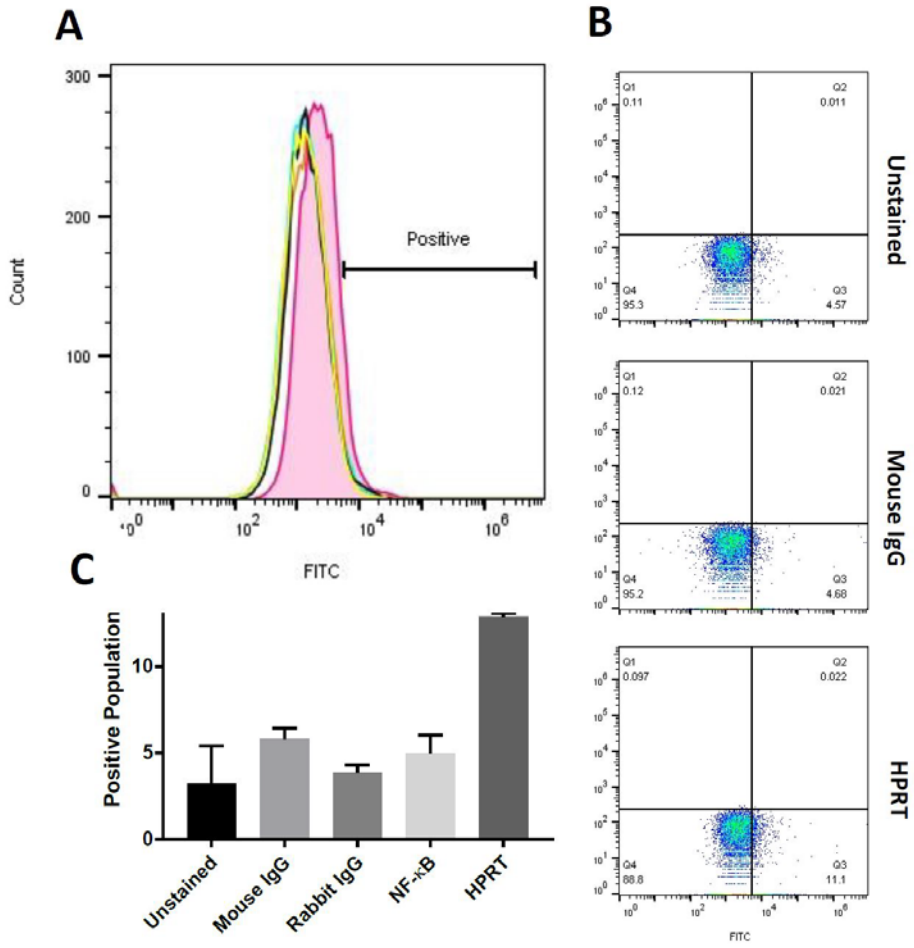

Figure 5-2. *HPRT surface expression on A549 non-small-cell lung cancer cells.* Notes: The following samples were utilized in order to evaluate the expression of APRT, DCK, and HPRT on the surface of H460 cells: unstained (autofluorescence), mouse IgG (nonspecific binding), rabbit IgG (isotype control), NF-κB (cytosolic protein control), and CD44 (positive surface antigen). (A) Although not as prominent as the population shift in H460 cells (Figure 5-1C), A549 cells treated with anti-HPRT antibody (pink) have a clear shift in the population toward a higher fluorescent value, indicating the presence of HPRT antigen on the surface of A549 cells. (B) When treated with anti-HPRT antibody there is a shift in the cell population from Q4 to Q3 of an average of 8% when populations are compared to unstained and mouse IgG Q3 populations. (C) Statistical analysis reveals significant HPRT binding on the surface of A549 cells (P=0.0245) when compared to controls. ***P<0.001.

Abbreviations: APRT, adenine phosphoribosyltransferase; DCK, deoxycytidine kinase; HPRT, hypoxanthine guanine phosphoribosyltransferase.

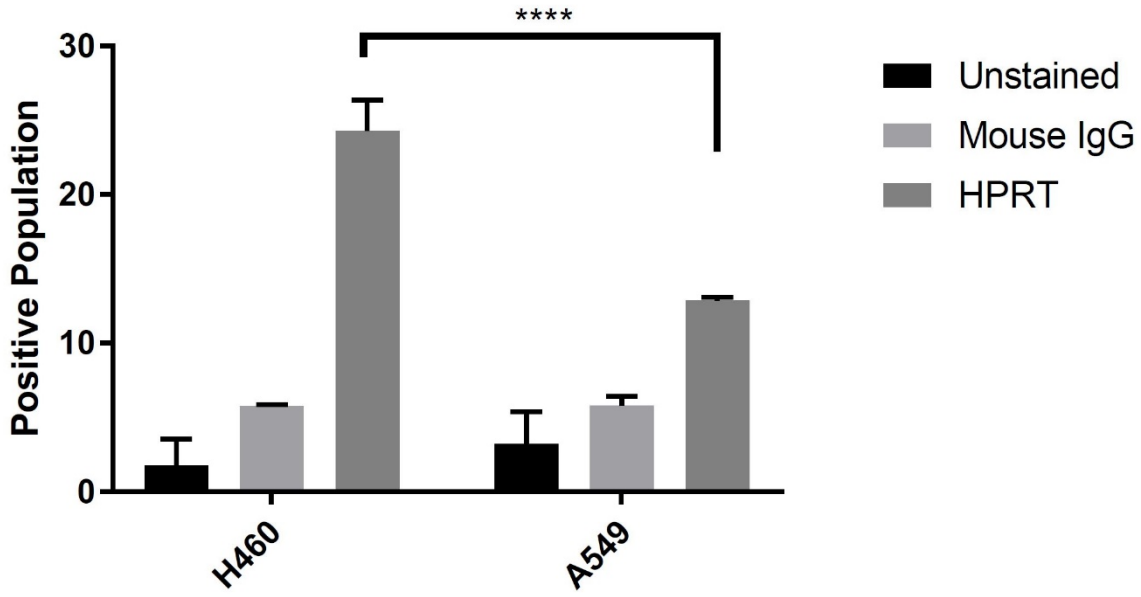

Figure 5-3. *Levels of HPRT expression compared between A549 and H460 cells.* Notes: While both A549 and H460 cells show a statistically significant increase in the surface expression of HPRT, H460 cells had a significantly higher expression (P,0.0001). H460 cells are a faster growing cell line, with a growth rate almost double that of A549 cells. As a result, HPRT expression on the surface of non-small-cell lung cancer cells may directly correspond to cell proliferation. ****P<0.0001.

Abbreviation: HPRT, hypoxanthine guanine phosphoribosyltransferase.

Confocal microscopy confirms that HPRT is bound to the surface of the cell

In order to confirm that HPRT was not bound to cytoplasmic protein, the surface expression of HPRT was further evaluated with confocal microscopy (Figure 5-4). Images obtained from cells treated with membrane dye and FITC antibody stain were overlapped to show colocalization of treated antigen on the plasma membrane of the cancer cell. When cells are treated with anti-HPRT antibody, a yellow pigment appears in the merged image, which indicates a direct relationship between the plasma membrane dye and the FITC dye. No other

treatment experienced this same overlapped pigmentation, which confirms the relationship between HPRT and the plasma membrane of H460 cells.

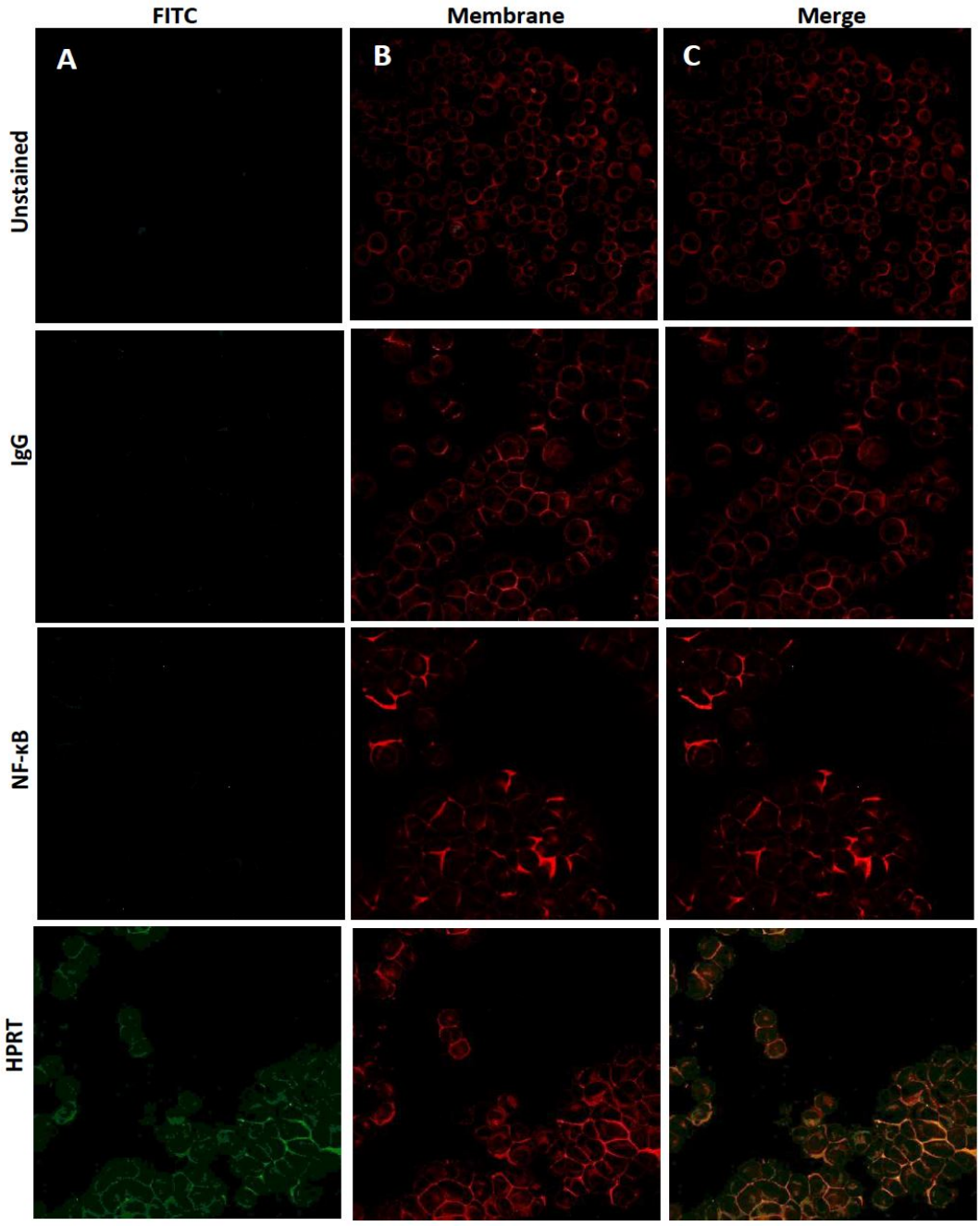

Figure 5-4. *Plasma membrane colocalization with HPRT in H460 cells*. Notes: H460 cells were dyed with both a FITC dye and a Rhodamine Red membrane dye to label antibody treatments and the plasma membrane, respectively. Utilizing unstained cells, IgG-treated cells, and NF-κB-treated cells as controls, plasma membrane associations were evaluated to determine whether any of the treatments significantly bound to the membrane of H460 cells. (A) Each sample was analyzed and imaged by a 488 nm laser to illuminate FITC-positive cells. These images show the binding of the respective antigen treatment. (B) Samples were also imaged in a 594 nm laser to show rhodamine-positive cells. This dye binds to the plasma membrane of all cells. (C) The two images obtained

from columns A and B were merged to show associations between treated antibodies and the plasma membrane of cells. These results show a clear overlap between cells treated with anti-HPRT antibody and those treated with the membrane dye. This demonstrates a clear association between HPRT and the plasma membrane of H460 cells.

Abbreviation: HPRT, hypoxanthine guanine phosphoribosyltransferase.

HPRT antigen is scattered randomly across the surface of H460 cells

The location of the HPRT protein on the surface of H460 cells was also analyzed with scanning electron microscopy (Figure 5-5). The gold elemental peak along with the elemental composition of each sample reveals the changes in the surface gold percentages when cells are exposed to primary antibodies. Images obtained from this analysis show HPRT on the cell surface, but there is no apparent clustering of the antigen as gold particles are scattered across the cell randomly. EDAX analysis showed that cells treated with anti-HPRT antibody had an increase in the average gold weight percentage of 10.39% in comparison with only 8.75% for IgG controls. With a P-value of 0.012 (Figure 5-6), these data indicate a statistically significant presence of HPRT on the surface of H460 cells while also demonstrating that the antigen shows no patterns of expression.

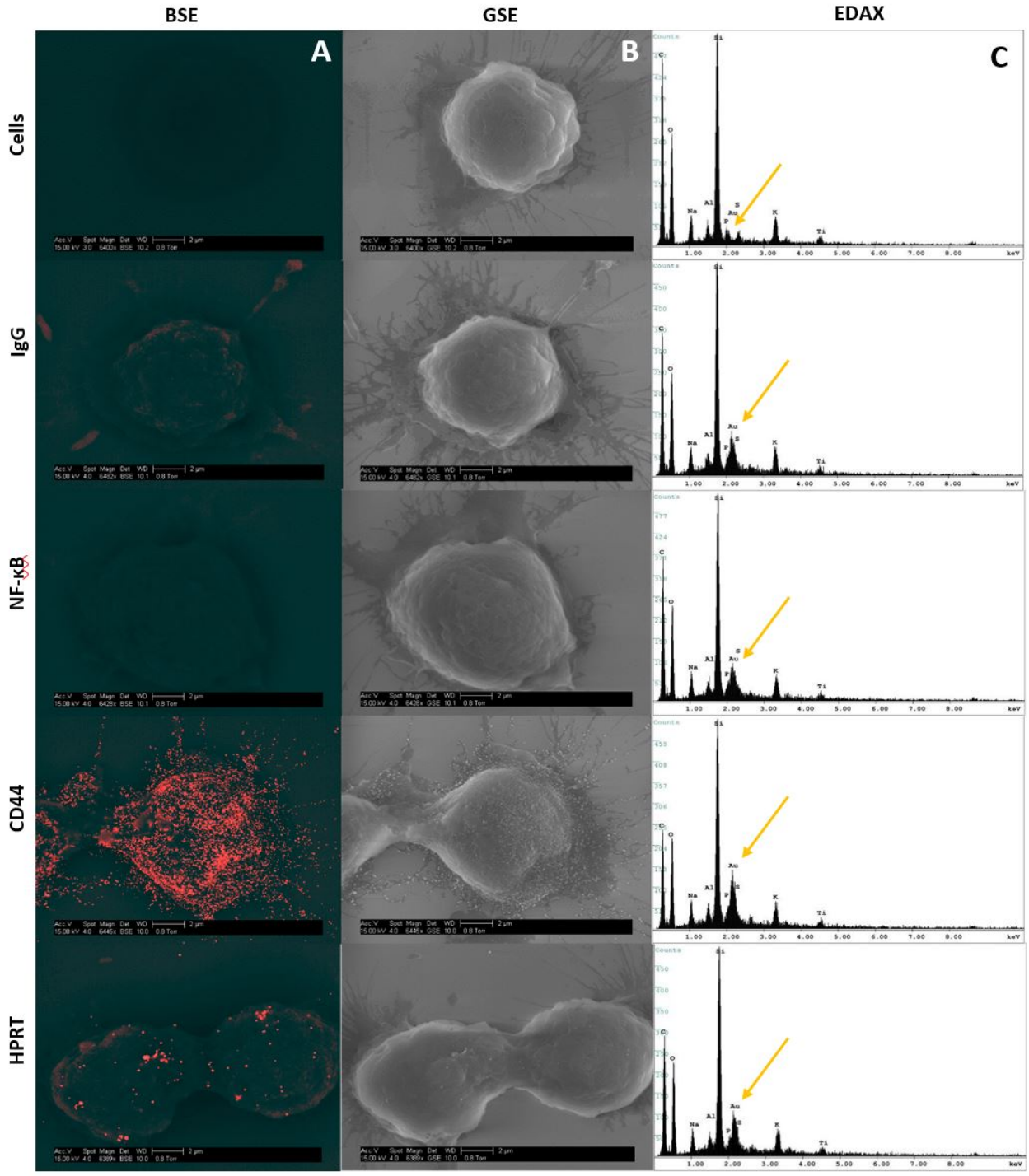

Figure 5-5. *Scanning electron microscopy images and resulting EDAX in H460 cells.* Notes: Cells were labeled with gold toward their respective antibody treatment. (A) Images were obtained using a BSE . This detector is specialized to image heavy metals within samples and highlights enhanced gold within the sample. Any distinguishable large particles of gold represent a bound antibody enhanced with gold. (B) Images were also obtained with a GSE , which showed cell morphology to ensure correct cell structure and integrity. (C) EDAX analysis of each sample showed the gold elemental peaks for all the elements present within the sample. Silicon is the highest represented element

because cells were mounted on silicon cover slips for analysis. The gold elemental peak is indicated with a gold error. Images obtained from this analysis show the exact location of the HPRT bound to the surface of the cell and show no clear pattern indicating a random distribution of the antigen across the surface of the cell.

Abbreviations: BSE , back scatter electron; EDAX, energy-dispersive analysis X-ray; GSE , gaseous side electron; HPRT, hypoxanthine guanine phosphoribosyltransferase.

HPRT expression in H460 cells is higher than expression within A549 cells

While HPRT is present on both H460 and A549 cells, there is a statistically significant difference between the amount of the protein expressed between the two cell lines (Figure 5-3).

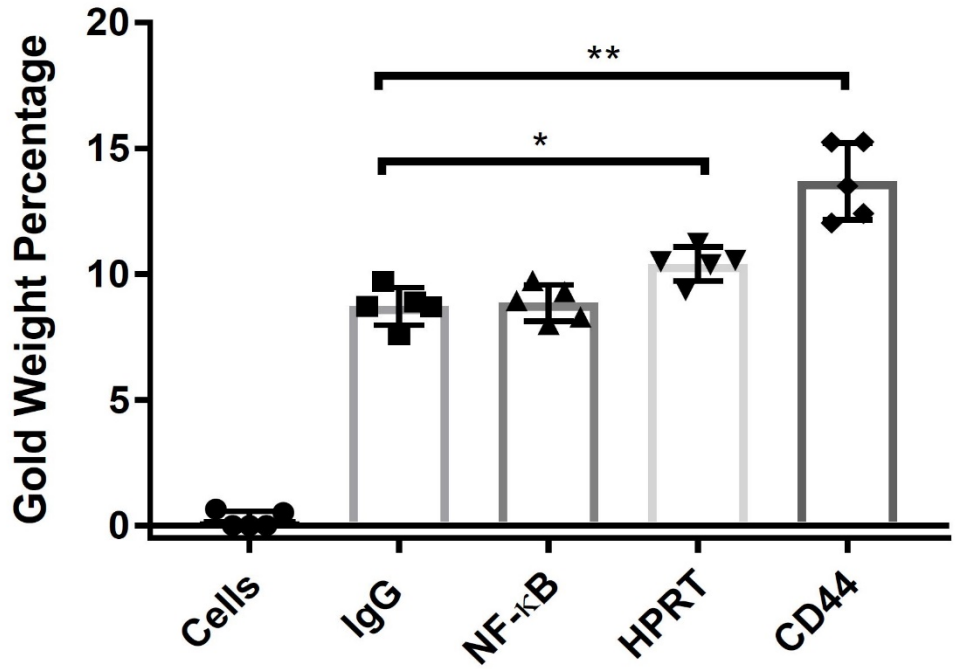

Figure 5-6. *Gold percentage of H460 cells*. Notes: The gold elemental composition of each sample is denoted on the Y-axis. The increase in the gold percentage when cells were exposed to HPRT and CD44 shows a quantifiable increase in the gold present on the outside of the cell. Cells exposed to HPRT antibody had a gold weight of ~10.4%, which is statistically significant to the IgG controls used for background binding (P=0.0159). These data indicate a statistically significant presence of HPRT on the surface of H460 cells. *P<0.05; **P<0.01.

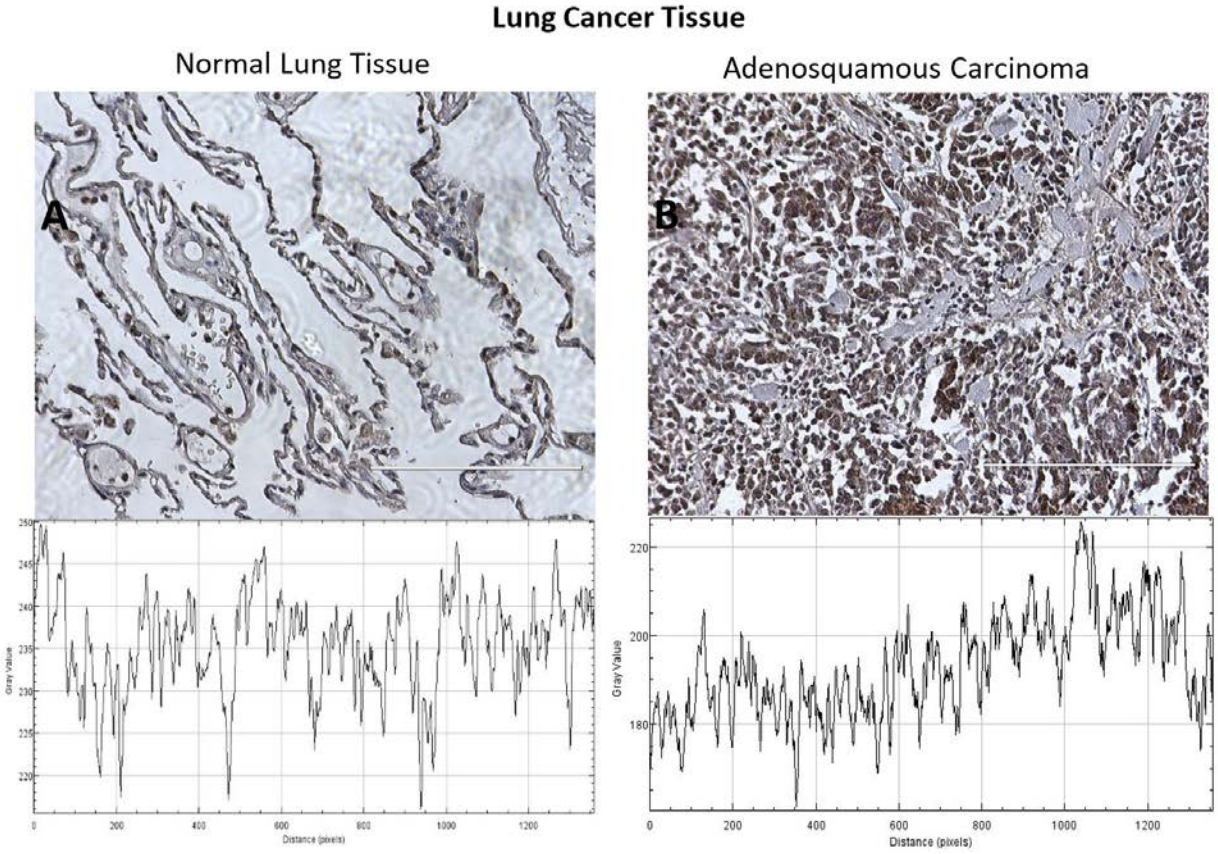

Figure 5-7. *Evaluation of HPRT expression within patient tissue*. Notes: All tissues were stained with a monoclonal anti-HPRT antibody. The gray plots for each of the tissues are imaged below. (A) Tissue from a 69-year-old female patient with stage III basaloid carcinoma and (B) normal tissue from a 59-year-old female patient. The malignant tissue is significantly darker than the corresponding normal tissue. These tissues show an upregulation of HPRT within malignant cells.

Abbreviation: HPRT, hypoxanthine guanine phosphoribosyltransferase.

H460 cells have ~50% more protein on the surface when compared to A549 cells. This altered expression may directly correspond to tumor proliferation as H460 cells grow at a much faster rate, approximately double that of A549 cells. These results suggest that HPRT surface expression may be more prevalent in rapidly proliferating cells as the need for protein is increased.

HPRT is elevated in half of the patients with lung carcinoma

In ~50% of patients evaluated, there was a significant increase in HPRT expression (Figure 5-7). This increase in protein was significant when compared to normal lung tissue, whose expression was minimal. This different expression demonstrates HPRT variability between patients as only half of the patients experienced this increase in protein levels. In addition, the presence of HPRT also appears to be dependent on cell proliferation. On average, there was an increased expression of HPRT in stage III tissues in comparison with other tissue types (P=0.049). This indicates that HPRT overexpression may depend on cell proliferation as stage III tissue is more aggressive and has a higher proliferative capacity than stage II or stage I tissue (Figure 5-8).

Discussion

HPRT is a salvage pathway enzyme involved in the production of both guanine and inosine bases. The enzyme functions by transferring phosphoribose from PRPP to hypoxanthine or guanine bases to form IMP and GMP, respectively [10,12]. Because of the proliferative capabilities of cancer cells and the large demand for nucleotide production, an upregulated expression at the HPRT locus is hypothesized in these environments [484]. We have found that there is significant HPRT colocalization with the plasma membrane in H460 and A549 cancer cells. This same expression is not observed for the salvage pathway enzymes DCK and APRT, indicating that HPRT may possess a role in cancer that is not shared by other salvage pathway enzymes and could be a useful biomarker target for non-small-cell lung cancer.

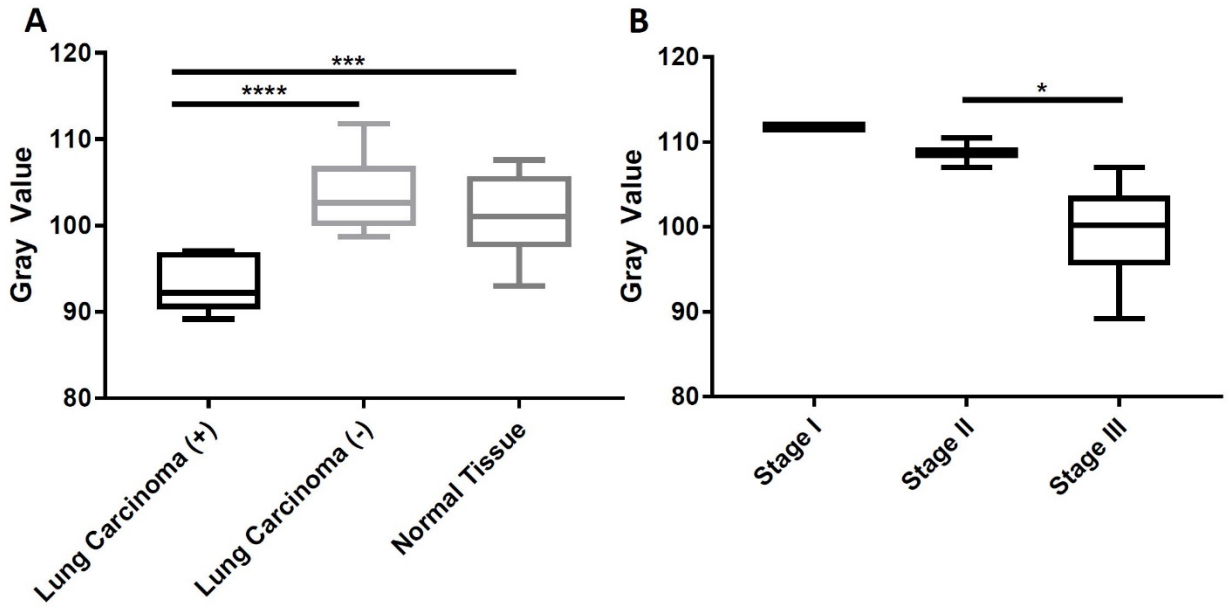

Figure 5-8. *Statistical analysis of HPRT expression within patient tissue.* Notes: Quantification of tissue was conducted utilizing a gray scale. The lower the gray value, the darker the tissue is stained. (A) There is a statistically significant presence of HPRT in approximately half of the tissues obtained from patients. This increased expression shows that in some patients there is an upregulation of the protein. As HPRT is a housekeeping gene, there is a basal level of expression present within the tissue. An isotype control was run to establish the gray value of unstained tissue and to account for nonspecific antibody binding. (B) Of the tissues evaluated there was a significant difference in HPRT presence in stage III tissue, indicating an increase in HPRT presence as cancer progressed and proliferated. *P<0.05; ***P<0.001; ****P<0.0001.

Abbreviation: HPRT, hypoxanthine guanine phosphoribosyltransferase.

The reason for the surface expression of HPRT is currently unknown, and the purpose of its external presentation in lung cancer cells can only be speculated [485]. We hypothesize that this unique surface expression may point to a secondary function of HPRT that goes beyond its primary role as a purine synthesis enzyme. HPRT is already known to have a secondary regulatory role in neural development and purine synthesis as patients who have a deficiency of the enzyme develop a disease known as Lesch–Nyhan syndrome. This disease is characterized by severe neurological illness, hyperuricemia, and purine overproduction. Purine overproduction is directly related to the loss of HPRT function and demonstrates the enzyme's necessary

responsibility in cells to regulate and control certain pathways. The regulatory role of HPRT may be important for its unique role within cancer. Loss of strict HPRT regulation may enhance cellular proliferation and may contribute to tumor development as cells no longer have regulation of processes normally controlled or limited by HPRT. Further defining these secondary functions may provide additional information about the unique cellular interactions present in the tumor microenvironment [22,486].

Although there is significant HPRT expression on A549 and H460 cells, the relative protein level is not equal between the cell lines. The differential expression of HPRT between these two cancer cell lines may be attributed to the growing capacity of the cells, as H460 cells grow at a rate that is nearly double the rate of A549 cells. In addition, H460 cells are known to be highly aggressive due to their increased vascularity and ability to metastasize [487,488] It is likely that the surface expression of HPRT may correspond with proliferation and tumor aggressiveness. This is further explored as stage III tissue stained with HPRT appears to be more prevalent in patient tissue.

We have shown this phenomenon in vitro, but further research into the in vivo expression is required to confirm whether HPRT could be utilized as a biomarker within patients, although we report a significant increase in HPRT within some patients. If found expressed in vivo, HPRT could be utilized in therapies to effectively treat non-small-cell lung cancer.

Conclusion

HPRT is expressed on the surface of NCI-H460 and A549 non-small-cell lung cancer cells and may be used as a biomarker target.

Acknowledgments

We thank the Simmons Center for Cancer Research for funding this work. We also thank Connor Peck for his editorial comments on the manuscript

CHAPTER 6

Examination of Hypoxanthine Guanine Phosphoribosyltransferase as a biomarker for colorectal cancer patients.

Michelle H. Townsend, Abigail M. Felsted, Weston Burrup, Evita G. Weagel, Edwin J. Velazquez, K. Scott Weber, Richard A. Robison, and Kim L. O'Neill.

Citation: Michelle H. Townsend, Abigail M. Felsted, Weston Burrup, K. Scott Weber, Richard A. Robison, and Kim L. O'Neill. Examination of Hypoxanthine Guanine Phosphoribosyltransferase as a biomarker for colorectal cancer patients. Molecular and Cellular Oncology. 2018. DOI: https://doi.org/10.1080/23723556.2018.1481810

The following chapter is taken from an article published in Molecular and Cellular Oncology. All content and figures have been formatted for this dissertation.

Abstract

The aim of this study is to investigate these enzymes as possible biomarkers in two colorectal cancer cell lines: HT29, SW480, SW620, and Colo205. With 1,168,929 individuals currently diagnosed with colorectal cancer in the United States, there remains a need to find biomarkers to improve diagnosis and expand treatment options for patients. Due to their role in proliferation and cell cycle regulation, we hypothesized an increase in salvage pathway enzyme (APRT, DCK, and HPRT) expression and possible presentation within colon cancer cells. Enzyme surface localization was assessed utilizing confocal microscopy, flow cytometry, and scanning electron microscopy. General protein expression was evaluated utilizing immunohistochemistry and Western blot analysis. While we found no statistically significant presence of either APRT or DCK on the membranes of SW620, Colo205, and HT29 cells, we found significant expression of HPRT on the surface of HT29, SW480, and SW620 cells. The average population fluorescence increased by 28%, 58%, and 40% in HT29, SW620, and SW480 cells, respectively, when compared to isotype controls. Confocal microscopy images revealed direct overlap between SW620 cells stained with a membrane dye and anti-HPRT antibody, indicating co-localization on the plasma membrane. In addition, cells treated with gold labelled HPRT antibody experienced significant changes in gold weight percentage on both SW620 and HT29 cells when compared to isotype controls. When evaluating expression within normal tissue, there was insignificant levels of HPRT binding. These data collectively suggest that HPRT may be a possible biomarker target for the identification and treatment of colorectal cancer.

Introduction

Colorectal Cancer (CRC) is one of the leading causes of death in the United States. Every year 49,700 individuals die as a result of CRC while an estimated 1,168,929 are currently diagnosed with the disease [462]. CRC is one of the most common cancers in the western world as 1 in 21 men and 1 in 23 women are predicted to develop the disease[489–491].

In order to combat disease progression, a variety of markers have been identified that act as useful tools for predicting tumor aggressiveness, mucin content, and aneuploidy in cancer DNA [492–494]. These markers are valuable when determining treatment options for individuals with a unique blend of cancer characteristics. Recent research using cultured cancer cells have identified cancer biomarkers such as the 1,25-Dihydroxyvitamin D3 receptor that may act as a marker for colon carcinoma cell differentiation and growth. Receptors such as Vitamin D receptor are upregulated on colon cancer cell surfaces and can serve as a target for tumour reduction and elimination. Additionally, markers such as CD133 and CD44 have also been identified for the elimination of cancer stem cells [489,495]. While a number of tumor antigens have been identified, additional markers will aid in better understanding colorectal cancer disease progression and could lead to additional treatment options.

In the search to further characterize colorectal cancer cells, we decided to evaluate the salvage pathway enzymes Hypoxanthine Guanine Phosphoribosyltransferase (HPRT), Adenine Phosphoribosyltransferase (APRT) and Deoxycytidine Kinase (DCK) as a possible upregulated targets. Salvage pathway enzymes act as recycling agents, reusing the components of old nucleotides to skip energetically expensive steps in the formation of nucleotide bases [9]. The salvage pathway is the chosen method of nucleotide synthesis for a majority of the cell cycle in humans as 90% of free purines are recycled [10]. Responsible for the salvage of adenine in the cell cycle, APRT is found constitutively expressed in a majority of mammalian cells [496]. DCK is

primarily involved in the phosphorylation of deoxycytidine in the production of cytosine [497]. HPRT functions by transferring phosphoribose from phosphoribosyl pyrophosphate (PRPP) to hypoxanthine or guanine bases in the purine biosynthesis of inosine and guanine [10,12].

A deficiency of HPRT results in a spectrum of diseases that directly correspond with the availability of the protein. Individuals with a complete lack of functional HPRT will develop Lesh-Nyhan syndrome, while individuals with a partial deficiency will develop gout-like symptoms characteristic of Kelley-Seegmiller syndrome [21,22,498]. Because the gene is located on the X chromosome, it is an X-linked recessive condition that predominantly affects males of diseased families. Evaluation of the HPRT gene has become a common biomarker for mutational assessment, and over 500 mutations in the gene have been described [23].

Having functional salvage pathway enzymes is important in the survival and functionality of mammalian cells. Salvage enzymes, such as HPRT, are known as common housekeeping genes, and are integral in several daily cellular functions regulating cell proliferation and cell cycle progression [10,499]. We evaluated these enzymes because of their intimate role in the production of nucleotides necessary to maintain rapid cell proliferation. Additionally, these enzymes maintain responsibility for synthesizing GTP and ATP which provide the critical energy source for several cellular processes that are found upregulated within malignant cells [2,500,501].

The aim of this study was to evaluate HPRT, APRT, and DCK as potential biomarkers for CRC. We assessed the expression of the proteins on the surface of four CRC cell lines in addition to evaluation within tumor tissue and normal tissue to determine the clinical relevance of the protein expression. Results from these experiments could provide an additional marker for the characterization of colorectal cancer.

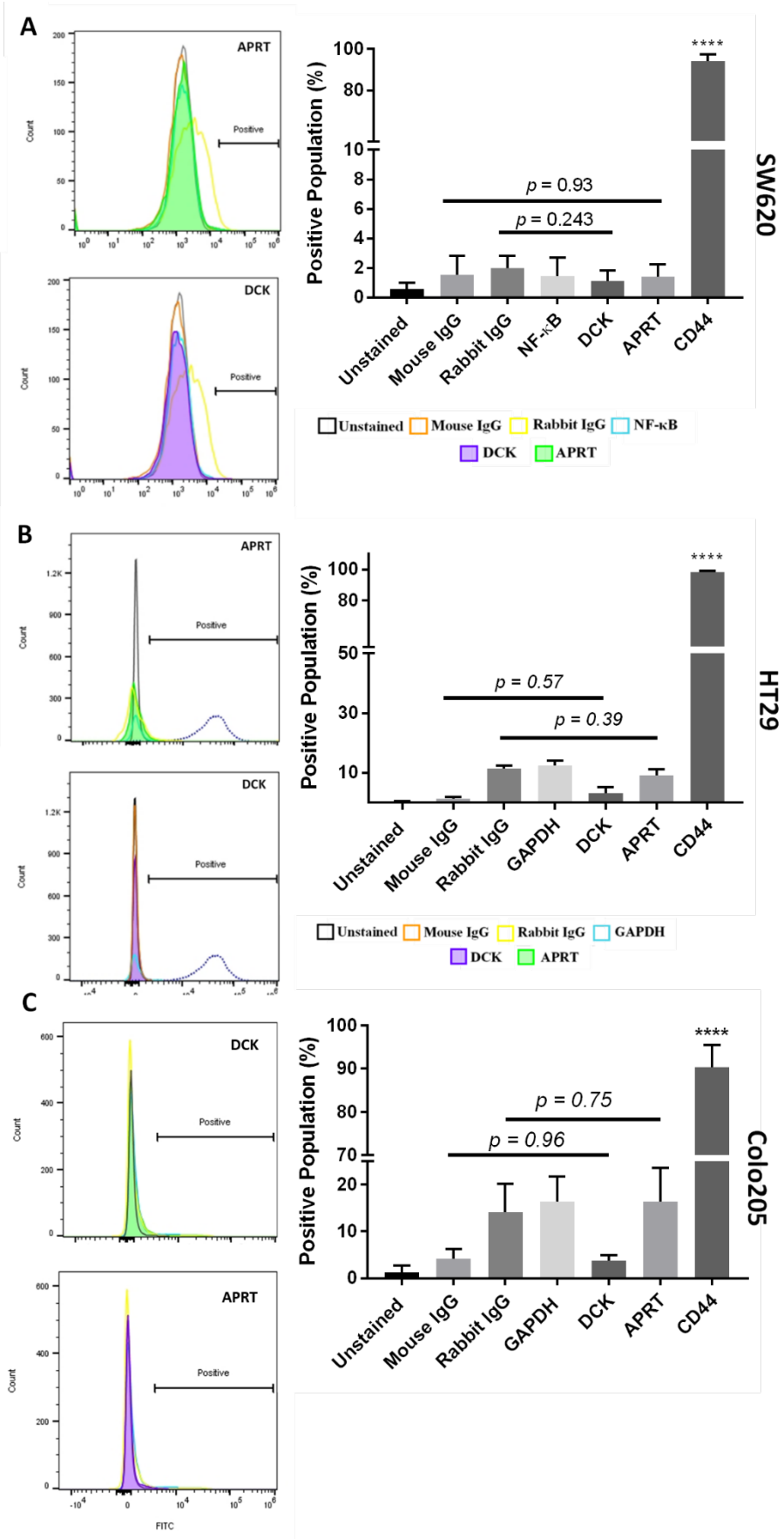

Figure 6-1. *Analysis of APRT and DCK expression on SW620 and HT29 colon cancer cells*. A, Cells treated with APRT antibodies experienced no shift in the fluorescent population and had similar fluorescent signatures to isotype controls. B, Cells treated with DCK antibodies experienced an insignificant change in the population when compared to isotype controls, indicating no surface presence. Statistical analysis of APRT and DCK binding reveal insignificant levels of either protein on the surface of SW620 cells. APRT antibodies were mouse and were compared against mouse isotype controls, and DCK antibodies were rabbit and were compared against rabbit isotype controls for statistical analysis. Insignificant shifts in the fluorescent intensity of the cells was observed when treated with both B, APRT and DCK antibodies. Statistical analysis of APRT and DCK binding in HT29 cells showed insignificant levels of the proteins on the surface. C, Insignificant surface binding was also observed in Colo205 cells as well with no shifts in the fluorescent population upon treatment with either APRT or DCK antibodies.

Results

Flow cytometry reveals an overall increase in fluorescence when colon cancer cells were exposed to HPRT antibody, but not when treated with DCK or APRT antibodies.

Flow cytometry revealed no significant presence of APRT (p-value = 0.93) or DCK (p-value = .243) on the surface of SW620 cells (Figure 6-1). There was also no statistically significant presence of both enzymes (APRT, p-value = 0.39; DCK, p-value = 0.57) on the surface of HT29 cells or Colo205 cells (APRT, p-value = 0.75; DCK, p-value = 0.96). We did find that SW480, SW620, and HT29 cells had statistically significant HPRT expression on the surface of the cells. The average fluorescence of the cell population increased by 27.73% in HT29 (p-value = 0.013), 39.6% in SW480 (p-value = 0.0095), and 58.85% in SW620 cells (p-value = 0.0079) when compared to isotype controls (Figure 6-2). This indicates a strong presence of HPRT on the surface of the cells. Figure 6-2 shows insignificant isotypic binding, lower than 3% average of the total population (p-value = 0.374) in SW620 cells, 7% (p-value = 0.11) in HT29 cells, and 3.94% (p-value = 0.058) in SW480 cells. While these cell lines showed positive

HPRT surface localization, Colo205 cells showed no significant increase in the surface presence of HPRT (p-value = 099). All cells were gated to exclude dead cells and cell doublet populations.

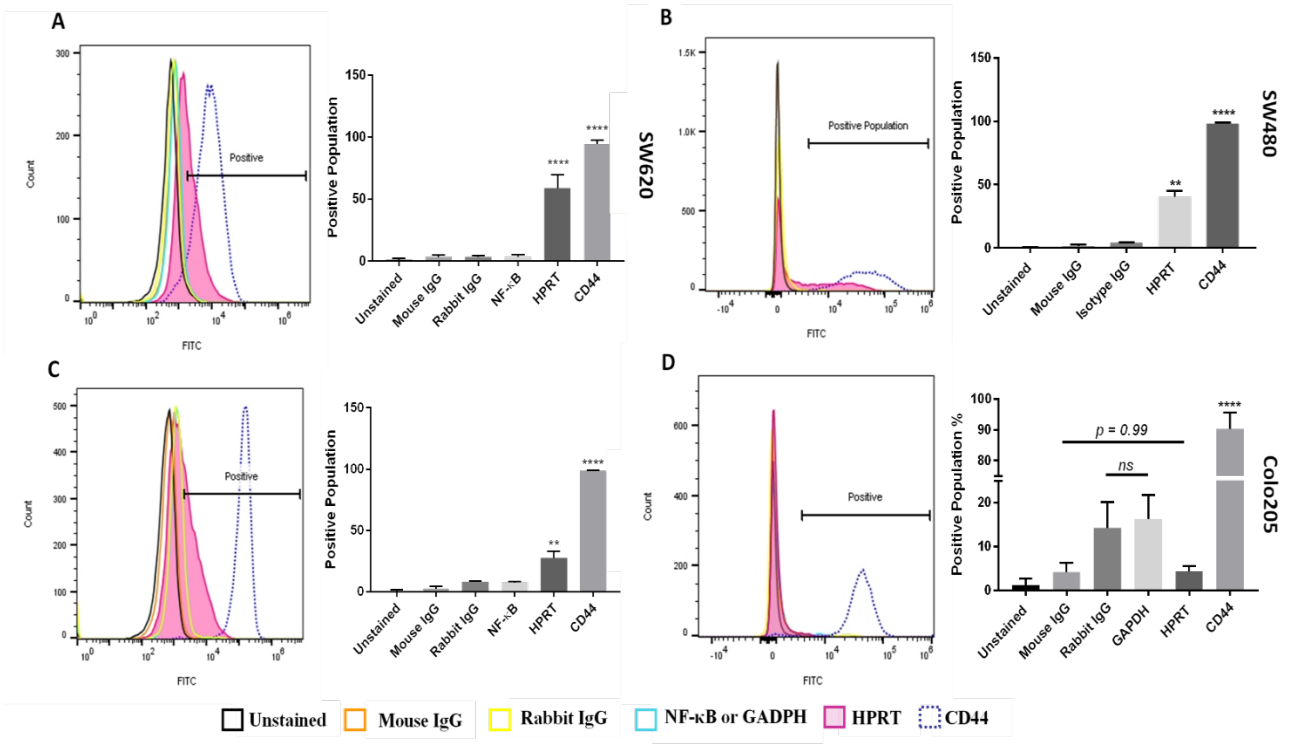

Figure 6-2. *Flow cytometry analysis of HPRT expression on HT29, SW480, and SW620 cells.* The following samples were utilized in order to evaluate the expression of HPRT on the surface of CRC cells: Unstained (auto-fluorescence control), Mouse IgG (Non-specific binding control), Rabbit IgG (Isotype control), NF-κB (cytosolic protein control), and CD44 (positive surface antigen). A, When treated with anti-HPRT antibody (pink), the histogram representation of the cell population showed a definitive shift in the population towards a higher fluorescence. Statistical analysis shows significant HPRT binding on the surface of SW620 cells (p value < 0.0001). B, SW480 cells treated with anti-HPRT antibody experienced a shift in fluorescent intensity, indicating HPRT surface localization. Upon statistical evaluation anti-HPRT treated cells show a significant difference when compared to isotype antibody controls (p-value = 0.0095). C, The same fluorescent shift in the population is seen when HT29 cells are exposed to anti-HPRT antibody. There was a shift in the population equivalent to 20%, which is statistically significant from the IgG controls (p value = 0.0016). While HPRT is statistically significant in both cell lines, the difference between the cell line expression is also statistically significant as SW620 cells have over 25% higher expression (p value = 0.0002). D, There was no significant change in the fluorescent population upon HPRT antibody treatment on the surface of Colo205 cells (p-value = 0.99).

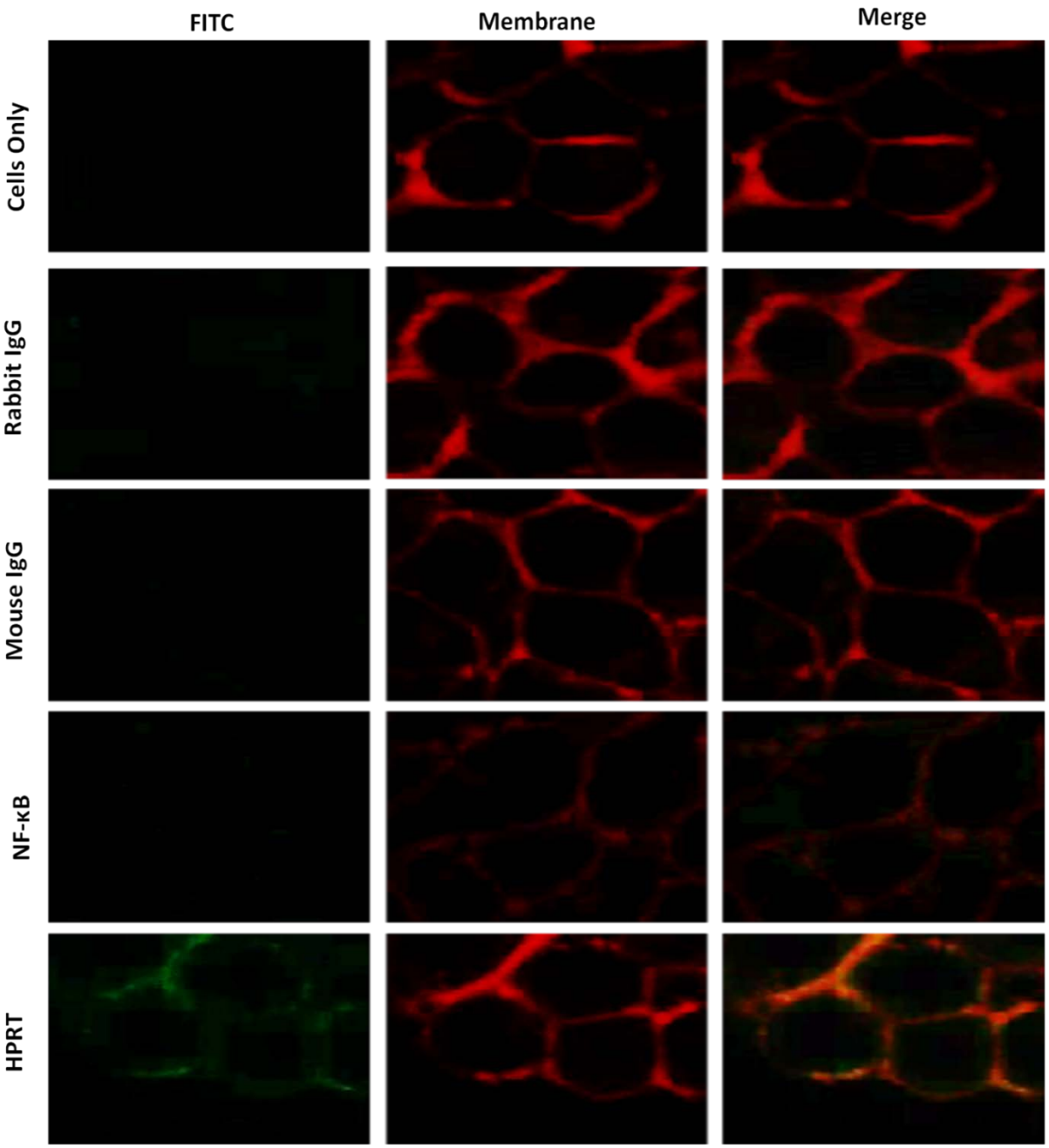

Figure 6-3. *Plasma membrane co-localization of HPRT in SW620 cells.* SW620 cells were dyed with both a FITC dye and a Rhodamine Red membrane dye to label antibody treatments and the plasma membrane respectively. A, Each sample was analyzed and imaged by a 488nm laser to illuminate FITC positive cells. These images show the binding of the respective antigen treatment. B, Samples were also imaged in a 594nm laser to show rhodamine positive cells. This dye binds to the plasma membrane of all cells. C, The two images obtained from column A and B were merged to show associations between treated antibodies and the plasma membrane of cells. These results show a clear overlap between cells treated with anti-HPRT antibody and those treated with the membrane dye.

HPRT is strongly associated with the plasma membrane of SW620 cells.

To ensure antibody binding was towards surface HPRT and not cytoplasmic HPRT, confocal microscopy was performed to visualize protein localization on SW620 cells (Figure 6-3). In all controls we observed a minimal FITC signal, indicating insignificant antibody binding, with the exception of samples treated with anti-HPRT. SW620 cells treated with anti-HPRT FITC antibody had a noteworthy association with the plasma membrane. These images reveal a direct overlap between the plasma membrane and antibodies targeting HPRT. In addition, the FITC channel reveals a distinguishable external presence of HPRT as fluorescent antibody binding is only seen on the periphery of the cells.

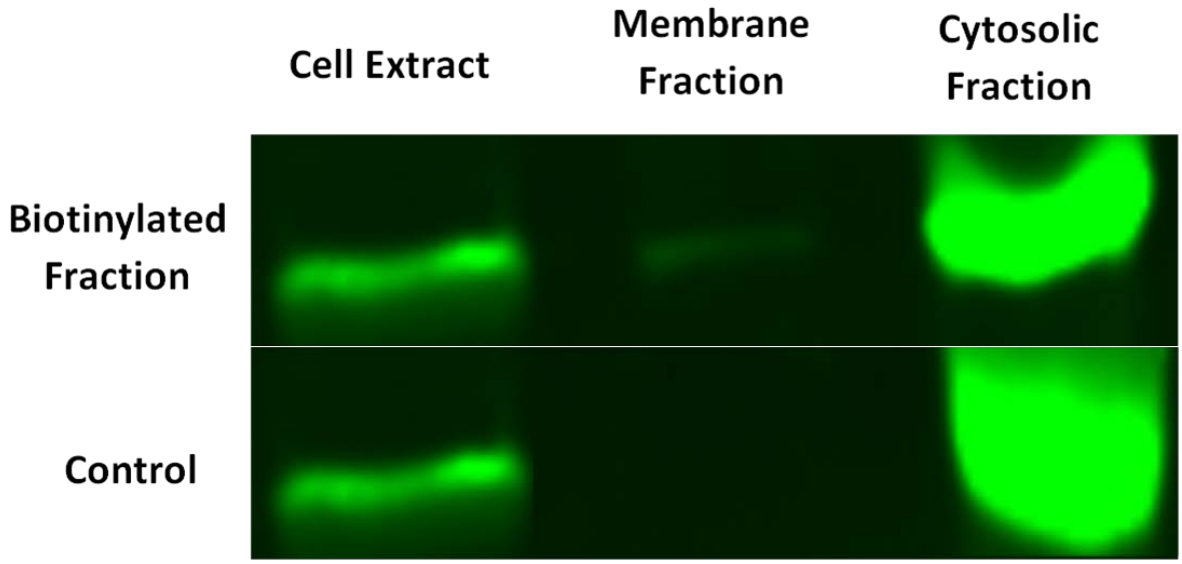

Figure 6-4. *Western analysis of HPRT expression in both cytosolic and membrane fractions*. Surface proteins were biotinylated and isolated for analysis. SW620 cell extract, membrane fractions, and cytosolic fractions were probed for HPRT along with a non-biotinylated control. This data shows that there is a very significant presence of HPRT within SW620 cytosol in addition to a clear presence on the surface of the cells.

Western Blot analysis shows there is a significant presence of HPRT within SW620 cancer cells. Along with a clear presence of the protein, this analysis also confirmed HPRT as a membrane associated protein, as it is found in the biotinylated fraction of the cells (Figure 6-4).

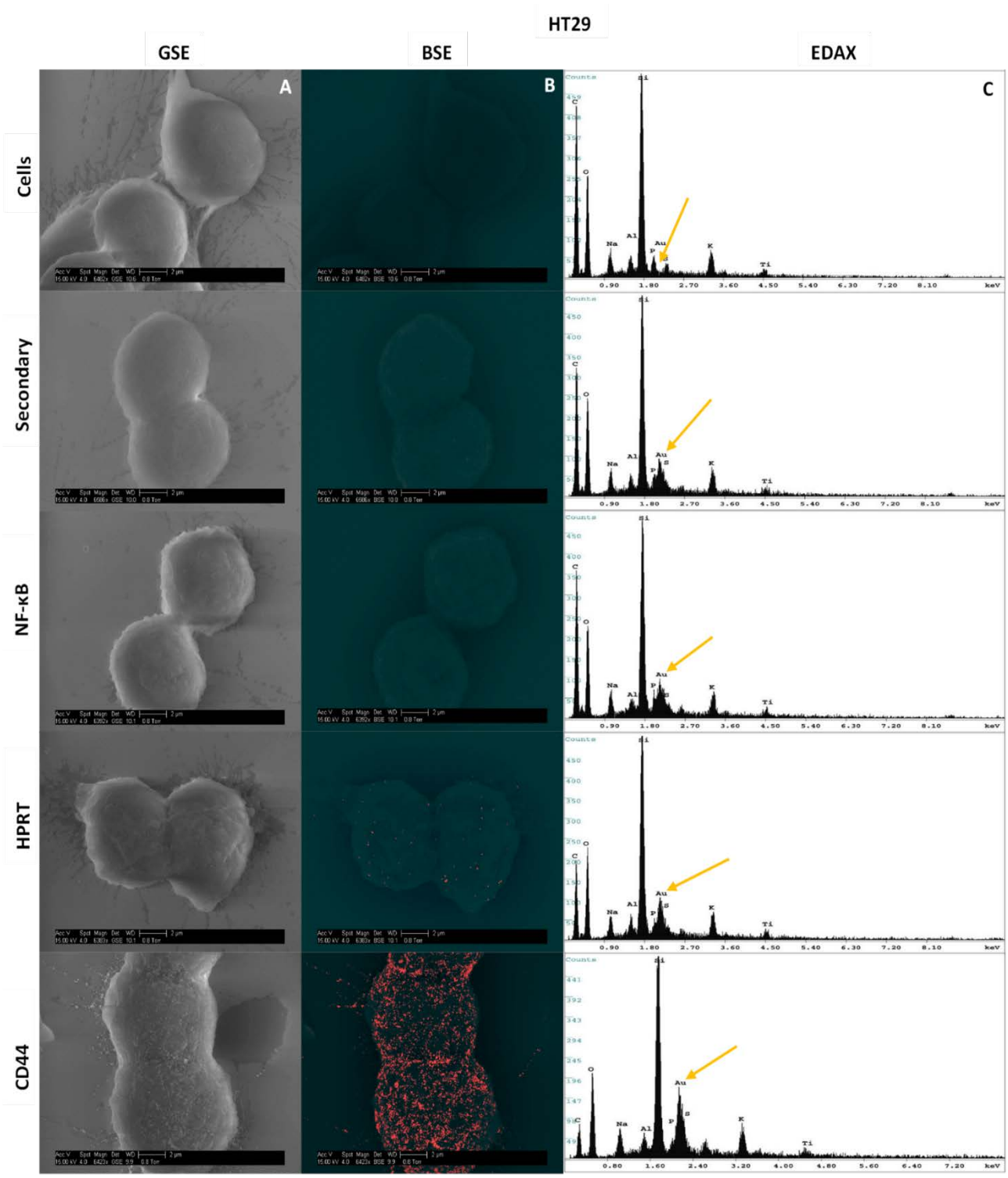

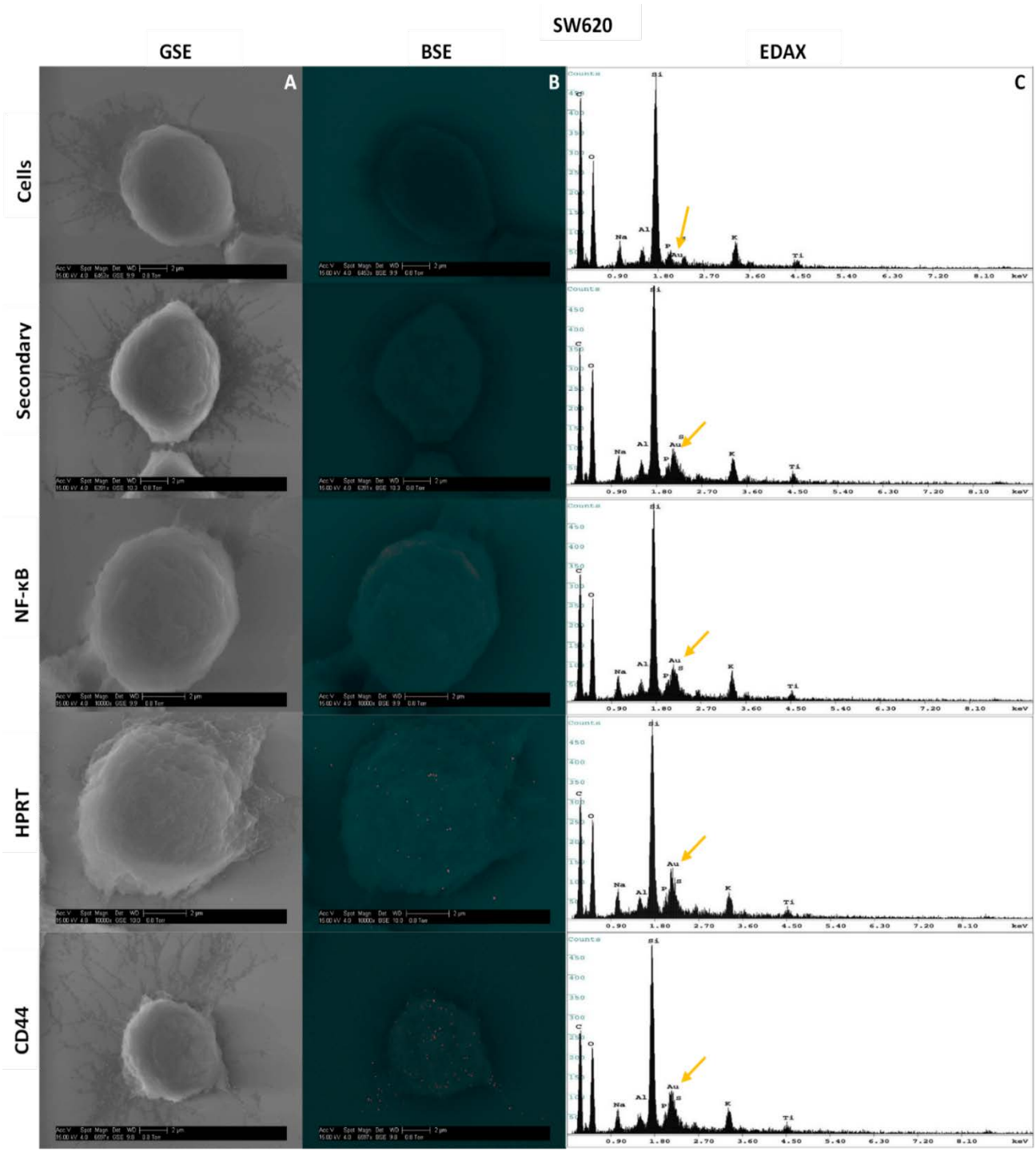

Figure 6-5. *Scanning Electron Microscopy Images and resulting EDAX in HT29 and SW620 cells.* Cells were labelled with gold towards their respective antibody treatment. The size scale is shown in each image and represents a 2µm distance. 5a-A & 5b-A, Images were obtained using a Back Scatter Electron (BSE) detector. This detector is specialized to image heavy metals within samples, and highlights enhanced gold within the sample. Any distinguishable large particles of gold represent a bound antibody. 5a-B & 5b-B, Images were also obtained with a Gaseous Side Electron (GSE) detector, which showed cell morphology to ensure correct cell structure and integrity.

5a-C & 5b-C, EDAX analysis of each sample showed the gold elemental peaks for all the elements present within the sample. Silicon is the highest represented element because cells were mounted on silicon cover slips for analysis. The gold elemental peak is indicated with a gold arrow. Images obtained from this analysis show the exact location of the HPRT bound to the surface of the cell, and show no patterns indicating a random distribution of the protein across the surface of the cell.

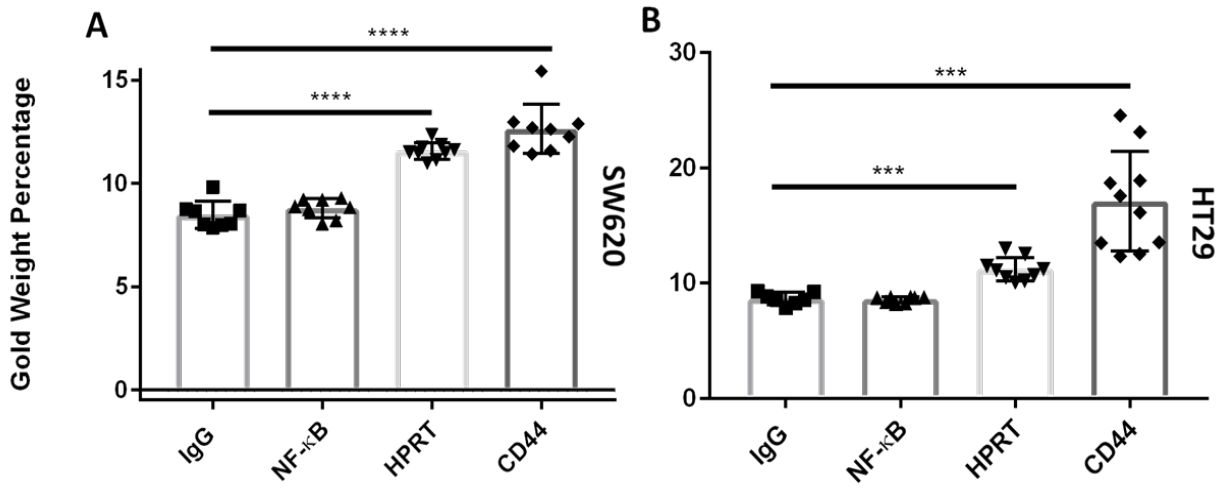

Figure 6-6. *Gold percentage of SW620 and HT29 cells.* The gold elemental composition of each sample is denoted on the Y-axis. The increase in the gold percentage when cells were exposed to HPRT and CD44 shows a quantifiable increase in the gold present on the outside of the cell. A, Gold elemental percentages in SW620 cells exposed to HPRT antibody had a gold weight of approximately 11.2%, which is statistically significant to the IgG controls used for background binding (p value < 0.0001). These data indicate a statistically significant presence of HPRT on the surface of SW620 cells. B, Gold elemental percentages in HT29 cells. Gold weight was approximately 10.4% with a p value < 0.0001.

Scanning Electron Microscopy reveals a random distribution of the protein across the surface of HT29 and SW620 cells.

To evaluate whether surface HPRT binding was distributed across the membrane randomly, we utilized scanning electron microscopy to physically visualize the position of the enzyme on the surface of the cells. As pictured in Figures 6-5 and 6-6, both cell lines show an increase in gold particle binding when exposed to anti-HPRT antibodies. This same increase in expression is not seen with isotype controls and further implicates HPRT on the surface of the

cells. The protein appears to be randomly presented across the plasma membrane with no clear pattern of expression. EDAX analysis (Figure 6-6) for each sample shows an increase in the gold percentage when cells were treated with anti-HPRT antibodies. A significant increase in sample elemental gold percentages is seen as SW620 cells (p-value of 8.14x10-6) and HT29 cells (p-value of 1.74x10-4) were treated with gold labelled HPRT antibodies. This analysis provides a further confirmation that HPRT is present on the surface of SW620 and HT29 colon cancer cells.

Within normal colon samples from patients, there is insignificant levels of HPRT binding.

To evaluate whether HPRT would be useful as a biomarker target for CRC patients, we measured the proteins levels on the surface of normal tissue. Flow cytometry revealed insignificant HPRT presence within normal colon tissue from healthy patients when compared to isotype controls (p value = 0.998) and unstained controls (p value = 0.996). When compared to a CD44 control, HPRT levels were minimal and shared similar binding to that of the isotype control, indicating its presence to be negligible in normal tissue (Figure 6-7).

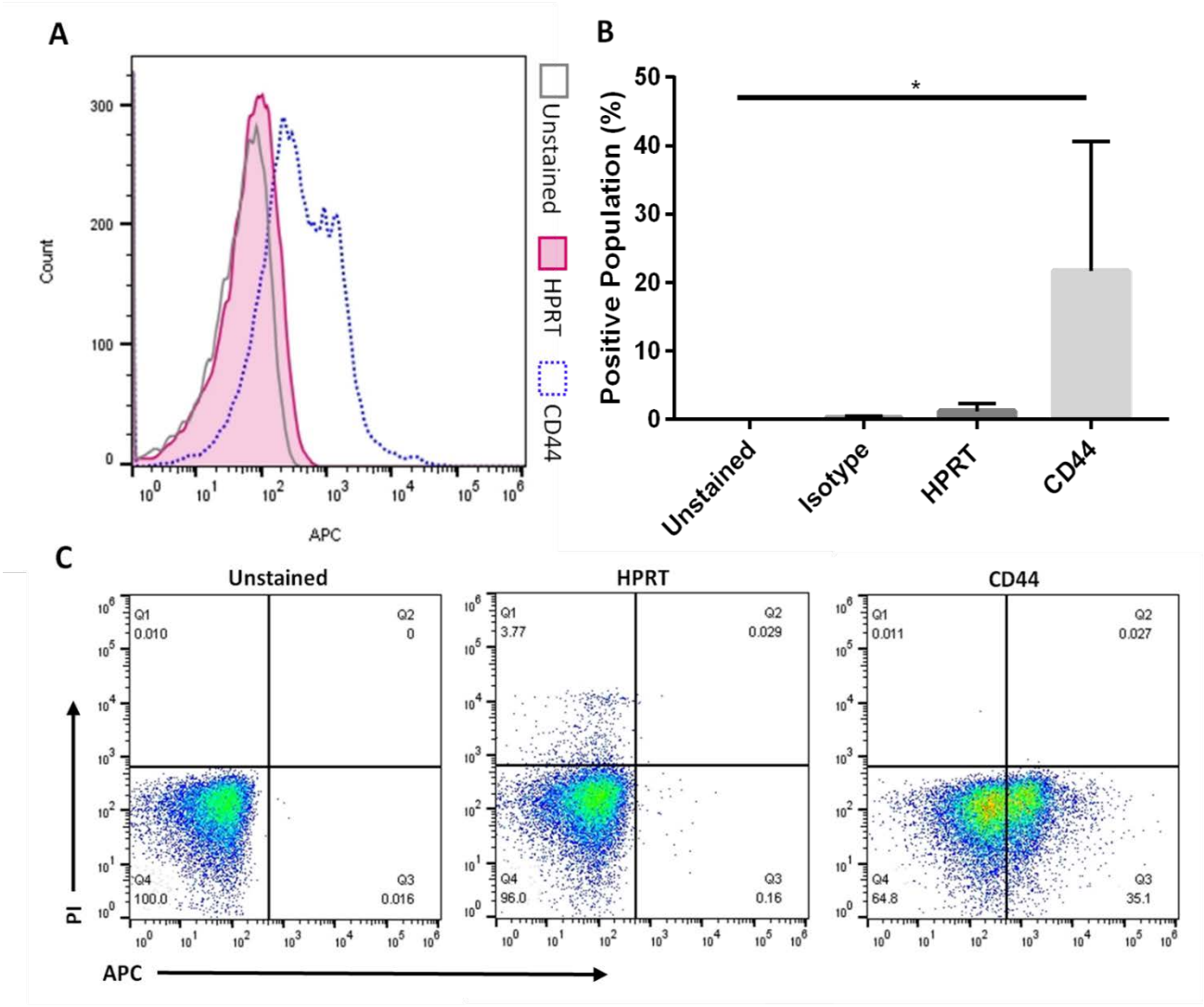

Figure 6-7. *Normal colon tissue stained with HPRT antibodies shows no significant increase in fluorescence*. A, Normal colon cells were treated with a variety of antibodies in order to select the correct cell population. Once this population was established, the fluorescent profile of each sample was obtained and graphed. Shown is the unstained control, CD44 positive control, and HPRT. There is a significant shift in the population when cells were exposed to anti-CD44 fluorescent antibodies, but a minimal shift is seen for anti-HPRT treated cells. B, Statistical analysis shows that HPRT had insignificant fluorescent increases when compared to isotype controls. C, These images portray the cell population of interest in quadrant Q3, which are CD45- and PI-, ensuring that cells analysed were not inherit lymphocytes within the tissue or dead cells.

HPRT expression within malignant cells and tissue demonstrates the variable nature of HPRT upregulation.

In order to evaluate HPRT expression levels within malignant tissue, 94 patient samples were stained (Table 6-1). While the overall average staining intensity of all malignant samples (p-value = 0.545) was insignificant when compared to normal patients, in 59% of the malignant tissue stained for HRPT, there was a substantial increase in the protein expression, while 41% of the patient samples showed insignificant increases in HPRT expression (Figure 6-8). This elevation was statistically significant from normal tissue ($p < 0.001$) and demonstrates unique HPRT production within a cohort of the patients (Figure 6-9). This expression was also significant when compared to the GAPDH control, which was utilized to assess housekeeping levels of protein expression. As the presence of HPRT is variable among cancer cell lines, this variation between patients would be expected as the mutational load of each patient is unique.

Table 6-1. *HPRT levels within malignant and normal colon tissue.*

Tissue Type	Number of Patients	Grade Range	Age Range	M/F	Overall Gray Intensity
Adenocarcinoma (+)	16	1-3	31-79	12/15	97.85
Adenocarcinoma (-)	11				114.92
Metastatic Adenocarcinoma (+)	11	2-3	30-79	15/12	92.01
Metastatic Adenocarcinoma (-)	16				106.12
Tubular Adenoma	10	-	31-69	6/4	99.09
Cancer Adjacent Normal Colon Tissue	20	-	32-81	16/4	103.01
Normal Colon Tissue	10	-	29-42	10/0	105.00

M/F; Male/Female patients.

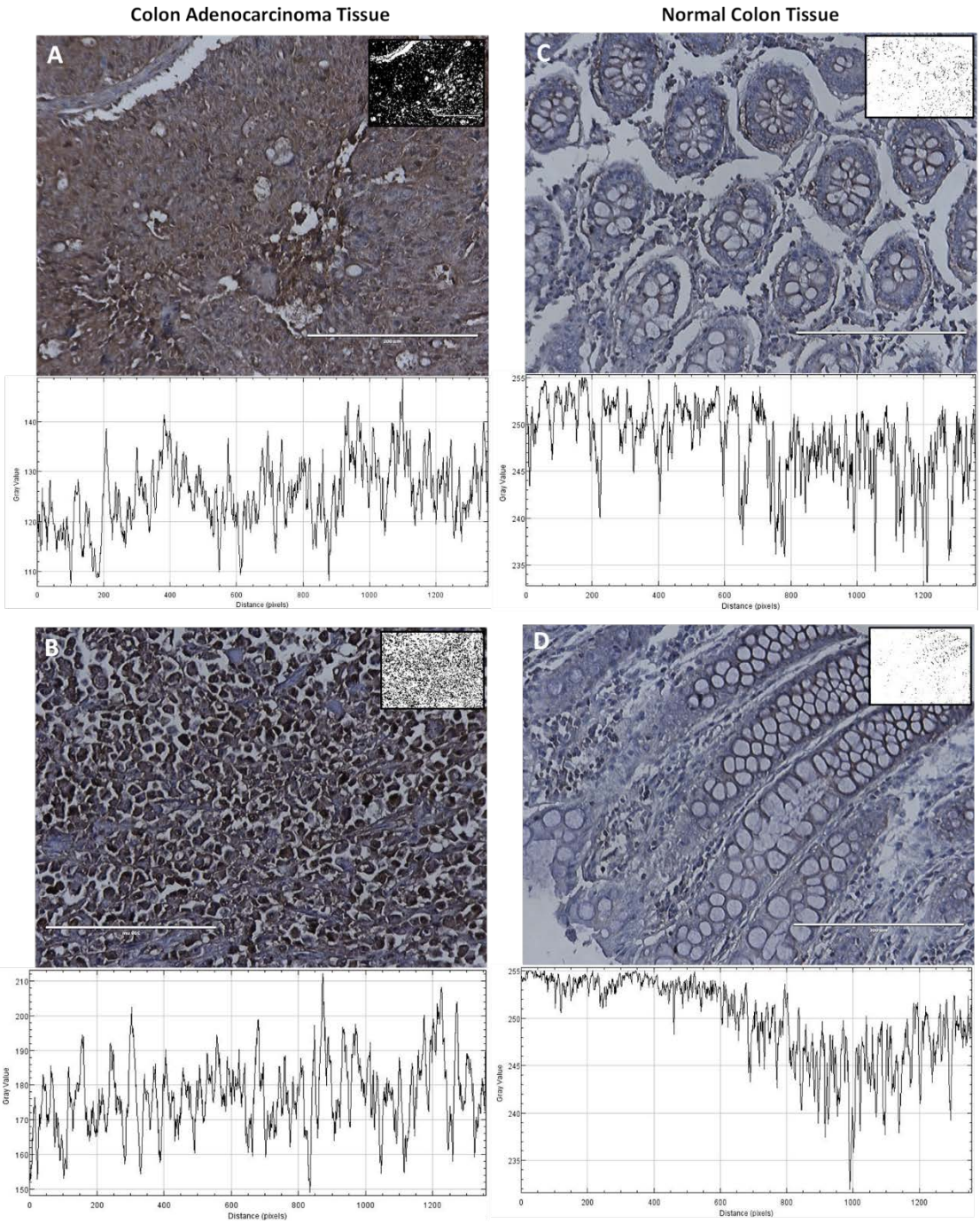

Figure 6-8. *Evaluation of HPRT expression within patient tissue.* All tissues were stained with a monoclonal anti-HPRT antibody. The resulting converted grayscale image is pictured in the top left corner of each image while the grayscale plot is below. A, Tissue from a 79-year-old female patient with stage IIB colon adenocarcinoma and B, tissue from a 48-year-old female patient with stage IV colon adenocarcinoma. These malignant tissues are significantly darker stained than normal colon tissue. C, Normal colon tissue from a 36-year-old male patient and D, tissue from a 31-year-old male patient. These tissues show an upregulation of HPRT within malignant cells.

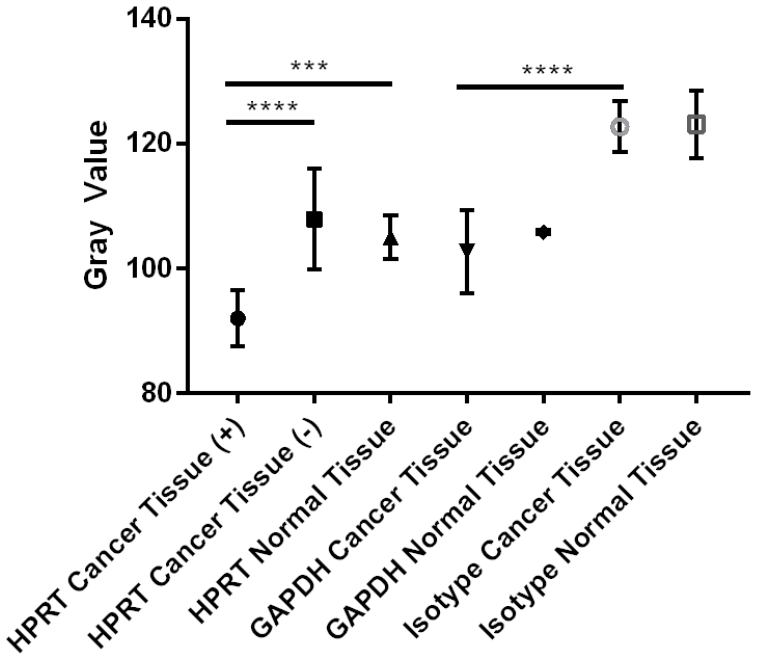

Figure 6-9. *Statistical Analysis of HPRT expression within patient tissue*. Quantification of tissue was conducted utilizing a grayscale. The lower the gray value, the darker the tissue is stained. An isotype control was run to establish the gray value of unstained tissue and to account for non-specific antibody binding. There is a statistically significant presence of HPRT in approximately half of the tissues obtained from patients which are labelled as HPRT Cancer Tissue (+). Patient tissue that did not show significant staining are labelled as HPRT Cancer Tissue (-). This increased expression shows that in some patients there is an increased expression of the protein when compared to normal tissue. GAPDH served as a positive control to establish housekeeping levels of staining and showed no statistical difference in expression between normal tissue and cancer tissue. This data indicates that HPRT may be upregulated within some patients and provides insight into how the protein may present on the surface of the cell.

Analysis within malignant colon samples confirms the variable nature of HPRT surface localization within patients.

Three malignant samples were obtained from patients with colorectal cancer. Of the three samples obtained, two of them had no HPRT surface localization, while one of the samples had elevated surface HPRT (Figure 6-10). This confirms the variation found within the tissues and the cell lines evaluated as the observed HPRT over-expression and subsequent surface presentation was not found within all the patients. Patients without surface localization had

expression similar to the Colo205 cell line, while patients with surface localization had HPRT expression similar to SW620, HT29, and SW480 cell lines. As one of the patients had a significant level of HPRT on the surface of their tumor cells, it demonstrates there is potential for the protein to be targeted within those individuals who experience an up-regulation of the enzyme within their tumors.

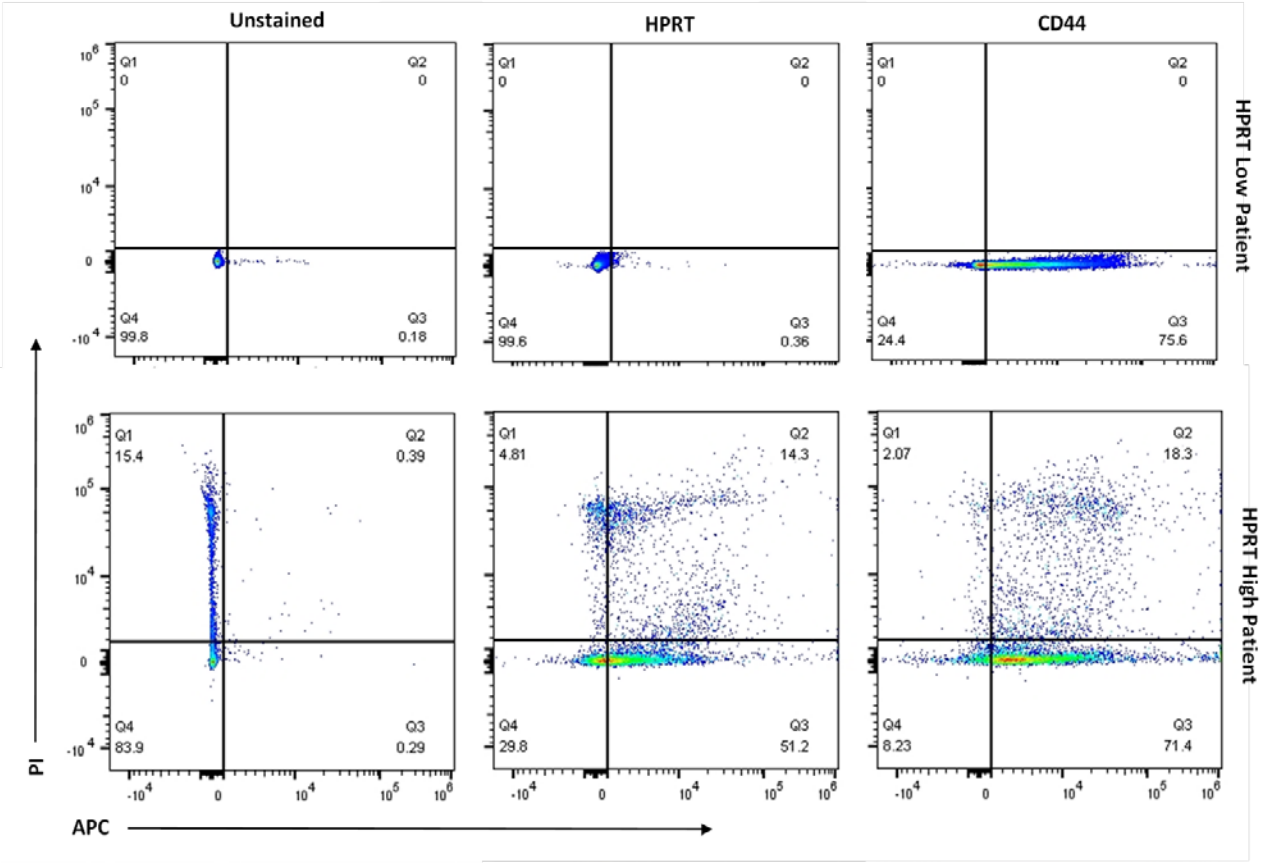

Figure 6-10. *Evaluation of HPRT surface expression in malignant HPRT tissue*. Malignant tissue was treated with PI and anti-CD45 antibodies in order to isolate the correct cell population. Upon analzying three separate patients with colon cancer, there were two patients with "HPRT low" tumors and one patient with an "HPRT High" tumor.

Discussion

HPRT is a common housekeeping gene critical to the successful production and regulation of nucleotides within the cell cycle [10]. Our results show a significant presence of HPRT on the

surface of HT29, SW620, and SW480 colorectal cancer cell lines. These results show a different role of HPRT within a malignant environment that has not been reported. Currently, HPRT is understood to be expressed at a relatively constant level within tumor cells as it is commonly used as an endogenous control for several molecular techniques [502–507]. Our results question the current view of HPRT within colon cancer tissue as it has shown to possess unique characteristics within cancer cell lines in addition to within malignant colon tissue. HPRT expression appears to be very similar to the expression of other biomarkers for colorectal cancer, such as the Vitamin D3 receptor which also shows presence on the surface of colon cancer cells and serves as a marker for cell differentiation and growth [508]. This marker is currently used to reduce tumors and it is likely that HPRT could serve this same purpose within colon cancer tissue as it seems to be related to cell proliferation and appears to be absent on the surface of healthy tissue.

There is other evidence of salvage enzymes serving as diagnostic and prognostic biomarkers to diagnose and monitor cancer development in patients [509]. Thymidine Kinase 1 (TK1), another salvage pathway enzyme, serves as a serum biomarker for cancer recurrence and has shown to have potential as a therapeutic biomarker as well [32,38,40,510]. HPRT may also be used in a similar setting to aid in diagnosing cancers as it appears to only be upregulated in cancer tissue. Unlike TK1, it does not appear to be stage dependent, which would be useful as an early diagnostic companion tool to detect early stage cancers [61]. While pathologists analyze patient biopsy tissue, HPRT could also be evaluated to help in the initial diagnosis.

While HPRT is present on SW620, SW480 and HT29 cells, the relative abundance of the protein is not equal between the cell lines. SW620, the highest expressing cell line, has upwards of 25% more protein on the surface when compared to the lowest expressing HT29 cells. SW620

cells are derived from a metastatic lymph node and are aggressive, fast growing cancer cells. In contrast, HT29 cells are derived from a colorectal adenocarcinoma originating in the mucus glands in the colon and rectum and are consequently less aggressive. Our results potentially indicate that HPRT surface expression may be more abundant in aggressive, rapidly proliferating cells, but this needs to be further explored.

We hypothesize the observed surface expression of HPRT in these cell lines may point to a regulatory element of HPRT expression that has lost function in cancer cells within certain patients [61]. The HPRT gene has several regulatory transcription factors that control its expression (P53, NF-κB, FOXL1, etc…) which may be altered in SW620, SW480 and HT29 cells due to mutation. Loss of HPRT gene control may increase levels of the protein in the cell and subsequently result in the export of the protein to the extracellular matrix where it may transiently reside on the surface of the cell. Further investigation into the mechanism by which this cytosolic protein is transported to the plasma membrane of these cancer cells needs to be evaluated to elucidate how HPRT is able to localize to the surface, and if it provides any functional advantage to the cancer cell. Furthermore, HPRT has shown to have a unique expression profile within a cohort of patients as determined by IHC staining. The over-expression of HPRT within these patients also points to a loss of HPRT regulation and may aid in determining which patients may experience this unique surface expression HPRT. While we were able to evaluate a few malignant cell lines and tumors for HPRT surface presentation, further testing with more patient samples will need to be done to determine how prevalent HPRT surface expression is and which patients could benefit from potentially targeting the protein. As colo205 cells do not show significant HPRT surface localization, further investigation into the

mechanism of surface presentation needs to be conducted to determine the reason some cells express HPRT on the surface while others do not.

HPRT could be used as a valuable marker for studies evaluating biomarker targeting [62]. Testing against this antigen could provide researchers with significant advantages when evaluating therapy efficiency and may lead to a new biomarker target for the treatment of a subset of colorectal cancer patients who experience an upregulation and surface presentation of the protein.

Conclusion

As a surface biomarker that is not present in normal cells, HPRT could be used as a valuable target for immunotherapies. Patients who experience an elevation in HPRT within their tumors may use the protein as a means to reduce tumor burden by targeting HPRT+ cells.

Materials and Methods

Chemicals

Anti-HPRT monoclonal antibody (Thermo Fischer Scientific) was aliquoted and stored at -20°C. Mouse-FITC and Rabbit-FITC antibodies (Sigma Aldrich) were stored at 4°C and were used in dark conditions. Bovine Serum Albumin (Sigma Aldrich) and Sodium thiosulfate (Macron Fine Chemicals) were dissolved in PBS at a 1% concentration and stored at 4°C. 50% Glutaraldehyde stock (Electron Microscopy Sciences) was stored at -20°C and workable solutions were diluted to 0.25% in PBS and stored at 4°C. Glycine (Thermo Fischer Scientific) was diluted to 0.2mM in PBS and stored at 4°C. NF-kB polyclonal antibody (Bioss Antibodies), DCK polyclonal antibody (rabbit: Abnova) and monoclonal antibody (mouse: Santa Cruz, Dallas TX) and APRT polyclonal antibodies (mouse: One World Labs, San Diego, Cal; rabbit: Abnova)

were stored at -20°C. CD44 monoclonal antibody (One World Lab) was stored at -20°C. Propidium Iodide (Sigma Aldrich Inc.) was stored at 4°C and aliquoted for use. Fc Block was purchased from Biolegend and stored at 4°C. An APC-Conjugation Kit (Abcam) was stored at -20°C.

Cell Culture Conditions

The human colon carcinoma cell lines SW620, SW480, Colo205 and HT29 were obtained from the American Type Culture Collection. HT29 and Colo205 cells were grown in RPMI 1640 medium supplemented with 10% fetal bovine serum and 2mM L-Glutamine (all from Hyclone). SW620 and SW480 cells were grown in DMEM medium supplemented with 10% fetal bovine serum and 4mM L-Glutamine (all from Hyclone). The cell media was replaced every 48 hours and cells were trypsinized and the cell population was reduced by half once 90% confluence was obtained. Cells were treated with Acutase (Stem Cell Technology) when utilized for flow cytometry and when plated for all other applications. Cell viability was evaluated using a trypan blue staining, and cells were utilized for all applications when the viability was greater than 98%. All cells were grown at 37°C and 5% CO_2. Cell lines were authenticated in May of 2016 by the University of Arizona Genetics Core.

Flow Cytometry

The surface presence of HPRT, APRT, and DCK in cultured cells was evaluated measuring the fluorescence intensity of antibodies against each of the salvage pathway enzymes. All samples were analyzed on a Blue/Red Attune (Applied Biosystems), and 25,000-50,000 events were recorded per sample. Briefly, 3-5x105 cells were incubated with 200µL of PBS containing 1µg of primary antibody treatment for 15 minutes on ice. Cells were then labelled

with FITC-conjugated secondary (mouse or rabbit) antibody for 15 minutes on ice. Isotypic IgG and unstained cells served as negative controls to ensure correct cell gating. The forward/side-scatter plots were used to gate out cell doublets, dead cells, and cell debris. Using unstained and isotype controls as guides, the positive population was determined by the overall shift in the fluorescent intensity. Each cell line was independently analyzed four times and the data was plotted using FlowJo Software (FlowJo Enterprise). Cells were washed appropriately after each step of the protocol.

Patient Tissue Dissociation and analysis

Healthy and malignant colon tissue samples were obtained from the Utah Valley Regional Medical Center. Tissue samples were minced using sterile scalpels into pieces ranging from 2-3mm in length and were suspended in Hanks media (5% FBS). Minced tissue was then placed in a solution of Collagenase IV on a shaker for 1-4 hours depending on the fat percentage of the tissue. Once dissociated the solution was washed through a 100 micron filter, to produce a single cell suspension. These cells were then washed and treated with an Fc block to minimize non-specific antibody binding. Following blocking, cells were treated with anti-CD45 FITC, anti-HPRT APC and PI to aid in the selection of correct cell populations for analysis. Cells were gated on CD45- and PI- populations to avoid analysis of lymphocytes resident in the tissue and dead cells.

Biotinylation and Western Blot Analysis

Cells were analysed for surface presence along with general expression within the cell utilizing the Pierce Cell Surface Protein Isolation Kit (Thermo Scientific). Briefly, 3 flasks of SW620 cells were grown to 95% confluency, washed, and treated with a kit-provided biotin

solution. Following rocking on a shaker for 30 minutes at 4°C, the cells were treated with a quenching solution. Cells were detached from the flask via cell scraping and transferred to a 50mL conical vial for washing. Then, cells were treated with a lysis solution and incubated for 30 minutes at 4°C. Cell lysis was added to a neutravidin gel and incubated for 60 minutes at room temperature. This solution was then passed through a filter and proteins bound to biotin are trapped within the column. The neutravidin gel was washed 4 times and the flow through was collected and labelled "cytosolic fraction". The biotin labelled protein was then eluted from the column utilizing a 50mM DTT solution and labelled "membrane fraction".

Both membrane fractions and cytosolic fractions along with cell extract from SW620s were evaluated for protein expression utilizing standard Western Blotting techniques described in Sewda et al. with slight modifications [22]. Briefly, each sample was boiled for 5 minutes prior to running on a 12% polyacrylamide gel under reducing conditions. Gels were then transferred to a nitrocellulose membrane (Biorad Laboratories), blocked, and treated with an anti-HPRT monoclonal antibody overnight at 4°C. Following primary antibody treatment, membranes were washed and treated with a rabbit fluorescent secondary antibody (Licor) for 1 hour. Membranes were then imaged on a Licor Odyssey CLx. SW620 cells were utilized for this analysis because their expression of HPRT on the membrane is significantly higher than that of HT29 cells.

Confocal Microscopy

Flourescently-stained cells were examined under an epiflouresence microscope (Olympus, Tokyo, Japan) equipped with a laser confocal system (Bio-Rad Laboratories, Hercules, CA) containing a 15mW Krypton/Argon laser. Image processing was carried out with Laser Sharp Computer Software (Bio Rad Laboratories). After treatment with acutase, cells were

plated at a concentration of 400,000 cells/mL on glass coverslips. Following one to two days of growth, cells were incubated in 500uL of PBS containing 2.5µg of anti-HPRT antibody for 15 minutes on a shaker at 4°C. Cells were then labelled with 2.5µg of FITC-conjugated secondary antibody for 15 minutes on a shaker at 4°C. Then, cells were incubated at 37°C for 10 minutes with a 1:1000 dilution of a Cell Mask Deep Red plasma membrane dye (Fisher Scientific).

Electron Microscopy

Following acutase treatment, cells were plated at a concentration of 400,000 cells/mL on glass coverslips. After one to two days of growth, cells were placed in 6 well plates and washed with PBS three times and with 1% PBS-BSA for 5 minutes at 4°C followed by a sodium azide wash. Cells were then incubated with 2.5µg or 5µg of primary antibody conjugated to Biotin for 15 minutes on a shaker at 4°C. After primary incubation, cells were washed with 1% PBS-BSA followed by two washes with PBS. Then, cells were washed with 1% PBS-BSA and 1% PBS-sodium thiosulfate for 5 minutes on a shaker at 4°C. Cells were incubated with 2.5µg of Streptavidin-gold conjugate (Nanoprobes, Yaphank, NY) for 15 minutes on a shaker at 4°C. This is followed by a 1% PBS-BSA wash and three PBS washes. Cells were then fixed with a 0.25% Glutaraldehyde solution diluted in PBS for 5 minutes. The reaction was then extinguished by adding a 0.2mM PBS-Glycine Solution and incubating for 10 minutes until the solution turned a slight yellow color. Cells were then washed three times with ddH_2O. Solutions A and B from the Nanoprobes gold enhancement kit (Nanoprobes Inc.) were incubated together for 5 minutes. Solutions C and D were then added, vortexed, and 40µL of the gold enhancement were added to each sample and incubated for 5 minutes. Each sample was put through a series of dehydrations with 70%, 80%, 90%, and 100% ethanol. Gold labelled samples were examined under a Phillips XL-30 ESEM using a 15kV electron stream under low vacuum conditions at 1 Torr. A Gaseous

Side Electron (GSE) detector was utilized to image the cell morphology and topography. A Back Scatter Electron (BSE) detector was utilized to visualize gold particles on the cell surface. Once images for the cells were obtained, the elemental composition of the cells was evaluated using energy dispersive spectroscopy (EDAX) and X-rays. EDAX analysis will provide a k-ratio, a Z value, an A value, and an F value. The k-ratio represents the element's peak height compared to a sample of the pure element collected under the same conditions. The Z value represents a correction in the atomic number taking backscattered election yield of the pure element and the sample. The A value represents a compensation for X-rays generated in the sample that are cannot emit energy. The F value represents a correction for the generation of X-rays. We used these EDAX output values to normalize our samples gold weight percentages using the following equation:

$$Normalized\ Weight\ Percentage = \frac{k - ratio * 100}{Z * A * F}$$

Immunohistochemistry

Colorectal Adenocarcinoma tissue arrays were obtained from BioMax. These tissues contain various stages of cancer along with corresponding benign and normal tissue from 100 different patients. HPRT levels were assessed utilizing standard immunohistochemistry staining. Tissues were rehydrated in a series of ethanol washes before treatment with a DIVA (Biocare Medical) solution to retrieve antigen. Tissues were then incubated with a Background Sniper (Biocare Medical) solution to reduce non-specific antibody binding. Following blocking, a primary antibody is added to the tissue at a concentration of 1:100 to 1:200 and incubated overnight at 4°C. Following primary staining, tissues were washed and then treated with secondary antibody conjugated to a HRP polymer (Biocare Medical) and incubated for an hour.

Following washing, a DAB Peroxidase solution was incubated with the tissues. Areas of antibody binding converted the colorless substrate to a brown product, effectively highlighting the target protein. Tissues were treated with hematoxylin (Biocare Medical) to stain the nucleus of the cells. Along with HPRT treatment, a universal negative antibody (Biocare Medical) was used as a negative control, and a GAPDH antibody was used as a positive control.

Tissues were quantified utilizing ImageJ software. All images were evaluated using the IHC toolbox ImageJ plugin. The DAB option is chosen and the tissue image is then removed of all other staining except for DAB. Following this analysis, the image is then converted to a grayscale and a threshold is applied in order to eliminate areas of no staining inherit within the tissue image. Once the threshold is applied the average gray value of the tissue is collected. The same threshold is applied to all tissue samples in order to ensure consistency.

Statistical Analysis

ANOVA statistical analysis with the multiple comparison method were used to determine the differential surface expression of the various treatments for flow cytometry data on all cell lines. In addition, two-way ANOVA tests were performed to compare the mean expression of HPRT between SW620 and HT29 cells. EDAX data was analyzed using an ANOVA with the multiple comparison method in addition to unapired t tests to determine significance between samples. All statistical analysis was evaluated using GraphPad Prism 7 software. Differences were considered significant when the p value was <0.05.

CHAPTER 7

Elevated expression of Hypoxanthine Guanine Phosphoribosyltransferase within malignant tissue

Michelle H. Townsend, Abigail M. Felsted, Zachary E. Ence, Stephen R. Piccolo, Richard A. Robison, and Kim L. O'Neill

Citation: MH Townsend, AM Felsted, ZE Ence, SR Piccolo, RA Robison, KL O'Neill. Elevated expression of hypoxanthine guanine phosphoribosyltransferase within malignant tissue. Cancer and Clinical Oncology. 2017. Vol 6, No 2. DOI: https://doi.org/10.5539/cco.v6n2p19

The following chapter is taken from an article published in Cancer and Clinical Oncology. All content and figures have been formatted for this dissertation

Abstract

Hypoxanthine Guanine Phosphoribosyltransferase (HPRT) is a housekeeping enzyme involved in the purine synthesis of guanine and inosine in the salvage pathway. While other salvage pathway enzymes, such as TK1, have been established as biomarkers for both cancer cell proliferation and cancer development, little has been done to evaluate whether HPRT has the same potential as a cancer biomarker. We designed this study to determine if HPRT has value as an identifier of malignancy within the most common types of cancer. We utilized histological samples from lung, colon, prostate, and breast cancer with additional normal tissue to evaluate whether there was any elevation within malignant samples. In addition, we also assessed general HPRT expression within patient's samples from The Cancer Genome Atlas (TCGA) to confirm clinical relevance. We found that within a subset of patients there was significant elevation of HPRT when compared to normal tissue controls. This elevation was seen in 33-55% of the malignant samples and appears to have no dependence on stage. There were slight differences in staining patterns among all the organ types, but overall each organ displayed the same pattern of 'HPRT high' and 'HPRT low' populations within malignant samples. We found that in our TCGA samples there was a similar elevation of HPRT that was significant when compared to normal controls. Overall, as an upregulated enzyme that does not directly correlate with stage, HPRT could become a valuable marker in the early diagnosis of a variety of solid tumors.

Introduction

With 14 million new cases diagnosed and 8.2 million deaths reported worldwide in 2012, cancer is a leading global health concern[511]. In 2016, the most common malignancies reported are lung, breast, prostate, and colon which comprised approximately 44.5% (Lung - 224,390; Breast - 249,260; Prostate - 180,890; Colon - 95,270) of all new cancer cases in the United States[417,512,513]. As the most common cancers throughout the world, new biomarkers are constantly needed to identify cancer in early stages to decrease mortality rates. While several cancer markers have been identified for each of these diseases, Hypoxanthine Guanine Phosphoribosyltransferase (HPRT) has the potential to provide an additional diagnostic tool for several cancer types.

HPRT is a transferase responsible for the salvage of both guanine and inosine nucleotides throughout the cell cycle[10,12,514]. As an established human reporter gene, HPRT is currently utilized to provide understanding of somatic mutations and mutagenesis in both *in vitro* and *in vivo* systems[43,44,515]. Mutation events in this locus are extensively monitored in population studies to evaluate the effects of continuing exposure to mutagens and detect carcinogenic agents that lead to increased cancer risk[49,51,516]. In at-risk populations including smokers, patients with DNA repair deficiency syndromes, and atom bomb survivors, there are significant mutations in the HPRT locus, which directly correspond with higher cancer incidence[45,52,54,55,57,58,516,517]. While its role as a standard mutational biomarker for cancer development has been well established, the relevance of HPRT to the proliferative capacity and tumorigenesis of cancer has not been evaluated. It has established that other salvage enzymes, such as TK1, have a direct relevance to cancer stage and aggressiveness as serum detection of the enzyme is correlated to cancer stage and recurrence[29,38,509,518,519]. To address whether this same stage-dependent protein

elevation pattern existed for HPRT, we have evaluated the expression of the enzyme in hundreds of patient samples to determine if HPRT could also serve as a cancer biomarker for early cancer detection. We compare HPRT expression in the most commonly diagnosed cancers throughout the world (lung, breast, prostate, and colon).

Methods

Chemicals/Reagents

DIVA Decloaker 10x, Background Sniper, Mach 4 HRP polymer, DAB Peroxidase, Hematoxylin, Hydrophobic pen, and Universal Negative antibodies were all obtained from Biocare Medical, Concord, CA. Anti-HPRT monoclonal antibody (Abcam, Cambridge, UK) was aliquoted and stored at -20°C. GAPDH polyclonal antibody (One World Labs, San Diego CA) was aliquoted and stored at -20°C. Tween20 (Fisher Reagents, Waltham MA) was stored at room temperature. 30% Hydrogen Peroxide (Fisher Reagents, Waltham MA) was stored at 4°C.

Patient Samples

All tissue microarrays were obtained from Biomax and stained for HPRT, GAPDH, and an isotype antibody to evaluate protein expression and upregulation. Lung samples were evaluated from 54 patients ranging in age from 39-77 containing malignant (n=17), normal (n=18), and marginal tissue (n=17) samples. Malignant tissue ranged from grade 1-3 and included female (n=4) and male (n=13) patients with either large cell carcinoma (n=3), adenocarcinoma (n=5), or squamous carcinoma (n=6). Colon samples were evaluated from 100 patients ranging in age from 30-79 with colon adenocarcinoma (n=30), metastatic adenocarcinoma from the colon (n=30), tubular adenoma (n=10), cancer adjacent normal tissue (n=20), and normal colon tissue (n=10). Sex (male, n=63; female, n=37) and grade (1-3) were

variable between samples. Breast samples were analyzed from 63 patients ranging in age from 29-68 containing malignant (n=18), normal (n=24), and margin of carcinoma samples (n=21). Prostate samples were analyzed from 63 patients ranging in age from 60-87 containing adenocarcinoma (n=60) and hyperplasia (n=3) samples.

Immunohistochemistry

HPRT levels were assessed using standard immunohistochemistry staining. Tissues were treated with Histoclear (National Diagnostics, Charlotte, North Carolina) and subsequently rehydrated in a series of ethanol washes before treatment with a DIVA Decloaker solution to retrieve antigens. Tissues were washed with a diluted hydrogen peroxide solution followed by a Tris Buffered Saline-Tween20 (TBST) wash. Following washing, tissues were incubated with a blocking Background Sniper solution to reduce non-specific antibody binding. Following blocking, a primary antibody was added to the tissue at a concentration of 1:100 and incubated overnight at 4°C. Following primary staining, tissues were then washed and then treated with secondary antibody conjugated to a HRP polymer and incubated for an hour. Following washing, a DAB Peroxidase solution was incubated with the tissues. Areas of antibody binding converted the colorless substrate to a brown product, effectively highlighting the target protein. Tissues were treated with hematoxylin to stain the nucleus of the cells. Along with HPRT treatment, a universal negative antibody was used as a negative control, and a GAPDH antibody was used as a positive control.

Tissue Quantification

Tissues were quantified utilizing ImageJ software. All images were evaluated using the IHC toolbox ImageJ plugin. The DAB option is chosen and the tissue image is removed of all

other staining. Following this modification, the image is then converted to a grayscale and a threshold is applied in order to eliminate areas of negative space inherit within the tissue image. Once a universal threshold was applied, the average gray value of the tissue was collected. The same threshold was applied to all tissue samples within the same organ in order to ensure consistency and reduce bias.

Bioinformatic analysis

We evaluated differences in expression levels of the HPRT gene in 3,147 tumor and 316 normal samples from The Cancer Genome Atlas (TCGA). RNA-sequencing data that had been processed using the *featureCounts* algorithm to transcripts-per-million values was utilized. The normal expression data were from adjacent normal tissue or blood samples and were not necessarily matched to the tumor data on a per-sample basis. We parsed and prepared the data using the Python[520] (v3.6.1) programming language. In making graphs, we used the R (v3.2.2) statistical software and the *ggplot2* package (v.2.2.1).

Statistical analysis

Comparison between tissue samples was conducted utilizing ANOVA statistical analysis with the multiple comparison method. Unpaired t tests were utilized in conjunction to confirm statistical significance. All statistical analysis were evaluated using GraphPad Prism 7 software. Differences were considered significant when the p value was < 0.05.

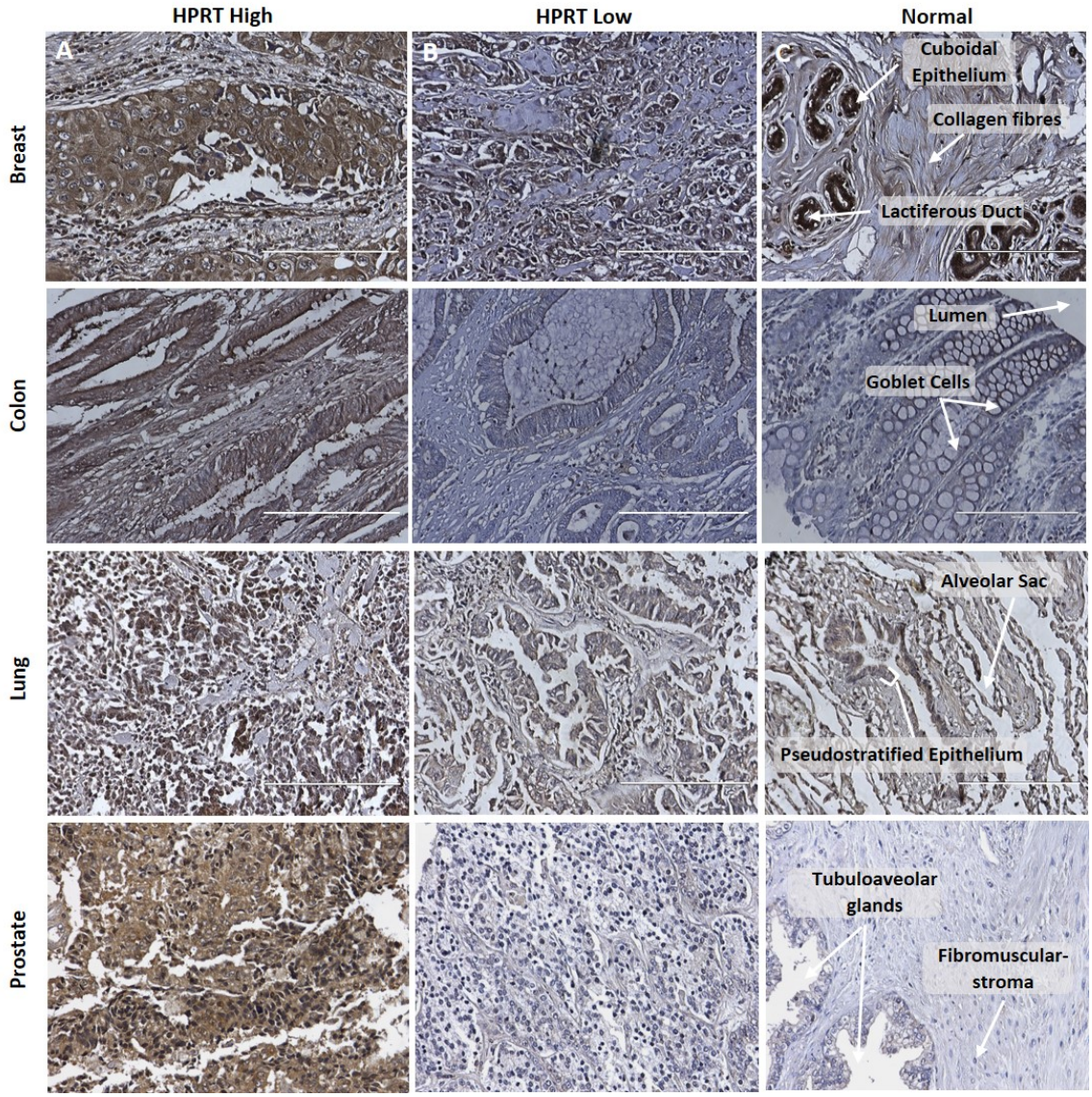

Figure 7-1. *HPRT staining within malignant and normal breast, colon, lung, and prostate.* A) All organs observed contained a population of patients who had a significant increase in HPRT staining, which are labeled "HPRT High". These tissues were significant when compared to normal controls. B) Organs also contained a population of patients who did not experience an increase in HPRT when compared to normal controls and are labeled "HPRT Low". C) Normal tissue was stained within all organs to provide a standard to compare expression. Normal tissue is labeled with identifying features.

HPRT has variable expression in several cancers and shows an upregulation in malignancy.

Within all malignant tissue there were populations of patients with high HPRT expression and populations with relatively low HPRT expression. We have labeled these patients as "HPRT high" and "HPRT low" (Figure 7-1). Patients with high levels (Figure 7-1A) were significantly separated from patients with low levels (Figure 7-1B), which had staining characteristics similar to normal tissue (Figure 7-1C). The variability of HPRT within malignant tissue was also variable between cancer types as each organ had a different percentage of patients who experienced an upregulation (Lung- 33%, Breast-55%, Colon-33%, Prostate-47%).These data indicate that HPRT is only elevated within some patients, and may serve as a diagnostic marker for characterizing tumors.

Table 7-1. *HPRT staining in malignant and normal tissue.*

Organ		Mean Gray Intensity	High Expression	Low Expression
Lung	Normal	101.08	4	11
	Malignant	100.24	6	12
Breast	Normal	91.91	2	9
	Malignant	81.86	10	8
Colon	Normal	105.00	0	7
	Malignant	102.59	18	36
Prostate	Hyperplasia	134.20	0	3
	Malignant	120.69	25	28

While a majority of staining was limited to malignant tissue, there were instances within normal lung and breast tissue where there was significant HPRT staining (Table 7-1). As HPRT is a housekeeping gene present within all somatic tissue, we expected to have a basal level of staining within normal tissue, and all analysis were performed against normal tissue staining to highlight any upregulation. Upon further analysis with protein expression data from clinical samples in TCGA, we found that there was a significant overall upregulation of HPRT within all

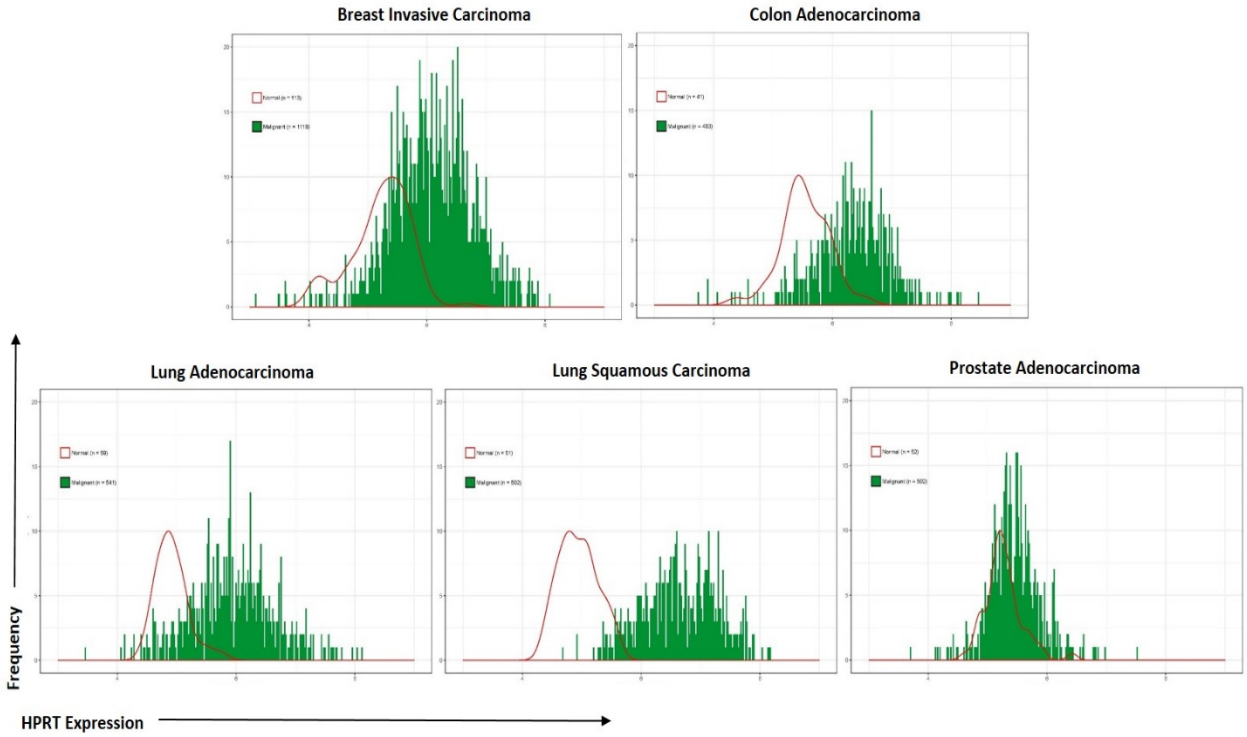

Figure 7-2. *Expression of HPRT within TCGA tumor and normal samples.* Clinical samples from 1119 patients with various cancer types were evaluated for HPRT elevation in malignant samples when compared to normal tissue. All cancer evaluated showed a significant shift in the population of malignant samples (green) when compared to normal controls (red).

cancer types evaluated when compared to normal controls (Figure 7-2). Samples from 1119 breast invasive carcinoma, 483 colon adenocarcinoma, 541 lung adenocarcinoma, 502 lung squamous carcinoma, and 502 prostate adenocarcinoma patients were compared to normal individuals and showed significant shifts in the expression of HPRT in malignant tumors, with lung samples showing the highest shift. Within each of the cancer types evaluated we observed

the same pattern of 'HPRT high' and 'HPRT low' populations in the patient cohorts. Several patients with malignancy had expression levels of HPRT comparable to normal samples, however, there was a population of patients that had elevated HPRT beyond that of normal tissue staining. This data exhibited a very standard normal distribution and there were some healthy patients with relatively high HPRT expression. These results indicate that there is a subset of patients that experience unusually high levels of HPRT expression, which could be used to further characterize tumors and provide a means for early detection of malignancy.

Table 7-2. *Distribution of HPRT staining in malignant breast tissue and normal breast tissue.*

Tissue Type	Number of Patients	Age Range	Overall Gray Intensity
Adenocarcinoma High	10	29-68	76.32
Adenocarcinoma Low	8	29-61	88.79
Normal Breast Tissue	11	43-69	91.91
Hyperplasia	3	49-68	100.87
Adenosis	7	28-61	89.91
Collagen Fiber Tissue	3	47-49	97.30
Marginal Tissue	21	32-74	90.07

Evaluation of HPRT within breast cancers tissue demonstrates its potential as a biomarker for malignancy

Of the 18 malignant breast tissues evaluated, 10 patients experienced a significant ($p = 0.0025$) increase in HPRT expression with an average total gray intensity of 76.32 when compared to normal breast tissue, which had an average gray intensity of 91.91 (Table 7-2). Normal and malignant tissue stained for HPRT were significant when compared to GAPDH positive and Isotype negative controls (Figure 7-3A). In addition to normal breast tissues, adenosis, fiber tissue, and hyperplasia were evaluated and showed insignificant upregulation compared to normal samples (Figure 7-3B & 7-3D). As a majority of the malignant tissue

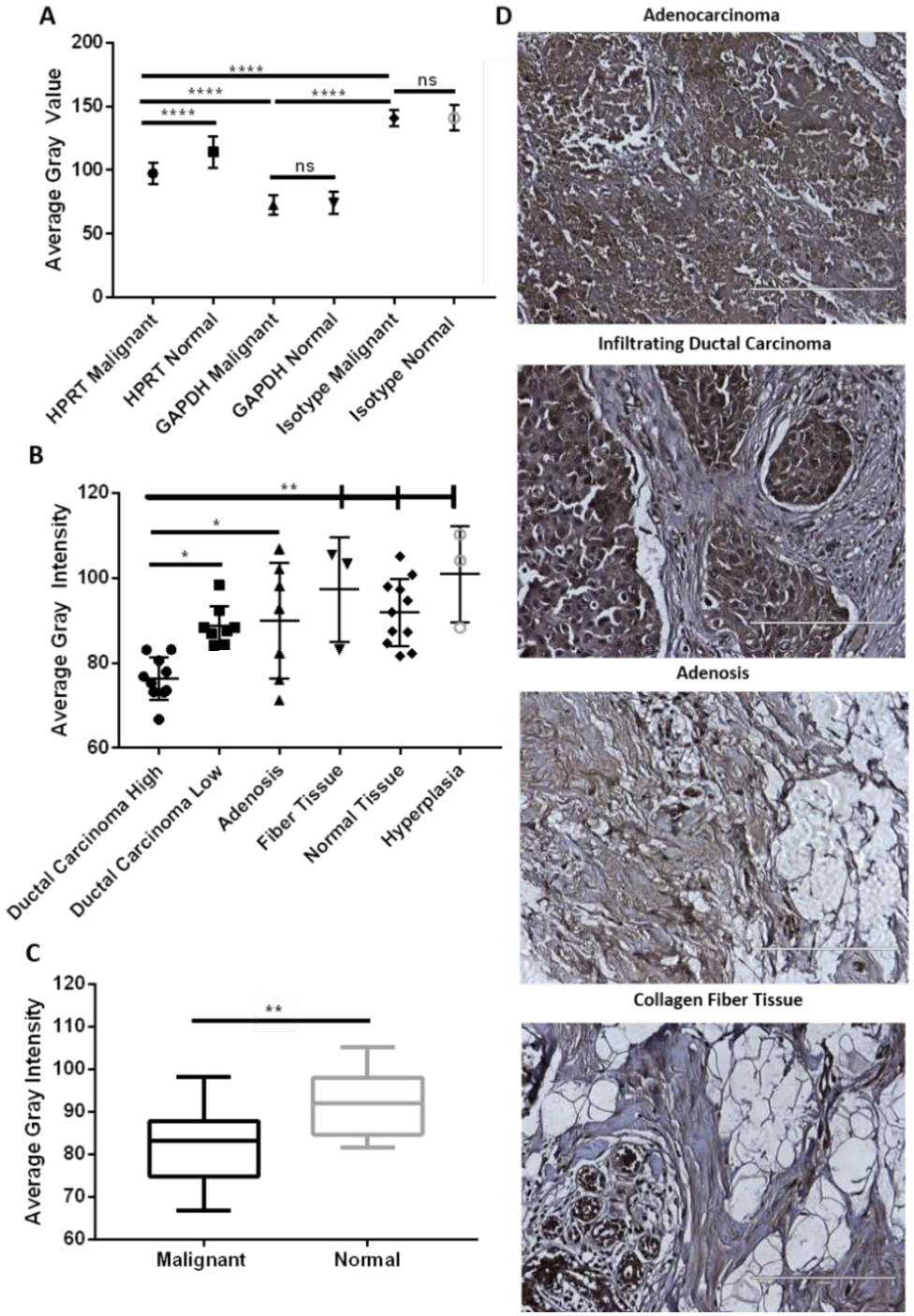

Figure 7-3. *Statistical evaluation of breast tissue.* A) Malignant and normal breast HPRT staining compared to GAPDH and Isotype controls. GAPDH and Isotype samples were not statistically significant between malignant and normal tissue. HPRT samples had a significant increase in expression when comparing malignant tissue to normal tissue. B) HPRT expression analysis between various tissue types. There were 10 patients who had significant HPRT elevation and are labeled 'Ductal Carcinoma High', while the remainder 8 patients are labeled 'Ductal Carcinoma Low' as they had staining similar to normal controls. C) Overall HPRT staining results of malignant and normal tissue within all samples. D) Tissue images of HPRT staining in various breast tissue samples.

experienced an upregulation of HPRT, there was still a significant ($p=0.0026$) difference between normal tissue and malignant samples when 'HPRT low' tissue was included within the analysis (Figure 7-3C).

In addition to evaluating malignant tissue, marginal tissue was analyzed to determine whether HPRT could be used to indicate unusual cell proliferation around the tumor. This analysis revealed that there was a distribution within the marginal tissue in regards to HPRT expression. We found that 6 marginal tissues were 'HPRT high' and 10 samples were 'HPRT low' (Figure 7-4). Each tissue showed variability, and demonstrates the ability of HPRT to aid in distinguishing potentially malignant tissue. Marginal tissue elevated in HPRT expression may indicate signs of malignancy and proliferative capacity.

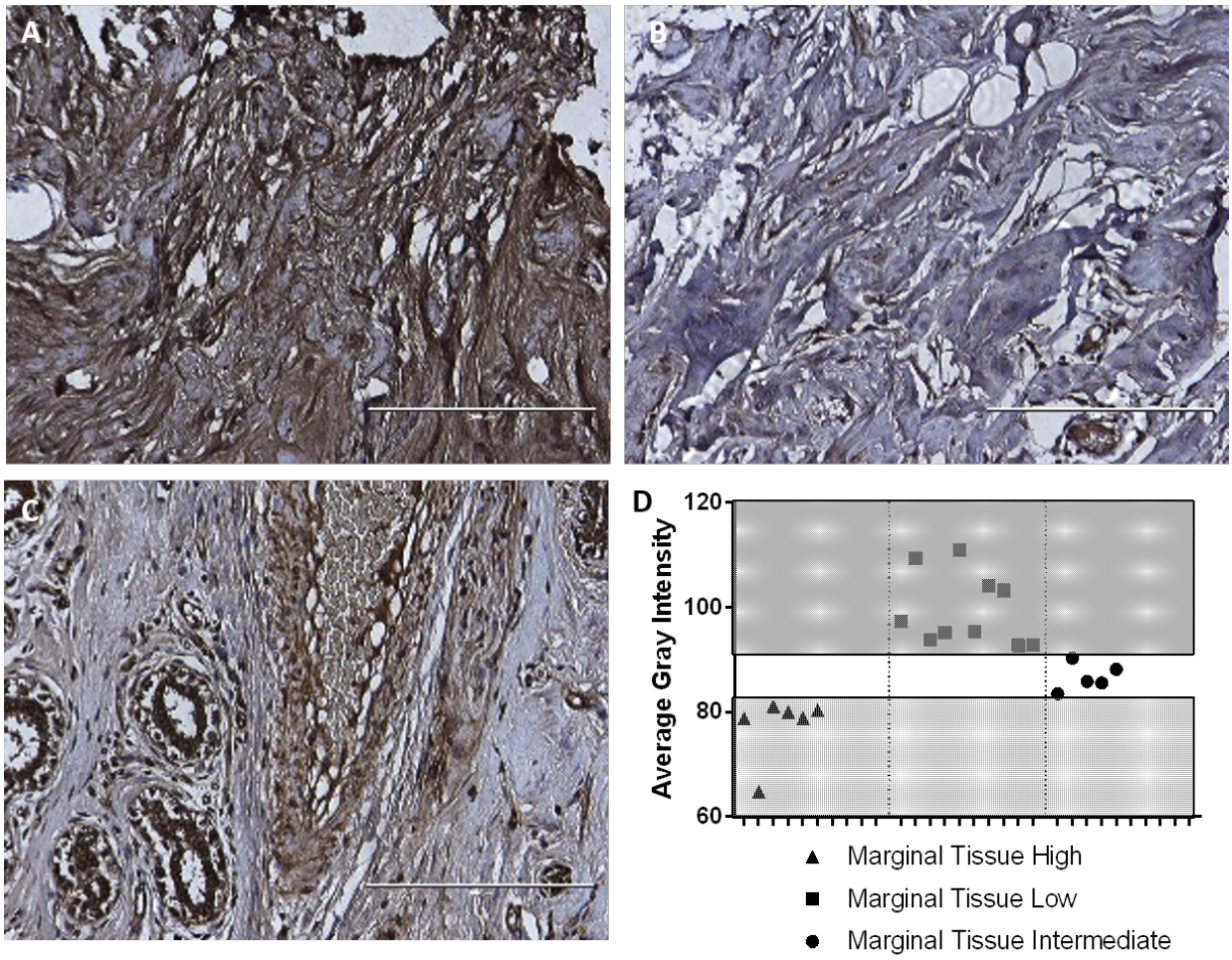

Figure 7-4. *HPRT analysis of margin of carcinoma tissue*. Margin of breast carcinoma tissue that stains A) 'HPRT High'; B) 'HPRT low'; and C) 'HPRT intermediate' staining. D) graphical representation of the quantity of patient samples within each HPRT staining level.

Interestingly, we found that in normal tissue HPRT expression was localized to the ductal tissue. There was clear staining within the inner lining of the lactiferous ducts of the breast with minimal staining in other portions of the tissue (Figure 7-5). This expression is localized and may indicate HPRT involvement in cell proliferation.

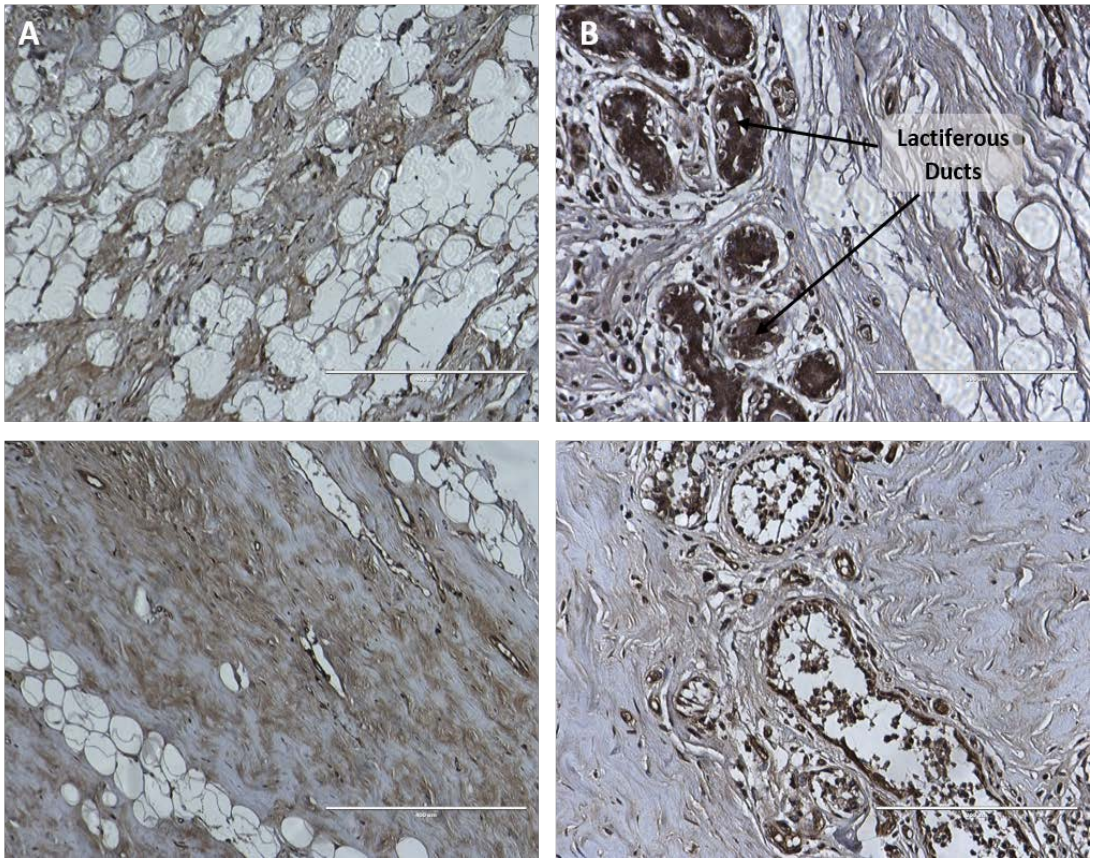

Figure 7-5. *Normal breast tissue stained for HPRT*. A) Within normal tissue we found minimal HPRT staining. B) While normal tissue showed no significant HPRT expression, ductal openings of normal breast tissue had unusually high staining. This may point to the involvement of HPRT in cellular proliferation.

Lung cancer shows insignificant variability of HPRT expression between cancer types and stage.

Multiple different lung malignancies were evaluated to determine if there were any differences between the cancer types as they have significantly different origins within the lung itself. All samples were evaluated against corresponding normal, isotype controls, and GAPDH positive controls to compare

expression (Figure 7-6A). We found that there was no statistically relevant difference between the malignant lung samples in regards to HPRT expression (Figure 7-6B).

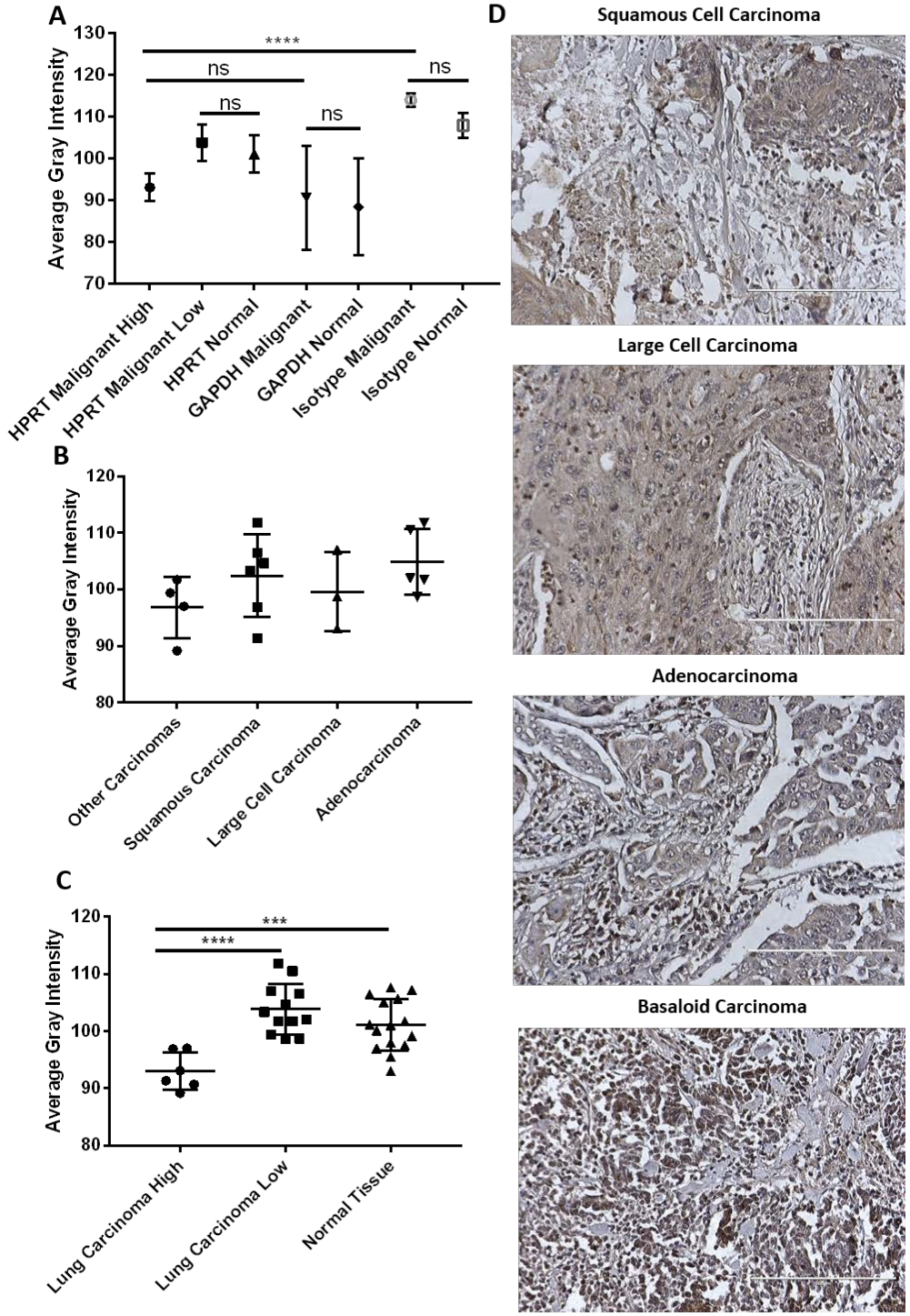

Figure 7-6. *Statistical evaluation of HPRT expression in lung cancer.* A) Malignant and normal lung tissue stained with HPRT, GAPDH, and Isotype controls. GAPDH and Isotype samples were not statistically significant between malignant and normal. B) HPRT expression analysis between various tissue types. There was no significance

between lung cancer types in regards to HPRT expression. C) There were 6 patients that had elevated HPRT labeled 'Lung Carcinoma High' and 12 patients that had insignificant HPRT expression labeled 'Lung Carcinoma Low'. D) Tissue images of HPRT expression in various lung cancers.

Adenosquamous samples had the highest average HPRT expression with a mean gray intensity of 94.12, while large cell carcinoma samples had the lowest average HPRT expression with a mean gray intensity of 104.24 (Table 7-3 & Figure 7-3D). These values were not statistically significant and indicate that there was no difference between the cancer types. Within malignant samples 33% of patients experienced significant upregulation when compared to normal tissue controls as 6 patients had expression characterized as 'HPRT High' (Figure 7-6C).

Table 7-3. *Distribution of HPRT staining in malignant lung tissue and normal lung tissue.*

Tissue Type	Number of Patients	Grade Range	Age Range	M/F	Overall Gray Intensity
Squamous Carcinoma	3	2-3	46-58	3/0	101.68
Large Cell Carcinoma	3	2-3	30-66	3/0	104.24
Adenocarcinoma	6	1-3	46-77	5/1	102.56
Alveolar Carcinoma	2	NA	39-59	1/1	96.26
Adenosquamous Carcinoma	2	3	60-69	2/0	94.12
Other Carcinomas	2	3	59-69	0/2	95.45
Normal Lung Tissue	18	-	39-77	14/4	101.08
Marginal Tissue	18	-	30-77	14/4	100.74

M/F; Male/Female patients.

Lung tissue was the only organ that we observed a stage-dependent increase in HPRT expression (Figure 7-7). As there was only one stage I tissue to analyze, the significance observed was between stage II and stage III tissue, where there was a significant increase in HPRT expression in stage III tissue ($p = 0.05$). As this pattern was not observed within any other organ, we hypothesize it may be an artifact of the small cohort size and a larger sample size is needed to determine any relevant significance.

HPRT elevation in metastatic colon tumors was significant when compared to primary tumors.

Within colon cancer tissue, there was a population (n = 18) that had a significant upregulation of HPRT when compared to isotype controls (Figure 7-8A). With an average gray intensity of 92.00 (Table 7-4), this was significant when compared to both the normal colon

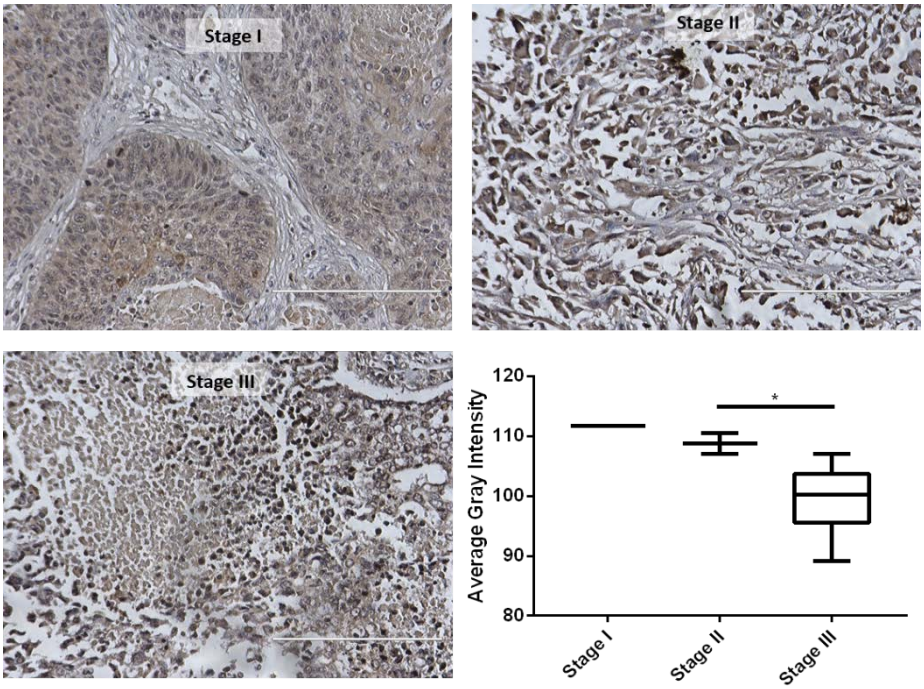

Figure 7-7. *Stage Evaluation of malignant lung tissue.* Lung tissue showed significant variations in HPRT expression in relation to stage. Stage I, II, and III tissue are evaluated and imaged to show any variations between tissue intensity.

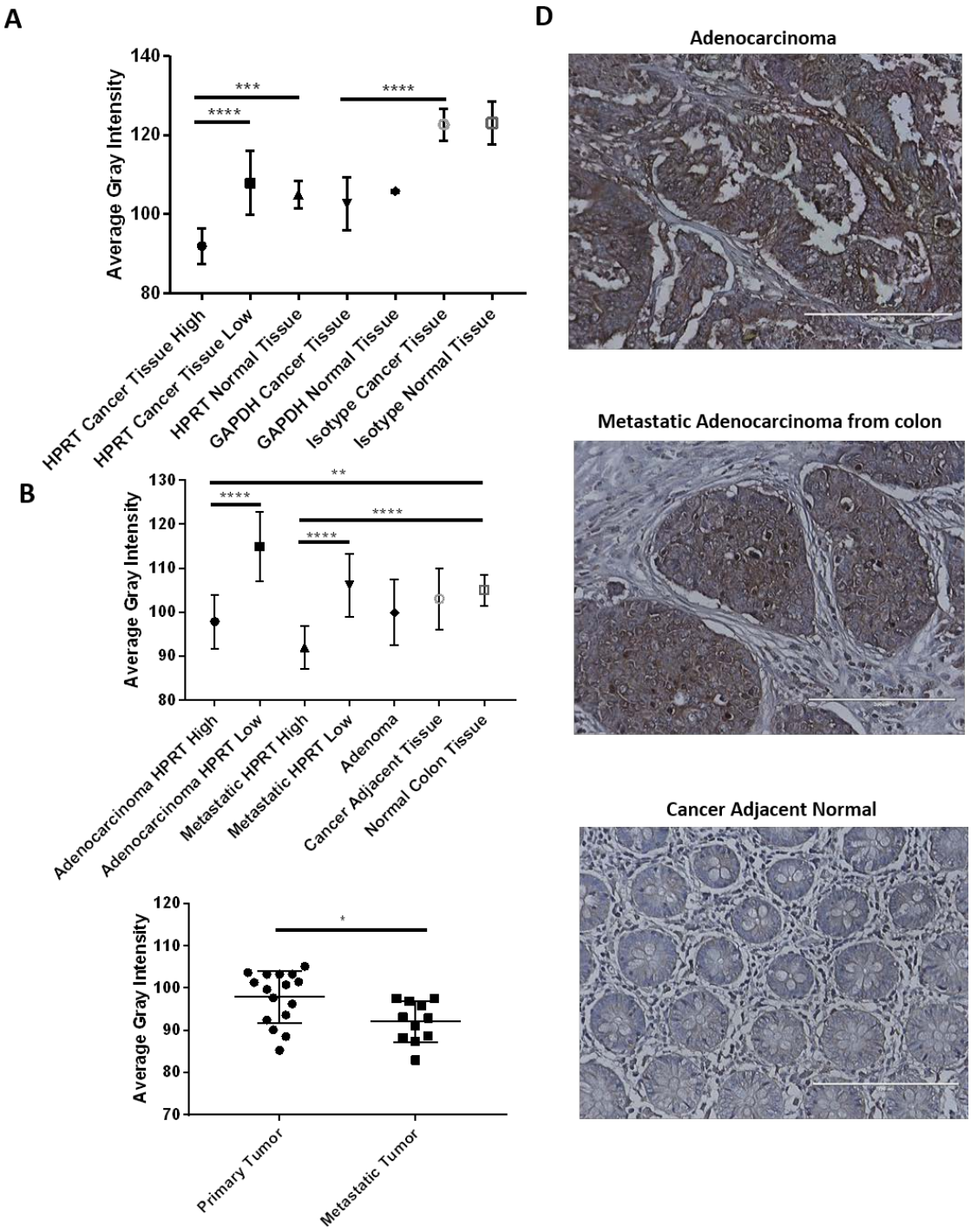

Figure 7-8. *HPRT expression within colon primary tumors, metastatic tumors from the colon, and normal colon tissue.* A) Malignant and normal tissue analysis in tissue stained with HPRT, GAPDH, and an Isotype antibody. B) HPRT staining within all colon sample tissues. C) 16 primary tumor samples and 11 metastatic tumor samples experienced 'HPRT High' staining.

tissue controls ($p < 0.0001$) and isotype controls ($p < 0.0001$). Additionally, we also evaluated primary and metastatic colon tumors to determine whether there was any difference in HPRT expression between aggressive, malignant cells that had successfully metastasized and primary tumor cells.

Table 7-4. *Distribution of HPRT staining in malignant colon tissue and normal colon tissue.*

Tissue Type	Number of Patients	Grade Range	Age Range	M/F	Overall Gray Intensity
Adenocarcinoma	30	1-3	31-79	14/16	104.81
Metastatic Adenocarcinoma	30	2-3	30-79	17/13	100.37
Tubular Adenoma	10	-	31-69	6/4	99.09
Cancer Adjacent Normal Colon Tissue	20	-	32-81	16/4	103.01
Normal Colon Tissue	10	-	29-42	10/0	105.00

M/F; Male/Female patients.

We found a similar pattern to other primary tumors evaluated where a subset of patients were 'HPRT High' and a subset of patients who had similar levels to normal controls and were labeled 'HPRT Low' (Figure 7-8B&D). We also found that metastatic samples had an overall increase in HPRT compared to primary tumors ($p = 0.014$), indicating that metastatic cells may express more HPRT (Figure 7-8C).

Prostate cancer tissue exhibits significant HPRT expression that is not dependent on stage or grade.

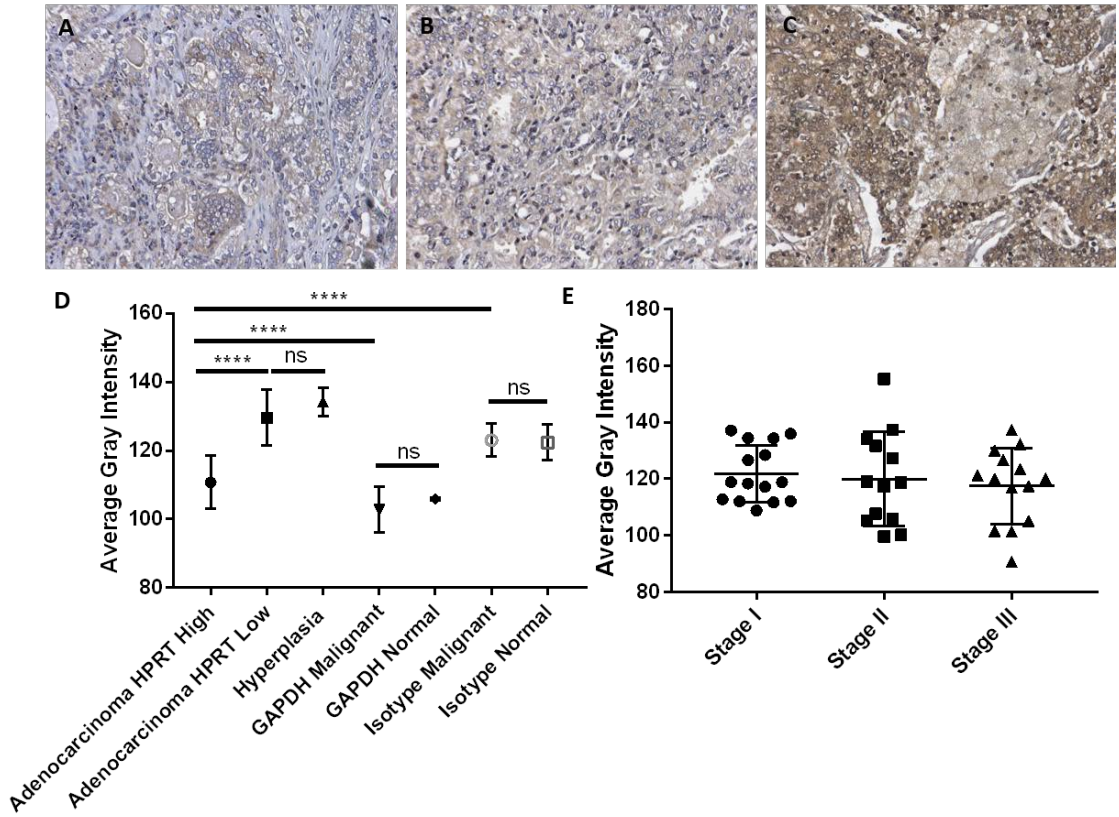

Figure 7-9. *Stage analysis of HPRT expression in prostate cancer stage.* Tissue images of A) Stage I; B) Stage II; and C) Stage III Prostate cancer tissue stained with HPRT. D) Staining of prostate tissue with HPRT, GAPDH, and Isotype antibodies. E, Stage evaluation of prostate tissue stained with HPRT shows no statistically relevant differences between cancer stage.

Of the 53 malignant patients analyzed (Table 7-4) we found a high percentage (55%) of the prostate patient cohort analyzed that were elevated in HPRT when compared to controls (Figure 7-9). Following a stage evaluation, we found no statistically relevant correlation between HPRT expression and the cancer stage even though there appears to be a slight average decrease in gray intensity within the samples (Figure 7-9E). This data, along with data presented in Figure 7-2 indicates there is a significant population of prostate cancer patients that experience an upregulation of this gene.

Discussion

As an enzyme that is significantly upregulated in several malignant tumors, HPRT has the potential to become an additional biomarker for the characterization of several cancers. As Figure 7-2 indicates, there is significant variability within patients in regards to their relative expression of HPRT both in normal and malignant tissue with the overall trend showing upregulation of the protein in cancerous tissue. We have evaluated this expression profile in several of the most common malignancies including lung, colon, breast, and prostate cancer with each showing a similar pattern of expression. This leads us to believe this general upregulation within a subset of patients may be a common trend in several cancer types. While there is a basal level of expression due to the housekeeping nature of HPRT, this expression was generally weak in normal tissue (Table 7-1) and patients who experienced an upregulation had significantly elevated HPRT orders of magnitude higher than isotype controls. Any upregulation that was observed was also independent of cancer grade or stage with the exception of Lung cancer. With this in mind, HPRT could be utilized as an early biomarker because it appears to be upregulated in all stages of cancer, including Stage I. This study has expanded the role HPRT currently has as a mutational biomarker to also encompass a possible involvement in cancer development within some patients[49,521].

Table 7-5. *Distribution of HPRT staining in malignant prostate tissue and normal prostate tissue.*

Tissue Type	Number of Patients	Age Range	Overall Gray Intensity
Adenocarcinoma High	25	66-85	110.77
Adenocarcinoma Low	28	60-82	129.56
Hyperplasia	3	63-75	134.20

Of interesting note is the use HPRT currently plays as a common endogenous control for several cancer-related studies. Due to its housekeeping nature, HPRT is often utilized as a

control for expressional studies and transcriptional analysis in a variety of studies[502–507,522,523]. Yet, the literature is inconsistent when reporting HPRT expression levels within cancer. After comparing various housekeeping genes such as GAPDH, β-2 microglobulin, 18s ribosomal RNA, etc., some researchers have reported HPRT as the most consistent endogenous control[523]. Meanwhile, other researchers have reported HPRT levels to be significantly lower than other controls in cancer tissue[524]. Finally, other studies have reported HPRT as an unsuitable standard in certain cell types due to varying expression in response to growth factor stimuli[525]. Recently, Homey et al. reported the expression of HPRT was detectable in cultured cancer cells, primary tumors, and metastatic tumors, but was found undetectable in normal lung tissue[60]. This data supports our observations and indicates that HPRT has widely variable expression that would deem it unsuitable as a transcriptional control standard.

Conclusions

Our results indicate that HPRT expression has significantly higher expression in malignant tissue when compared to normal controls, and has potential as a biomarker for the characterization of several malignancies including breast, lung, prostate, and colon cancers.

Acknowledgements

We would like to thank the Simmons Center for Cancer Research for funding this work.

CHAPTER 8

Falling from grace: HPRT is unsuitable as an endogenous control for cancer related studies

Michelle H. Townsend, Abigail M. Felsted, Zac E. Ence, Stephen R. Piccolo, Richard A. Robison, and Kim L O'Neill

Citation: MH Townsend, AM Felsted, ZE Ence, SR Piccolo, RA Robison, and KL O'Neill. (under review). Falling from Grace: HPRT is unsuitable as an endogenous control for cancer related studies. PLOS ONE.

The following chapter is taken from an article submitted in PLOS ONE. All content and figures have been formatted for this dissertation.

Abstract

HPRT is a housekeeping enzyme involved in recycling guanine and inosine in the purine salvage pathway. As a housekeeping gene, HPRT has been widely used as an endogenous control for molecular studies evaluating changes in gene expression. Yet, recent evidence has shown that HPRT exhibits high variability within malignant samples with a trend of elevated expression. To determine whether this observed upregulation is found for other molecular techniques and in other organs, we designed this study to thoroughly evaluate the expression of HPRT within both malignant and normal tissues to determine whether it is suitable as an endogenous control. Utilizing protein and RNA-seq expression, we found that malignant and normal patient samples vary significantly both within the same tissue type and across organ sites. Upon staining for HPRT expression via immunohistochemistry, we found that expression is highly variable in malignant samples (Lung; 89.2-111.8, Breast; 66.7-98.3, Colon; 85.3-129.7, Prostate; 90.8-155.4, Pancreas; 74.1-132.1). Similarly, we observed high variability across cell lines via western blotting ($p<0.0001$). RNA sequencing further confirmed these findings; we observed clear variability in expression across 90 different cell lines from five organ sites. Comparing normal and malignant patient samples, we observed consistent upregulation of HPRT expression within malignant samples relative to normal samples (p-value = 0.0001). These data indicate that HPRT is unsuitable as an endogenous control for cancer-related studies because its expression is highly variable and exceeds that of an appropriate control; therefore, we recommend its discontinued use as a normalization gene.

Introduction

Nucleotides provide the essential building blocks to support DNA replication and cell growth [1]. As cell division is controlled by a balance of external factors, the processes that control nucleotide production are tightly regulated [4]. The salvage pathway is a nucleotide synthesis pathway that operates by recycling nucleotides and supplies the majority of the nucleotide pool needed during the s-phase of the cell cycle [9]. Hypoxanthine Guanine Phosphoribosyltransferase (HPRT) is a salvage pathway enzyme involved in the synthesis of both Guanine and Inosine and is responsible for the majority of Guanine production, as 90% of free purines in humans are recycled [10,11]. The enzyme transfers phosphoribose from phosphoribosyl pyrophosphate (PRPP) to hypoxanthine or guanine bases to form IMP and GMP, respectively [10,12]. Due to the constant requirement for GTP, as both a nucleotide for DNA synthesis and as energy currency throughout the cell, HPRT is reliably produced as a housekeeping gene and is found in all somatic tissue in low levels [19–21].

Due to its housekeeping nature, HPRT is commonly used as a standard endogenous control for transcriptional and protein-level analysis [502,504–507,522]. Yet, the literature is inconsistent when reporting HPRT expression levels, particularly in cancer. After comparing various housekeeping genes such as GAPDH, β-2 Microglobulin, 18s ribosomal RNA, etc., some researchers have reported HPRT as the most consistent endogenous control [523], while others have reported HPRT levels to be significantly lower than other controls in cancer tissue [503]. Further studies have reported HPRT as an unsuitable standard in certain cell types due to varying expression in response to growth factor stimuli [525]. Other sources have reported HPRT to be expressed in breast carcinoma cell lines, primary tumors, and metastatic lungs, but undetectable in healthy lung tissue [60]. In addition, further evidence shows that HPRT demonstrates significant

variability between normal patients and those with cancer [61,62]. The inconsistency present in the literature is concerning as HPRT is widely used to standardize both RNA and protein levels.

This study was designed to investigate the use of HPRT as a suitable endogenous control for cancer-related studies. The most essential characteristic of endogenous controls is their relatively constant expression in all cells regardless of experimental conditions. As a critical component of several molecular techniques evaluating small discrepancies in mRNA and protein content, using accurate endogenous controls to standardize expression is paramount in correctly representing data.

Results

HPRT expression varies widely between cancer patients

Due to the housekeeping status of HPRT, protein expression within patient tissue was directly compared against normal tissue samples to highlight additional upregulation above that of normal cells. We found significant variability between normal and malignant patient samples with an overall trend of elevated HPRT expression upon malignancy (Table 8-1). This variability is seen across several different organ types with prostate cancer patients exhibiting the highest discrepancy between normal, 154.93 average gray value, and malignant, 120.83 average gray value. Most notably, the range of staining intensity greatly varied amongst the malignant samples (lung; 89.2-111.8, breast; 66.7-98.3, colon; 85.3-129.7, prostate; 90.8-155.4, pancreas; 74.1-132.1) demonstrating that within each organ type, HPRT expression is significantly variable. This same variability was greatly reduced within the normal tissue samples as the overall range of average gray intensity decreased (lung; 93.0-107.6, breast; 81.6-105.1, colon; 101.5-108.7, prostate; 129.4-136.9, pancreas; 51.0-103.6). Pancreatic tissue showed an inverse relationship when compared to all organ types, as HPRT expression was generally reduced ($p<0.0001$) in

malignant tissue, 154.95 average gray value, when compared to normal tissue, 137.33 average gray value (Figure 8-1).

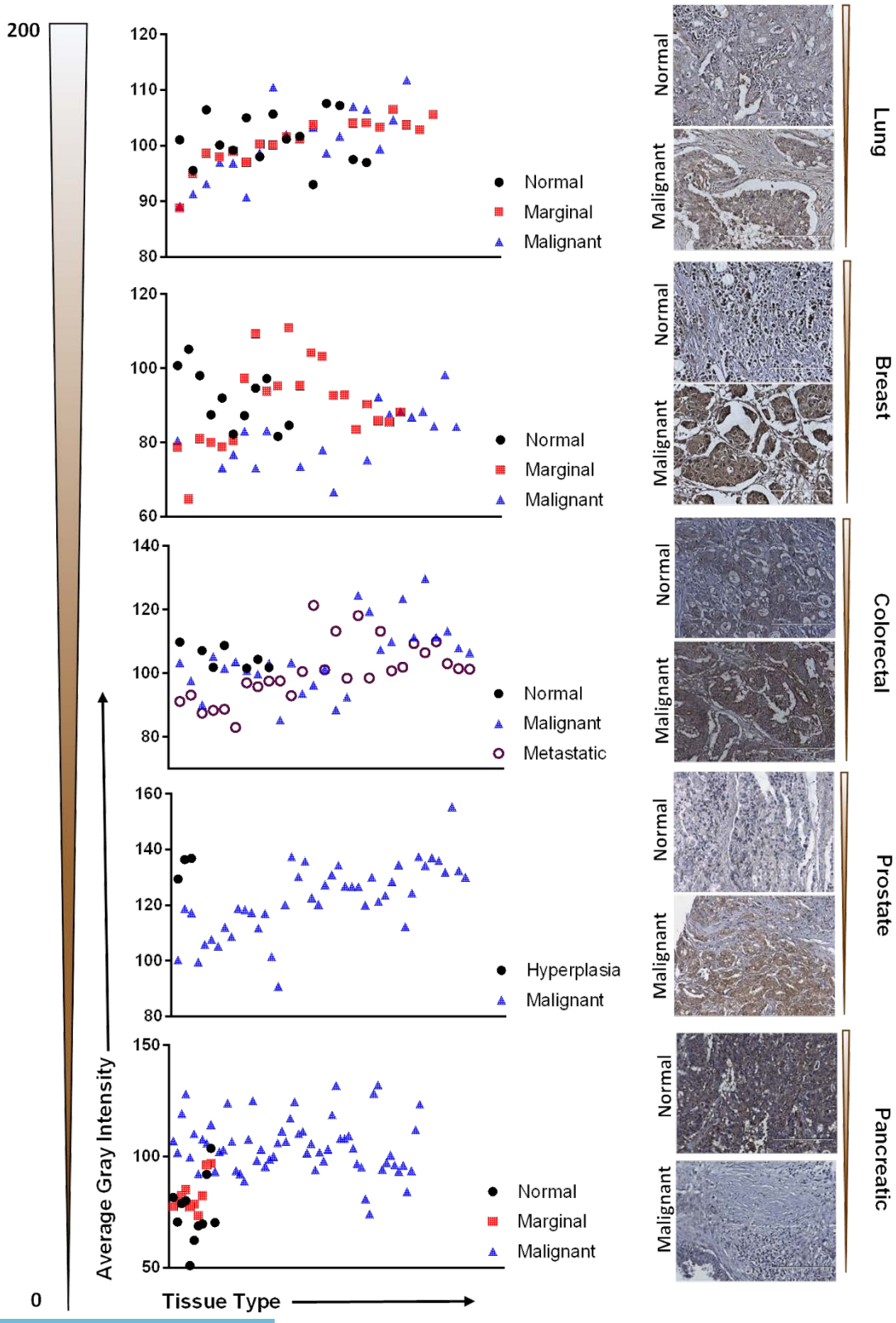

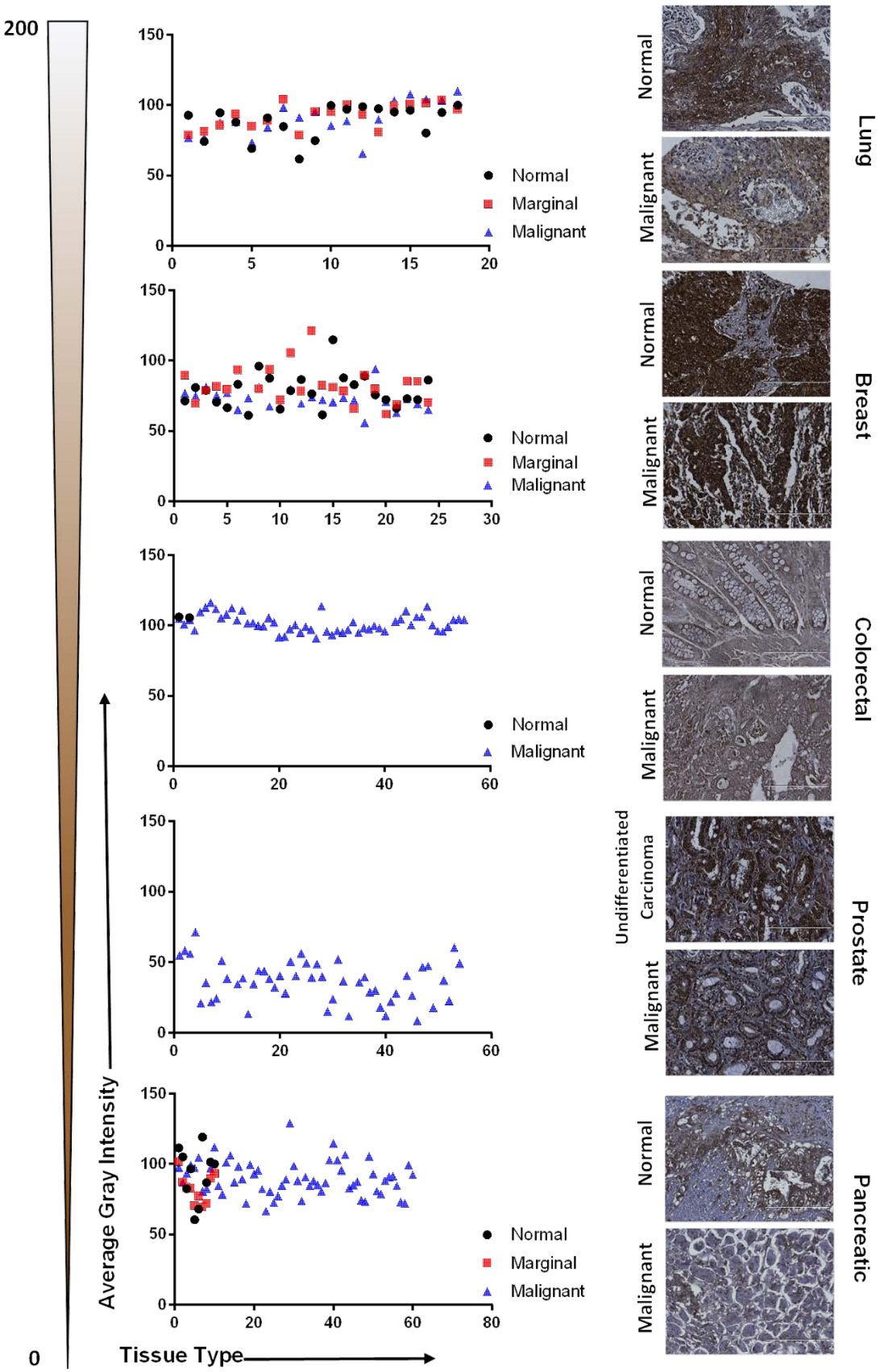

Figure 8-1. *Immunohistochemistry staining of HPRT compared to GAPDH in a variety of organ types*. Lung, Breast, Colon, Prostate, and Pancreatic malignant and normal tissue were stained with antibodies against HPRT and GAPDH to determine any trends in expression between cancerous and healthy tissue. Tissues were quantified on a gray scale and lower values indicate a darker stain and higher protein binding. A, HPRT showed a significant variability between malignant and normal tissue samples with an overall trend of increased HPRT upon malignancy. B, GAPDH had significantly elevated levels of expression in both malignant and normal tissue samples.

Additionally, upon comparing HPRT expression across malignant organ types, we found significant variation with breast tissue showing the highest average HPRT (97.33) and prostate tissue showing the lowest average HPRT (120.83). The discrepancy between the different organ sites was also experienced within normal tissue, but with less severity (Figure 8-2). Breast and colon samples showed significant ($p=0.0183$) changes in HPRT expression, while pancreatic samples were significantly lower than other organ sites ($p<0.0001$). These data indicate that not only is HPRT expression inconsistent between healthy and malignant tissue, but also shows that there is significant variability between various tissue types. On average, the marginal tissue had intermediate HPRT expression between normal levels and malignant levels, which is consistent with our analysis indicating a general trend of increased HPRT expression with cancer development.

Less variability was observed in the box plots of GAPDH samples when compared to the HPRT box plots as they were generally tighter in prostate, colon, and breast samples. GAPDH also showed some significance between normal tissue, but was not as severe as the variability observed in malignant samples.

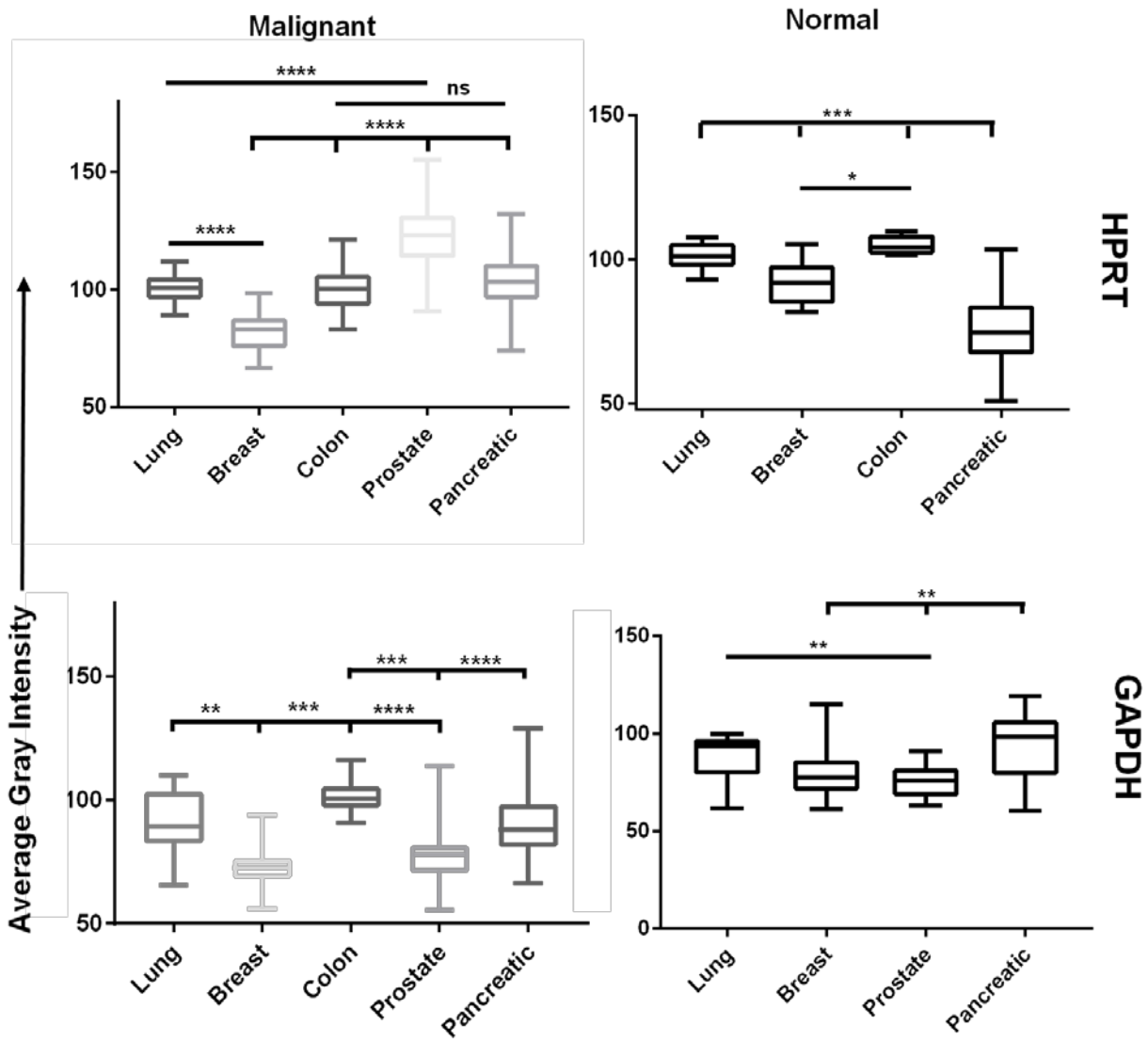

*F*igure 8-2. *Statistical analysis of HPRT and GAPDH expression in patient tissue.* Tissues were quantified on a gray scale and lower values indicate darker staining. Both GAPDH and HPRT had significant variability between organ systems. HPRT showed less significance within normal tissue, with pancreatic tissue showing the greatest significance from other tissue types ($p<0.001$). In malignant samples, HPRT showed more significant variability with all organs showing significance from each other with the exception of Colon and Pancreatic tissue samples. GAPDH showed similar patterns as HPRT with significant expression between malignant organ sites.

Protein expression varies significantly between cell lines

We found that the expression of HPRT protein varied significantly between various cell lines from a variety of organ origins. As protein volumes were standardized against GAPDH, we found that EEF2 had no significant differences in protein expression between cell lines. B2M

showed similar consistent expression, with the exception of Jurkat cells which had significantly ($p=0.0012$) lower expression from other cell line samples. While both B2M, TBP, and GAPDH show very small changes in total protein expression, HPRT had significant variability between all cell types (Figure 8-3). Consistent with tissue data, normal PBMC cells had the lowest total amount of protein ($p<0.0001$), while A549 and U937 cells had the highest total protein content ($p<0.0001$).

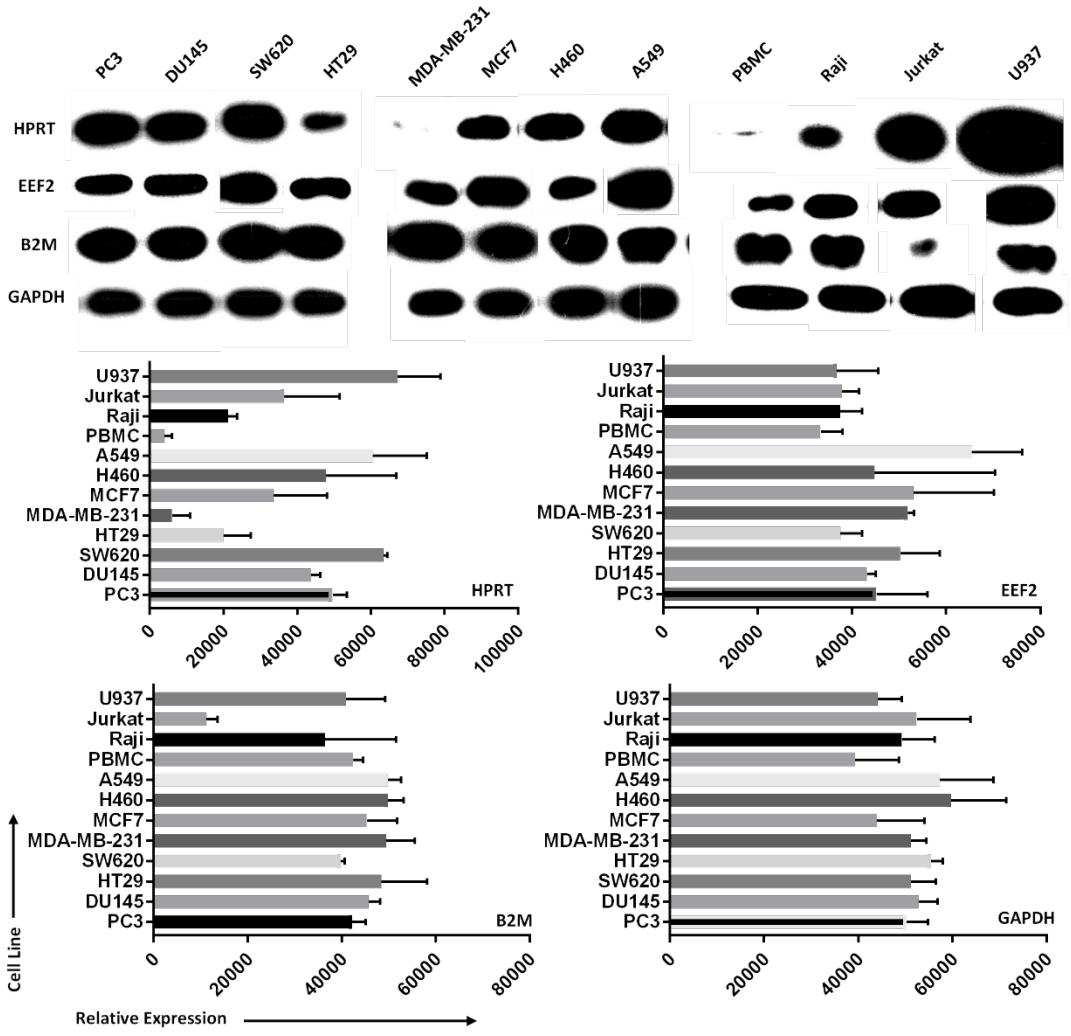

Figure 8-3. *Protein expression between cell lines shows significant variability in HPRT when compared to other endogenous controls*. Samples were originally standardized to GAPDH expression and B2M, EEF2, and HPRT were measured in comparison to that standard. Cell lysates were isolated for 2 cell lines from each organ tissue type. We

find that HPRT expression varies significantly in comparison to both EEF2 and B2M expression when standardized against GAPDH.

PC3 and DU145 prostate cancer cell lines had equal HPRT expression (p>0.999), along with H460 and A549 lung cancer cells (p=0.87). All other organ pairs had significant differences in expression. SW620 and HT29 colon cancer cells (p=0.043), MDA-MB-231 and MCF7 breast cancer cells (p=0.043) all show significant differences in HPRT expression. When comparing normal PBMC lysate to other mononuclear cells, we found Raji cells (p=0.0007), Jurkat cells (p=0.0212), and U937 cells (p=0.0007) each show significant elevation. These data also show that HPRT protein levels within cancer cells are significantly different from one another, especially when compared to other endogenous proteins.

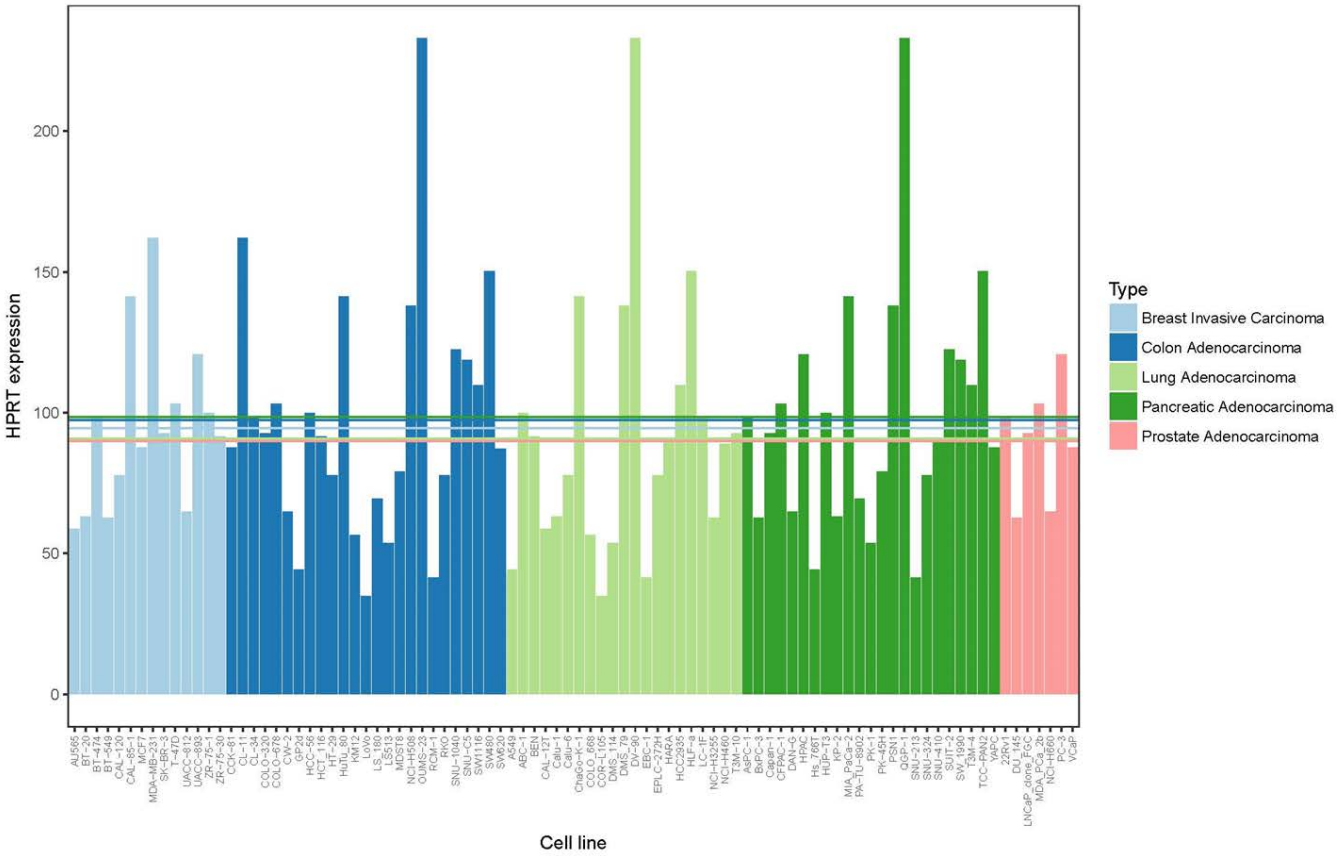

Figure 8-4. *RNA expression in cell lines show a range of HPRT expression. RNA* expression of HPRT was plotted in a range of malignant cell lines (7-25 cell lines) from five different organs sites. The horizontal lines are the average expression levels across all cell lines within a given organ type, which is corresponded to the labeled organ color.

These data show the significant variability in HPRT expression between various cancer cell lines in regards to RNA levels.

RNA levels are inconsistent between various cancer cell lines

To determine whether HPRT was suitable as a control in terms of RNA expression, we evaluated RNA levels of 90 cancer cell lines from a variety of different organ origins (lung, breast, colon, prostate, pancreas). We found statistically significant variability in expression not only between different cancer cell lines within the same organ site, but also found variation between different organ sites (Figure 8-4). The highest expressing cell lines according to RNA expression were QGP-1 (pancreas), DV-90 (lung), and OUMS-23 (colon), while the lowest expressing cell lines were LoVo (colon), COR-L105 (lung), and SNU-213 (pancreas). Although the overall average levels of all cell lines evaluated from each tissue type show some similarity, as indicated by the horizontal lines, the variability between the individual cell lines within and between each organ type is significant.

Table 8-1. *Patient tissue quantification.*

Organ	Tissue Type	Grade Range	Number of Patients	Age Range	Male/Female	Overall gray intensity
Lung	Normal	-	18	30-77	14/4	101.08
	Marginal	-	18			100.74
	Malignant	1-3	18			100.26
Breast	Normal	-	24	28-69	0/24	113.04
	Marginal	-	21	32-74	0/21	107.90
	Malignant	-	18	29-68	0/18	97.33
Colon	Normal	-	8	29-42	8/0	104.37
	Marginal	-	18	32-81	15/3	103.30
	Malignant	1-3	53	30-79	27/26	102.59
Prostate	Normal	-	3	63-75	3/0	134.2
	Malignant	1-3	53	60-85	53/0	120.83
Pancreas	Normal	-	10	19-40	29/28	154.93
	Marginal	-	10	49-73	6/4	137.33
	Malignant	1-3	54	40-84	4/6	154.95

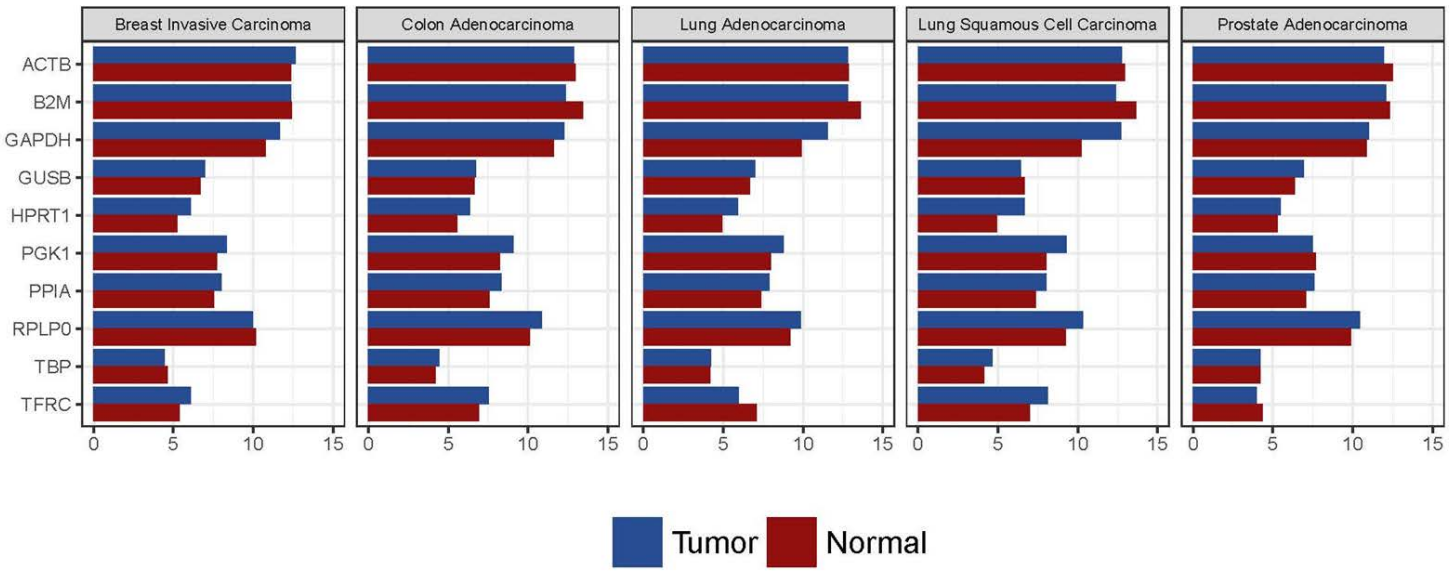

Figure 8-5. *RNA expression in normal and malignant patient tissue.* RNA expression of 10 different endogenous control genes was graphed between tumor and normal samples. We found significant variability between several of the control genes in regard to expression in normal and tumor samples.

Endogenous control variation is dependent on the original organ tissue

We also evaluated RNA expression levels between malignant and normal samples to determine if the same variability observed within cell line data also existed within patient samples. We found that there was an overall significant increase in HPRT upon malignancy, as was observed in other assays (*p-value* = 0.0007, Prostate adenocarcinoma; 0.0001, lung squamous carcinoma; 0.0001, Lung adenocarcinoma; 0.0001, Colon adenocarcinoma; 0.0001, Breast invasive carcinoma). The most significant difference was found within lung squamous cell carcinoma patients. Upon analyzing 9 other endogenous control genes we found that their expression levels also varied, but this was according to the organ tissue type (Figure 8-5). ACTB and TBP generally were elevated in normal patients when compared to malignant patients but showed relatively consistent expression across samples (p-values ACTB: 0.8178, colon adenocarcinoma; 0.4614, lung adenocarcinoma; 0.9974, lung squamous carcinoma; TBP:

0.2615, lung adenocarcinoma; 0.3142, prostate adenocarcinoma). Meanwhile GAPDH, GUSB, PGK1, PP1A, RPLPO, and B2M all generally showed elevation of expression in malignant tumors. TFRC was the only gene that had a variation of elevation, with lung adenocarcinoma and prostate adenocarcinoma patients showing elevated levels in normal samples and lung squamous cell carcinoma, colon adenocarcinomas, and breast carcinoma showing elevation in tumors.

To show how HPRT variability can affect experimental results and conclusions we mapped the other endogenous control genes utilizing either normal HPRT as the standard or malignant HPRT as the standard. Here we see that gene expression can vary. TFRC goes from showing an elevation when normalized to normal HPRT to a decrease in protein expression when standardized to malignant HPRT. This demonstrates that utilizing HPRT in malignant samples does not provide an adequate representation of gene elevation or reduction compared to normal cells (Figure 8-6).

Discussion

This study analyzed the gene expression of HPRT to determine whether the protein is suitable as a normalized control for cancer-related studies. Because HPRT has been used extensively as an endogenous control for a several studies, it is important to provide a clear understanding of how it's expression changes in a cancerous setting [526–532]. Here we have shown that HPRT is not a suitable control in cancer-related experiments as it exhibits expression variability at both protein and transcriptional levels. When comparing normal samples to malignant samples, HPRT showed variation that is not consistent with a good normalized control. Additionally, the levels of HPRT also varied across different organ tissue in malignant samples and, to a lesser extent, normal samples.

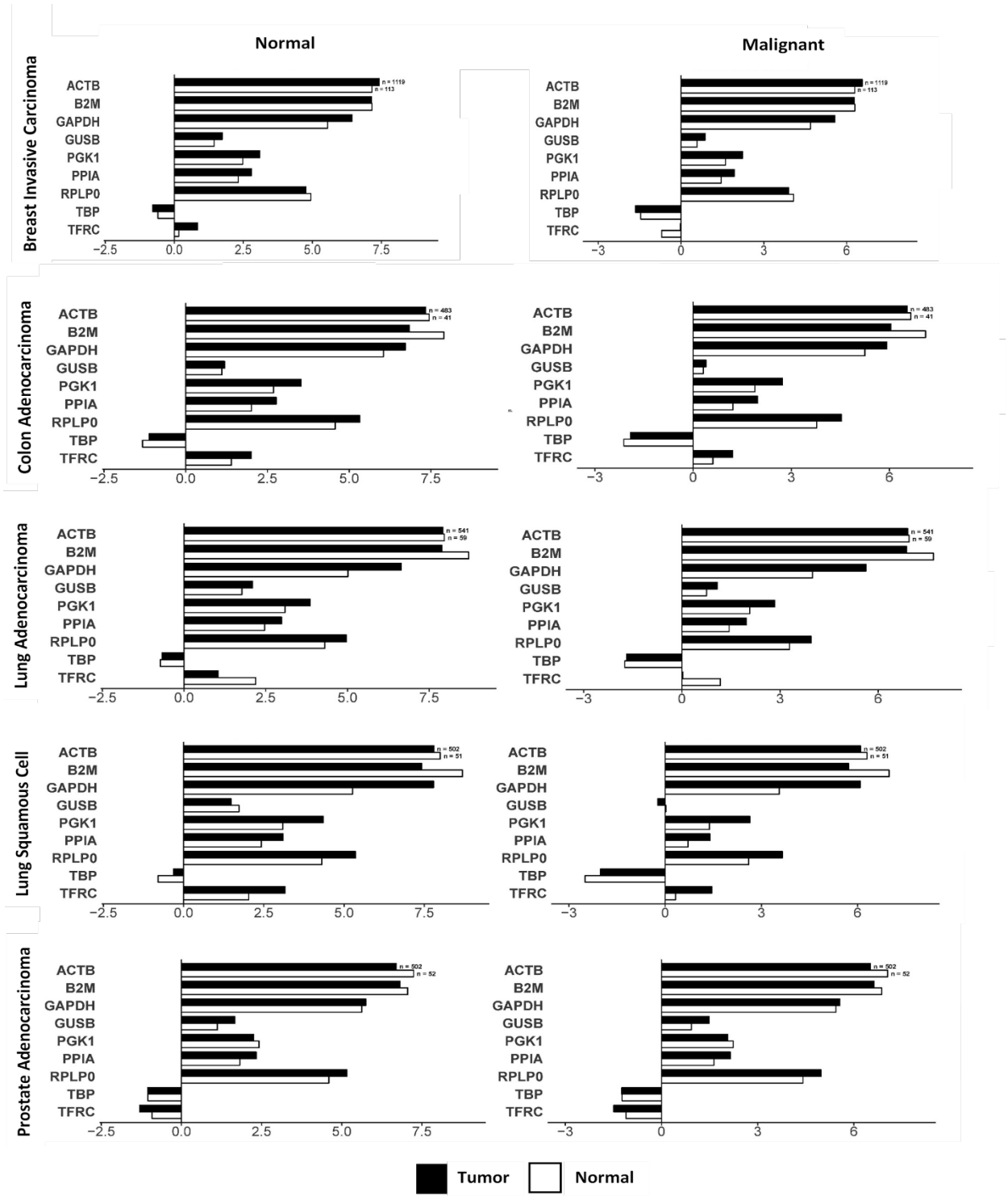

Figure 8-6. *Impact of using HPRT as a normalization standard on gene expression*. Normal and malignant HPRT levels were used as a normalization to compare the expression of the remaining 9 endogenous control genes. We found that when utilizing either normal or malignant HPRT levels there was significant variability in the other endogenous control gene expression profiles.

HPRT has been utilized as the sole housekeeping standard for several studies involving cancer [533,534]. As there is a significant increase in HPRT expression in most tissue types upon developing malignancy, the increased target gene expression observed in several studies may be more significant than originally detected, as some increases in gene expression may be masked by the concomitant increase in malignant HPRT expression. This inherent elevation of HPRT may also conceal genes with increased expression that would have otherwise been significant if a different endogenous control was chosen for the analysis. With this in mind, we would recommend research utilizing HPRT as a single standard to re-evaluate their data to determine if a different control would result in more accurate results. In addition, we propose the discontinued use of HPRT as a standard control as the variability seen within malignant patients renders it unsuitable for normalization.

When comparing 10 different common endogenous controls, we found that their relative expression between malignant and normal tissue was dependent on the originating organ. TBP showed insignificant differences between malignant and normal cells in lung adenocarcinoma but exhibited significant differences in lung squamous cell carcinoma. Some genes also had inverted expression depending on the tissue type. PGK1 had elevated levels in normal prostate, but also had elevated levels in colon adenocarcinoma. These results indicate that it may be in the best interest of the researcher to select the endogenous control genes based upon previously determined expression levels and change the selected control gene according to the experimental conditions and tissue used.

Previous work has already shown that HPRT is an unsuitable endogenous control in some experimental systems, such as embryonic stem cells [525], and has pseudogenes that affect gene

normalization in QPCR [535]. Considering this previous data and the results obtained in our evaluation, HPRT appears to be unsuitable as an endogenous control for cancer-related studies.

Methods

Chemicals/Reagents

Anti-HPRT rabbit polyclonal antibody (ab10479) used for Western blot analysis were purchased from Abcam (Cambridge, United Kingdom) and stored at 4°C. Western bright western blotting detection kit was purchased from Advansta (Menlo Park, CA, USA) and stored at room temperature. DIVA Decloaker 10x, Background Sniper, Mach 4 HRP polymer, DAB Peroxidase, Hematoxylin, Hydrophobic pen, and Universal Negative antibodies were all obtained from Biocare Medical, Concord, CA. GAPDH polyclonal antibody (One World Labs, San Diego CA) was aliquoted and stored at -20°C. Tween20 (Fisher Reagents, Waltham MA) was stored at room temperature. Hydrogen Peroxide, 30% (Fisher Reagents, Waltham MA) was stored at 4°C.

Lysate Preparation

Raji, HT-29, Jurkat, U937, PC3, DU145, NCI-H460, SW620, MCF-7, MDA-MB-231, and A549 human cell lines were obtained from the American Type Culture Collection (Rockville, MD, USA). Raji, HT-29, Jurkat, U937, PC3, DU145 and NCI-H460 cells were grown in RPMI 1640 medium supplemented with 10% fetal bovine serum (FBS) and 2mM L-Glutamine. SW620, MCF-7, and MDA-MB-231 cells were grown in DMEM medium supplemented with 10% FBS and 4mM L-Glutamine (Gibco, MD, USA). A549 cells were grown in F-12K medium supplemented with 10% FBS and 2mM L-Glutamine. Cell media was replaced every 48 hours to maintain exponential conditions. Cell viability was evaluated using trypan blue

staining. All cells were grown at 37°C and 5% CO_2. Cell lines were authenticated in May of 2016 by the University of Arizona Genetics Core.

Whole blood was collected from healthy volunteers under IRB approval (BYU X090281) with written informed consent. Blood was further diluted with PBS at a 1:1 ratio and layered on Lymphocyte Separation Medium (LSM) (Corning Incorporated, Corning, NY, USA) before being centrifuged for 30 minutes at 400xg. The buffy layer was collected and treated with a red blood cell lysis buffer before used for experimentation.

Once confluent, cells were washed with cold PBS and added to a RIPA buffer solution with freshly added protease and phosphatase inhibitor (Thermo Fisher Scientific, MA, USA). Cells were then thoroughly vortexed and incubated on ice for 30 minutes with an additional vortex step performed every 10 minutes. The lysed solution was then pelleted at 15,000xg for 15 minutes at 4°C and aliquoted to avoid freeze-thawing samples. All lysates were stored at -80°C.

Immunohistochemistry

Tissue microarrays were purchased from Biomax. Patient details and information are found in Table 8-1 and include lung, prostate, colon, breast, and pancreatic cancer patients and corresponding normal samples.

HPRT levels were assessed using standard immunohistochemistry staining. Following treatment with Histoclear (National Diagnostics, Charlotte, North Carolina), tissues were rehydrated with a series of ethanol washes. To retrieve antigen, tissues were treated with a DIVA Decloaker. Tissues were washed with a hydrogen peroxide solution followed by a Tris Buffered Saline-Tween20 (TBST) wash. Following washing, tissues were incubated with a blocking Background Sniper solution to reduce non-specific antibody binding. Following blocking, primary antibody was added at a 1:100 dilution and incubated overnight at 4°C. Tissues were

then washed and treated with secondary HRP conjugated antibodies and incubated for an hour. DAB peroxidase was added to the tissues along with hematoxylin to highlight target protein and the cell nuclei, respectively. A universal negative antibody was used as the negative control for background binding, and GAPDH was utilized as a positive control to ensure protocol functionality.

Tissue Quantification

Quantification of tissues was carried out using ImageJ software. An IHC toolbox ImageJ plugin with the DAB more option was chosen and tissues were removed of all non-DAB stain. Following this modification, the image was converted to a grayscale and a threshold was applied to eliminate areas of negative space. This same threshold was applied to all tissue samples within the same organ to ensure consistency and reduce sample bias.

Western Blot and quantification

Cell lysates were blotted for GAPDH, B2M, EEF2, and HPRT expression utilizing standard Western Blotting techniques described in Sewda et al., with minor modifications [22]. Briefly, each sample was boiled for 5 minutes prior to running on a 12% polyacrylamide gel under reducing conditions. Gels were then transferred to a nitrocellulose membrane (Biorad Laboratories Hercules, CA, USA), blocked, and treated with primary antibody overnight at 4°C on a shaker. Following primary antibody treatment, membranes were washed and treated with secondary HRP antibodies (Abcam, Cambridge, United Kingdom) for 1 hour at room temperature. Membranes were then washed and treated with a Western Bright (Advansta, California, USA) HRP substrate before capturing the image with X-ray film. Western images were imported into ImageJ and converted to an 8-bit image. Lanes were then selected and

plotted. The area under the individual bands were calculated to determine the relative protein expression of the samples.

Transcriptomic analysis

We evaluated expression levels for 90 cell lines from the Cancer Cell Line Encyclopedia using data that had been generated using Illumina-based RNA-Sequencing[536,537]. The data values were originally calculated at the isoform level using the *kallisto* software[538]; we calculated gene-level values by summing the isoform values for each gene. Next we log-transformed these values and converted them to transcripts-per-million values. We sorted the cell lines according to HPRT1 expression level, from high to low expression per sample.

We obtained gene-level expression values for tumors and normal tissues from The Cancer Genome Atlas[539]. The Illumina-based, RNA-Sequencing data had been prepared previously using the *featureCounts* algorithm and the *Rsubread* package[540–542]. In cases where RNA expression had been profiled for the same patient multiple times, we averaged expression on a per-gene basis across the replicates. Next, we log-transformed the data and normalized the data to transcripts-per-million values. The normal data came from tissue of the same organ type or from blood samples; however, these samples did not necessarily come from the same patients as the tumor samples.

We preprocessed the RNA expression data using scripts written in the Python programming language (https://python.org, v.3.6.1). To make graphs for this analysis, we used the ggplot2 package (v.2.2.1) and the Superheat package (v.0.1.0) implemented for the R (v.3.4.3) statistical software[543–545].

Statistical analysis

ANOVA using the multiple comparison method was used to determine significance differences between patient tissue samples in immunohistochemistry staining and western blotting data. These statistical analyses were evaluated using GraphPad Prism 7 software.

In calculating differences in transcriptome between tumor and normal samples, we used a permutation-based test. For a given gene, we repeatedly (n = 10,000) permuted the tumor/normal labels and calculated the difference in mean expression; then we compared the actual difference in expression for a given gene against its respective permuted distribution; lastly, we calculated an empirical p-value by determining the proportion of times that the actual difference was greater than the permuted differences. Differences were considered significant when the p value was < 0.05. These tests were performed using the R (v.3.4.3) statistical software.

CHAPTER 9

Evaluation of the upregulation and surface expression of Hypoxanthine Guanine Phosphoribosyltransferase on B cell malignancies

Michelle H. Townsend, Zac E. Ence, Abigail M. Felsted, Taylor P. Cox, John E. Lattin, Weston Burrup, Michael K. Boyer, Stephen R. Piccolo, Richard A. Robison, and Kim L. O'Neill

Citation: Townsend MH, Ence ZE, Felsted AM, Cox TP, Lattin JE, Burrup W, Boyer MK, Piccolo SR, Robison RA, O'Neill KL. (under review). Evaluation of the upregulation and surface expression of Hypoxanthine Guanine Phosphoribosyltransferase on B cell malignancies. Biomarkers Research.

The following chapter is taken from an article submitted in Biomarkers Research. All content and figures have been formatted for this dissertation.

Abstract

Background: The aim of this study is to determine whether Hypoxanthine Guanine Phosphoribosyltransferase (HPRT) could be used as a biomarker for the diagnosis and treatment of B cell malignancies. With 4.3% of all new cancers diagnosed as Non-Hodgkin lymphoma, finding new biomarkers for the treatment of B cell cancers is an ongoing pursuit. HPRT is a nucleotide salvage pathway enzyme responsible for the synthesis of guanine and inosine throughout the cell cycle.

Methods: Raji cells were used for this analysis due to their high HPRT internal expression. Internal expression was evaluated utilizing western blotting and RNA sequencing. Surface localization was analyzed using flow cytometry, confocal microscopy, and membrane biotinylation. To determine the source of HPRT surface expression, a CRISPR knockdown of HPRT was generated and confirmed using western blotting. To determine clinical significance, patient blood samples were collected and analyzed for HPRT surface localization.

Results: We found surface localization of HPRT on both Raji cancer cells and in 77% of the malignant ALL samples analyzed and observed no significant expression in healthy cells. Surface expression was confirmed in Raji cells with confocal microscopy, where a direct overlap between HPRT specific antibodies and a membrane-specific dye was observed. HPRT was also detected in biotinylated membranes of Raji cells. Upon HPRT knockdown in Raji cells, we found a significant reduction in surface expression, which shows that the HPRT found on the surface originates from the cells themselves. Finally, we found that cells that had elevated levels of HPRT had a direct correlation to XRCC2, BRCA1, PIK3CA, MSH2, MSH6, WDYHV1, AK7, and BLMH expression and an inverse correlation to PRKD2, PTGS2, TCF7L2, CDH1, IL6R, MC1R, AMPD1, TLR6, and BAK1 expression. Of the 17 genes with significant correlation, 9 are involved in cellular proliferation and DNA synthesis, regulation, and repair.

Conclusions: As a surface biomarker that is found on malignant cells and not on healthy cells, HPRT could be used as a surface antigen for targeted immunotherapy. In addition, the gene correlations show that HPRT may have an additional role in regulation of cancer proliferation that has not been previously discovered.

Introduction

Non-Hodgkin lymphomas (NHL) and lymphocytic leukemia (Chronic Lymphoblastic Leukemia and Acute Lymphoblastic Leukemia) are hematological cancers that include more than 30 different cancers of B and T lymphocytes [546]. Non-Hodgkin lymphoma diagnoses made up 4.3% of all new cancer cases in 2017, demonstrating the prevalence of the disease in the United States [547]. In addition, leukemia is the most common malignancy in children, with ALL comprising approximately 26% of all childhood cancers [548,549].

Cancer biomarkers are typically categorized as diagnostic, prognostic, or predictive. While diagnostic biomarkers identify the onset or presence of cancer, prognostic biomarkers inform physicians of clinical outcomes for their patients throughout treatment, and predictive biomarkers suggest how patients will respond to various treatment regimens [550]. A new category of surface biomarkers has emerged; these biomarkers function as targets for immunotherapy [551–555]. Currently, the most prominent immunotherapy biomarker for B cell malignancies is CD19 [180,556–559]. CD19 is a type I transmembrane protein expressed in normal and neoplastic B cells, and follicular dendritic cells [560]. CD19 has been used as a direct target for chimeric antigen receptors (CARs) as well as an antibody in bi-specific T-cell that directs cytotoxic T-cells to CD19 expressing B cells [560]. Currently, the only FDA approved CAR therapy targets are against CD19; these include Yescarta and Kymriah [561]. A disadvantage of utilizing this biomarker target is that patients' healthy B cell populations decrease because CD19 is not specific to cancer cells. Another disadvantage of targeting CD19 is that some tumors experience antigen loss which confers resistance to CD-19-targeted immunotherapy, and approximately 10%-20% of patients relapse following treatment with CD19-CAR therapy [562,563]. To aid in reducing antigen loss, researchers seek to identify new immunotherapy biomarkers that can be targeted to eliminate B cell malignancies. New targets such as CD22, CD20, andROR1 have all shown promise in

eliminating certain B cell malignancies, but further research is needed to expand targetable antigens on the surface of malignant B cells [564–567].

Previous studies have found that there is variability in regards to hypoxanthine guanine phosphoribosyltransferase (HPRT) expression within malignant tissue [61], and as such it has been suggested that HPRT could be used as targetable biomarker for some solid malignancies [62]. We have designed this study to determine whether HPRT could be used as a targetable biomarker in the treatment of B cell malignancies [61,514]. In doing this, we hope to identify additional biomarkers options to lessen the growing concern of antigen loss.

Materials and Methods

Chemicals

Anti-HPRT mouse monoclonal antibody (MA5-15274) used for flow cytometry was aliquoted and stored at -20°C (Thermo Fischer Scientific, Waltham, MA, USA). Anti-HPRT rabbit polyclonal antibody (ab10479) used for Western blot analysis were purchased from Abcam (Cambridge, United Kingdom) and stored at 4°C. Anti-Mouse-FITC and anti-Rabbit-FITC antibodies (Sigma Aldrich, St. Louis, MO, USA) were stored at 4°C and were used in dark conditions. Goat-anti-rabbit-HRP secondary antibody was purchased from Abcam and stored at 4°C. NF-κB polyclonal antibody (Bioss Antibodies, Wodburn, MA, USA) was stored at 4°C and used as an internal negative control for surface expression. CD44 monoclonal antibody and GAPDH polyclonal antibody (One World Lab, San Diego, CA) were stored at -20°C and used as positive control and negative controls for surface expression, respectively. Propidium Iodide (Sigma Aldrich Inc., Milwaukee, WI, USA) was stored at 4°C and aliquoted for use. Fc Block was purchased from Biolegend (San Diego, CA, USA) and stored at 4°C. An APC-Conjugation

Kit (Abcam, Cambridge, United Kingdom) was stored at -20°C and following conjugation, antibodies were stored at 4°C.

Cell Culture Conditions

The Raji (CCL-86- human Burkitt's B cell lymphoma) cell line was obtained from the American Type Culture Collection (Rockville, MD, USA). Raji cells were grown in RPMI 1640 medium supplemented with 10% fetal bovine serum (FBS) and 2mM L-Glutamine (all from Hyclone, Logan, UT, USA). Cell media was replaced, and cells were cut to maintain exponential conditions throughout experimentation. Cell viability was evaluated using trypan blue staining, and cells were utilized for all applications when viability exceeded 98%. All cells were grown at 37°C and 5% CO_2. Raji cells were authenticated in May of 2016 by the University of Arizona Genetics Core.

Flow Cytometry

The surface presence of HPRT was evaluated by measuring the fluorescence intensity of antibodies against the enzyme. All samples were analyzed on a Blue/Red Attune (Applied Biosystems), and 25,000-50,000 events were recorded per sample. Briefly, 3-5x105 cells were incubated with 200µL of PBS containing 1µg of primary antibody for 15 minutes at 4°C. Cells were then labelled with FITC-conjugated secondary (mouse or rabbit) antibody for 15 minutes 4°C. Isotypic IgG and unstained cells served as negative controls to ensure correct cell gating. The forward/side-scatter plots were used to gate out cell doublets, dead cells, and cell debris. Using unstained and isotype controls as guides, the positive population was determined by the overall shift in the fluorescent intensity. Each cell line was independently analyzed and the data

was plotted using FlowJo Software (FlowJo Enterprise). Cells were washed appropriately after each step of the protocol.

Mononuclear cell separation

Whole blood was collected from healthy volunteers under IRB approval (BYU X090281) with written informed consent. Blood was further diluted with PBS at a 1:1 ratio and layered on top of Lymphocyte Separation Medium (LSM) (Corning Incorporated, Corning, NY, USA) before being centrifuged for 30 minutes at 400xg. The buffy layer was collected and treated with a red blood cell lysis buffer before used for experimentation.

ALL Patient Samples

Acute lymphoblastic leukemia (ALL) samples were collected at diagnosis or relapse from patients after informed consent utilizing a biobank protocol at the Huntsman Cancer Institute in Salt Lake City, UT. Samples were frozen with dimethyl sulfoxide (DMSO) and albumin and further aliquoted for analysis. Following sufficient thawing at 37°C, samples were washed with Dulbecco's phosphate-buffered saline (DPBS). After careful washing, cells were used for flow cytometry analysis and stained with similar procedures as previously described.

Surface Biotinylation and Western Blot Analysis

Cells were analyzed for surface presence of HPRT along with general expression within the cell using the Pierce Cell Surface Protein Isolation Kit (Thermo Scientific, Waltam, MA, USA). Briefly, 3 flasks of Raji cells were grown to 95% confluency and normal lymphocytes were obtained from healthy donors under appropriate IRB approval (#090281). These cells were washed and treated with a biotin solution. Following rocking on a shaker for 30 minutes at 4°C,

the cells were treated with a quenching solution. Then, cells were treated with a lysis solution and incubated for 30 minutes at 4°C. Cell lysate was added to a neutravidin gel and incubated for 60 minutes at room temperature. This solution was then run through a filter and proteins bound to biotin were trapped within the column. The neutravidin gel was washed 4 times and the flow through was collected and labelled "cytosolic fraction". The biotin-labelled protein was then eluted from the column utilizing a 50mM DTT solution and labelled "membrane fraction".

Both membrane and cytosolic fractions were evaluated for HPRT presence using standard Western Blotting techniques described in Sewda et al. with slight modifications [22]. Briefly, each sample was boiled for 5 minutes prior to running on a 12% polyacrylamide gel under reducing conditions. Gels were then transferred to a nitrocellulose membrane (Biorad Laboratories Hercules, CA, USA), blocked, and treated with an anti-HPRT polyclonal antibody overnight at 4°C on a shaker. Following primary antibody treatment, membranes were washed and treated with a goat anti-rabbit HRP antibody (Abcam, Cambridge, United Kingdom) for 1 hour at room temperature. Membranes were then washed and treated with a Western Bright (Advansta, California, USA) HRP substrate and the image was captured with X-ray film.

Confocal Microscopy

Image processing was carried out with Laser Sharp Computer Software (Bio Rad Laboratories). Cells were incubated in 200uL of PBS containing 1µg of anti-HPRT monoclonal antibody for 15 minutes at 4°C. Cells were then labelled with 1µg of FITC-conjugated secondary antibody for 15 minutes at 4°C. Then, cells were incubated at 37°C for 10 minutes with a 1:1000 dilution of a Cell Mask Deep Red plasma membrane dye (Fisher Scientific, Waltham, MA, USA). Cells were imaged using an epiflourescence microscope (Olympus, Tokoyo, Japan)

equipped with a 15mW Krypton/Argon laser (Bio-Rad Laboratories, Hercules, CA). Images were captured and processed using Laser Sharp Computer Software (Bio Rad Laboratories).

HPRT knockdown

The pSpCas9(BB)-2a- GFP CRISPR vector was purchased from Addgene (Cambridge, MA, USA) and guide RNA design was conducted using the CRISPR Design tool created by MIT [568]. Briefly, Raji cells were grown to a concentration of 4x105 cells per mL and seeded in a 6-well plate. Following 24 hours of growth, cells were transfected with a lipofectamine LTX reagent (Invitrogen Waltam, MA, USA). Briefly, 150µL of Opti-MEM (Gibco, Gaithersburg, MD) was incubated with 5-7µL of Lipofectamine LTX reagent while 250µL of Opti-MEM was incubated with approximately 2x103ng of the CRISPR vector. The solutions were mixed together and incubated at room temperature for 30 minutes. The lipofectamine-DNA solution was then added to the Raji cells in a drop-wise fashion. Cells were grown for 3 days and then treated with media containing 6-Thioguanine (6-TG) at a final concentration of 10µg/µL. 6-TG is a nucleoside analog that is toxic to cells with a functional HPRT gene. Cells that survived the 6-TG treatment were grown to sufficient quantities to produce cell extract. This extract was analyzed by Western blotting using similar techniques described previously, to confirm surviving cells were HPRT-/-.

Bioinformatic gene expression analysis of malignant B cell lines

We evaluated gene-expression levels for 105 genes across 79 cell lines from the Broad Institute's Cancer Cell Line Encyclopedia [537]. We used RNA-Sequencing data for protein-coding transcripts that had been generated using Illumina-based, short-read sequencing. These data had been processed using the kallisto software [538], then log- transformed and converted to transcripts-

per- million values [536]. This data can be found at https://osf.io/gqrz9/files/ (matrices/CCLE/CCLE_tpm.tsv.gz). We summed the transcript-level values to gene-level values and sorted the cell lines according to HPRT expression level, from high to low expression per sample. We parsed and prepared the data using Python (https://python.org, v.3.6.1) scripts. In making the heat map, we used the R (v.3.4.3) statistical package [569] and the Superheat package (v.0.1.0) [543].

Statistical analysis

ANOVA statistical analysis with the Tukey-Kramer multiple comparison method were used to analyze the flow cytometry data from all cell lines, representing the differential surface expression of HPRT for the various treatments. In addition, two-way ANOVA tests were performed to compare the mean expression of HPRT between wild type Raji and knockdown cells. All statistical analyses were performed using GraphPad Prism 7 software. Differences were considered significant when a p value was <0.05.

When assessing relationships between HPRT expression and other genes, we used a Spearman correlation test to calculate correlation coefficients and two-sided p-values. In performing these calculations, we used the cor.test function in the stats package of the R (v.3.4.3) statistical software.

Results

Raji cells show a significant increase in HPRT localization on the plasma membrane while healthy cells have insignificant expression.

Raji cells treated with antibodies against HPRT had an average fluorescent population shift of 81.39% which was significantly different (p-value < 0.0001) from the isotype controls,

which only experienced a 1.50% shift in the fluorescent population (Figure 9-1A&C). Lymphocytes from healthy donors treated with antibodies against HPRT had insignificant fluorescent shifts in the population (1.53%) when compared to isotype controls (p-value = 0.98)(Figure 9-1B&D). These results indicate that HPRT has substantial presence on the surface of Raji cells and has insignificant presence on the surface of their normal counterparts.

To confirm surface localization, malignant and normal cells were analyzed using confocal microscopy to visualize direct overlap between the plasma membrane and HPRT binding. Raji cells had a direct overlap between the membrane specific dye and the FITC conjugated HPRT antibody resulting in a yellow merged image (Figure 9-2B). This same overlap was not observed in normal lymphocytes as the HPRT binding was similar to that of the isotype control, showing that these cells had minimal HPRT expression (Figure 9-2A). This analysis shows that HPRT associates strongly with the plasma membrane and has a significant surface presence on malignant Raji cells.

Biotinylated surface proteins show HPRT bound to the plasma membrane of Raji cells.

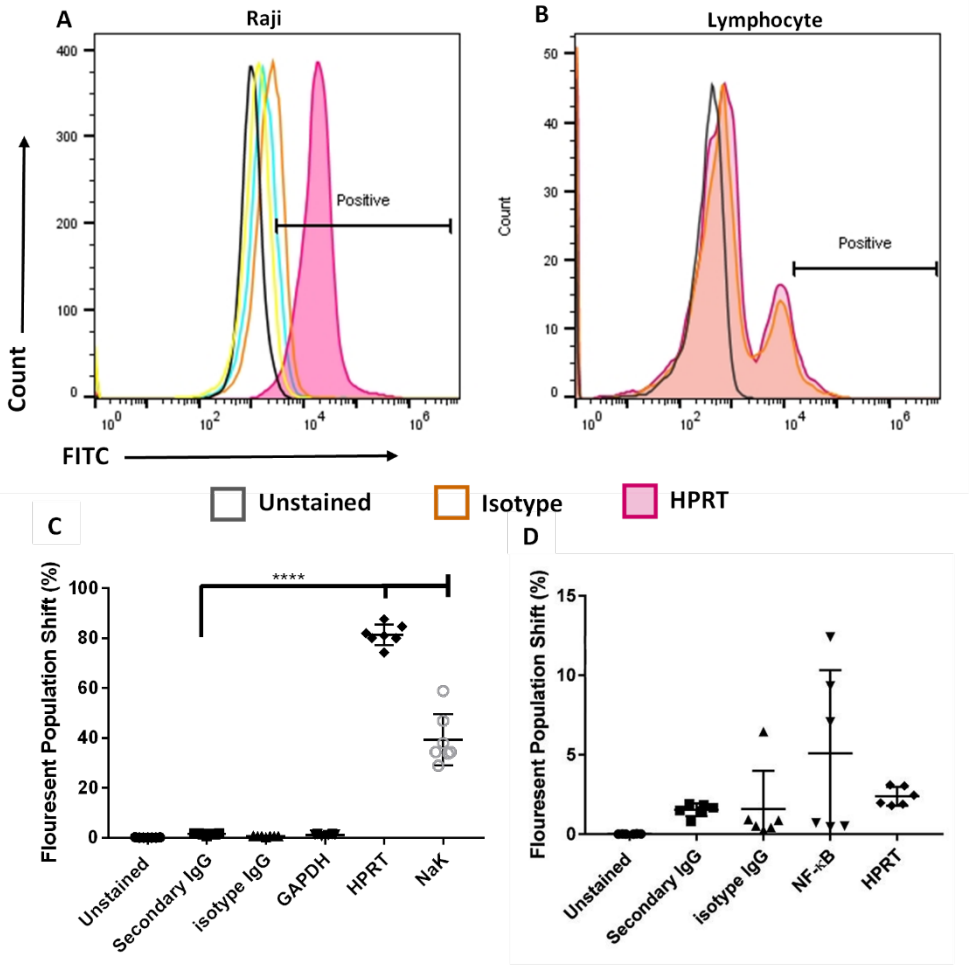

Figure 9-1. *HPRT surface localization in Raji and normal cells.* A, Raji cells treated with a fluorescent anti-HPRT antibody experienced a significant shift (p-value < 0.0001) when compared to isotype controls. B, Normal lymphocytes from healthy donors treated with fluorescent anti-HPRT antibodies did not experience a significant shift in the fluorescent population when compared to isotype controls. C, Statistical analysis reveals a significant elevation of HPRT expression on the surface of Raji cells, and D, an insignificant elevation of HPRT on healthy lymphocytes.

To further confirm whether HPRT was bound to the plasma membrane of Raji cells, we biotinylated the surface proteins of Raji cells and normal cells, and probed for HPRT presence. This analysis revealed a band in the Raji membrane biotin sample that was absent from the normal lymphocyte membrane biotin sample and all other membrane controls. As expected, the band observed in the membrane fraction was smaller than that of the cytosolic fraction as the amount of HPRT on the cell surface would be significantly less than the internal levels of the protein (Figure 9-3). This analysis further confirmed the localization of HPRT on the cell surface of Raji cells and the absence of the enzyme on normal cells.

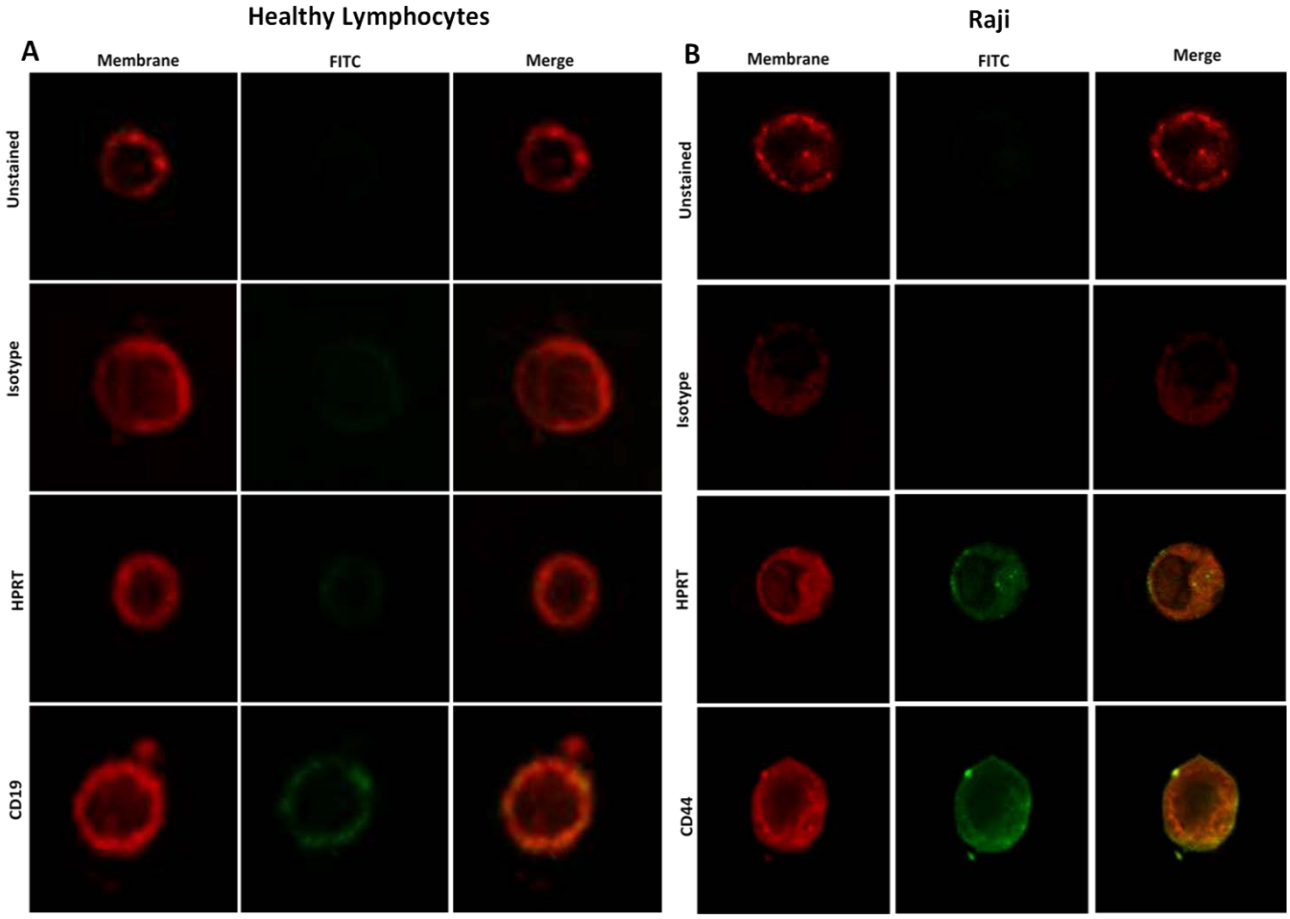

Figure 9-2. *HPRT directly overlaps with the plasma membrane of Raji cells*. Fluorescent HPRT antibodies were compared against a membrane specific dye to highlight overlap in binding. CD19 and CD44 were used as positive controls and isotype controls were used as negative controls to highlight nonspecific antibody binding A, Healthy lymphocytes did not have a significant presence of HPRT on the cell surface and levels were similar to isotype controls. B, Raji cells showed a clear increase in fluorescence when analyzed for HPRT and there was a direct

overlap between the membrane dye and the antibody treatment, indicating that HPRT is co-localized with the plasma membrane of Raji cells.

HPRT knockdown cells exhibited reduced levels of surface HPRT expression.

To help confirm that the surface HPRT originated from the cells themselves, we created a knockdown of HPRT in Raji cells using a CRISPR system. Following adequate selection, we determined that there was sufficient reduction of HPRT within the cells for analysis (Figure 4). The average relative expression of the enzyme went from 47,628 in wild type Raji cells to 2,254 in knockdown cells (p-value = 0.0002). In conducting this analysis, we also observed that the HPRT expression within Raji cells was significantly different than the expression within normal PBMCs. This further demonstrates the variability of HPRT expression between malignant and normal samples.

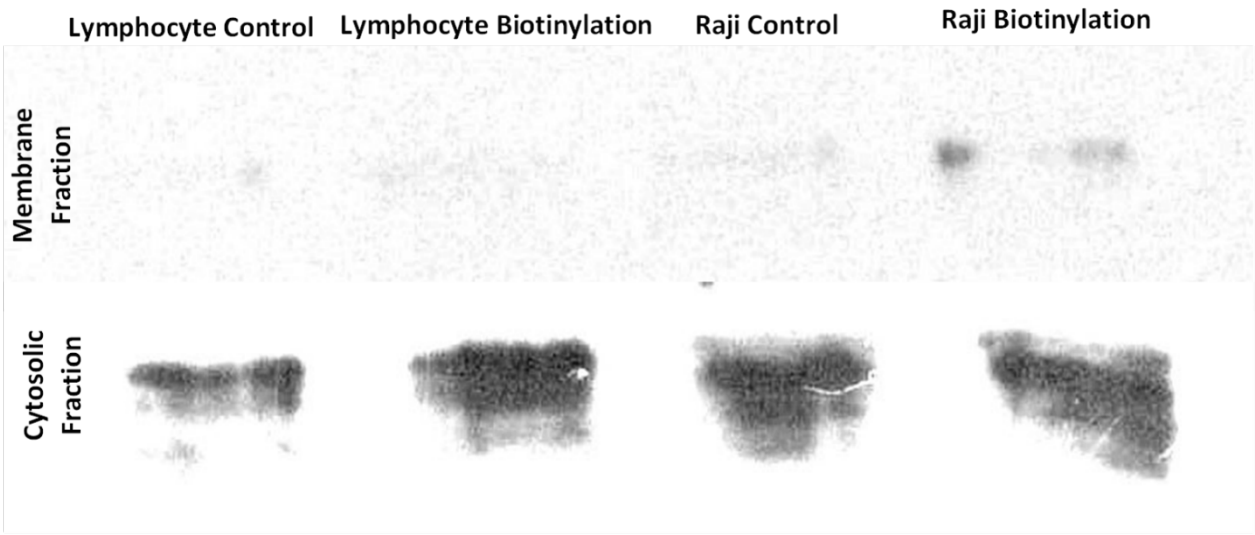

Figure 9-3. *Biotinylated surface proteins reveal HPRT presence and confirms surface presence of the protein.* 'Membrane Fraction' shows the total surface proteins on both lymphocytes and Raji samples. 'Cytosolic Fraction' shows the total HPRT within the cell. A band is observed in the 'Raji Biotinylation' sample as the membrane fraction of Raji cells and healthy lymphocytes are probed for HPRT presence.

When evaluating HPRT knockdown cells for surface expression we found a significant (p-value = 0.039) decrease in the presence of the protein on the surface compared to the WT Raji counterparts (Figure 5). We observed a shoulder in the population that we hypothesize are a result of the sample not being a true knockout, but a knockdown. While the knockdown cells did show slight significance in expression when compared to isotype controls (p-value = 0.029), this was far less than the surface expression of HPRT in WT Raji cells (p-value = 0.0001). The overall average reduction in HPRT expression upon protein knockdown was approximately 20%. Further analysis with a true knockdown cell line will need to be evaluated to confirm these initial findings, but these data indicate that surface HPRT is in some way directly produced within the cells.

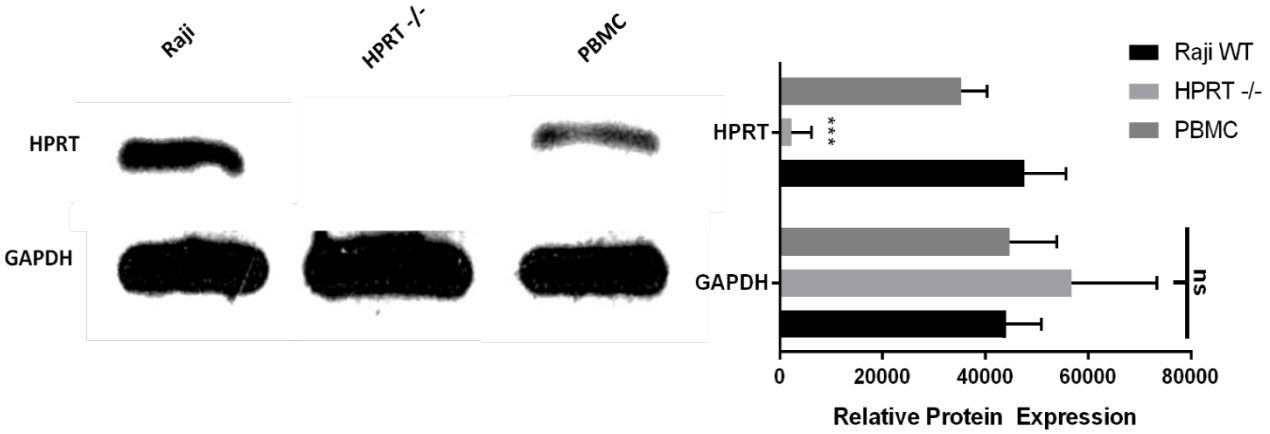

Figure 9-4. *HPRT knockdown confirmation.* Following knockdown of HPRT, a western blot was performed to both confirm knockdown status and to also quantify the expression of HPRT within Raji cells and healthy PBMC. Knockdown cells had significantly decreased levels of HPRT in total cell lysate, indicating successful knockdown (p-value = 0.0002). Healthy PBMCs had significantly lower total HPRT than Raji samples.

Analysis of patient samples shows that HPRT surface expression has clinical relevance. To determine whether the presence of HPRT was an artifact of cell culturing conditions or cell immortalization, we analyzed samples from patients with ALL to determine whether the

phenomenon was also found within these patients. We found that 7 out of the 9 patient samples were positive for elevated HPRT on the cell's surface and we saw an overall increase in fluorescence (p-value < 0.0001) upon anti- HPRT treatment when compared to isotype controls. The highest expression observed was approximately 34%, while the lowest expression was 6.7%, with the average fluorescence shift around 25% for ALL patients (Figure 9-6). This analysis

showed that HPRT has relevance within a proportion of patients. This analysis also confirmed

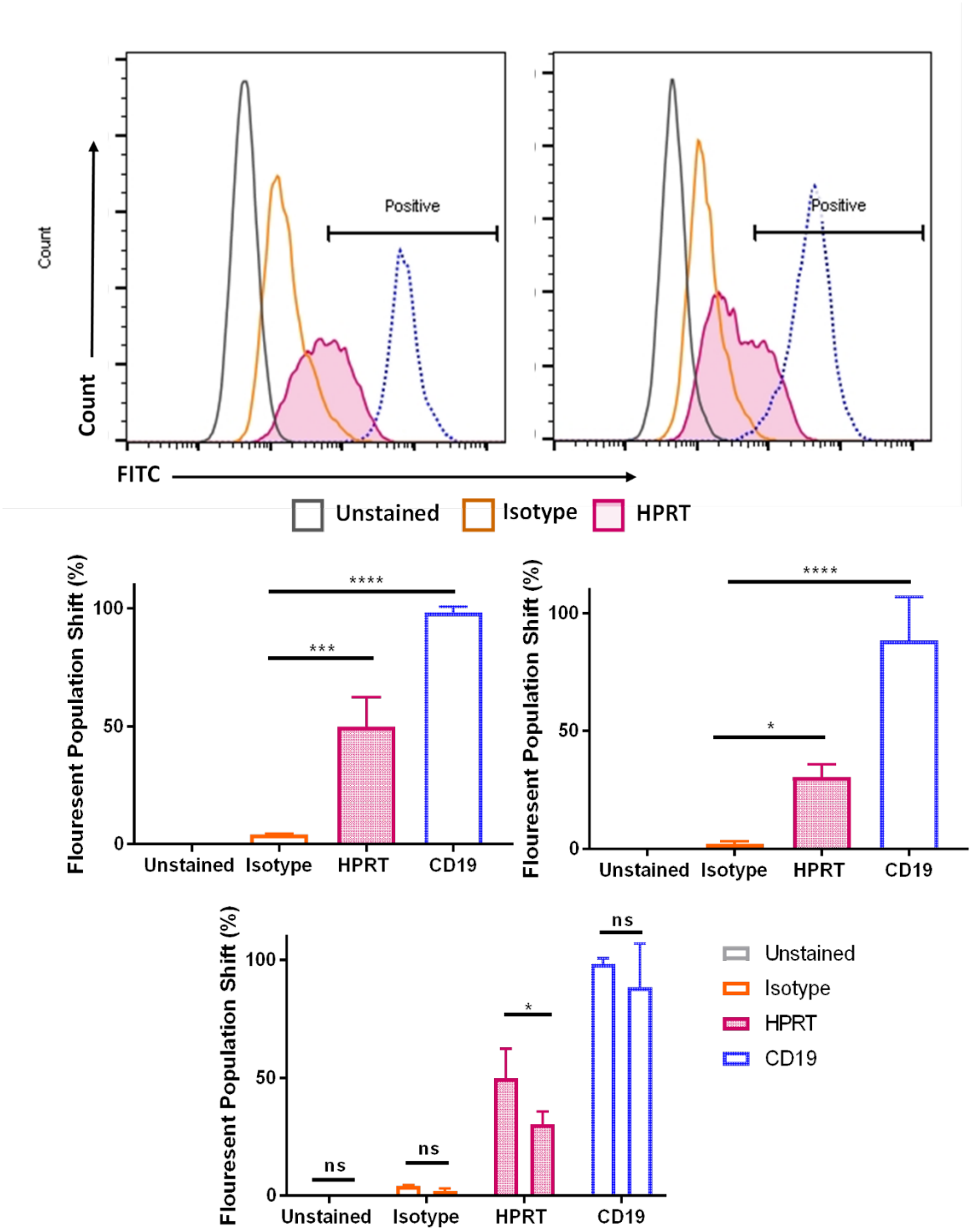

Figure 9-5. *Flow analysis of HPRT knockdown Raji cells reveal a reduction in surface binding*. Following knockdown of the HPRT gene in Raji cells, we analyzed surface HPRT expression in both knockdown Raji and wild type Raji cells. We found that there was a significant decrease in HPRT surface localization in the knockdown when compared to the wild type Raji cells.

that HPRT surface localization is not a universal characteristic of malignant cells and patients should be evaluated on an individual basis.

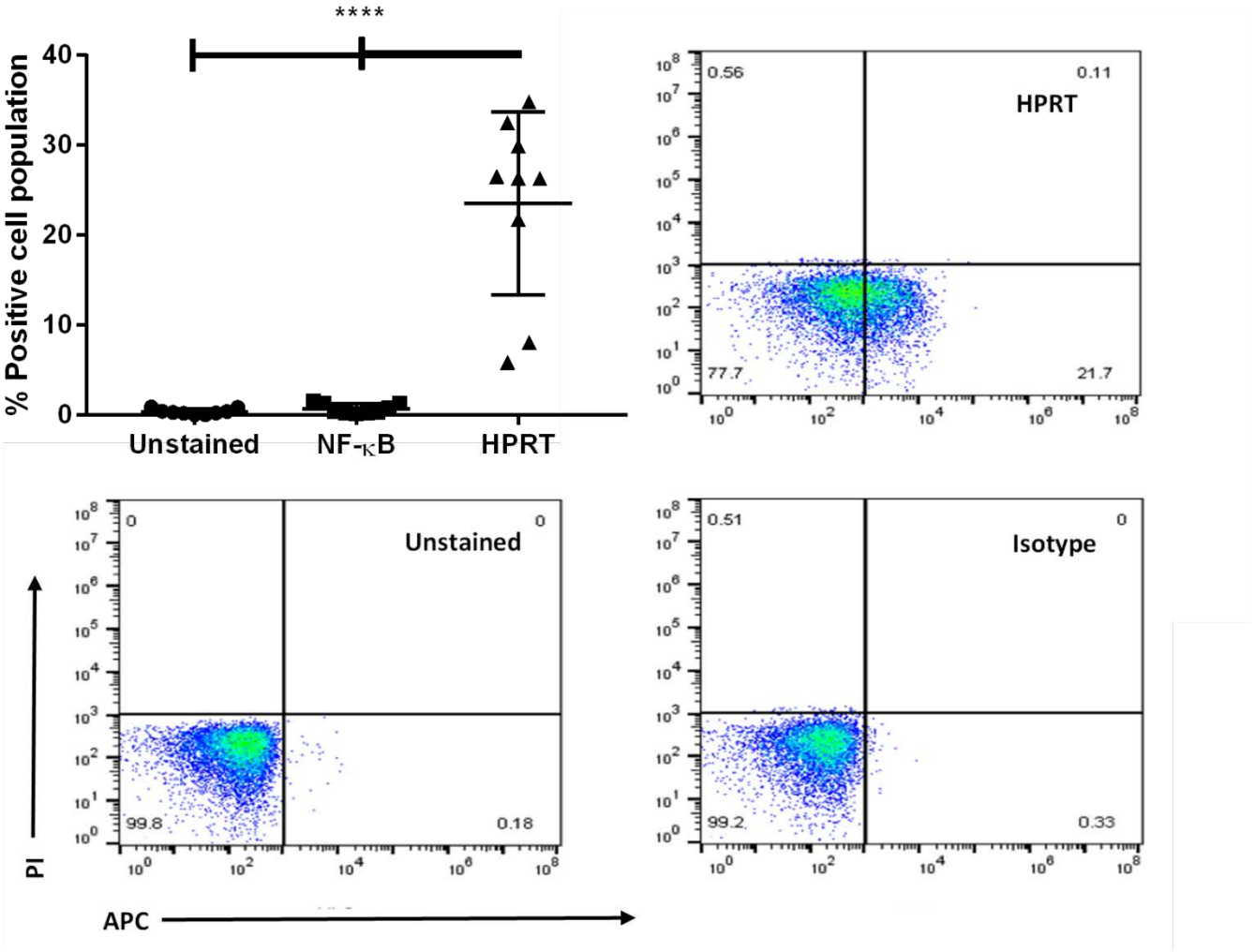

Figure 9-6. *ALL patients show elevated surface HPRT*. Patient samples were stained with PI to discriminate against dead cells. APC was used to stain proteins of interest. Upon evaluation of 9 ALL patient samples, we found that 7 of them had elevated HPRT surface localization with an average fluorescent population shift of 25%. This indicates that the surface localization observed in Raji cells is also found within patients.

Differential gene expression between HPRT low and HPRT high expressing cancer cells.

As we found variability between normal cells and malignant cells in regard to their relative HPRT expression, we further evaluated changes in gene expression between high-expressing and low-expressing cells to determine whether HPRT could have any potential influence on other cancer-associated genes. We assessed 79 different malignant B cell lines and ranked them according to their relative HPRT expression. Raji cells had the third highest expression of all cell lines evaluated, which we predicted, as there is significant surface presentation of the enzyme in Raji cells.

Many other genes experienced a significant trend correlating to HPRT expression (Table 9-1). Genes that showed a direct positive correlation to HPRT were XRCC2 (p-value = 0.0045), BRCA1 (p-value = 0.0032), PIK3CA (p-value = =0.0034), MSH2 (p-value = 0.0445), MSH6 (p-value = 0.019), WDYHV1 (p-value = 0.0066), AK7 (p-value = 0.0452), and BLMH (p-value = 0.0498). Genes that showed an inverse correlative relationship to HPRT were PRKD2 (p-value = 0.0109), PTGS2 (p-value = 0.0046), TCF7L2 (p-value = 0.0032), CDH1 (p-value = 0.0201), IL6R (p-value = 0.0054), MC1R (p-value = 0.0487), AMPD1 (p-value = 0.0227), TLR6 (p-value = 0.0401), and BAK1 (p-value = 0.0052). Although HPRT is not the sole contributor to these changes in gene expression, there may be a cascading relationship between HPRT levels and these genes as there are general trends either towards higher expression or lower expression when HPRT is elevated within the cells.

Table 9-1. *HPRT gene correlations.*

Gene Name	Gene	General Function	p-value
Direct Correlation			
	XRCC2	DNA repair protein involved in homologous recombination.	0.0045
Breast cancer type 1 susceptibility protein	BRCA1	Tumor suppressor gene that maintains genomic stability via DNA damage repair, chromatin remodeling, transcriptional regulation and apoptosis.	0.0032
Phosphatidylinositol 4,5-bisphosphate 3-kinase catalytic subunit alpha	PIK3CA	Involved in cell growth, survival, proliferation, motility and morphology. Also participates in cellular signaling in response to growth factors.	0.0034
	MSH2	Involved in mismatch repair system.	0.0445
	MSH6	Involved in mismatch repair system.	0.019
Protein N-terminal glutamine amidohydrolase	WDYHV1	Involved in the N-end rule pathway in protein degradation.	0.0066
Adenylate kinase 7	AK7	Nucleoside monophosphate kinase that transfers phosphate groups between nucleoside triphosphates and monophosphates.	0.0452
Bleomycin hydrolase	BLMH	Cysteine peptidase, hydrolyzes homocysteine thiolactone	0.0598
Inverse Correlation			
Serine/threonine-protein kinase D2	PRKD2	Regulation of cell proliferation via MAP1/3 signaling.	0.0109
Prostaglandin G/H synthase 2	PTGS2	Production of inflammatory prostaglandins	0.0046
	TCF7L2	Involved in the Wnt signaling pathway and modulates MYC expression.	0.0032
Cadherin-1	CDH1	Involved in mechanisms regulating cell-cell adhesion, mobility, and proliferation.	0.0201
Interleukin-6 receptor	IL6R	Potent pleiotropic pro-inflammatory cytokine that regulates cell growth and differentiation.	0.0054
Melanocyte-stimulating hormone receptor	MC1R	Produces melanin pigment	0.0487
AMP deaminase 1	AMPD1	Energy metabolism	0.0227
Toll-like receptor 6	TLR6	Innate immune response to Gram-positive bacteria and fungi	0.0401
Brassinosteroid insensitive 1-associated receptor kinase 1	BAK1	Controls the expression of genes associated with innate immunity in the absence of pathogens or elicitors.	0.0052

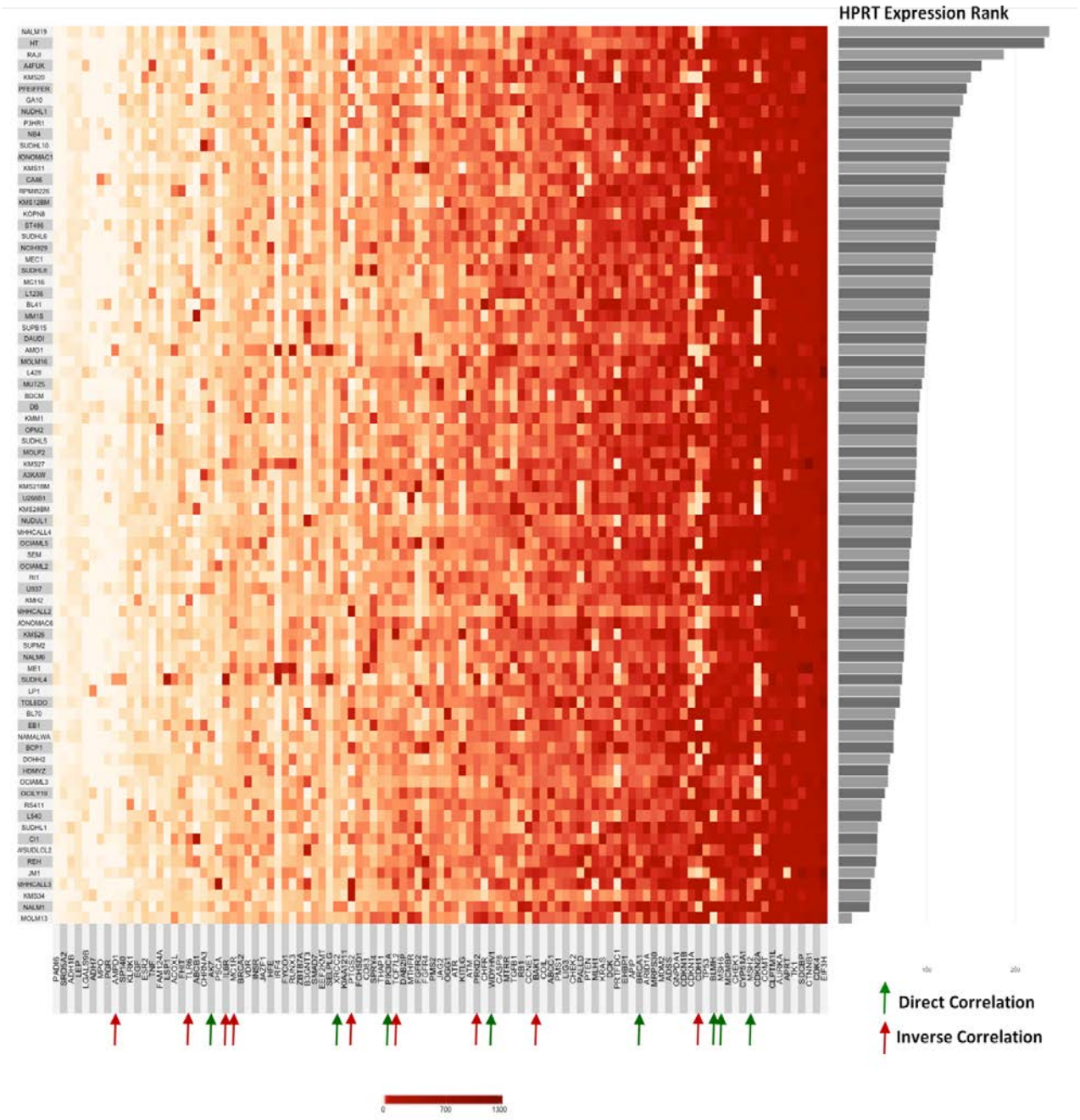

Figure 9-7. *Gene-expression evaluation of HPRT high vs HPRT low expression B cell lines.* 79 Cancerous B cell lines are ranked on the Y-axis according to their relative HPRT expression, which is portrayed on the right-hand Y-axis. The expression of 105 cancer-associated genes are labeled on the X-axis. The expression of each of these genes is portrayed with higher expression scaled to darker color. We found significant variability within B cell lines in terms of HPRT expression and also identified correlative relationships between the gene expression of HPRT and other cancer-associated genes.

Discussion

HPRT is an enzyme that plays a critical role in the cell cycle by providing essential nucleotides that support cell division and DNA replication. We have shown that HPRT is significantly elevated in some patient malignancies. This elevation appears to manifest via co-localization to the plasma membrane of the cell. Yet, this surface expression is not found on all malignant cells and we have shown that many cell lines have significant variation in regard to their expression of HPRT. As cell cycle regulation is a common target for mutation in malignant cells, we hypothesize that enzymes controlling the cell cycle are the most likely contributing factor to the differential HPRT expression within these cells [500,570]. Additionally, we hypothesize that surface presence of the enzyme is related to an overabundance of the protein internally, and we predict that cell lines with an unusually high level of HPRT will have significant surface expression.

As a protein that is presented on the surface of malignant cells and absent on the surface of normal cells, HPRT could be used as a cancer-associated epitope for immunotherapy targeting. New epitopes are required as cancer is an evolving disease and adapts to avoid immune detection [554]. There has been unprecedented success using CD19 Chimeric Antigen Receptors to target and kill malignant B cells [556–558,560]. Yet, this therapy is not cancer-specific and targets healthy cells as well. As a protein that appears to be found only on malignant cells, HPRT could serve as a safer target for patients with B cell malignancies, as they may maintain their healthy supply of B cells. HPRT could also serve as a novel biomarker to aid in increasing numbers of CD19-resistent cancers [71,562]. Targeting HPRT could serve as an additional treatment to target cells that become resistant to current treatment regimes.

While HPRT is present on the surface of Raji cells, we hypothesize that only cells with significantly elevated HPRT production express the enzyme on the plasma membrane. Screening

patients for surface HPRT would be feasible; a simple blood test would confirm whether a patient was positive or negative. Our data indicates that HPRT surface localization is a relatively common occurrence in these B cell malignancies and could be a valuable biomarker in future therapeutic treatments. Future work will need to be conducted using a larger number of patient samples to determine whether targeting HPRT would be technically feasible and beneficial from a therapeutic standpoint.

While the surface expression of HPRT may be useful as a biomarker for diagnosis and treatment, novel correlations between HPRT and other genes may highlight possible regulatory roles that HPRT play within the cell. Of the 17 genes that had a significant correlation to HPRT expression, 9 are involved in cellular proliferation and DNA synthesis/repair. With this is mind, HPRT may be responsible for additional regulation of cellular proliferation outside of nucleotide synthesis and may interact or direct other genes. Another possibility is that the same genes that are regulating cellular proliferation in these genes may also influence HPRT expression. On an interesting note, of the 9 genes with an inverse correlative relationship with HPRT expression, 4 genes (PTGS2, IL6R, TLR6, and BAK1) are involved in the regulation and activation of the immune system. This may suggest that the upregulation of HPRT could have a side effect of downregulating the immune system.

In addition, we also noted some interesting cell lines that have gene profiles significantly different from any other cell line. SUDHL4, AMO1, and L428 cells appear to have inverse gene expression to the average B cell line. This highlights that any observed correlations between gene expression are the result of several different contributing factors, and not just HPRT expression within these cells.

Conclusions

Because HPRT is localized to the surface of malignant lymphocytes, it has the potential to be used as a targetable biomarker for immunotherapy. As antigen escape is emerging as a significant concern with targeted immunotherapy, the need to find and use new biomarkers is always increasing. In addition, the genes that are correlated with HPRT expression may elucidate a new role of HPRT in cancer proliferation.

List of abbreviations

HPRT; hypoxanthine guanine phosphoribosyltransferase, ALL; acute lymphoblastic leukemia, CLL; chronic lymphoblastic leukemia, BRCA1; Breast cancer type 1 susceptibility protein, PIK3CA; Phosphatidylinositol 4,5-bisphosphate 3-kinase catalytic subunit alpha, WDYHV1; Protein N-terminal glutamine amidohydrolase, AK7; Adenylate kinase 7, BLMH; Bleomycin hydrolase, PRKD2; Serine/threonine-protein kinase D2, PTGS2; Prostaglandin G/H synthase 2, CDH1; Cadherin-1, IL6R; Interleukin-6 receptor subunit alpha, MC1R; Melanocyte-stimulating hormone receptor, AMPD1; AMP deaminase 1, TLR6; Toll-like receptor 6, BAK1; Brassinosteroid insensitive 1-associated receptor kinase 1

CHAPTER 10

Aiding in diagnosis: new cancer biomarkers for endometrial cancer

Michelle H. Townsend, Zac E. Ence, Abigail M. Felsted, Alyssa C. Parker, Stephen R. Piccolo, Richard A. Robison, and Kim L. O' Neill.

Citation: Townsend MH, Ence ZE, Feslted AM, Parker AC, Piccolo SR, Robison RA, O'Neill KL. (in review). Aiding in diagnosis: new cancer biomarkers for endometrial cancer.

The following chapter is taken from an article in review for publication. All content and figures have been formatted for this dissertation.

Abstract

Background: Incidence of endometrial cancer are rising both in the United States and worldwide. As endometrial cancer becomes more prominent, the need to develop and characterize biomarkers for early stage diagnosis and the treatment of endometrial cancer has become an important priority. Several biomarkers currently used to diagnose endometrial cancer are directly related to obesity. Epigenetic and mutational biomarkers have been identified for endometrial cancer, and have resulted in treatment options for patients with specific aberrations, but many tumors who do not harbor those specific aberrations. A promising alternative is to develop biomarkers based on differential gene expression, which can be used to estimate prognosis. There remains a need to identify additional biomarkers to help physicians identify and characterize endometrial cancer and to optimize patient treatments.

Objective: Due to their significant elevation within other cancer types, we have evaluated expression levels of JAG2, AURKA, PGK1, and HPRT1 in endometrial tumors to determine whether they show promise as diagnostic, prognostic, or treatment biomarkers.

Study Design: We evaluated 589 patients to determine differential expression between normal and malignant patient samples. We then supplemented these evaluations with immunohistochemistry staining of endometrial tumors and normal tissues. Additionally, we used the Library of Integrated Network-based Cellular Signatures to evaluate the effects of 1769 chemotherapy drugs on 26 cell lines to determine the effects of each drug on HPRT1 and AURKA expression.

Results: Expression of all four genes was elevated when compared to normal samples, and HPRT1 and PGK1 showed a stepwise elevation in expression that was significantly related to cancer grade. To determine the prognostic potential of these genes, we evaluated patient outcome

and found that levels of both HPRT1 and AURKA were significantly correlated with overall patient survival. When evaluating drugs that had the most significant effect on lowering the expression of HPRT1 and AURKA, we found that Topo I and MEK inhibitors were most effective at reducing HPRT1 expression. Meanwhile, drugs that were effective at reducing AURKA expression were more diverse (MEK, Topo I, MELK, HDAC, etc.). The responses of these drugs on the expression of HPRT1 and AURKA provides insight into their role within cellular maintenance.

Conclusions: Collectively, these data show that JAG2, AURKA, PGK1, and HRPT1 have the potential to be used independently as diagnostic, prognostic, or treatment biomarkers in endometrial cancer. Expression levels of these genes may provide physicians with insight into tumor aggressiveness and chemotherapy drugs that are well suited to individual patients.

Introduction

Endometrial cancer is the fourth most common cancer in women with 12,990 new diagnoses and 4,120 deaths in 2016 in the United States[417]. Over 710,200 women are living with endometrial cancer in the United States, and approximately 2.8% of women will be diagnosed with the disease at some point during their lifetime. As the most significant risk factor for endometrial cancer is obesity, a majority of the biomarkers used to detect and monitor endometrial cancer development are related to metabolic and endocrine alterations[571]. Androgens, estrogens, prolactin, thyroid stimulating hormone, leptin, and adiponectin are a few of the biomarkers utilized to highlight risk of endometrial cancer development. While these biomarkers can be useful, they are oftentimes somewhat subjective as the levels of these hormones fluctuate naturally, are generally elevated with obesity, and are not necessarily unique to cancer development[571,572]. In order to find new biomarkers that may act as diagnostic biomarkers for endometrial cancer, we evaluated Jagged2 (JAG2), Aurora Kinase A (AURKA), Phosphoglycerate Kinase 1 (PGK1), and Hypoxanthine Guanine Phosphoribosyltransferase 1(HPRT1) due to their role in cellular proliferation and cancer development. We evaluated these genes because of their upregulation and diagnostic potential in other cancer types[61,573–577].

JAG2 is a notch transmembrane ligand. Notch signaling is a conserved signaling pathway linked to the development of several cancers due to its role in cell fate, cellular proliferation regulation, and cell death[578]. This is exemplified by the fact that Notch signaling regulates stem cell proliferation and differentiation[579]. Within cancer, Notch signaling mediates hypoxia, invasion, and chemoresistance[580], and JAG2 expression in primary tumors has been correlated with vascular development and angiogenesis[581]. In addition, elevated levels of JAG2 result in significant chemoresistance, and when JAG2 is knocked down in mice, tumor cells become

sensitive to chemotherapeutics (doxorubicin)[576]. Notch signaling has been identified as an important pathway for carcinogenesis of the endometrium[582]. Additionally, JAG2 has been shown to be a promising target in several cancer cell lines, as specific antibody-drug conjugate have resulted in tumor reduction[583].

AURKA is a cell-cycle regulated kinase that functions in spindle formation and chromosome segregation during the M phase of the cell cycle. AURKA has been shown to be a downstream target of MAPK1, which is a major force in cellular proliferation in several cancer cells[584]. The protein is also elevated in a variety of cancer and has a significant association with disease recurrence[574,575]. Because AURKA is upregulated in cancers, efforts have been made to target the protein to aid in tumor reduction. Upon AURKA suppression, cancer cells become sensitive to chemotherapeutics and overall tumor growth is suppressed in a variety of cancer cells (docetaxel & taxane)[585,586]. The role AURKA may play as a diagnostic biomarker in endometrial cancer has not been well studied, although it has shown promising results in other cancer types[575,587–590].

PGK1 is involved in the glycolysis pathway and functions by transferring a phosphate group from 1,3-bisphosphoglycerate to ADP to form ATP[591,592]. As an enzyme involved in generating valuable energy for the cell, especially in hypoxic conditions, PGK1 has been correlated with cancer development and progression in a variety of tumor types[577,593,594]. It's role in promoting tumor proliferation is linked to PGK1's ability to promote tumor angiogenesis[595,596], DNA replication and repair[597598], and cancer metastasis[594,599]. While the protein is elevated internally in several cancers, it is also actively secreted from tumor cells, where it cleaves plasminogen to create angiostatin[600]. PGK1 has been shown to be upregulated in several cancer types, but has not been evaluated for upregulation in endometrial cancer[594,601].

HPRT1 is a nucleotide salvage enzyme involved in the cell cycle[498,514]. This enzyme is a transferase responsible for producing guanine and inosine nucleotides by transferring a phosphoribose from PRPP to guanine and inosine bases, respectively, during cellular maintenance[10,28]. As cells rapidly divide, the need for nucleotides increases, and subsequently HPRT1, has been shown to be elevated in several malignant settings[61,62]. As the enzyme shows upregulation in malignant tissue while maintaining stable levels in normal tissue, it has the potential to be used as a biomarker for cancer development in several cancer types.

We decided to evaluate these enzymes in endometrial cancer because they have all shown promising diagnostic potential in other tissue types as biomarkers for disease development and progression but have not been evaluated in endometrial cancer. As malignant endometrial biomarkers are less established, we hope to identify additional markers for malignancy to aid in the early diagnosis and possible treatment of endometrial cancer.

Materials and Methods

Chemicals/Reagents

DIVA Decloaker 10x, Background Sniper, Mach 4 HRP polymer, DAB Peroxidase, Hematoxylin, Hydrophobic pen, and Universal Negative antibodies were all obtained from Biocare Medical, Concord, CA. Anti-JAG2 (LifeSpan Biosciences, Inc. Seattle, USA), Anti-AURKA (Sigma-Aldrich, St. Louis, USA), and anti-PGK1 (Abcam, Cambridge, UK) were stored at -20°C. Anti-HPRT monoclonal antibody (Abcam, Cambridge, UK) was aliquoted and stored at -20°C. GAPDH polyclonal antibody (Cell signaling) was aliquoted and stored at -20°C. Tween20 (Fisher Reagents, Waltham MA) was stored at room temperature. 30% Hydrogen Peroxide (Fisher Reagents, Waltham MA) was stored at 4°C.

Tissue Microarray Samples

Tissue microarrays were obtained from Biomax and stained for GAPDH, HPRT, JAG2, AURKA, PGK1, and with an isotype control. Patients were all female and ranged in age from 21 to 63. Normal (n=9), cancer adjacent (n=9), and malignant tissue (n=54) (grade 1-3) were included in the analysis (Table 1).

Immunohistochemistry

Protein levels were assessed using protocols described by Townsend et al. with slight modifications[61]. Briefly, tissues were rehydrated, washed, and treated with DIVA Decloaker. Following a hydrogen peroxide wash, tissues were treated with a Background Sniper followed by a primary antibody (1:100 dilution). After a series of washes, the tissues were treated with DAB Peroxidase and hematoxylin and imaged using a standard light microscope.

Tissue Quantification

ImageJ software was utilized to quantify staining intensity[602]. An IHC toolbox plugin was selected with the "DAB (more brown)" option to remove staining that is not resulting from DAB. After this modification, the images were converted to a grayscale and a threshold was applied to eliminate areas of negative space that could potentially bias the results. Once a universal threshold was applied, the average gray intensity of the tissue was collected.

Tumor Gene-expression Analysis

We obtained RNA-Sequencing and clinical outcomes data for Uterine Corpus Endometrial Carcinoma (UCEC) samples from The Cancer Genome Atlas (TCGA)[540]. We used

transcripts-per-million values, summarized at the gene level. These data were derived from tumor and normal samples.

Survival was calculated using a Cox proportional hazard model. Inaddition to gene expression (primary variable), covariates included gene expression and clinical factors such as age, race, and tumor purity. Kaplan-Meier curves were generated to compare survival of patients with the highest 20% of target gene expression against those with the lowest 20% of target gene expression. The statistical analyses and curve generations were calculated utilizing the TIMER program developed by Li et al. [603].

Drug Response Analyses

We evaluated the effects of chemotherapy treatments on cell lines using two publicly available databases. First, we examined data from the Cancer Cell Line Encyclopedia (CCLE)[537]. We obtained treatment-response data for 24 drugs that were available from the CCLE portal and used the area above the fitted dose-response curve (ActArea) as a metric of treatment response[604]. We obtained transcript-level expression levels for CCLE[536] and summed protein-coding transcript values to gene-level values using a custom Python script (https://python.org). For each of four genes (HPRT1, AURKA, JAG2, and PGK1), we identified cell lines for which drug-response and gene-expression data were available and then ranked the cell lines according to expression of the respective genes. Next, we selected the lowest- and highest-expressing cell lines for each gene and used a Mann-Whitney U test to evaluate differences in ActArea values between these cell-line groups. To perform these calculations, we used the R statistical software (version 3.4.3)[569].

Second, we evaluated data from the Library of Integrated Network-based Cellular Signatures, which contains gene-expression profiles for cell lines after drug perturbations. We wrote a Python (version 3.6.5) script to extract HPRT1 and AURKA expression values from the LINCS database for samples from 26 cell lines for which data were available. We used the Level 5 data, which were generated using the L1000 platform[605], normalized using a z-score methodology within each plate, and averaged across replicates. Using the R (version 3.4.4)[569] statistical software and the readr package (version 1.1.1)[606], we parsed the metadata file to identify experiments where the cell lines had been treated with chemotherapeutic compounds (pert_type = "trt_cp"). The summarized data values indicate relative gene-expression levels for cells treated with a given compound relative to control-treated cells. To perform this filtering and data transformation, we used the dplyr (version 0.7.4)[607] and reshape2 (version 1.4.3) packages [608]. Before plotting the data, we grouped the values for each cell line by compound name. We identified the median value for each group and sorted the values from lowest to highest. Then we used the superheat package (version 1.0.0) to create heatmaps with data from the seven cell lines with the most treatment data [543]. The code and data we used for this analysis can be found at https://bitbucket.org/alyssaparker99/lincs-heatmaps

Statistical Analysis

Staining intensity between tissue samples were analyzed using an ANOVA test with the multiple comparison method. Additionally, unpaired *t* tests were utilized in conjunction to confirm statistical significance. These statistical tests were performed in GraphPad Prism 7 software. Differences were considered significant when the p value was < 0.05. Asterisks were used in figures to indicate levels of significance with ns = $P > 0.5$, * = $P \leq 0.05$, ** = $P \leq 0.01$, *** = $P \leq 0.001$, and **** = $P \leq 0.0001$.

Results

JAG2, AURKA, PGK1, and HPRT1 had significant upregulation in malignant samples when compared to normal.

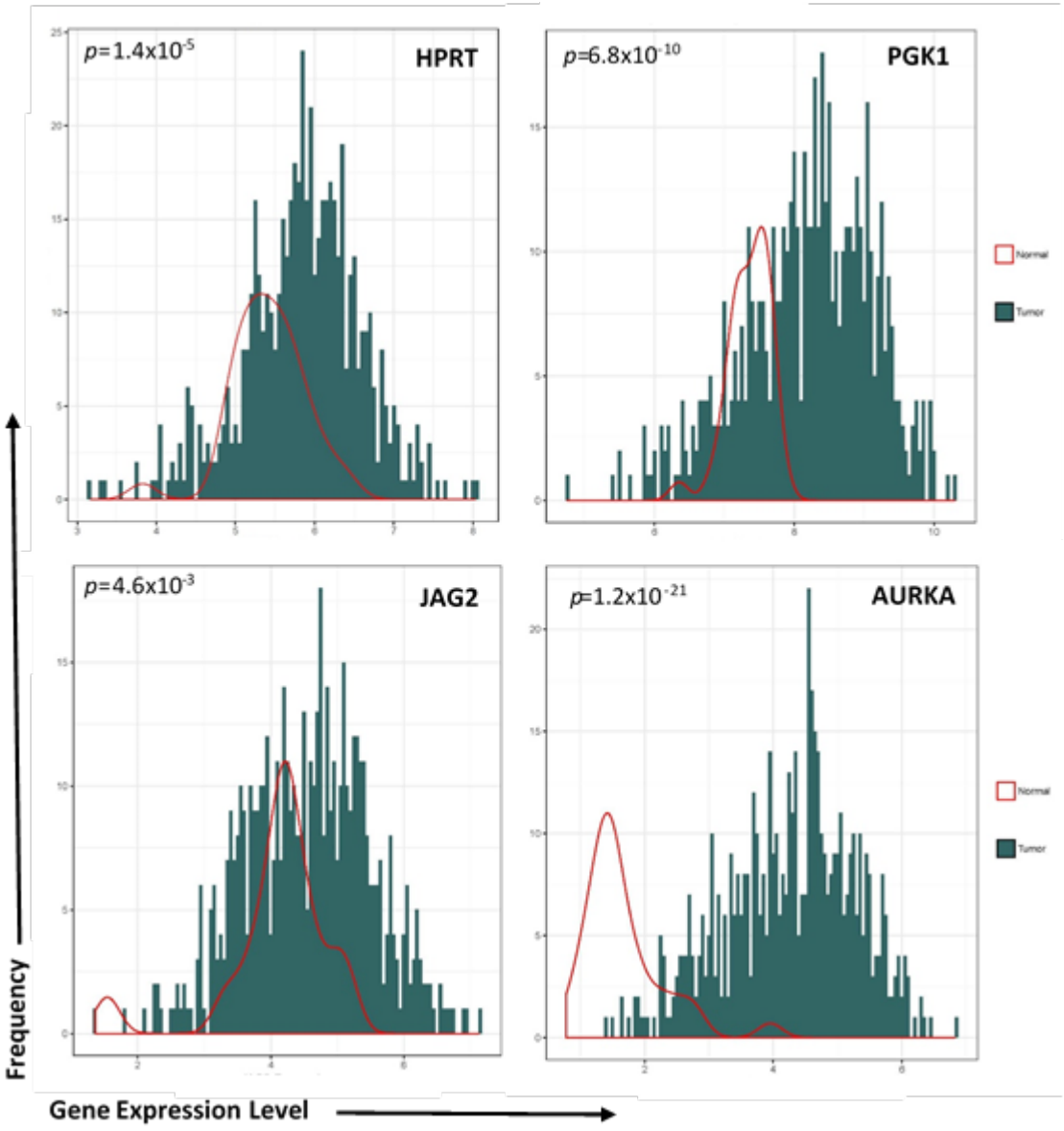

Figure 10-1. *Gene expression in patient samples.* HPRT, PGK1, JAG2, and AURKA were analyzed for gene expression in both normal (red line) and malignant (blue histogram) samples. Relative protein expression is quantified on the X-axis (represented as transcripts per million), while the frequency of the expression is plotted on the Y-axis.

We evaluated gene-expression levels for AURKA, JAG2, HPRT1, and PGK1 in tumors and normal tissues from TCGA. Upon comparing malignant and normal samples, we observed a consistent elevation of each of the genes in malignant tissues (Figure 1). JAG2 had the smallest elevation overall (*p-value* = 4.6×10^{-3}), while AURKA showed the largest increase (p-value = 1.2×10^{-21}). This upregulation indicates that these genes may be useful as diagnostic markers of endometrial cancer, as they have differential expression between normal and malignant samples.

When analyzing protein levels in tissue microarrarys from a separate cohort, we again found that all four genes were significantly elevated within malignant samples (Figure 2). This confirmed the initial analysis with gene expression data. In addition, we found that PGK1 and HPRT1 both showed significant differences between grades as there was a stepwise elevation of protein expression corresponding to grade. This indicates that HPRT1 and PGK1 may have a grade dependency, and could serve as biomarkers for tumor aggressiveness. All four genes showed a range of protein expression in both malignant and normal samples (Figure 3).

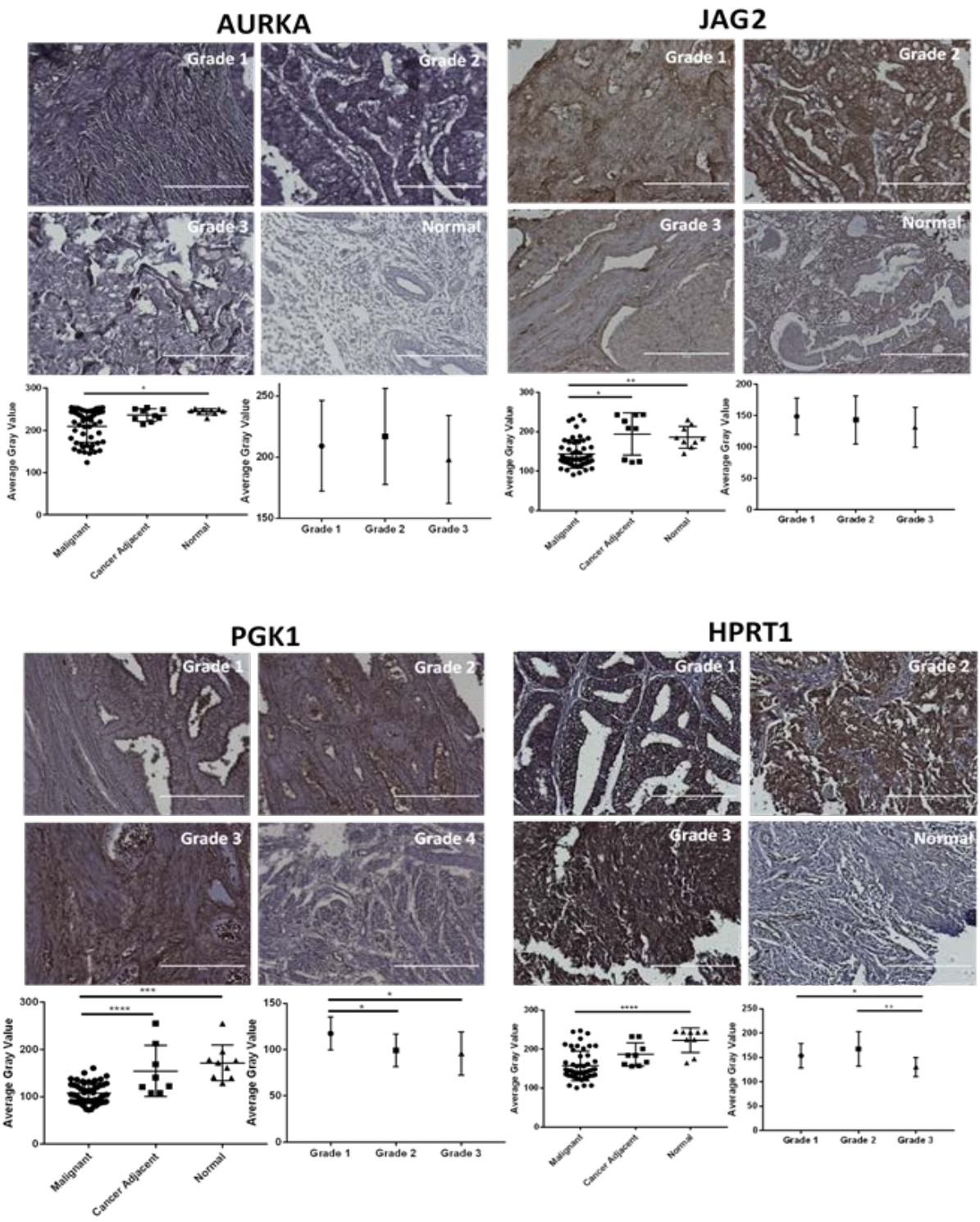

Figure 10-2. *Tissue evaluation of AURKA, JAG2, PGK1, and HPRT*. Tissues were quantified on a gray scale with lower values indicating darker staining intensity. A, AURKA expression and B, JAG2 expression was significant between malignant and normal samples, but showed no significance between cancer grade. C, PGK1 expression and D, HPRT expression showed significance both between normal and malignant samples in addition to between cancer grade.

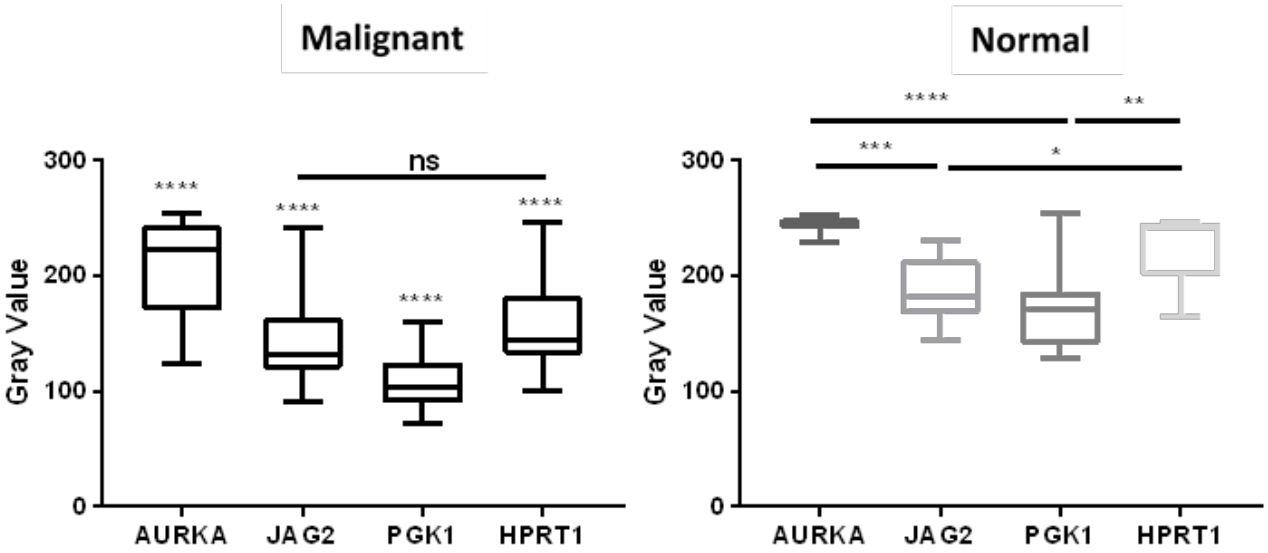

Figure 10-3. *Gene expression between normal and malignant patient samples.* Tissues were quantified on a gray scale with lower values indicating darker staining intensity. Across malignant samples, patients had a variety of expression of each of the genes evaluated that were all significant from each other with the exception of JAG2 and HPRT expression. In addition, normal samples also showed a variety of expression of the genes, with PGK1 showing the highest expression and AURKA showing the lowest expression.

To determine whether elevated expression of these genes occurred in the same patients, we plotted expression values for each patient jointly for all four genes. There was no pattern of concordant elevation across PGK1, AURKA, JAG2, and HPRT1. For example, patients with elevated levels of AURKA did not share the same high levels of HPRT1 or of the other genes (Figure 4). This was observed in all cancer stages. For example, there were cases where the patient with the lowest expression of AURKA (patient 7 in Stage 2) also had the highest expression of HPRT1. This indicates that these biomarkers may be useful in identifying different patients and that each biomarker may be independently used to benefit further characterization of individual patient cancer types.

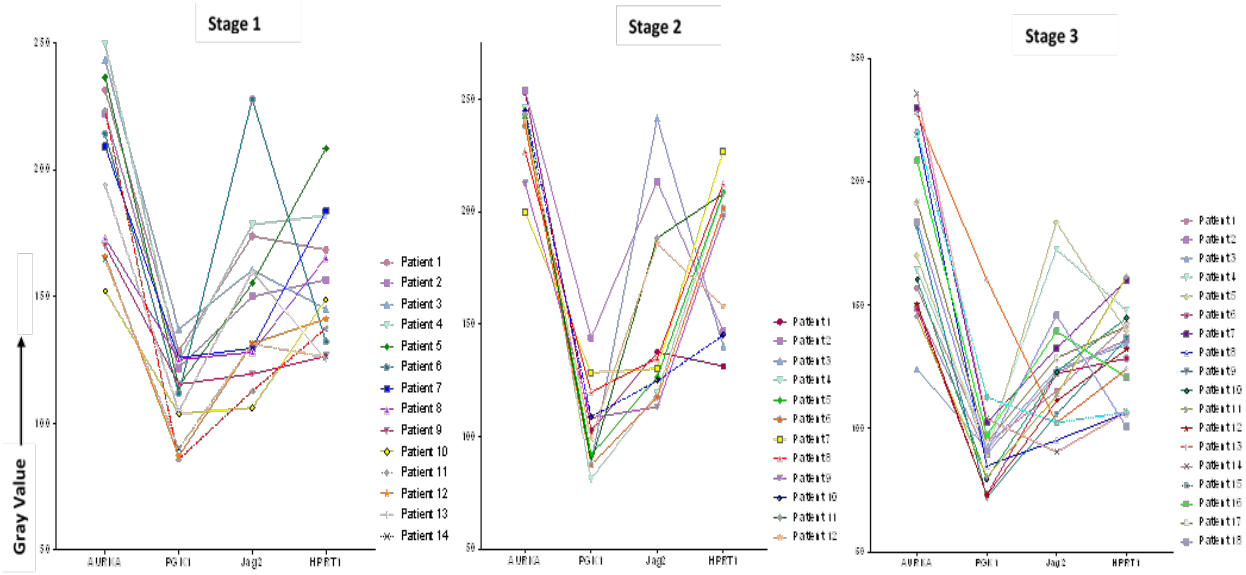

Figure 10-4. *Individual patient expression of biomarkers.* Each biomarker and their relative expression is plotted according to the patient. Relative expression is represented on the Y-axis, while the protein evaluated is represented on the X-axis. Individual patients did not show a pattern of biomarker elevation consistently in any of the stages evaluated.

AURKA and HPRT1 elevation have a significant impact on patient survival.

We evaluated overall patient survival in patients with the highest 20% of biomarker expression and patients with the lowest 20% biomarker expression to determine whether the elevation of these genes had any impact on survival. Both PGK1 (*p-value*=0.589) and JAG2 (*p-value*=0.46) showed insignificant differences in survival over the course of 100 months between high and low expressors. While there may be elevation of these genes within cancer, they do not seem to contribute to survival outcomes. Interestingly, both AURKA and HPRT1 showed significant differences in survival in high vs low expressing patients. Following 100 months, patients with the highest 20% of AURKA expression showed significant (*p-value*<0.0001) decreases in survival and AURKA elevation correlated with a lower survival rates (Figure 5). This same pattern was also observed for patients with elevated HPRT1 expression, as patients

with the highest 20% HPRT expression had significantly (*p-value*=0.041) decreased survival compared to their lower expressing counterparts. This shows that both AURKA and HPRT1 may have significance beyond diagnostic; they also may be useful, as prognostic biomarkers for uterine corpus endometrial cancer.

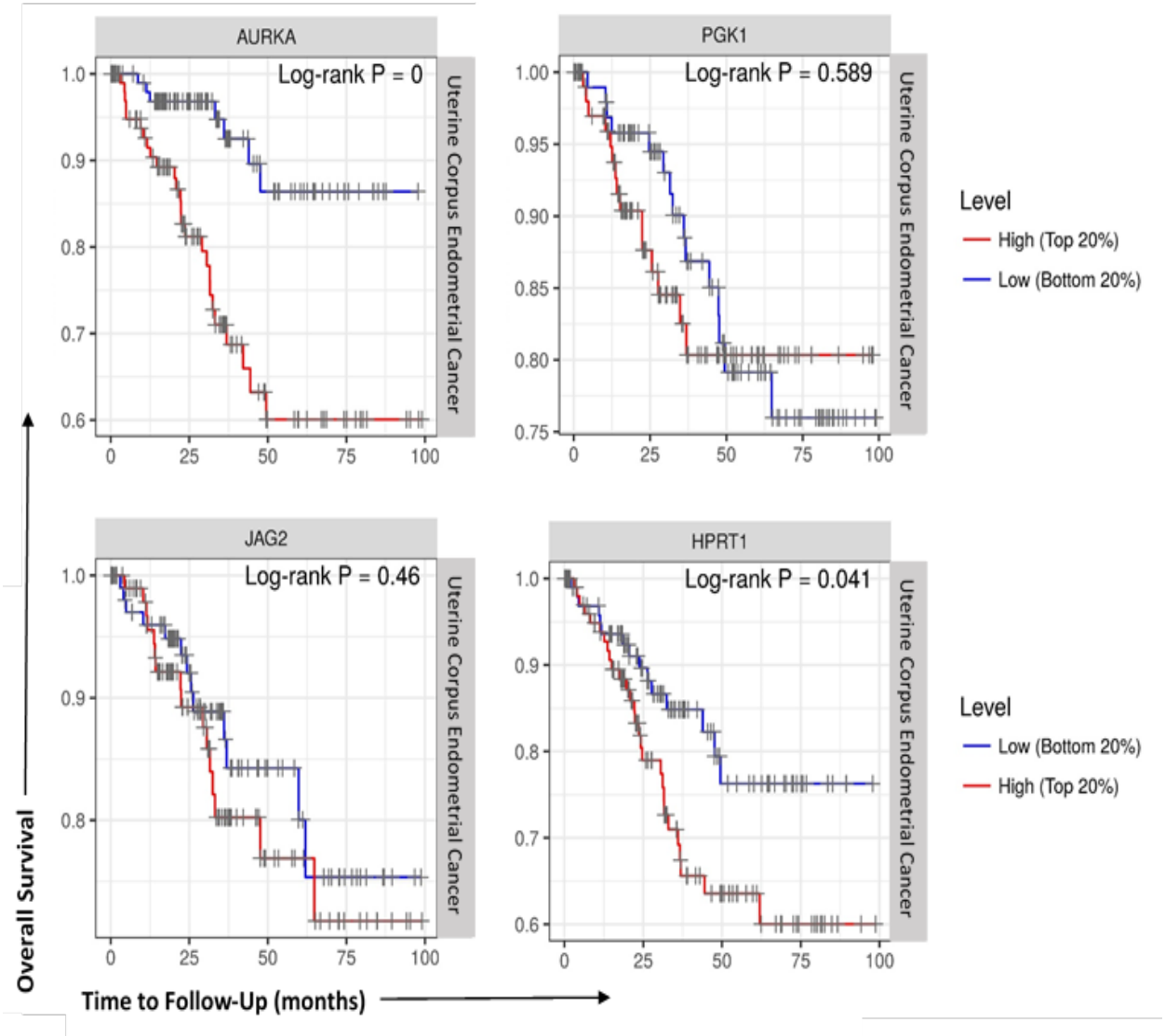

Figure 10-5. *Survival of patients with elevated levels of JAG2, AURKA, PGK1, and HPRT1.* We plotted the survival of patients with the highest 20% expression of each respective biomarker (red line) and compared them to the patients with the lowest 20% expression (blue line) over the course of 100 months. We found no statistically significant difference in survival in regards to high and low expression of PGK1 or JAG2, but found significant decreases in survival in patients with an elevation of AURKA (p-value <0.0001) and HPRT1 (p-value=0.041).

Drug treatments of cell lines with high and low target gene expression.

To determine whether these genes could be utilized as biomarkers for physicians when deciding treatment options, we analyzed the effects of 24 drugs on cell lines with relatively high and low expression of AURKA, JAG2, PGK1, and HPRT1. Cell lines were ranked according to their expression of each gene and highest and lowest expressing cell lines were chosen for analysis (Figure 6). Although there was no significance observed, there were some responses that appeared to have a larger impact than others. Drugs with the largest differences were PD-0325901 (MEK inhibitor), TAE684 (ALK inhibitor), AEW541 (IGF-1R inhibitor), and Nilotinib (tyrosine kinase inhibitor) in JAG2, PGK1, HPRT1, and AURKA, respectively. Several of the drug responses were negligible as the mean ActArea was almost identical in a majority of the responses between the high and low expression cell lines (Figures 7-10).

Table 10-1. *Protein expression within patient tissue.*

Protein	n	General Function	Average gray value Malignant	Average Gray Value CAT	Average Gray Value Normal
HPRT	68	Nucleotide Salvage	157.206	186.176	223.207
PGK1	71	Glycolytic Enzyme	107.273	154.437	171.748
AURKA	72	Cycle-regulated Kinase	209.994	236.147	244.352
Jag2	72	Protein Coding	143.635	194.297	186.269

Note. CAT; Cancer Adjacent Tissue

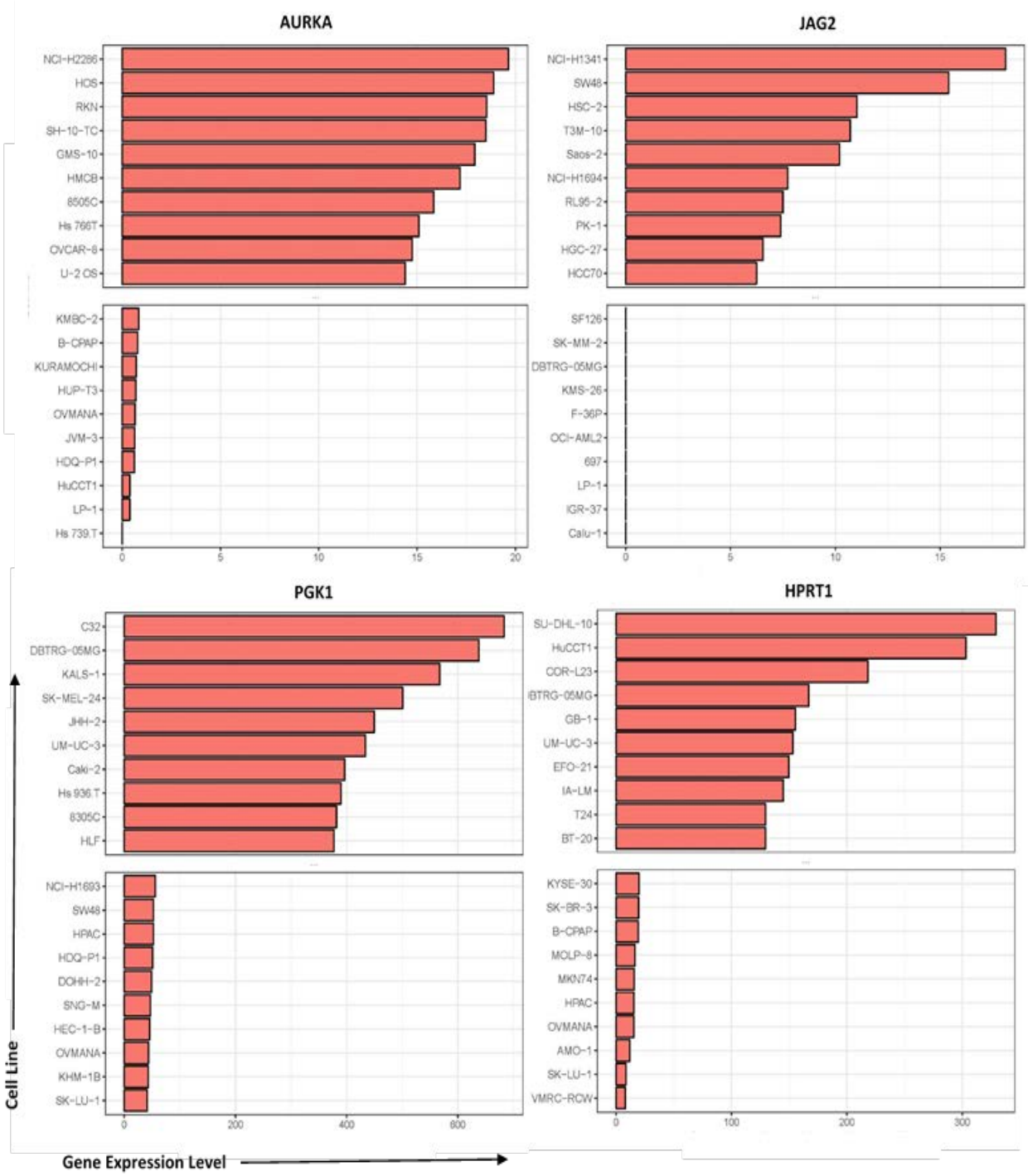

Figure 10-6. *Cell lines ranked by their relative expression of JAG2, AURKA, PGK1, and HPRT1.* Cell lines were ranked according to their gene expression level (transcripts per million) and the 10 highest expressing and 10 lowest expressing cell lines are shown.

Drugs with the largest impact on AURKA and HPRT1 expression.

As HPRT1 and AURKA elevation showed prognostic significance (Figure 5), we analyzed data from the LINCS, a publicly available resource that contains gene-expression responses signatures for 1769 chemotherapy drugs and 26 cell lines. We searched for drug treatments that caused significant declines in HPRT1 and/or AURKA expression. These responses varied widely across drug treatments and cell lines with some drugs increasing the expression of the genes and, other decreasing expression. The vast majority of drug treatments had no impact on HPRT1 or AURKA expression. We focused on seven cell lines for which data were most available (Figure 11). For both genes, over 12,000 drug-cell line interactions resulted in no effect. When evaluating AURKA expression, 78 interactions resulted in a severe reduction, 396 resulted in an intermediate reduction, while 14 resulted in a severe elevation and 141 resulted in an intermediate elevation of the gene. When evaluating HPRT1 expression 13 interactions resulted in a severe reduction, 233 resulted in an intermediate reduction, while 15 resulted in an intermediate elevation of the gene (Table 2). This indicates that AURKA may be a better prognostic biomarker than HPRT1 as there is a larger number of events where the protein was significantly decreased upon treatment.

Table 10-2. *Impact of drug treatment on AURKA and HPRT expression.*

	Description	PTEZ Score Range	# samples
AURKA	Severe Reduction	-10 → -6	78
	Intermediate Reduction	-6 → -2	396
	No Effect	-2 → 2	14,174
	Intermediate Elevation	2 → 6	141
	Severe Elevation	6 → 10	14
HPRT1	Severe Reduction	-10 → -6	13
	Intermediate Reduction	-6 → -2	233
	No Effect	-2 → 2	14553
	Intermediate Elevation	2 → 6	15
	Severe Elevation	6 → 10	0

Note. PTEZ; Post-treatment expression z-score

Figure 10-7. *Drug responses to cell lines with elevated JAG2.* The 20 cell lines with the highest and lowest expression for each target gene from the previous analysis in Figure 6 (X-axis) were evaluated via their Activity Area (ActArea) in response to drug treatments. Drug responses are represented by individual graphs with the mean ActArea plotted on the Y-axis. Drugs with a high ActArea indicate sensitivity, while drugs with a low ActArea indicate resistance. The mean ActArea is represented by a line within the figure to indicate the average increase or reduction between the high expressing and low expressing cell lines.

Figure 10-8. *Drug responses to cell lines with elevated PGK1.* The 20 cell lines from the previous analysis in Figure 6 were evaluated via their ActArea in response to drug treatments. The mean ActArea is represented by a line within the figure to indicate the average increase or reduction between the high expressing and low expressing cell lines.

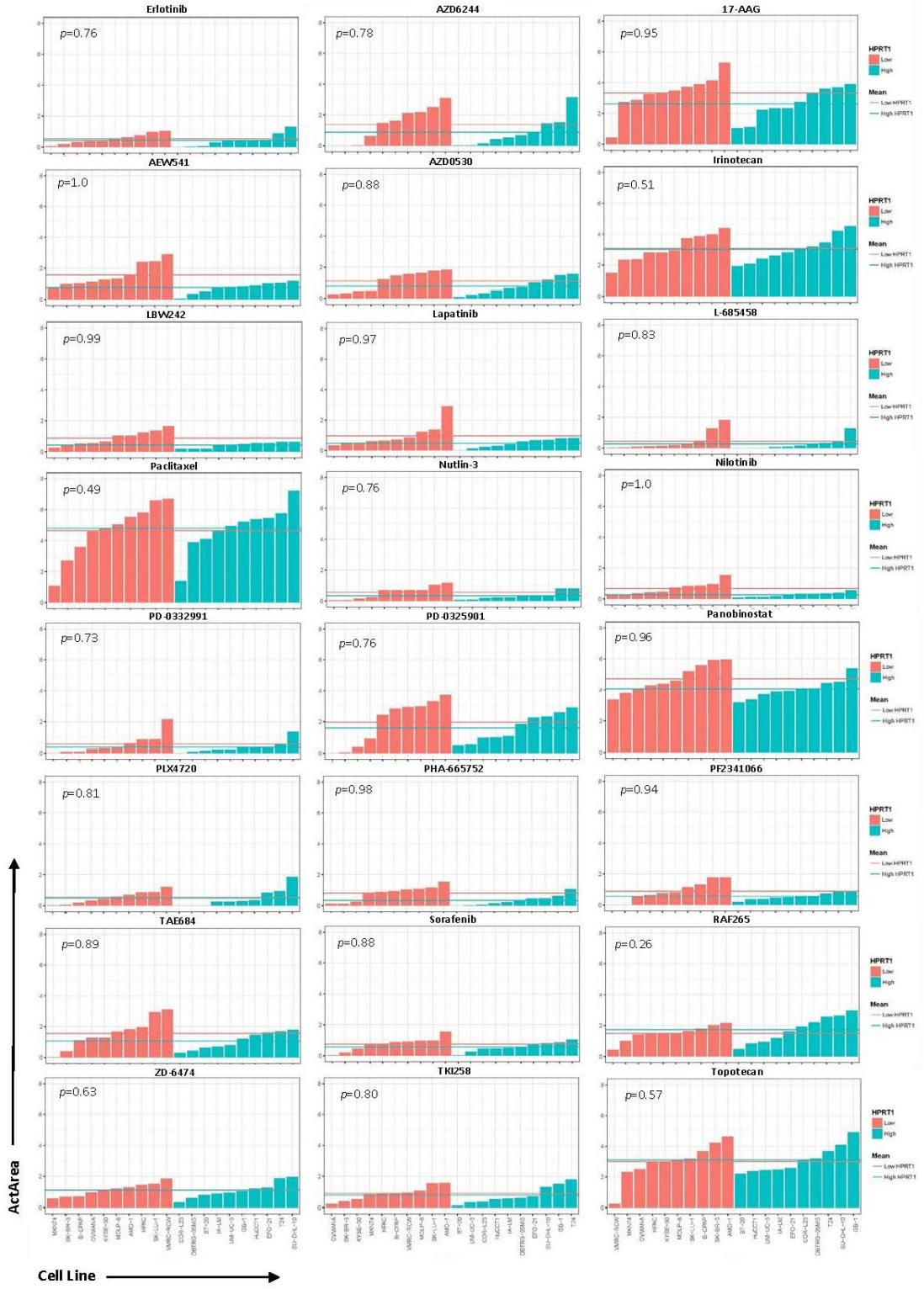

Figure 10-9. *Drug responses to cell lines with elevated HPRT1.* The 20 cell lines from the previous analysis in Figure 6 were evaluated via their ActArea in response to drug treatments. The mean ActArea is represented by a line within the figure to indicate the average increase or reduction between the high expressing and low expressing cell lines.

Figure 10-10. *Drug responses to cell lines with elevated AURKA*. The 20 cell lines from the previous analysis in Figure 6 were evaluated via their ActArea in response to drug treatments. The mean ActArea is represented by a line within the figure to indicate the average increase or reduction between the high expressing and low expressing cell lines.

The ten drugs with the largest reduction in AURKA expression were Ro-4987655, Genz-644282, OTS-167, Vorinostat, Pralatrexate, Epirubicin, Ro-4987655, Pralatrexate, JNJ-26481585, and R-547. Each of these drugs has a different mechanism of action but most ware involved in DNA synthesis and regulation. Of note, when analyzing the drugs that resulted in an increase in AURKA expression, we found that 9 of 10 drugs were directly involved in inhibiting microtubule function or inhibited PLK. This was consistent throughout our analysis and indicates AURKA may be connected in a regulatory fashion to these cellular mechanisms (Table 3).

Table 10-3. *Effective drugs for the reduction of AURKA.*

Cell Line	*Drug*	*Inhibition Target*	*Target Symbol*	*PTEZ Score*
Drugs with significant reduction in AURKA expression post treatment				
A375	Ro-4987655	Mitogen-Activated Protein Kinase	MEK	-10
A375	Genz-644282	Topoisomerase I	Topo I	-10
HUES3	OTS-167	Maternal Embryonic Leucine-Zipper Kinase	MELK	-10
HUES3	Vorinostat	Histone Deacetylase	HDAC	-10
A375	Pralatrexate	DNA synthesis	-	-9.838
MCF7	Epirubicin	Topoisomerase II	Topo II	-9.471
HT29	Ro-4987655	Mitogen-Activated Protein Kinase	MEK	-9.284
MCF7	Pralatrexate	Metabolic	-	-9.259
A375	JNJ-26481585	Histone Deacetylase	HDAC	-9.206
HT29	R-547	Cyclin Dependent Kinase	CDK	-8.938
Drugs with an increase in AURKA expression post treatment				
PC3	BIIB-021	Heat Shock Protein 90	HSP90	6.298
HT29	NMS-1286937	Polo-like Kinase 1	PLK	6.407
HELA	NMS-1286937	Polo-like Kinase 1	PLK	6.426
HT29	Docetaxel	Microtubule Function	-	6.458
HT29	Epothilone-b	Microtubule Function	-	6.518
HT29	Indibulin	Microtubule Function	-	6.552
HELA	Dolastatin-10	Microtubule Function	-	6.666
HELA	Volasertib	Polo-like Kinase 1	PLK	6.732
HT29	Epothilone-b	Microtubule Function	-	6.898
HELA	Combretastatin-A-4	Microtubule Function	-	7.007

Note. PTEZ; Post-treatment expression z-score

Drugs that resulted in the highest reduction in HPRT1 expression were AS-703026, OTS-167, BGT-226, genz-644282, AS-703026, SN-38, SN-38, TAK-733, paclitaxel, and KX2-391. Of these, six were of either Topoisomerase I (Topo I) or MEK. This may indicate a relationship between HPRT1 regulation and regulation of Topo I or the MEK pathway (Table 4).

Table 10-4. *Effective drugs for the reduction of HPRT1.*

Cell Line	*Drug*	*Inhibition Target*	*Target Symbol*	*PTEZ Score*
Drugs with significant reduction in HPRT1 expression post treatment				
HT29	AS-703026	Mitogen-Activated Protein Kinase	MEK	-9.822
HUES3	OTS-167	Maternal Embryonic Leucine-Zipper Kinase	MELK	-9.707
Jurkat	BGT-226	Phosphoinositide 3-Kinase	P13K	-8.533
MCF7	genz-644282	Topoisomerase I	Topo I	-7.601
A375	AS-703026	Mitogen-Activated Protein Kinase	MEK	-7.119
MCF7	SN-38	Topoisomerase I	Topo I	-6.904
A375	SN-38	Topoisomerase I	Topo I	-6.702
HT29	TAK-733	Mitogen-Activated Protein Kinase	MEK	-6.594
MCF7	paclitaxel	Microtubule Function	-	-6.537
MCF7	KX2-391	Sarcome	Src	-6.366
Drugs with an increase in HPRT1 expression post treatment				
MNEU	dinaciclib	Cyclin Dependent Kinase	CDK	2.362
NPC	SB-939	Histone Deacetylase	HDAC	2.39
MNEU	mitoxantrone	Topoisomerase II	Topo II	2.412
NEU	ischemin	P53 Transcription	-	2.454
ASC	mitoxantrone	Inflammation	-	2.551
NEU	NVP-BGJ398	Fibroblast Growth Factor Receptor	FGFR	2.668
Jurkat	tanespimycin	Heat Shock Protein	HSP	2.72
SKL	dinaciclib	Cyclin Dependent Kinase	CDK	3.137
ASC	dinaciclib	Cyclin Dependent Kinase	CDK	3.195
Jurkat	dinaciclib	Cyclin Dependent Kinase	CDK	5.414

Note. PTEZ; Post-treatment expression z-score

Discussion

We have determined that there is a significant elevation of JAG2, HPRT1, AURKA, and PGK1 expressionin endometrial cancer. With elevated expression upon malignancy, these genes can be utilized as a companion diagnostic tool to both identify and characterize endometrial cancer. As cancer specific biomarkers, these genes may serve as useful markers when analyzing endometrial cancer development within patient tissue. Additionally, HPRT and PGK1 show additional promise as possible biomarkers for cancer grade as the levels of the proteins elevated in a stepwise manner with higher cancer grade. These biomarkers have already shown utility in other cancer types [61,573,574,576,577,584] and we have shown that their use may also extend to endometrial cancer.

While there are several epigenetic biomarkers for endometrial cancer (p52, KRAS, VEGF. PTEN, etc.)[609,610], there remains a need to find suitable protein biomarkers for not only endometrial diagnosis, but also as possible targets for future therapies. Future directions to this work include evaluating a larger cohort of patients to determine whether the expression of these biomarkers could have clinical application. Especially in the case of both HPRT1 and AURKA, it may be beneficial to develop therapies to reduce their expression, thereby determining whether these genes play a critical role in cancer survival and proliferation as they show significant impact on overall patient survival.

In addition, the conserved pathways that HPRT1 and AURKA have in terms of drugs that inhibit or induce their expression, may indicate a regulatory relationship between the inhibited pathway and the proteins that have not yet been identified. The merit of this hypothesis is demonstrated as AURKA has a reciprocal regulation with PLK1 in mitotic entry and within spindle assembly[611]. This corresponds to the data we have observed as the drugs with the largest

impact on AURKA elevation with the highest consistency are inhibitors of PLK1 and microtubule formation. Yet, the consistent relationship between drugs that inhibit HPRT1 expression are both inhibitors of Topo I and the MEK pathway. There has not been any investigation into the relationship between HPRT1 and these proteins/pathways and our initial data show that a possible link exists. With this in mind, this potential relationship merits further examination and could potentially elucidate novel gene interactions specific to cancer.

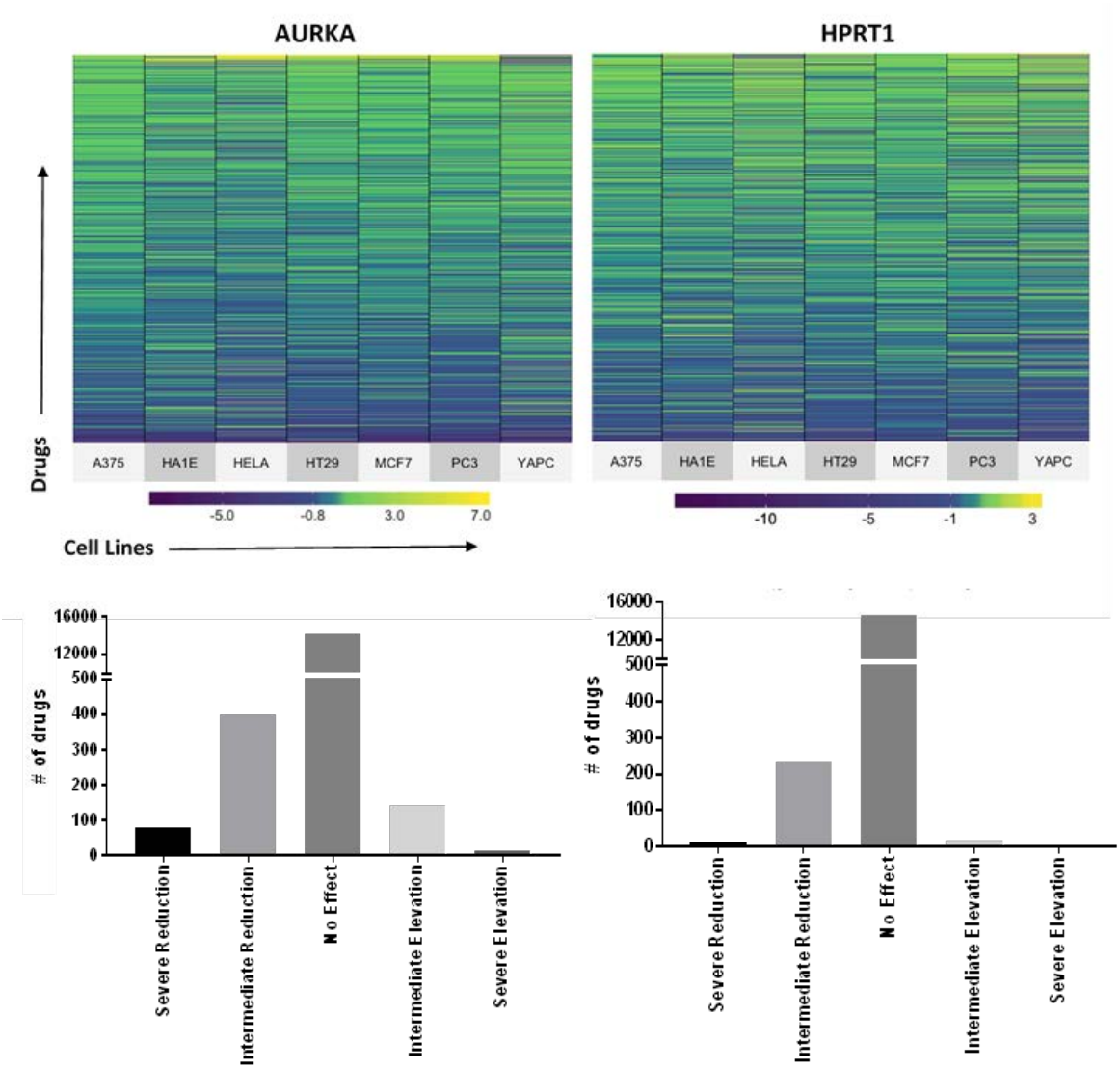

Figure 10-11. *Drugs that lower the expression of JAG2, HPRT1, AURKA, and PGK1.* Cell lines (x-axis) were evaluated for their expression of AURKA and HPRT1 pre and post treatment with drugs (y-axis). The relative changes in protein expression is indicated by the heat map legend and show the variety of responses to various drugs. The events and their effects on target gene expression are indicated by the bar graphs.

APPENDIX 1

HPRT surface localization in malignant prostate cancer cells and the influence of gain of function p53 mutations on HPRT expression.

Michelle H. Townsend, Abigail M. Felsted, Zac E. Ence, Weston Burrup, John E. Lattin, Stephen R. Piccolo, Richard A. Robison, and Kim L. O'Neill

The following data contains data published in an abstract in Cancer Research and presented at the American Association for Cancer Research Annual Meeting in 2018. This appendix contains data for a manuscript in preparation for publication and all contents and figures have been formatted for this dissertation.

Abstract

Prostate cancer is the second most lethal cancer in men, and an estimated 26,730 men will die from the disease in 2017. We chose to evaluate the HPRT enzyme due to its involvement in nucleotide synthesis and cell cycle progression. Two prostate cancer cell lines were used for this analysis (PC3 and DU145) along with malignant tissue. The surface localization of HPRT was determined utilizing flow cytometry and scanning electron microscopy, while upregulation within tissue was assessed using immunohistochemistry. Additionally, RNA-seq data was used to evaluate general HPRT upregulation in patients with prostate cancer (n = 502) when compared to healthy individuals (n = 52). Throughout our investigation, we found a significant association between HPRT and the plasma membrane of DU145 cells, but found no presence on PC3 cells. Flow cytometry showed insignificant ($p = 0.14$) changes in fluorescence when PC3 cells were exposed to HPRT antibodies, while there was a significant increase in fluorescence on DU145 cells ($p = 0.0004$). To determine the distribution of HPRT across the membrane, gold conjugated antibodies were used for analysis with an electron microscope. The distribution of the gold on the cell surface showed random HPRT binding across the membrane with no patterns of localization. This analysis aided in confirming HPRT surface presence as the gold weight % of DU145 cells increased significantly when exposed to HPRT antibodies ($p < 0.0001$). In addition to being presented on the surface of DU145 cells, tissue samples revealed variable HPRT expression as approximately 53% of prostate cancer patients had elevated levels of HPRT compared to normal controls, while 47% of patients had no upregulation. TCGA data revealed a significant ($p = 1.53 \times 10^{-4}$) increase in HPRT levels upon malignancy. While some patients had levels consistent with healthy controls, there was a significant number of patients with increased protein expression upon cancer development. The control of HPRT expression within these cancer cells has been linked preliminarily to p53 functionality. While PC3 cells are null for p53,

DU145 cells have a p53 mutation than may exhibit gain of function (GOF) properties. GOF p53 mutations are known to influence salvage pathway enzyme expression and is an influential gene in HPRT expression in these cancer cells. These results strongly indicate a unique relationship between prostate cancer cells and HPRT and suggest the protein as a possible biomarker for the detection and treatment of patients with prostate cancer.

Introduction

As the second leading cause of cancer related deaths in males, prostate cancer is a principal health concern. In 2018, approximately 164,690 new cases of prostate cancer are estimated and 29,430 men are expected to die in the United States[612]. This is the second most frequently diagnosed cancer in males following lung cancer[462]. While incidence rates in younger men are relatively low, rates increase by 2.8% every year after the age of 65[512]. While many environmental factors, such as diet and hormone treatments, have shown to lower the risk of cancer development by 25% in some cases, there is a need to find suitable biomarkers for cancer diagnosis and treatment.

Currently, the most routine diagnostic methods for prostate screening are measuring prostate-specific antigens (PSA), conducting digital rectal examinations, and histological examinations of biopsied prostate tissue[613]. PSA, a kallikrein serine protease encoded by the KLK3 gene, is the routinely tested antigen when screening for prostate cancer. As PSA levels are often elevated in the blood of prostate cancer patients, measuring PSA can aid physicians in determining the risk of cancer along with the stage of developed tumors. Yet, these evaluations can be subjective and variable between patients, making diagnosis difficult when considering assay sensitivity and specificity[614]. Another drawback from PSA screening is the lack of specificity for prostate cancer which results in negative biopsies and over diagnosis[615]. Although measuring PSA is a useful tool for the early identification of prostate cancer, there are many shortcomings that make it less than ideal for several patients[613,616,617].

In addition to PSA characterization, several prostate cancer specific antigens have been identified as autoantibodies present in the serum of patients through phage microarrary analysis[618]. This method of screening measures patient antibodies against 22 tumor associated

peptides, and can detect tumor development with 88.2% accuracy and a sensitivity of 81.6%. In comparison to PSA tests, these antibody screenings have significantly increased performance[619]. Additionally, other overexpressed antibodies have been used in the identification of prostate cancers such as huntingtin interacting protein-1, prostasomes, and human kallikrein-related peptidase 2 [620–622]. Antibodies towards these antigens show a definitive increase in patients with prostate cancer and are used to improve diagnosis often in combination with PSA screening.

mRNA-based biomarkers have also been shown as dependable biomarkers for prostate detection. PCA3 (Prostate cancer antigen 3) and ERG (ETS-related gene) are both mRNA biomarkers that are shown elevated expression in prostate cancer. PCA3 is a prostate-specific gene that encodes a non-coding mRNA, and the overexpression of the gene was observed in 95% of prostate cancer patients[623,624]. ERG gene fusions between TMPRSS2, SLC45A3 or NDGR1 with ERG, and are also extremely common as 50% of prostate cancer patients have the fusion[625,626]. This gene fusion results in increased expression of ERG oncogene and high levels of ERG transcripts[615].

Several different surface expressed protein have been identified for their potential therapeutic use in prostate cancer. Prostate-specific membrane antigen (PSMA) are found on the surface of prostate cancer cells and are useful for both diagnosis and treatment[627]. There are currently several clinical trials investigating PSMA as a target for CAR T cell therapy (NCT03356795, NCT03089203, NCT03185468, NCT01140373). PSCA is a glycoprotein that is expressed on the cellular surface of prostate cancer and is detected via immunohistochemistry[624]. PSCA also serves as a direct target for CAR T cell therapy and there are three clinical trials testing the efficacy and safety of anti-PSMA CAR T cells (NCT03198052, NCT02744287, NCT03267173). Hepsin is a membrane-bound serine protease that is widely expressed

throughout the body, but is upregulated in malignant prostate tissue and is used as a diagnostic tool[628]. There are several other surface antigens, such as Sca-1, CD133, and CXCR4, used to identify cancer stem cells that possess progenitor cell properties and can serve as targets for initiating prostate tumorigenesis[629,630].

Because the characterization of prostate cancer cells is so integral to the effective treatment of the disease, we designed this project to identify possible cancer biomarkers that could be used diagnostically as well as therapeutically. Hypoxanthine Guanine Phosphoribosyltransferase (HPRT1) has been shown to have potential as a surface antigen in lung cancer, colorectal cancer, and Burkitt's lymphoma and has also showed elevated expression within malignant tissue[61,62,388,573,631]. HPRT is a salvage enzyme involved in nucleotide recycling and production throughout the cell cycle[28,632,633]. We evaluated the expression of HPRT in prostate cancer to determine if it had a similar potential.

Materials and Methods

Chemicals

Mouse-anti-human HPRT monoclonal antibody clone 1F8D11 (Thermo Fischer Scientific, Waltham, MA) was aliquoted and stored at -20°C. Anti-mouse-FITC and anti-rabbit-FITC antibodies (Sigma Aldrich, St. Louis, MO) were stored at 4°C and were used in minimal light conditions. Bovine Serum Albumin (Sigma Aldrich, St. Louis, MO) and sodium thiol sulfate (Macron Fine Chemicals, Center Valley, PA) were dissolved in PBS at a 1-3% concentration and stored at 4°C. A 50% Glutaraldehyde stock solution (Electron Microscopy Sciences, Hatfield, PA) was stored at -20°C and workable solutions were diluted to 0.25% in PBS and stored at 4°C. Glycine (Thermo Fischer Scientific, Waltham, MA) was diluted to

0.2mM in PBS and stored at 4°C. NF-κB polyclonal antibody (Bioss Antibodies, Wodburn, MA) was stored at -20°C. GAPDH polyclonal antibody and CD44 monoclonal antibody (One World Lab, San Diego, CA) were stored at -20°C.

Cell Culture Conditions

The human prostate cancer cell lines PC3 and DU145 were obtained from the American Type Culture Collection (Rockville, MD). Both cell lines were grown in RPMI 1640 medium supplemented with 10% fetal bovine serum and 2mM L-Glutamine (all from Hyclone, Logan, UT). Cell media was replaced every 48 hours and cells were trypsinized and cut upon 90% confluency. Cells were treated with Acutase (Stemcell Technologies, Vancouver, Canada) when utilized for flow cytometry, and when plated for all other applications. Cells were grown at 37°C and 5% CO2. Cell lines were authenticated in May of 2016 by the University of Arizona Genetics Core. Cell viability was assessed using trypan blue staining and only cell samples with a viability over 98% were used for testing.

Immunohistochemistry

Prostate tissue arrays were obtained from Cybrdi. The expression of HPRT was assessed utilizing standard immunohistochemistry staining outlined in Townsend et al. [62]. Briefly, tissues were soaked in histoclear to remove paraffin, rehydrated in ethanol, and treated with a DIVA solution to retrieve antigen. Slides were incubated in block and subsequently treated with primary antibody overnight at 4°C. Tissues were then washed and treated with secondary HRP conjugated antibodies followed by a DAB peroxidase solution to highlight areas of antibody binding. A universal negative antibody and a GAPDH antibody were used as the negative and positive controls, respectively.

Tissue arrays were imaged blind to ensure each tissue core was accurately represented without bias. Tissues were then quantified utilizing ImageJ software. All images were evaluated using the IHC toolbox ImageJ plugin. The DAB option is chosen and the tissue image is removed of all other staining. Following this analysis, the image is converted to a grayscale and a threshold is applied in order to eliminate areas of negative space inherit within the tissue. Once the threshold is applied, the average gray value of the tissue is collected. The same threshold is applied to all tissue samples in order to ensure consistency.

Flow Cytometry

To evaluate HPRT surface localization on cultured cells (DU145 and PC3), fluorescent antibodies were used to label target proteins. Briefly, approximately 250,000 cells per sample were incubated with 1µg of primary antibody at 4°C after washing. Cells were then labeled with FITC-conjugated secondary (mouse or rabbit) antibodies for 15 minutes at 4°C. Isotype IgG and NF- κB served as negative controls to account for non-specific antibody binding. CD44 was used as a positive control. Forward/side scatter plots were used to gate out cell doublets and the resulting data was analyzed and plotted using FlowJo Software (FlowJo Enterprise).

Confocal Microscopy

Cultured cells were also analyzed using an epifluorescence microscope (Olympus, Tokyo, Japan) under a laser confocal system (Bio-Rad Laboratories, Hercules, CA) using a 15mW krypton/argon laser. Image processing was conducted using Laser Sharp Computer Software (Bio Rad Laboratories). Briefly, cells were treated with acutase and plated at a concentration of $4x10^5$ cells/mL in a 6-well plate. Following one day of growth, cells were washed and treated with 2.5µg of primary antibody and incubated at 4°C for 15 minutes on a

shaker. Cells were then treated with FITC-conjugated secondary antibody under the same conditions as primary antibody. Finally, cells were treated with a 1:1000 dilution of Cell Mask Deep Red plasma membrane dye (Fisher Scientific, Waltham, MA) and incubated at 37°C for 10 minutes prior to imaging.

Scanning Electron Microscopy

Samples were analyzed under a scanning microscopy using procedures outlined by Weagel et al. [389]. In brief, cells were washed thoroughly with BSA, Sodium Thiol Sulfate, and sodium azide, before treatment with biotin-labeled primary antibodies. Cells were then washed and treated with gold-conjugated streptavidin. Following cell staining, the samples were fixed with a 0.25% flutaraldehyde solution and treated with a gold enhancement kit. Finally, samples were dehydrated in a series of ethanol washes before imaged in low vacuum conditions with a Phillips XL-30 ESEM 15kV electron stream. A gaseous side electron detector (GSE) and Back Scatter electron detector (BSE) were used to visualize gold particles on the surface of cell samples. Due to the gold enhancement step, the background elemental gold percentage of gold are approximately 8%

Once images for the cells were obtained, the elemental composition of the cells was evaluated using energy dispersive spectroscopy (EDAX). EDAZ analysis provides a k-ratio, a Z-value, an A-value, and an F-value. The k-ratio represents the element's peak height compared to a sample of the pure element collected under the same conditions. The Z value represents a correction in the atomic number taking backscattered election yield of the pure element and the sample. The A value represents a compensation for X-rays generated in the sample that are cannot emit energy. The F value represents a correction for the generation of X-rays. We used

these EDAX output values to normalize our samples gold weight percentages using the following equation:

$$Normalized\ Weight\ Percentage = \frac{k - ratio * 100}{Z * A * F}$$

Cell lysate preparation and Western Blot analysis

DU145 and PC3 cells were grown to 95% confluency and trypsinized. Following washing, cells were treated with a RIPA buffer with freshly added protease and phosphatase inhibitor (all from Thermo Fisher Scientific, Waltham, MA). The solution was vortexed thoroughly and incubated for 30 minutes on ice with an additional vortex step performed every 10 minutes. The lysed solution was then pelleted at 15,000xg for 15 minutes at 4°C and aliquoted to eliminate freeze-thawing. All lysate were stored at -80°C.

Lysates were blotted for GAPDH, HPRT, and p53 expression utilizing standard western blotting techiques described by Sewda et al., with minor modifications[634]. Each sample was boiled for 5 minutes prior to running on a 12% polyacrylamide gel under reducing conditions. Gels were then transferred to a nitrocellulose membrane (Biorad Laboratories Hercules, CA, USA), blocked, and treated with primary antibody overnight at 4°C on a shaker. The, HRP conjugated secondary antibodies (Abcam, Cambridge, United Kingdom) were incubated with the membrane for 1 hour at room temperature. Membranes were washed and treated with Western Bright (Advansta, California, USA) HRP substrate before capturing the image with X-ray film. Films were imported into ImageJ and converted to an 8-bit image. Lanes were selected and plotted. The area under the individual bands were calculated to determine the relative protein expression of the samples.

Statistical Analysis

Standard ANOVA statistical analysis with the multiple comparison method was used to determine the differential surface expression of the various treatments for flow cytometry data on both PC3 and DU145 cells. In addition, two-way ANOVA tests were performed to compare the means of HPRT expression between PC3 and DU145 cells. EDAX data was analyzed using an ANOVA with the multiple comparison method in addition to unpaired t tests to determine significance between samples. All statistical analysis was evaluated using GraphPad Prism 7 software. Differences were considered significant when the p value was <0.05.

Results

Patients with prostate adenocarcinoma have variable levels of HPRT expression with an overall trend of elevated expression upon malignancy.

We found that variability in prostate cancer tissue regarding HPRT expression with an overall trend of increased expression within malignant samples. When compared to normal samples, there was a statistically significant increase in overall HPRT expression within malignant samples (*p-value < 0.0023*). While there was an overall increase in HPRT expression within cancerous samples, there was a separation between the patients with some individuals showing unusually high levels of HPRT ("High Adenocarcinoma") while other patients showed levels similar to normal controls ("Low Adenocarcinoma"). Of the patients evaluated 47% showed a 'high adenocarcinoma' profile (Figure A1-1B) while 53% of the patients experienced normal levels of HPRT and were 'low adenocarcinoma'. Within malignant samples, when separated, 'low' patients were statistically significant from 'high' patients (*p-value* < 0.0001). This differentiation between patients was observed in all stage levels, as Figure 1A&B show that within stage III tissue some patients have normal levels of HPRT (Figure 11-1A), while other

patients have a severe upregulation of the protein in lower, stage II, cancers (Figure A1-1B). This indicates that the expression of HPRT within tumors is considerably varied between patients. As there appeared to be no stage dependence, we hypothesized that the increase in HPRT within some individuals was mutational in cause, as it did not relate to the proliferative state of the tumor.

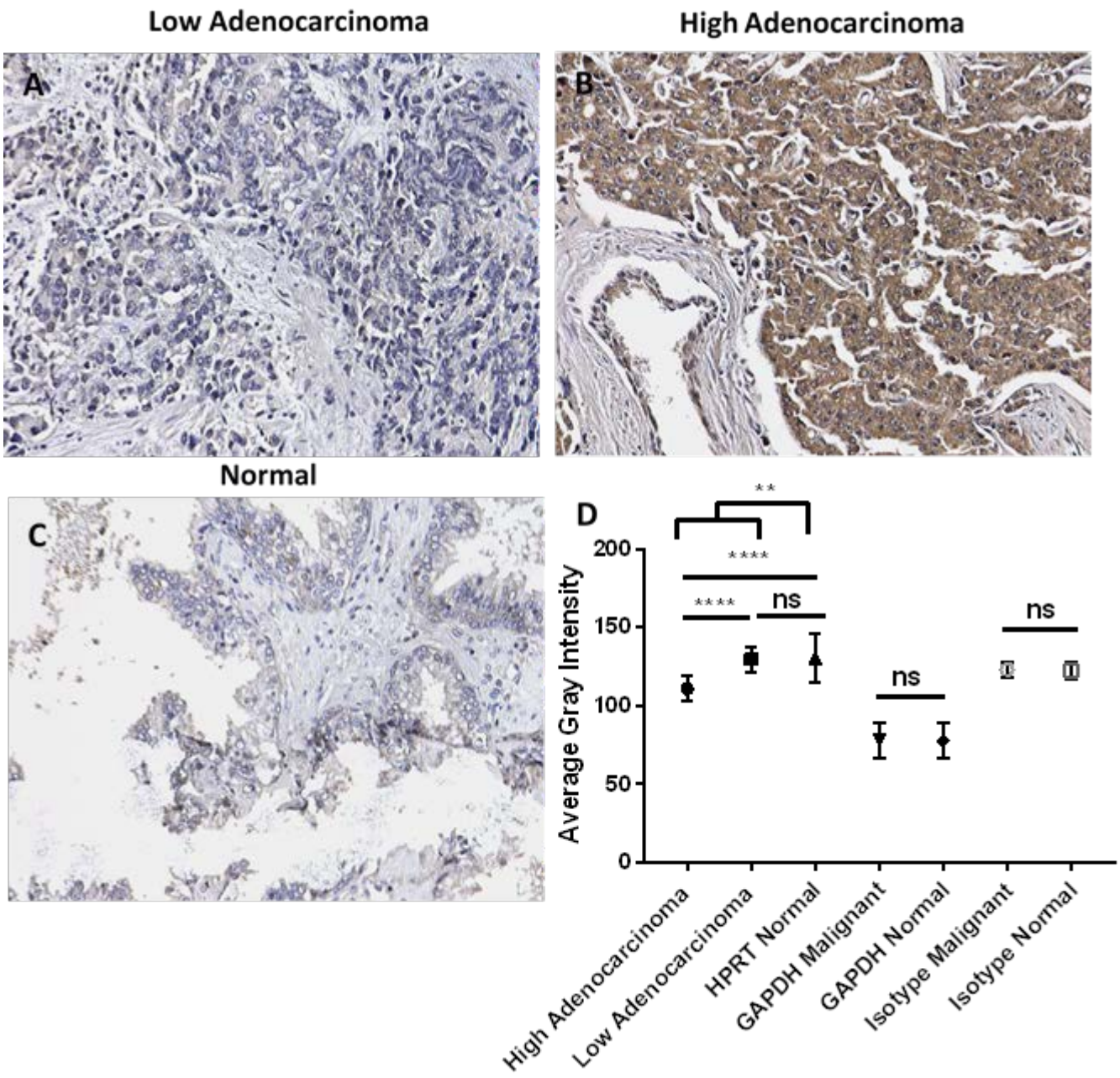

Figure A1-1. *HPRT expression in malignant and normal tissue demonstrate variability of expression.* Tissues were evaluated for HPRT expression along with GAPDH as a positive control and an isotype as a negative control. Images were quantified using a gray scale with lower values indicating a darker stain. A, Sample from a 62-year-old male with stage III prostate adenocarcinoma had very low levels of HPRT expression similar to those seen in normal controls. B, Sample from an 81-year-old male with stage II prostate adenocarcinoma had elevated levels of HPRT that were significant from normal controls. C, Sample from a 63-year-old normal male showed the expected low levels of HPRT expression within healthy adults. D, Statistical evaluation of HPRT expression along with controls.

HPRT is co-localized to the surface of DU145 cells, but not PC3 cells.

DU145 cells show statistically significant HPRT expression on the surface of the cell. There is a statistically significant (*p-value* < 0.0001) increase in the average fluorescent shift in the population (33.4%) when cells are exposed to fluorescent anti-HPRT antibodies when compared to isotype controls (Figure A1-2). This expression is not observed in PC3 cells and there is no statistically significant shift in the fluorescent population when cells are treated with anti-HPRT fluorescent antibodies (*p-value* =0.998). These results are similar to results found in patient tissue, as some cells have an upregulation of HPRT, which results in surface presentation of the protein, while other patients have lower levels of the protein that results in no surface localization.

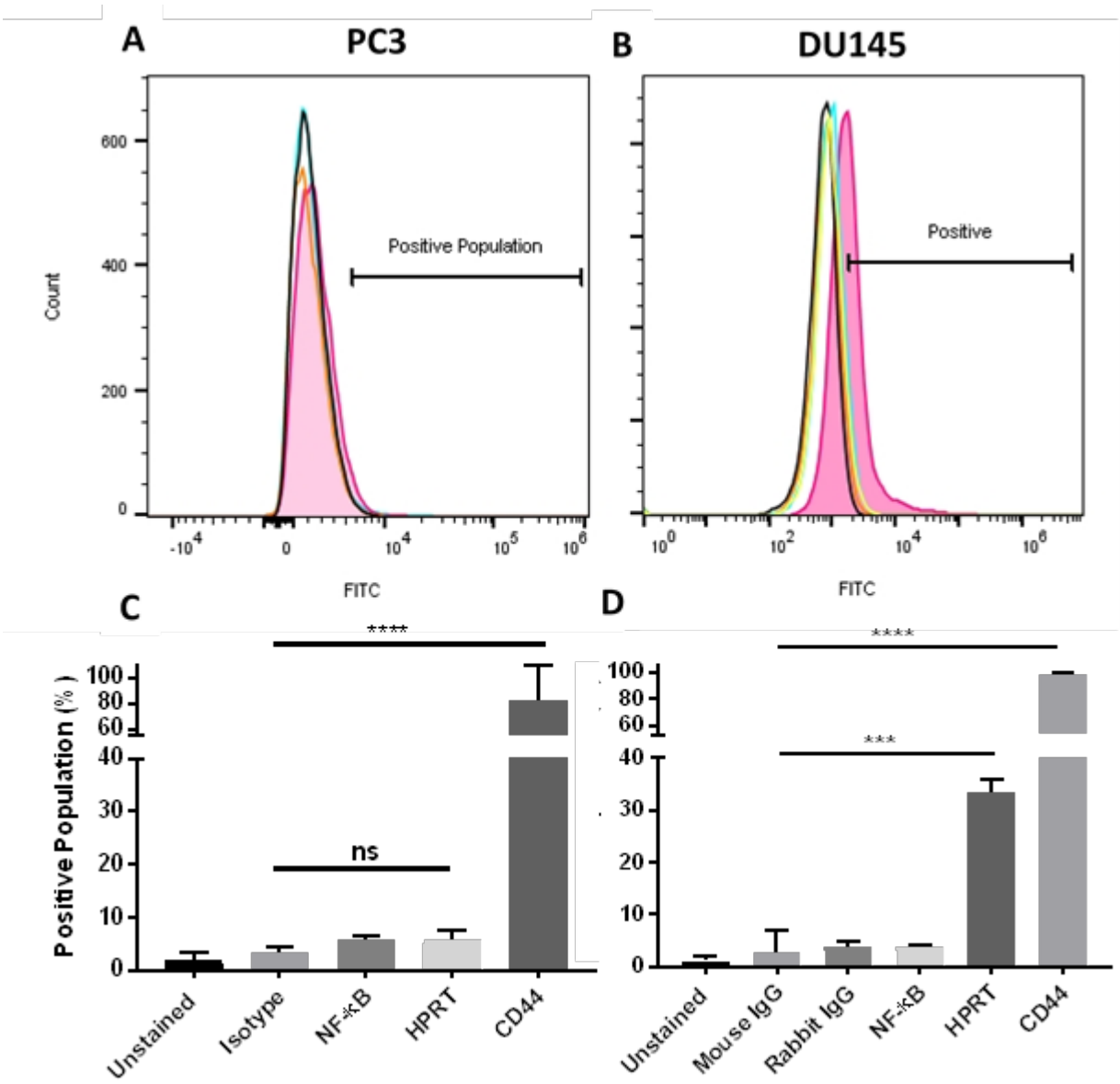

Figure A1-2. *Surface localization of HPRT in DU145 and PC3 cells.* Following treatment with fluorescent antibodies towards the target proteins, the resulting shifts in the fluorescent population were diagramed. Isotype and NF-κB were used as negative controls and CD44 was used as a positive control for expression. A, PC3 cells showed no change in fluorescence upon anti-HPRT treatment while B, DU145 cells show a shift in the population towards a higher fluorescence, indicating surface expression of the protein. C, Statistical evaluation of PC3 expression of HPRT and all controls. D, Statistical evaluation of DU145 expression of HPRT and all controls.

To confirm surface expression, we also imaged individual cells and merged them to a membrane specific dye. The overlap in these images confirms the association of HPRT to the

plasma membrane in DU145 cells and the lack of HPRT presence on the surface of PC3 cells. PC3 cells showed similar staining intensity as isotype controls and did not show co-localization with the membrane specific dye (Figure A1-3). DU145 cells showed a clear presence on the surface of the cell that was directly overlapped with the membrane-specific dye (Figure A1-4). This confirms the surface expression observed in flow cytometry.

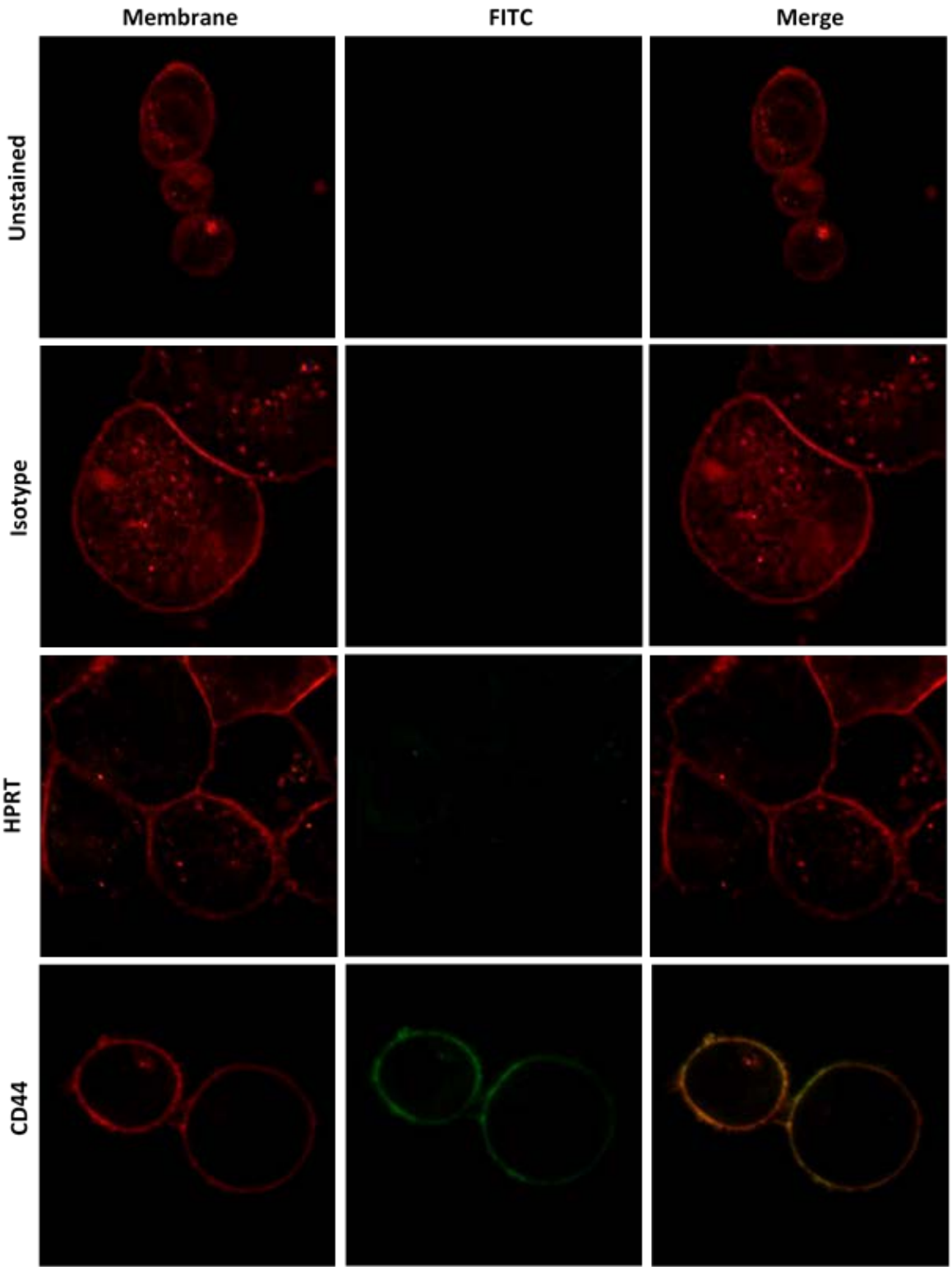

Figure A1-3. *PC3 cell images reveal insignificant HPRT surface localization.* Cells were treated with an isotype antibody, HPRT, and CD44 antibodies along with an unstained control. Each sample was imaged separately to highlight the cell membrane ("membrane") and the target ("FITC"). Both images were merged to show any overlap ("Merge").

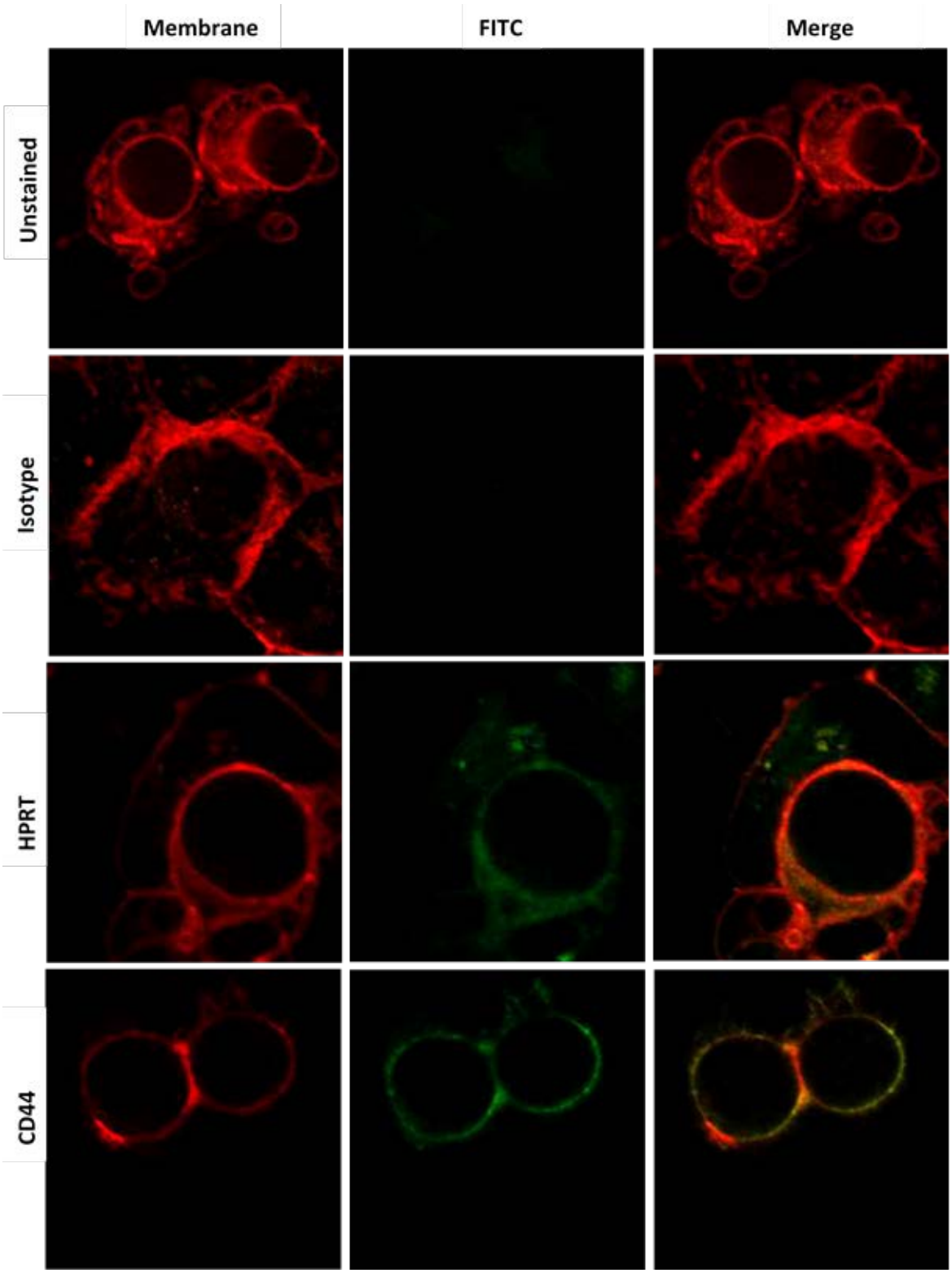

Figure A1-4. *DU145 cell images reveal significant HPRT surface localization.* Cells were treated with an isotype antibody, HPRT, and CD44 antibodies along with an unstained control. Each sample was imaged separately to highlight the cell membrane ("membrane") and the target ("FITC"). Both images were merged to show any overlap ("Merge").

To further determine the exact location of the HPRT protein on the cell surface, we performed scanning electron microscopy to visualize the exact position of antibody binding. We found that the unstained, isotype, and negative control all showed no distinguishable gold particles, indicating no antibody binding. Yet, both anti-HPRT and anti-CD44 treated cells showed distinct particles, highlighted in pink, that pinpoints the exact location of antibody binding on the cellular surface. Anti-CD44 shows some localization of binding as the antibodies appear to cluster. Anti-HPRT treated cells do not show this same pattern and gold particles are randomly dispersed across the cell (Figure A1-5).

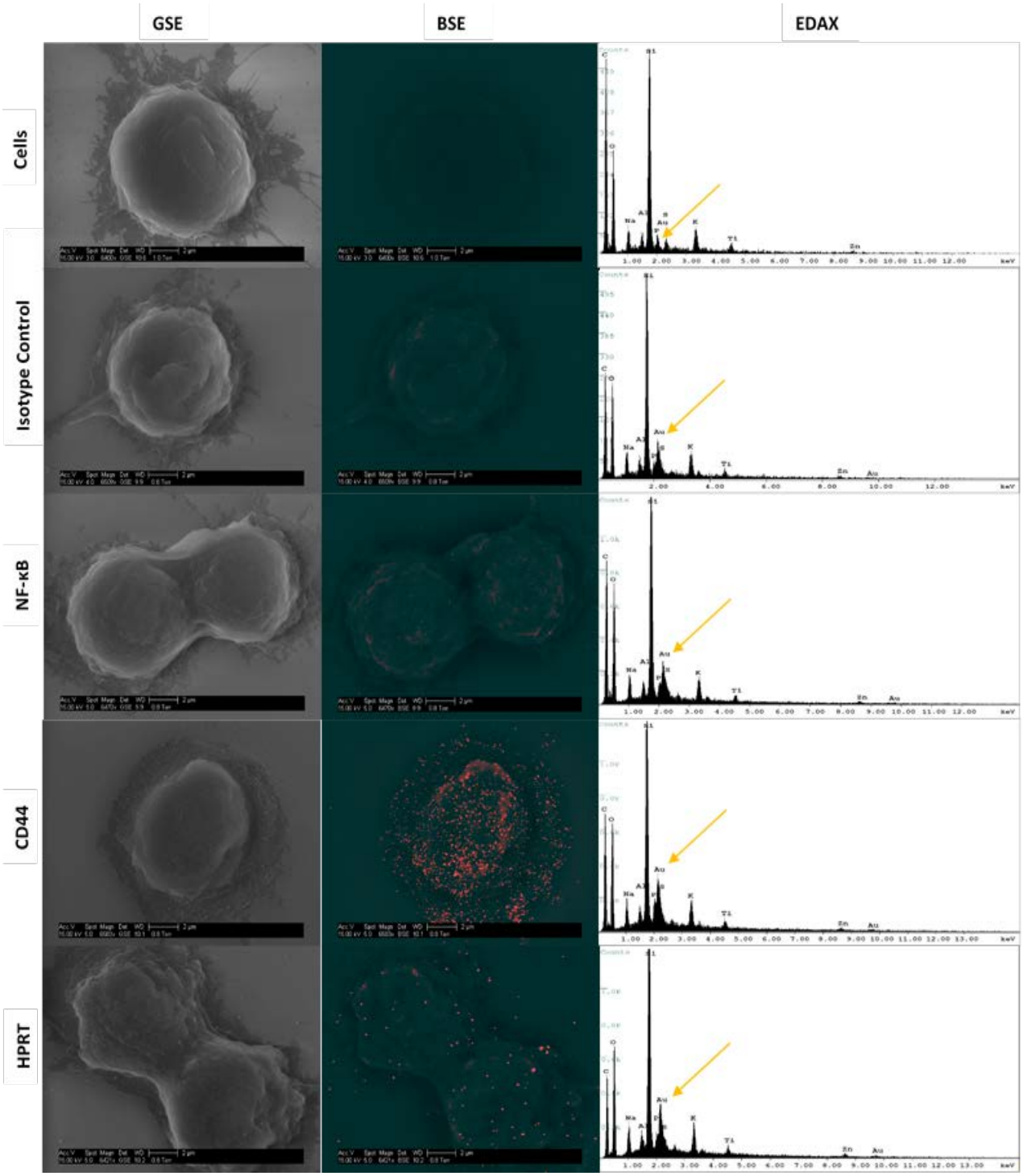

Figure A1-5. *Exact position of HPRT binding on the surface of DU145 cells.* Cells labelled with gold towards the respective antibody treatment were evaluated for gold weight percentage. The size scale shown in each image represents a 2µm distance. Images were obtained using a GSE detector to show cell morphology and correct structure and cellular integrity. Images were also obtained using a BSE detector which images heavy metals within the samples. EDAX analysis was also utilized to show the elemental composition of each sample. The gold elemental peak is indicated by a gold arrow.

When compared to isotype controls, there was a significant increase in HPRT expression on the surface of DU145 cells (*p-value* < 0.0001) as determined by increases in gold elemental weight percentage of the samples. The average gold percentage of anti-HPRT treated samples was 11.63%, while the average gold percentage of isotype controls was 8.58%. This increase in elemental gold shows the increase in gold binding, and subsequently anti-HPRT binding to the surface of the cells (Figure A1-6).

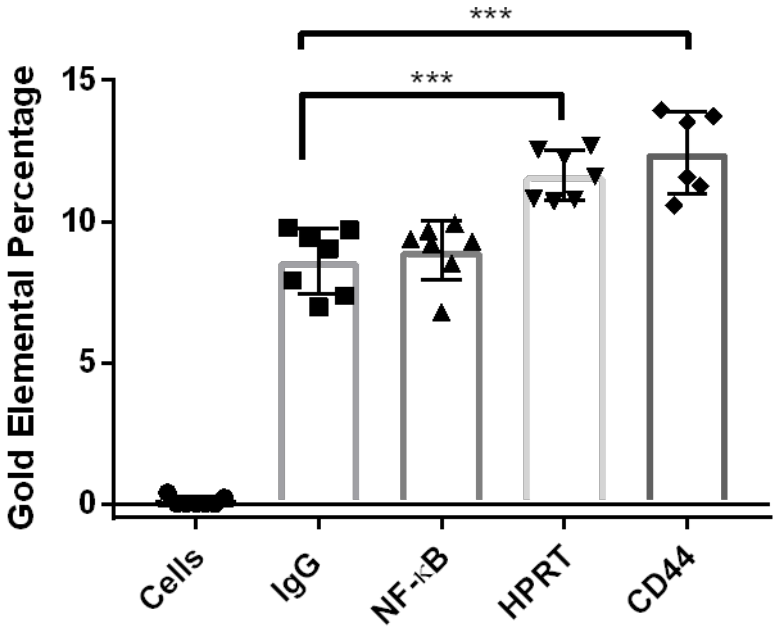

Figure A1-6. *Gold weight percentage of DU145 cells.* The gold weight percentage of each sample was calculated and compared to controls. Cells treated with anti-HPRT antibodies had a significant elevation in gold weight% when compared to isotype controls.

Influence of p53 mutations on HPRT expression.

In an effort to determine the molecular mechanism of HPRT elevation and surface expression we evaluated the differences in transcriptional regulation of the hprt gene between PC3, DU145, and other cell lines previously determined to have surface expression of the protein. We determined that cell lines with elevated levels of HPRT on the cell membrane all have a gain of function (GOF) mutation in p53, a transcription factor of the *hprt* gene. As GOF

p53 mutations have already shown to influence salvage enzyme expression, we hypothesized that this mutation may have an influence on HPRT expression and resulting surface localization, especially considering our initial hypothesis that the overexpression of HPRT in patients was mutational in origin. We utilized a protein that showed a historical strong correlation with GOF mutations (TK1) as our 'positive' control for increases in protein levels upon GOF mutations33.

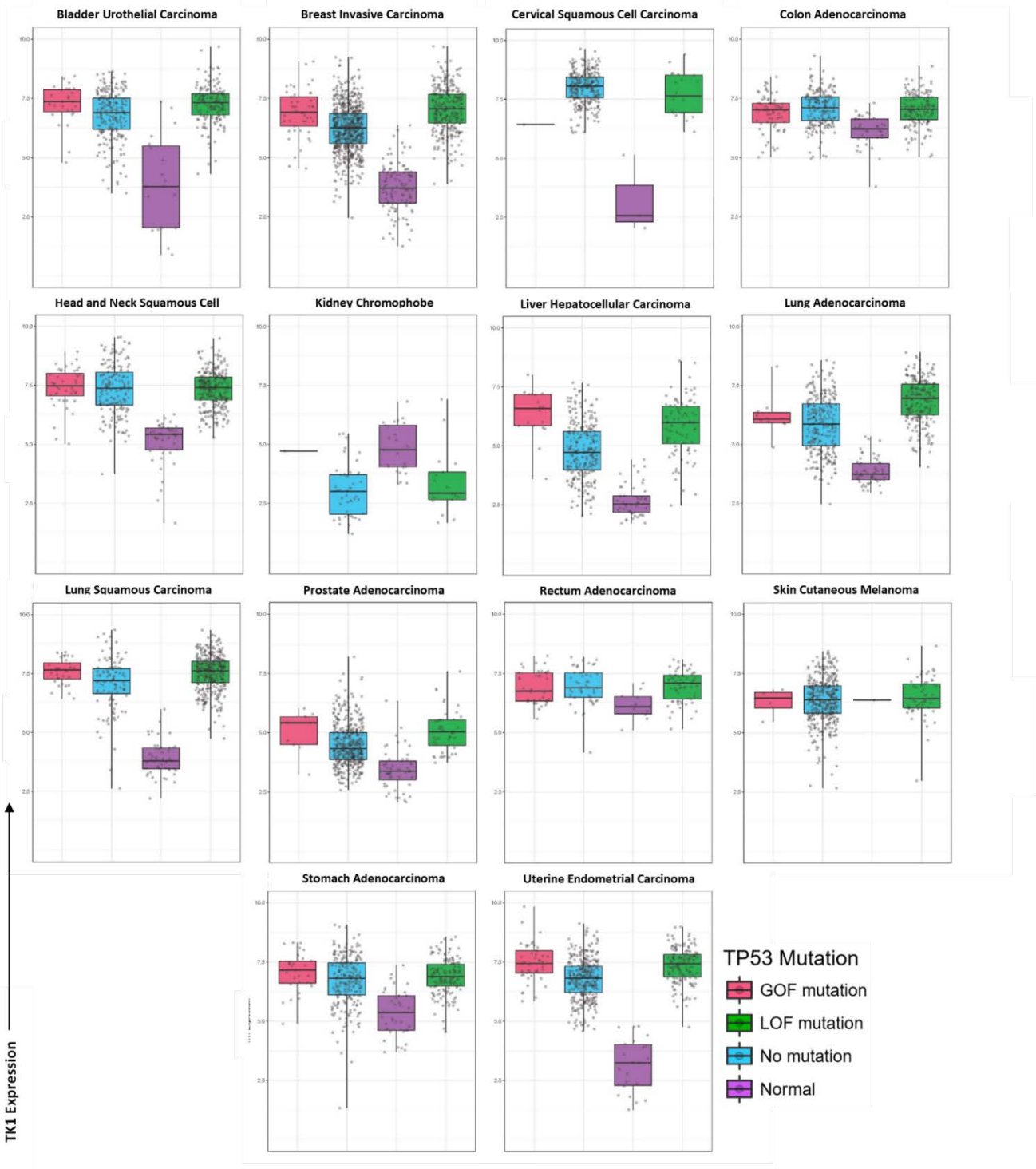

Figure A1-7. *TK1 expression between GOF, LOF, WT, and normal patients*. Patient samples were evaluated for their p53 status and plotted according to 'GOF' mutations (G245C, P151S, R175H, R248Q, R249S, R273H, R282W), 'LOF' mutations, and 'no mutations' (WT). Each diagram has been log2 transformed to better represent the data. We evaluated 14 different cancer types for expression changes in TK1 upon p53 mutation. TK1 expression was evaluated in transcripts per million.

We evaluated RNA-sequencing data and compared the relative expression of HPRT and TK1 between GOF mutations, Loss of function (LOF) mutations, WT ('no mutation'), and normal samples. This analysis led to conflicting results. We found very little change in TK1, our positive control, expression between GOF and LOF mutations within several cancer types (Figure A1-7). Throughout our analysis, only one cancer type showed statistical significance in TK1 expression between GOF and LOF mutations (Uterine Endometrial Carcinoma; p-value = 0.037). As such, it was difficult to evaluate the influence of GOF p53 mutations on HPRT expression as our results deviated from previous work. This discrepancy may be due to a small sample size, as gain of function mutations are somewhat infrequent within patient populations.

In our evaluation of HPRT expression, we found there were only 2 cancer types (diffuse large B-cell lymphoma & liver hepatocellular carcinoma) that had a significant difference between the expression of HPRT between LOF p53 mutations and GOF mutations (p-value = 0.0335 & 0.0236, respectively). Several cancer types did show a significant difference between GOF mutations and no p53 mutation (breast invasive carcinoma; p-value = 0.0028, colon adenocarcinoma; p-value = 0.0255, bladder urothelial carcinoma; p-value = 0.0052, liver hepatocellular carcinoma; p-value = 0.0024, and rectum adenocarcinoma; p-value = 0.0067), showing that mutations in p53 do impact the overall expression of HPRT in some cancer (Figure A1-8). In addition, a promising observation is in each cancer type regardless of p53 status, HPRT was significantly elevated between normal and malignant samples (p-value < 0.0001).

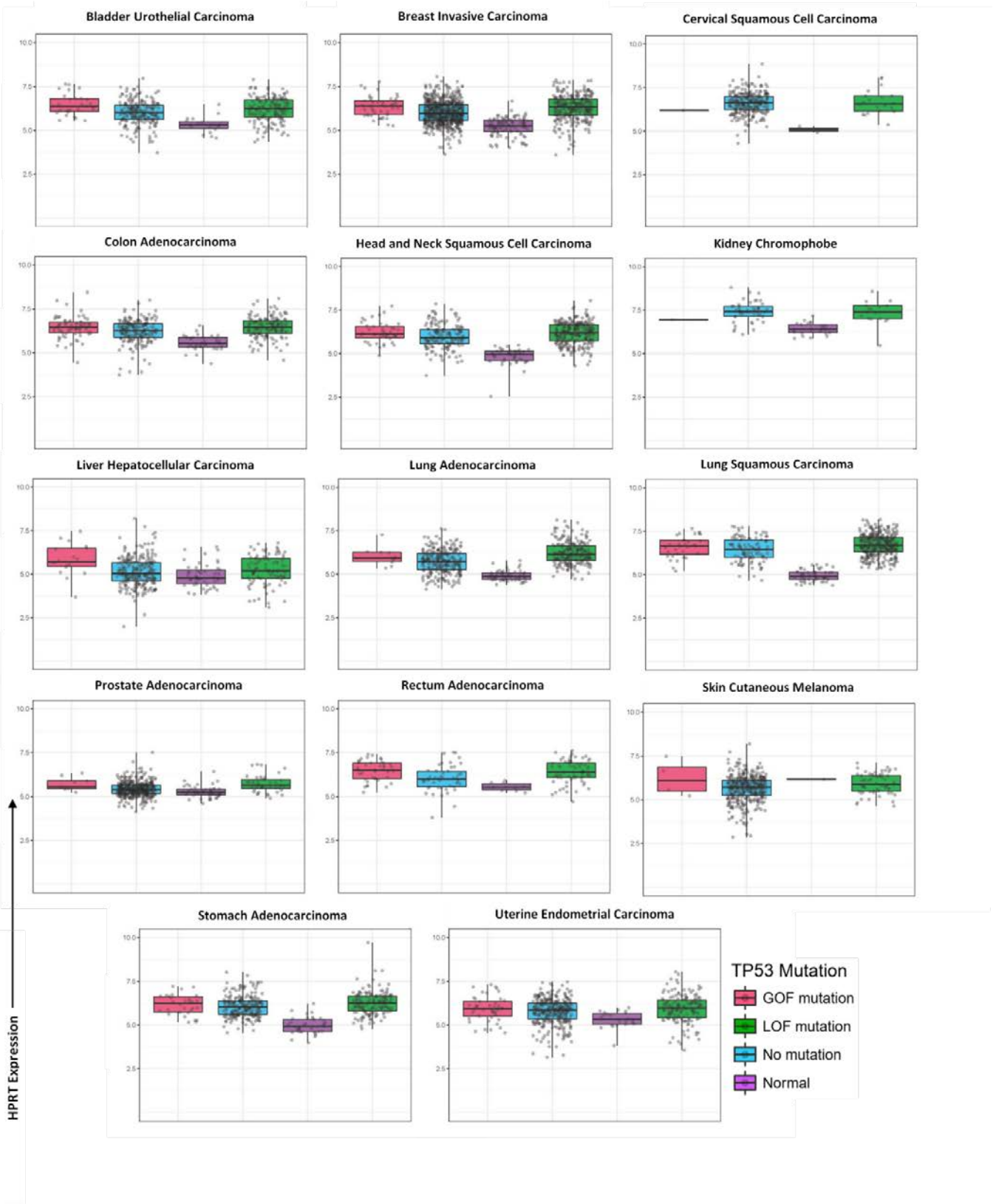

Figure A1-8. *HPRT expression between GOF, LOF, WT, and normal patients.* All diagrams were log2 transformed to better represent the data. GOF mutations (G245C, P151S, R175H, R248Q, R249S, R273H, R282W) were compared to other mutations for variations in HPRT expression upon mutation. HPRT expression was evaluated in transcripts per million.

Discussion

We have determined that HPRT has a significant elevation in prostate cancer both within certain patient tissue and also on the surface of some prostate cancer cells. It would appear that this overexpression is not a universal event in cancer, and is patient specific. The molecular mechanism has been preliminarily linked to gain of function p53 functionality within these cells. The exact mechanism behind the elevation and surface expression of HPRT will require further study and presents an opportunity to discover new molecular functions and/or control of the HPRT1 gene within cancer.

HPRT is already known to have a regulatory function as its role in neural development is critical for healthy growth as patients with a deficiency of the protein suffer from Lesch-Nyhan syndrome. This regulatory role may extend to a possible advantageous function within cancer cells, which may explain its subsequent upregulation in approximately 50% of prostate cancer patients.

Although an exact mechanism is not known, HPRT shows significant surface localization with prostate cancer cells in some patients and could serve as a biomarker for targeted immunotherapy, such as CAR T cell therapy. Especially, as HPRT is not found in normal patients at high levels it may be a beneficial target to limit on-target, off-tumor cytotoxicity.

APPENDIX 2

HPRT elevation has a direct impact on Guanosine production within cancer cells and induces a decrease in cytokine production in the tumor microenvironment.

Michelle H. Townsend, Claudia M. Tellez Freitas, Dallas Larsen, Stephen R. Piccolo, K. Scott Weber, Richard A. Robison, and Kim L. O'Neill

This appendix contains data for a manuscript in preparation for publication and all contents and figures have been formatted for this dissertation.

Introduction

Guanosine is a guanine nucleoside that has an important role in regulating inflammation within the central nervous system (CNS). Both guanosine and adenosine are aromatic organic molecules that present with one or more phosphates to form components of nucleotides essential for cellular survival. In addition to their basic role within cellular maintenance, both adenosine and guanosine act as intercellular messenger molecules.

Adenosine is established as a potent anti-inflammatory molecule that affects the activation of neutrophils, by inhibiting stimulated cell adhesions to the vascular endothelium[635,636], macrophages, by suppressing chemokine/cytokine production[637–639], and T cells. T regulatory cells (Tregs) express CD39 and CD73 on their cell surface, which produce adenosine to mediate anti-inflammatory regulatory effects on effector T cells[636,640,641]. These anti-inflammatory properties of adenosine have made it an attractive target for therapy in chronic inflammatory diseases[642–644].

Guanine and its derivatives have been identified as modulators of G-protein function, which are essential in signal transduction[645,646]. In addition, they have also shown a regulatory role in small monomeric G-proteins (Ras, Rab Ef-Tu, etc.)[647]. Guanosine itself has shown anti-inflammatory properties specifically within the brain and acts as a neuroprotectant. Specifically, guanosine has shown to inhibit LPS-induced pro-inflammatory responses[648] and reduce NF-kB signaling pathway and pro-inflammatory cytokine production[649]. Additionally, guanosine reduces apoptosis[650] and activates cell survival pathways, including P13K/Akt/PKB signaling in neural cells[651–653]. Extracellular guanosine has a regulatory role and controls the levels of extracellular adenosine[654,655]. An increase in guanosine leads to an increased level of adenosine and guanosine has been implicates as a potential therapeutic target for reducing inflammation[654].

We have previously shown that a salvage enzyme hypoxanthine guanine phosphoribosyltransferase (HPRT) is upregulated within several cancer types[61]. HPRT is responsible for salvaging GTP and is involved in the production of guanine and its derivatives[632]. We hypothesized that an increase in guanosine production within tumors may be persistent because of the immune protection it provides the tumor as guanosine has shown anti-inflammatory properties in the CNS. In addition, as the levels of guanosine have shown to elevate in hypoxic and hypoglycemic conditions, we believe the increase in HPRT expression within these tumors has a direct relationship with the conditions present within tumor microenvironment, which often supports a hypoxic and hypoglycemic state[656–660].

Materials and Methods

Cell Culture

Raji, Jurkat, and THP-1 human cell lines were obtained from the American Type Culture Collection (Rockville, MD, USA). All cells were grown and maintained in RPMI-1640 medium supplemented with 10% fetal bovine serum and 2mM L-glutamine. Cells were grown at 37°C and 5% CO_2 and were fed every 24-48 hours according to their proliferation. Cell lines were authenticated in May of 2016 by the University of Arizona Genetics Core.

HPRT Knockdown Raji cells

The pSpCas9(BB)-2a- GFP CRISPR vector was purchased from Addgene (Cambridge, MA, USA) and guide RNA design was conducted using the CRISPR Design tool created by MIT[568]. Briefly, Raji cells were grown to a concentration of 4x105 cells per mL and seeded in a 6-well plate. Following 24 hours of growth, cells were transfected with a lipofectamine LTX reagent (Invitrogen Waltam, MA, USA). Briefly, 150µL of Opti-MEM (Gibco, Gaithersburg,

MD) was incubated with 5-7µL of Lipofectamine LTX reagent while 250µL of Opti-MEM was incubated with approximately 2x103ng of the CRISPR vector. The solutions were mixed together and incubated at room temperature for 30 minutes. The lipofectamine-DNA solution was then added to the Raji cells in a drop-wise fashion. Cells were grown for 3 days and then treated with media containing 6-Thioguanine (6-TG) at a final concentration of 10µg/µL. 6-TG is a nucleoside analog that is toxic to cells with a functional *hprt* gene. Cells that survived the 6-TG treatment were grown to sufficient quantities to produce cell extract. This extract was analyzed by western blotting to confirm surviving cells were HPRT-/-.

Calcium Signaling Activation

Calcium mobilization was measured using flow cytometry and the high affinity calcium indicator Fluo-4 (ex:470–490 nm and em: 520–540 nm). Cells were loaded for 30 mins as previously published with pluronic acid and 1mM Fluo-4-acetoxymethyl ester (Invitrogen) in Ringer solution (150 mM NaCl, 10 mM glucose, 5 mM of HEPES, 5 mM of KCl, 1 mM MgCl2, and 2 mM CaCl2, pH 7.4). Intracellular calcium mobilization was initiated by adding 50 ng/ml of PMA (phorbol 12-myristate 13-acetate) and 1 µg/mml of ionomycin. For further analysis done in FlowJo, intracellular calcium flux was measured in the cell lines e using the FlowJo kinetics tool.

Kaplan-Meier Curves

Survival was calculated utilizing a Cox proportional hazard model. Covariates included gene expression and clinical factors such as age, race, and tumor purity. Uterine Corpus Endometrial Carcinoma (UCEC) samples were obtained from The Cancer Genome Atlas (TCGA)[539] and Kaplan-Meier curves were generated to compare survival of patients with the

highest 30% of target gene expression to those with the lowest 30% of target gene expression. The statistical analyses and curve generations were calculated utilizing the TIMER program developed by Li et al. [603].

Immune Infiltration and Gene correlations

The correlation of HPRT expression to each immune cell subset infiltration and with other tumor associated genes was generated using the TIMER program developed by Li et al. [603]. Gene-level expression values for tumor samples was obtained from The Cancer Genome Atlas[536,540]. Samples were purity-corrected and the Spearman's correlation and statistical significance were calculated.

Gene expression correlations

We used RNA-Sequencing data for protein-coding transcripts that had been generated using Illumina-based, short-read sequencing. These data had been processed using the kallisto software[538], then log- transformed and converted to transcripts-per- million values[536]. We summed the transcript-level values to gene-level values and sorted the cell lines according to HPRT expression level, from high to low expression per sample. We parsed and prepared the data using Python (https://python.org, v.3.6.1) scripts. In making the heat map, we used the R (v.3.4.3) statistical package[569] and the Superheat package (v.0.1.0)[543].

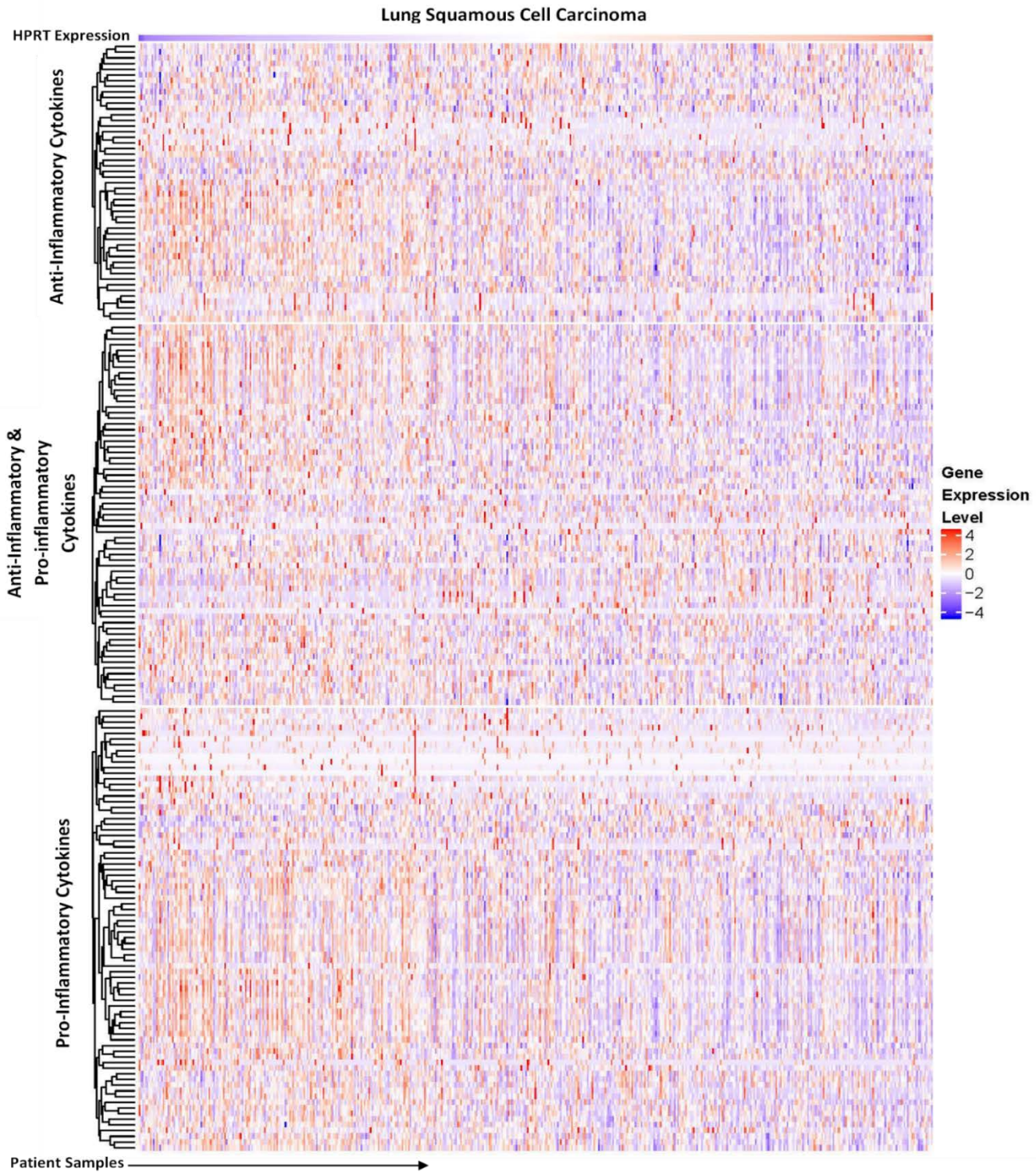

Figure A2-1. *Impact of HPRT elevation on immune gene expression.* We evaluated patients with lung squamous cell carcinoma and ranked them according to their relative expression of HPRT which is represented above the graph. Cytokine gene expression is organized into 'pro-inflammatory cytokines', 'pro-inflammatory and anti-inflammatory cytokines' and 'anti-inflammatory cytokines'. We found an overall trend of decreasing cytokine expression upon increased HPRT expression within all cytokine categories.

Table A2-1. *Gene correlations with HPRT expression.*

Anti-inflammatory and Pro-inflammatory								
Gene	*p-value*	Correlation	Gene	*p-value*	Correlation	Gene	*p-value*	Correlation
CD27	$2.18x10^{-14}$	-	LEP	0.001091	-	IL1RN	0.003788	-
CD40	$6.29x10^{-6}$	-	LEPR	$1.66Ex10^{-7}$	-	IL31	0.025384	+
CD40LG	$5.17x10^{-16}$	-	LIF	0.000363	-	IL33	$2.76x10^{-5}$	-
CD70	$5.71x10^{-13}$	-	LIFR	$1.73x10^{-5}$	-	IL36B	0.00013	+
EDA	0.007857	-	LTA	$1.55x10^{-11}$	-	IL36RN	0.041797	+
EDA2R	$1.6x10^{-15}$	-	LTBR	0.047026	+	IL6R	$3.63x10^{-5}$	-
EDAR	0.000857	-	OSM	$1.24x10^{-5}$	-	TNFSF8	$9.33x10^{-17}$	-
FAS	0.000486	-	OSMR	0.041817	-	TNFSF9	0.025906	-
FASLG	0.003111	-	RELT	$3.91x10^{-5}$	-	TNFRSF8	$7.49x10^{-13}$	-
IL11	0.0001	-	SIGIRR	$6.44x10^{-9}$	-	TNFRSF9	$4.32x10^{-9}$	-
IL11RA	$9.49x10^{-9}$	-	TNF	$8.82x10^{-11}$	-	TNFSF11	$3.06x10^{-11}$	-
IL18BP	$1.38x10^{-9}$	-	TNFRSF10B	$6.34x10^{-6}$	-	TNFSF12	$1.08x10^{-12}$	-
IL18R1	$1.66x10^{-6}$	-	TNFRSF10C	0	-	TNFSF13	$9.48x10^{-14}$	-
IL18RAP	$8.2x10^{-6}$	-	TNFRSF13C	0.014051	-	TNFSF13B	$3.31x10^{-7}$	-
IL1F10	0.00325	+	TNFRSF1A	0.041936	-	TNFSF14	$1.21x10^{-13}$	-
IL1R1	$1.48x10^{-13}$	-	TNFRSF1B	0	-	TNFSF15	0.000132	+
IL1RAPL1	4x10-08	-	TNFRSF21	0.001233	-	IL1RL1	5.8x10-9	-
IL1RAPL2	$1.17x10^{-7}$	+	TNFRSF6B	$1.02x10^{-19}$	-	TNFRSF8	$7.49x10^{-13}$	-
Pro-inflammatory								
Gene	*p-value*	Correlation	Gene	*p-value*	Correlation	Gene	*p-value*	Correlation
CCL1	0.000048	-	CNTF	0.000363	-	IFNA5	0.004918	-
CCL11	0.015893	-	CXCL10	0.035549	-	IFNAR1	$2.25x10^{-10}$	-
CCL13	0.000508	-	CXCL11	0.016643	-	IFNAR2	0	-
CCL14	$5.69x10^{-8}$	-	CXCL12	1.38x10-9	-	TNFRSF10D	$4.14x10^{-14}$	-
CCL15	$1.23x10^{-5}$	-	CXCL13	$4.46x10^{-7}$	-	TNFRSF4	0	-
CCL16	$2.14x10^{-15}$	-	CXCL14	0.047987	-	TNFSF4	$6.7x10^{-6}$	-
CCL17	$4.3x10^{-6}$	-	CXCL16	$4.46x10^{-7}$	-	CCR4	$2.09x10^{-17}$	-
CCL18	0.000121	-	CXCL17	$8.99x10^{-5}$	-	CCR5	$2.07x10^{-11}$	-
CCL19	$8.32x10^{-9}$	-	CXCL2	$6.77x10^{-8}$	-	CCR6	0	-
CCL20	0.00038	-	CXCL3	0.001412	-	CCR7	$4.1x10^{-14}$	-
CCL21	$3.3x10^{-16}$	-	CXCR1	$1.52x10^{-7}$	-	CCR8	$1.12x10^{-10}$	-
CCL22	$7.22x10^{-13}$	-	CXCR2	$1.04x10^{-8}$	-	CCRL1	$7.84x10^{-6}$	-
CCL23	$9.37x10^{-13}$	-	CXCR3	$1.84x10^{-12}$	-	FAM19A3	$8.78x10^{-11}$	-
CCL25	0.000173	-	CXCR4	$1.58x10^{-13}$	-	FAM195A5	$3.56x10^{-5}$	-
CCL26	3x10-16	+	CXCR5	$3.62x10^{-14}$	-	IFNA14	0.009756	-
CCL3	0.007677	-	CXCR6	$5.61x10^{-7}$	-	CCR1	$1.56x10^{-9}$	-
CCL4	0.000144	-	CXCR7	0.001016	+	CCR2	$8.12x10^{-15}$	-
CCL5	$4.02x10^{-6}$	-	FAM19A1	$3.11x10^{-8}$	-	CCR3	0.000869	-
CCL7	0.002324	-	FAM19A2	$9.01x10^{-11}$	-			
Anti-inflammatory								
Gene	*p-value*	Correlation	Gene	*p-value*	Correlation	Gene	*p-value*	Correlation
DCN	$1.41x10^{-11}$	-	IL22Rα2	$5.39x10^{-8}$	-	STAT5A	0	-
DPT	$2.33x10^{-14}$	-	IL24	0.009718	-	STAT6	$1.08x10^{-5}$	-
ENG	0	-	IL29	0.026208	-	TGFβ1	$2.26x10^{-8}$	-
IL10	$2.93x10^{-11}$	-	IL4	$2.56x10^{-5}$	-	TGFβ2	$4.46x10^{-9}$	-
IL10Rα	0	-	IL5	0.024097	-	TGFβ3	$6.74x10^{-13}$	-
IL10Rβ	0.029185	-	LTB	$4.53x10^{-18}$	-	TGFBR2	0	-
IL13	0.013039	-	SMAD5	0.034756	+	TNFRSF11B	$1.73x10^{-5}$	-
IL20	$6.38x10^{-9}$	-	STAT2	$1.76x10^{-8}$	-	TNFRSF12A	$2.55x10^{-6}$	-
IL22	$3.39x10^{-11}$	-	STAT3	$9.86x10^{-8}$	-	TNFRSF13B	$5.58x10^{-15}$	-
IL22Rα1	0.009197	+	STAT4	$8.23x10^{-17}$	-	TNFRSF14	0	-
TNFRSF17	$1.37x10^{-8}$	-	TNFRSF19	$4.27x10^{-6}$	-	TNFRSF25	$3.56x10^{-8}$	-

Results

HPRT expression showed an overall negative correlation to genes involved in immune function.

As HPRT levels vary significantly among patients, we evaluated the changes in immune gene expression in patients with high expression and compared them to patients with lower expression. For this analysis we evaluated lung squamous carcinoma as it showed the most distinct elevation of HPRT when compared to normal lung tissue[61,62]. Of the 194 total genes evaluated we found a that 68% were negatively correlated with HPRT elevation (31 of 49 anti-inflammatory, 54 of 67 anti-inflammatory and pro-inflammatory, and 47 of 78 pro-inflammatory). Interestingly, there was an overall decrease in both ant-inflammatory and pro-inflammatory cytokines with elevates expression of HPRT (Figure A2-1). Genes with a statistically relevant correlation are found in table 1 and show the significant effect elevated levels of HPRT have in the expression of immune-related genes. Of the genes that did show a statistically significant positive correlation to HPRT expression seven were pro-inflammatory (12% of total), two were anti-inflammatory and pro-inflammatory (3.6% of total), and two were anti-inflammatory (6% of total) in function (Table A2-1).

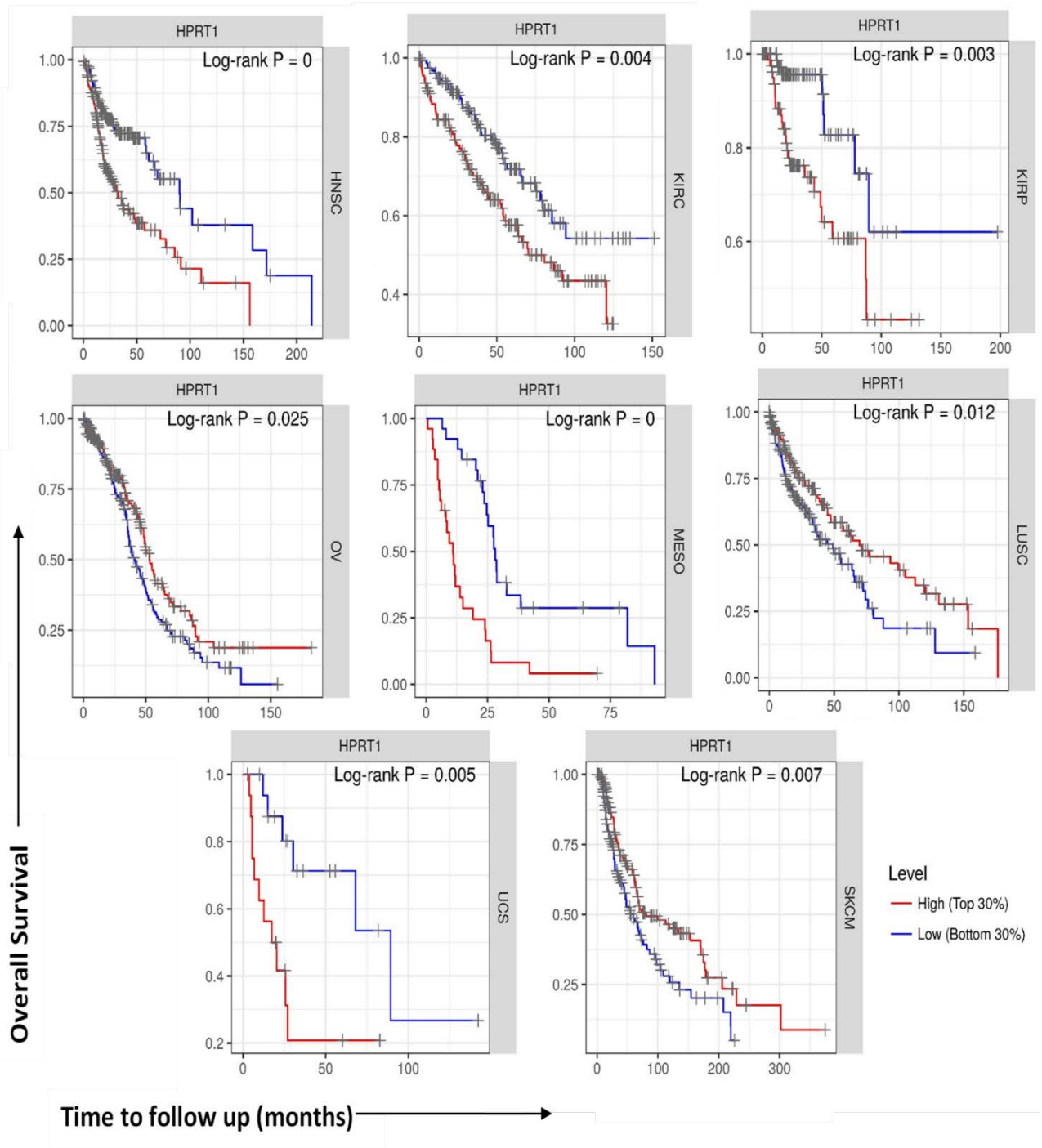

Figure A2-2. *HPRT influence on patient survival.* Patients were divided into the highest expressing 30% and lowest expressing 30% in regards to HPRT. Patient survival was monitored over an extended time (varied depending on the cancer as data permitted) and the percent survival was evaluated on the y-axis.

HPRT elevation has a significant impact on patient survival in several cancer types.

When comparing patients with the highest 30% and the lowest 30% of HPRT expression we found that low expressing patients had a significant increase in overall survival over a long term period in several cancer types (Figure A2-2). Most notable, head and neck squamous cell carcinoma experienced one of the most significant differences between patients. This is interesting because HPRT is involved in guanosine processing and guanosine is most influential in the CNS.

Increased HPRT expression correlates to decreased tumor infiltration by immune cell subsets.

We found that in several cancer types there was a significant negative correlation between HPRT expression and the immune infiltration of B cells, CD8+ T cells, D4+ T cells, macrophages, neutrophils, and dendritic cells (Figure A2-3). Within prostate adenocarcinoma (PRAD), lung squamous cell carcinoma (LUSC), and thyroid carcinoma (THCA) the tumor infiltration of all immune cell types were lessened upon HPRT elevation, with the exception of CD8+ T cells in THCA cancer. This shows that the expression of HPRT is significantly associated with the ability of immune cell subsets to penetrate and infiltrate the tumor microenvironment. Of the immune cell types evaluated, macrophages (42% of cancers) showed the least change in infiltration, while CD4+ T cells showed the most significant change (62.5% of cancers). Cancers that seemed to experience no changes in immune infiltration upon HPRT elevation were esophageal carcinoma (ESCA), kidney chromophobe (KICH), and uterine carcinosarcoma (UCS) (Table A2-2). In addition, when evaluating the immune infiltration of immune cells with a change in the copy number of the HPRT gene we found that in several cancer types there was a significant decrease in immune infiltration in ‘arm-level gain’ and ‘arm-level loss’ patients when compared to ‘normal’ patients (Figure A2-4).

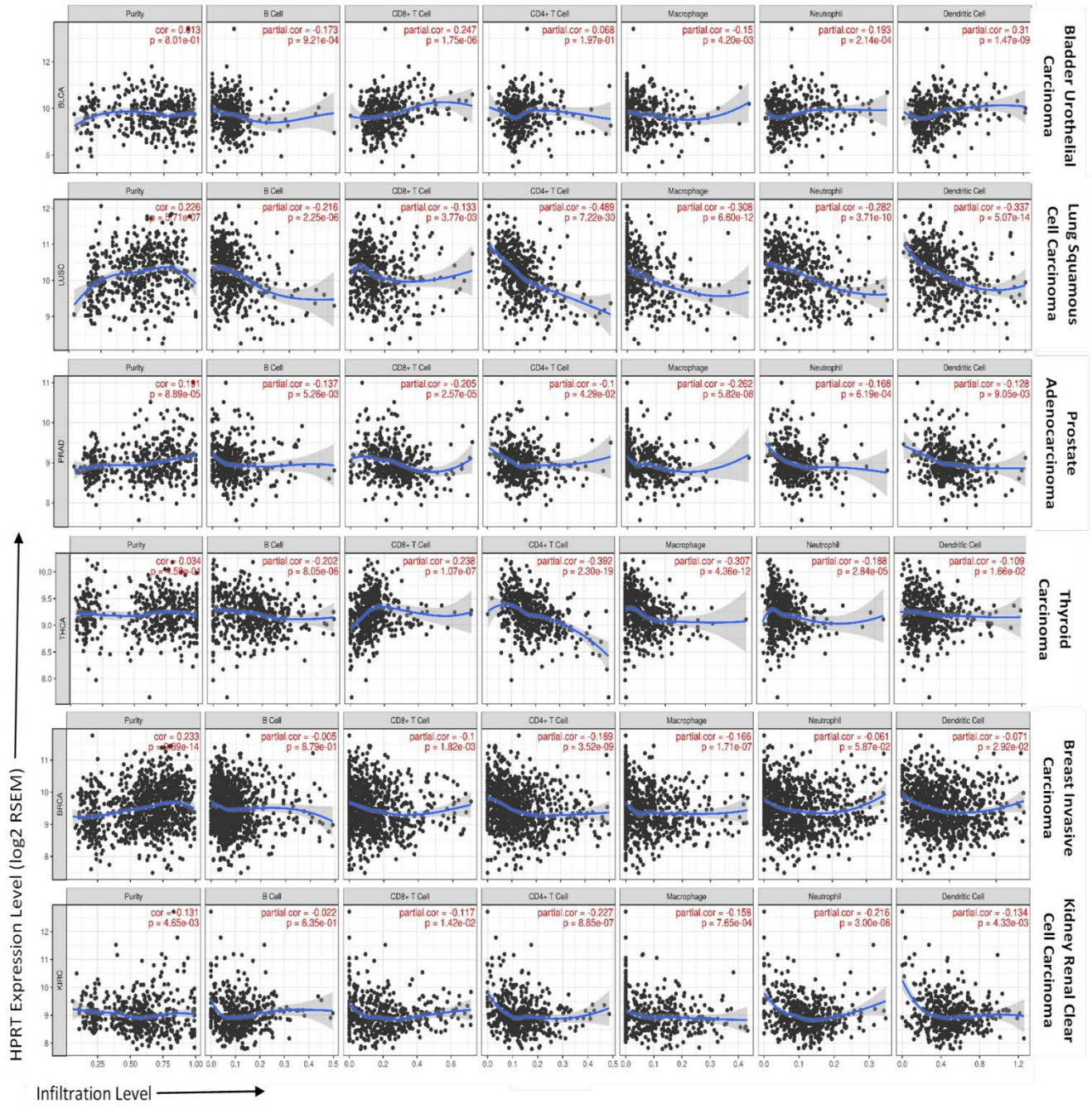

Figure A2-3. *Immune cell infiltration is decreased with high levels of HPRT.* HPRT expression levels is represented on the Y-axis and the infiltration level of B cells, CD8+ T cells, CD4+ T cells, macrophages, neutrophils, and dendritic cells is represented on the X-axis. Each cancer type is displayed on the right hand side. These data indicate that HPRT expression has a significant negative correlation with immune infiltration.

Table A2-2. *Immune cell infiltration according to cancer type and HPRT expression.*

	Purity		B Cell		CD8+ T Cell		CD4+ T Cells		Macrophage		Nuetrophil		Dendritic Cell	
Cancer Type	cor	*p*	cor	*p*	cor	*p*	cor	*p*	cor	*p*	cor	p	cor	*p*
ACC	0.12	0.29	-0.22	0.064	-0.18	0.13	-0.15	0.21	-0.38	$8.0x10^{-4}$	-0.24	0.04	-0.13	0.27
CESC	0.17	$4.4x10^{-3}$	-0.15	0.012	-0.10	0.14	-0.18	$2.2x10^{-3}$	-0.15	0.014	-0.04	0.55	-0.06	0.34
COAD	0.03	0.52	0.09	0.076	0.044	0.38	-0.30	$1.3x10^{-9}$	0.001	0.98	-0.05	0.28	-0.17	$5.5x10^{-4}$
DLBC	0.42	$6.1x10^{-3}$	-0.01	0.96	-0.09	0.76	-0.68	$6.9x10^{-4}$	0.16	0.48	-0.40	0.07	0.004	0.98
ESCA	0.18	0.02	-0.06	0.40	0.10	0.17	-0.12	0.11	0.06	0.46	-0.08	0.28	-0.06	0.42
GBM	-0.21	$1.5x10^{-5}$	-0.10	0.045	-0.12	0.02	-0.04	0.39	0.02	0.61	0.1	0.042	0.27	$3.2x10^{-8}$
HNSC	0.18	$7.0x10^{-7}$	-0.18	$6.8x10^{-5}$	0.12	0.01	-0.17	$1.8x10^{-4}$	-0.04	0.38	-0.12	$9.3x10^{-3}$	-0.15	$1.2x10^{-3}$
KICH	0.15	0.24	0.03	0.82	0.01	0.94	-0.08	0.54	0.04	0.77	-0.18	0.15	-0.23	0.064
KIRP	0.09	0.16	0.19	$2.3x10^{-3}$	0.32	$1.6x10^{-7}$	-0.17	$6.3x10^{-3}$	-0.04	0.54	-0.03	0.61	0.10	0.10
LIHC	0.17	$1.5x10^{-3}$	0.11	0.05	0.10	0.076	0.02	0.73	-0.01	0.82	-0.03	0.56	0.07	0.18
LUAD	-0.07	0.12	-0.07	0.14	0.1	0.028	-0.15	$8.5x10^{-4}$	-0.03	0.49	0.10	0.034	0.08	0.09
OV	-0.06	0.17	0.07	0.12	0.02	0.65	0.07	0.13	0.02	0.61	0.22	$1.7x10^{-6}$	0.16	$3.3x10^{-4}$
MESO	-0.08	0.46	0.08	0.48	0.11	0.33	0.21	0.051	0.048	0.66	-0.15	0.19	0.38	$3.7x10^{-4}$
PAAD	0.13	0.096	-0.21	$6.5x10^{-3}$	-0.22	$4.1x10^{-3}$	-0.34	$5.6x10^{-6}$	-0.39	$1.5x10^{-7}$	-0.38	$2.6x10^{-7}$	-0.34	$7.7x10^{-6}$
SKCM	-0.10	0.04	-0.04	0.47	0.14	$4.6x10^{-3}$	-0.19	$4.3x10^{-5}$	0.004	0.94	0.20	$1.4x10^{-5}$	-0.03	0.54
STAD	0.06	0.23	-0.19	$2.9x10^{-4}$	-0.008	0.87	-0.38	$6.4x10^{-14}$	-0.28	$3.7x10^{-8}$	0.004	0.95	-0.12	0.019
UCEC	-0.04	0.49	-0.03	0.62	0.12	0.047	-0.17	$4.5x10^{-3}$	-0.05	0.43	0.11	0.061	-0.008	0.89
UCS	-0.06	0.68	0.04	0.76	0.14	0.33	-0.12	0.40	-0.04	0.77	-0.01	0.93	0.074	0.60
BLCA	0.01	0.80	-0.17	$9.2x10^{-4}$	0.25	$1.8x10^{-6}$	0.07	0.20	-0.15	$4.2x10^{-3}$	0.19	$2.1x10^{-4}$	0.31	$1.5x10^{-9}$
LUSC	0.23	$5.7x10^{-7}$	-0.22	$2.3x10^{-6}$	-0.13	$3.8x10^{-3}$	-0.49	$7.2x10^{-30}$	-0.31	$6.1x10^{-12}$	-0.28	$3.7x10^{-10}$	-0.34	$5.1x10^{-12}$
PRAD	0.19	$8.9x10^{-5}$	-0.14	$5.3x10^{-3}$	-0.21	$2.6x10^{-5}$	-0.1	0.043	-0.26	$5.8x10^{-8}$	-0.17	$6.2x10^{-4}$	-0.13	$9.1x10^{-3}$
THCA	0.03	0.46	-0.20	$8.1x10^{-6}$	0.24	$1.1x10^{-7}$	-0.39	$2.3x10^{-19}$	-0.31	$4.4x10^{-12}$	-0.19	$2.8x10^{-5}$	-0.11	0.017
BRCA	0.23	$8.9x10^{-15}$	-0.01	0.88	-0.1	$1.8x10^{-3}$	-0.19	$3.5x10^{-9}$	-0.17	$1.7x10^{-7}$	-0.06	0.06	-0.07	0.03
KIRC	0.13	$4.7x10^{-3}$	-0.02	0.64	-0.12	0.014	-0.23	$8.9x10^{-7}$	-0.16	$7.7x10^{-4}$	-0.22	$3.0x10^{-6}$	-0.13	$4.3x10^{-3}$

Note. Green boxes indicate statistically significant correlations between immune cell infiltration and HPRT expression. Red boxes indicate samples with a negative correlation to HPRT expression.

Increased levels of HPRT correlate with decreased levels of costimulatory and coinhibitory molecules.

When evaluating the effect HPRT levels may have on immune activation, we found that elevated levels of the protein have a significant negative correlation to molecules involved in co-stimulation or co-inhibition. These results mirror those found in the initial evaluation of pro-inflammatory and anti-inflammatory cytokines. It appears that the increased expression of HPRT has a down-regulatory effect on all inflammatory molecules (Figure A2-5).

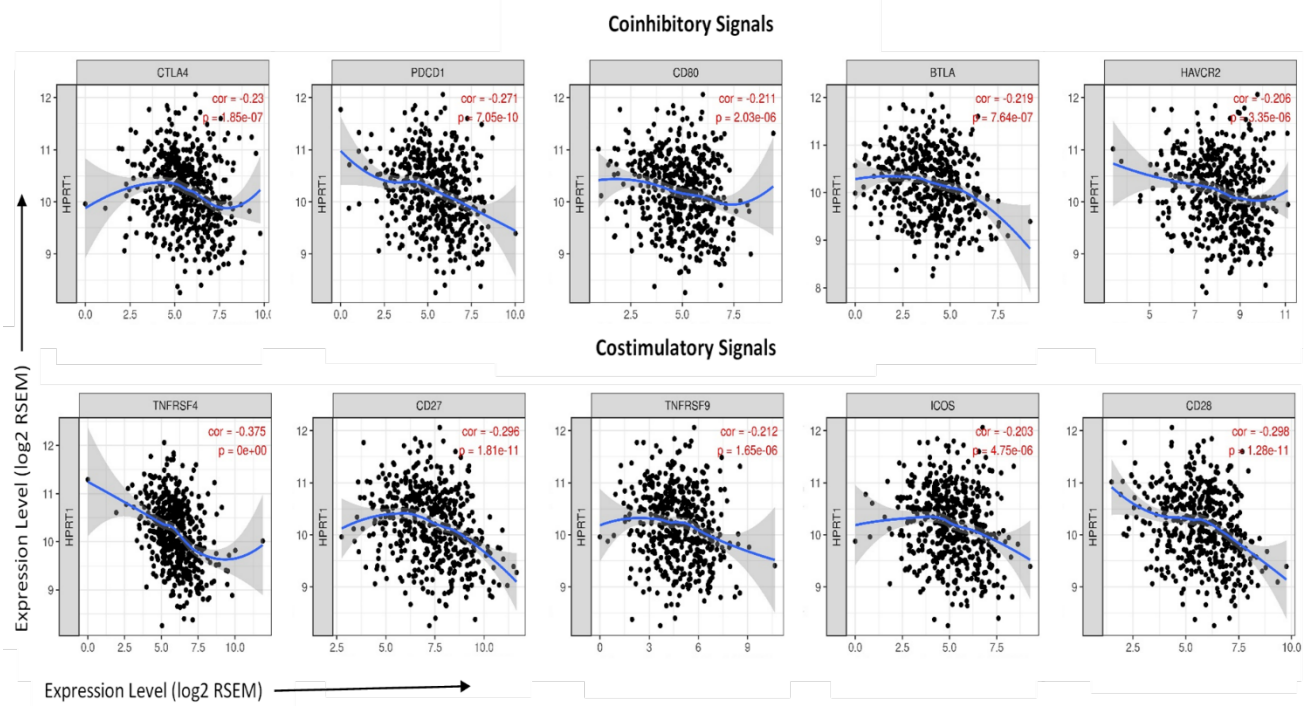

Figure A2-5. *Effects of high HPRT on coinhibitory and costimulatory signals*. The expression of HPRT was correlated to the expression of five coinhibitory molecules and five costimulatory molecules to determine relevance of HPRT expression in checkpoint immunotherapy. We found that HPRT had a statistically significant negative correlation to all molecules evaluated.

Guanosine has a significant impact on immune cell activation

When evaluating the impact on guanosine on immune cell activation, we found that guanosine significantly decreases the activation of Raji B cells. We found no significant change in activation in Jurkat T cells or THP-1 macrophages.

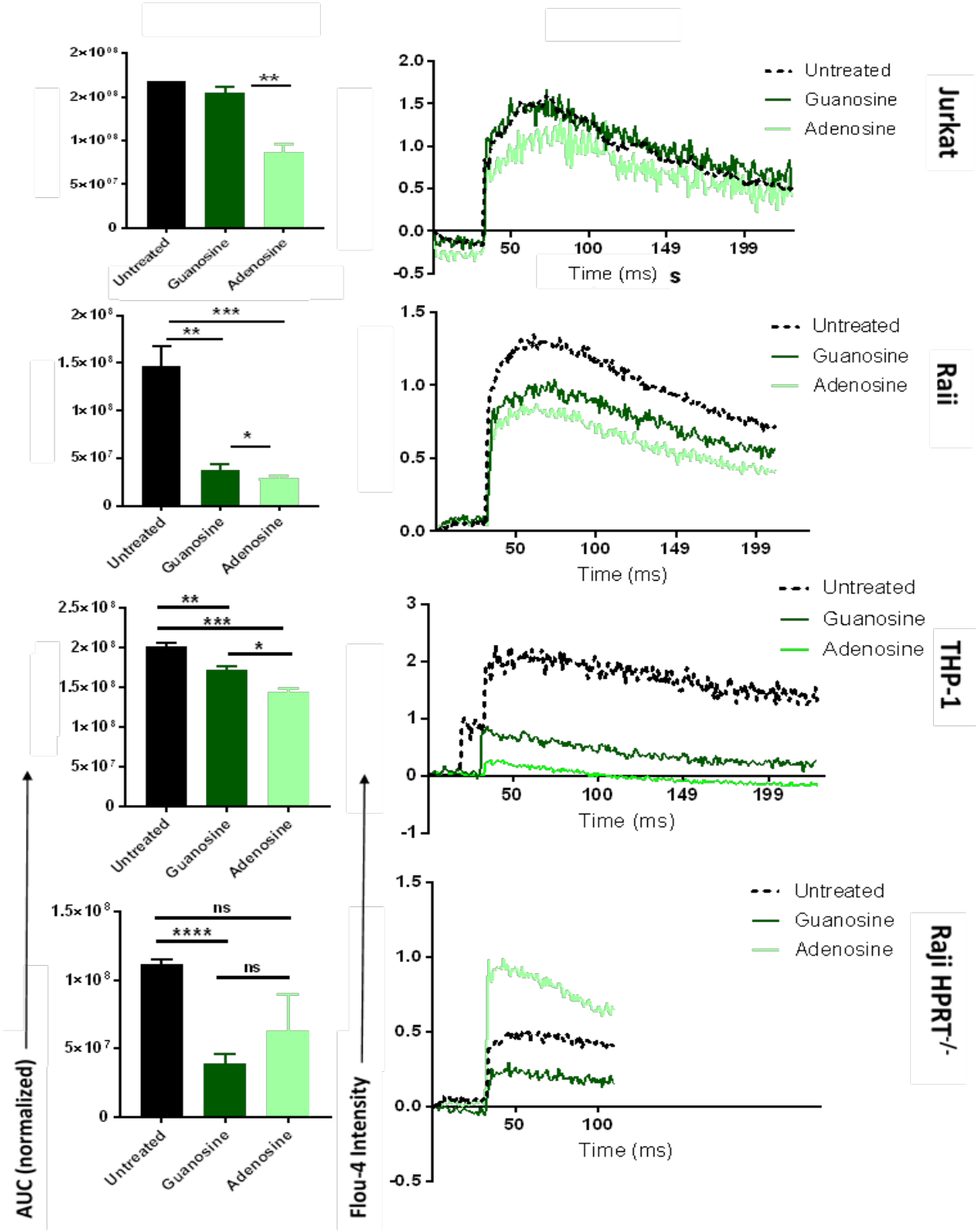

Figure A2-6. *Immune cell activation upon treatment with guanosine and adenosine*. Jurkat (T cells), Raji (B cells), THP-1 (macrophages), and a Raji HPRT knockdown were evaluated for their activation upon treatment with guanosine and adenosine. The normalized representation of the activation and the activation curve are shown for each respective cell type.

Conclusion

These data indicate that HPRT has a regulatory role in immune regulation in cancer cells that may stem back to the immuno-protective role it plays in the CNS to protect neurons from hypoxic and hypoglycemic conditions which are also common within the tumor microenvironment.

REFERENCES

1. Goodchild, J. Review of Their Synthesis and Properties. I, (1990).

2. Biochem, A. R., Kaziro, Y., Itoh, H., Kozasa, T. & Satoh, T. SIGNAL-TRANSDUCING STRlJCTURE AND FUNCTION OF GTP-BINDING PROTEINS. (1991).

3. Schneider, E. & Hunke, S. ATP-binding-cassette (ABC) transport systems : Functional and structural aspects of the ATP-hydrolyzing subunits / domains. 22, (1998).

4. Rajagopal, L., Vo, A., Silvestroni, A. & Rubens, C. E. Regulation of purine biosynthesis by a eukaryotic-type kinase in Streptococcus agalactiae. 56, 1329–1346 (2005).

5. Lane, A. N. & Fan, T. W. Regulation of mammalian nucleotide metabolism and biosynthesis. 1–20 (2015). doi:10.1093/nar/gkv047

6. Enzymatic, P. E. & Synthesis, P. N. A RTICLE. 3, 499–511 (2008).

7. Gross, A., Lewis, J. M. & George, M. Practical Synthesis of 5-Phospho-~-ribosyl. 7428–7435 (1983).

8. Tong, X., Zhao, F. & Thompson, C. B. The molecular determinants of de novo nucleotide biosynthesis in cancer cells. 32–37 (2009). doi:10.1016/j.gde.2009.01.002

9. Becerra, A. & Lazcano, A. THE ROLE OF GENE DUPLICATION IN THE EVOLUTION OF. 539–553 (1998).

10. Stout, J. T. & Caskey, C. T. Hprt: gene structure, expression, and mutation. (1985).

11. Caskey, C. T. & Kruh, G. D. The HPRT Locus Review. l, 1–9 (1979).

12. Wilson, J. M., Tarr, G. E. & Kelley, W. N. Human hypoxanthine (guanine)

phosphoribosyltransferase: an amino acid substitution in a mutant form of the enzyme isolated from a patient with gout. *Proc. Natl. Acad. Sci. U. S. A.* 80, 870–3 (1983).

13. Eads, J. C., Xu, Y. & Grubmeyer, C. The Crystal Structure with Bound GMP of Human Phosphoribosyltransferase. 78, 325–334 (1994).

14. Keough, D. T., Brereton, I. M., De Jersey, J. & Guddat, L. W. The crystal structure of free human hypoxanthine-guanine phosphoribosyltransferase reveals extensive conformational plasticity throughout the catalytic cycle. *J. Mol. Biol.* 351, 170–181 (2005).

15. Zhang, N. *et al.* Crystal structures of Apo and GMP bound hypoxanthine – guanine phosphoribosyltransferase from Legionella pneumophila and the implications in gouty arthritis. *J. Struct. Biol.* (2016). doi:10.1016/j.jsb.2016.03.007

16. Fuscoe, J. C., Fenwick, I. R. G., Ledbetter, I. D. H. & Caskey, C. T. Deletion and Amplification of the HGPRT Locus in Chinese Hamster Cells. 3, 1086–1096 (1983).

17. Wilson, J. M., Tarrt, G. E. & Kelley, W. N. Human hypoxanthine (guanine) phosphoribosyltransferase : An amino acid substitution in a mutant form of the enzyme isolated from a patient with gout. 80, 870–873 (1983).

18. Kim, S. H. *et al.* Nucleic Acids Research. 14, 3103–3118 (1986).

19. Melton, D. W., Mcewan, C., Reid, A. M. & Mckie, B. Expression of the Mouse HPRT Gene : Deletional Analysis of the Promoter Region of an X-Chromosome Linked Housekeeping Gene. 44, 319–328 (1986).

20. Caskey, C. T. In vitro translation of hypoxanthine / guamne phosphoribosyltrans- ferase mRNA : Characterization of a mouse neuroblastoma cell line that has elevated levels of

hypoxanthine / guanine phosphoribosyltransferase protein. 78, 6977–6980 (1981).

21. Zoref-shani, E., Frishberg, Y. & Bromberg, Y. Kelley-Seegmiller syndrome due to a unique variant of hypoxanthine-guanine phosphoribosyltransferase : reduced a ¤ nity for 5-phosphoribosyl-1-pyrophosphate manifested only at low , physiological substrate concentrations. 1500, 197–203 (2000).

22. Nyhan, W. L. & Diego, S. Lesch – Nyhan Syndrome. 1–6 (2012). doi:10.1002/9780470015902.a0001457.pub2

23. Kostalova, E., Pavelka, K., Vlaskova, H., Musalkova, D. & Stiburkova, B. Clinica Chimica Acta Corrigendum to " Hyperuricemia and gout due to de fi ciency of hypoxanthine – guanine phosphoribosyltransferase in female carriers : New insight to differential diagnosis ". *Clin. Chim. Acta* 447, 121 (2015).

24. Miller, A. D., Jollyt, D. J., Friedmannt, T. & Verma, I. M. A transmissible retrovirus expressing human hypoxanthine phosphoribosyltransferase (HPRT): Gene transfer into cells obtained from humans deficient in HPRT Biochemistry : 80, 4709–4713 (1983).

25. Rcas, J. O. M. A., Uño, A. N. S. B. & Eill, P. A. O. N. The Spectrum of Hypoxanthine-Guanine Phosphoribosyltransferase (HPRT) Deficiency Clinical Experience Based on 22 Patients from 18 Spanish Families. 80, 102–112 (2001).

26. Seegmiller, J. E., Rosenbloom, F. M. & Kelley, W. N. Enzyme Defect Associated with a Sex-Linked Human Neurological Disorder and Excessive Purine Synthesis. 155, 1682–1684 (2016).

27. Torres, R. J. & Puig, J. G. deficiency : Lesch-Nyhan syndrome. 10, 1–10 (2007).

28. Wilson, J. M. *et al.* A Molecular Survey of Hypoxanthine-Guanine Phosphoribosyltransferase Deficiency in Man. (1986).

29. Jagarlamudi, K. K., Hansson, L. O. & Eriksson, S. Breast and prostate cancer patients differ significantly in their serum Thymidine kinase 1 (TK1) specific activities compared with those hematological malignancies and blood donors : implications of using serum TK1 as a biomarker. 1–13 (2015). doi:10.1186/s12885-015-1073-8

30. Alegre, M. M. & Grose, J. Thymidine Kinase 1 : Diagnostic and Prognostic Significance in Malignancy. (2013).

31. Aufderklamm, S. *et al.* Thymidine kinase and cancer monitoring. *Cancer Lett.* 316, 6–10 (2012).

32. Li, H. X., Lei, D. S., Wang, X. Q., Skog, S. & He, Q. Serum thymidine kinase 1 is a prognostic and monitoring factor in patients with non-small cell lung cancer. *Oncol. Rep.* 13, 145–9 (2005).

33. O'Neill, K. L., Zhang, F., Li, H., Fuja, D. G. & Murray, B. K. Thymidine kinase 1 – A prognostic and diagnostic indicator in ALL and AML patients. *Leukemia* 21, 560–563 (2007).

34. He, Q. *et al.* The clinical significance of thymidine kinase 1 measurement in serum of breast cancer patients using anti-TK1 antibody. *Int. J. Biol. Markers* 15, 139–46

35. Nisman, B., Allweis, T., Kadouri, L., Hamburger, T. & Baras, M. Comparison of diagnostic and prognostic performance of two assays measuring thymidine kinase 1 activity in serum of breast cancer patients. 51, 439–447 (2013).

36. Carlsson, L., Larsson, A. & Lindman, H. Elevated levels of Thymidine kinase 1 peptide in serum from patients with breast cancer. *Ups. J. Med. Sci.* 114, 116–120 (2009).

37. Bolayirli, M. *et al.* Serum Thymidine Kinase 1 Activity in Solid Tumor (Breast and Colorectal Cancer) Patients Treated With Adjuvant. 226, 220–226 (2013).

38. Alegre, M. M. *et al.* Serum detection of thymidine kinase 1 as a means of early detection of lung cancer. *Anticancer Res.* 34, 2145–2152 (2014).

39. Zhang, F. *et al.* Thymidine kinase 1 immunoassay: a potential marker for breast cancer. *Cancer Detect. Prev.* 25, 8–15 (2001).

40. He, E. *et al.* Thymidine Kinase 1 is a Potential Marker for Prognosis and Monitoring the Response to Treatment of Patients with Breast, Lung, and Esophageal Cancer and Non-Hodgkin's Lymphoma. *Nucleosides, Nucleotides and Nucleic Acids* 29, 352–358 (2010).

41. Chang, Y.-J., Tseng, C.-Y., Lin, P.-Y., Chuang, Y.-C. & Chao, M.-W. Acute exposure to DEHP metabolite, MEHP cause genotoxicity, mutagenesis and carcinogenicity in mammalian Chinese hamster ovary cells. *Carcinogenesis* 38, 336–345 (2017).

42. Gobrecht, J., McDyre, C., Comotto, J. & Reynolds, M. Induction of cytotoxic and genotoxic damage following exposure of V79 cells to cadmium chloride. *Mutat. Res. Toxicol. Environ. Mutagen.* 816–817, 12–17 (2017).

43. Grist, S. a, McCarron, M., Kutlaca, a, Turner, D. R. & Morley, a a. In vivo human somatic mutation: frequency and spectrum with age. *Mutat. Res.* 266, 189–196 (1992).

44. Hirota, H., Kubota, M., Hashimoto, H., Adachi, S. & Mikawa, H. Analysis of hprt gene mutation following anti-cancer treatment in pediatric patients with acute leukemia Haruyo

Hirota a , Masaru Kubota a , Hisako Hashimoto a , Souichi Adachi a , Kousaku Matsubara a , Katsuji Kuwakado a , Yuichi Akiyama a , Tsutomu Tsut. 319, 113–120 (1993).

45. Robinson, D. R. *et al.* An analysis of in vivo hprt mutant frequency in circulating T-lymphocytes in the normal human population : a comparison of four datasets. 313, 227–247 (1994).

46. Enumeration of 6-thioguanine-resistant peripheral blood lymphocytes in man as a potential test for somatic cell mutations arising in vivo. *Mutat. Res. Mol. Mech. Mutagen.* 61, 353–379 (1979).

47. Albertini, R. J., Castle, K. L. & Borcherding, W. R. T-cell cloning to detect the mutant 6-thioguanine-resistant lymphocytes present in human peripheral blood. *Proc. Natl. Acad. Sci. U. S. A.* 79, 6617–21 (1982).

48. Compton, P. J. E., Hooper, K. & Smith, M. T. Human somatic mutation assays as biomarkers of carcinogenesis. *Environ. Health Perspect.* 94, 135–141 (1991).

49. Albertini, R. J. HPRT mutations in humans: Biomarkers for mechanistic studies. *Mutat. Res. - Rev. Mutat. Res.* 489, 1–16 (2001).

50. Hou, S., Yang, K., Nyberg, F., Hemminki, K. & Lambert, B. Hprt mutant frequency and aromatic DNA adduct level in non-smoking and smoking lung cancer patients and population controls. 20, 437–444 (1999).

51. Vacek, P. M. & Albertini, R. J. M e a s u r e m e n t of H P R T mutant frequencies in T-lymphocytes from healthy human populations R . F . Branda a , L . M . Sullivan a j . p . O ' Neill a M . T . Falta a , J . A . Nicklas a B . Hirsch c ,. 285, 267–279 (1993).

52. Sawada, M. *et al.* Prospective study of mutant frequencies at the hprt and T-cell receptor gene loci in pediatric cancer patients during chemotherapy. *Cancer Epidemiol Biomarkers* 7, 711–717 (1998).

53. Sawada, M., Kubota, M., Lin, Y. & Watanabe, K. Evaluation of mutant frequencies at the hprt and the T-cell receptor loci in pediatric cancer patients before treatment. (1998).

54. Branda, R. F., O'Neill, J. P., Jacobson-Kram, D. & Albertini, R. J. Factors influencing mutation at the hprt locus in T-lymphocytes: studies in normal women and women with benign and malignant breast masses. *Env. Mol Mutagen* 19, 274–281 (1992).

55. Cheng, T. *et al.* Mutant frequency at the hprt locus in human lymphocytes in a case-control study of lung cancer. 332, (1995).

56. Duthie, S. J. & Collins, R. The influence of smoking and diet on the hypoxanthine phosphoribosyltransferase mutant frequency in circulating T lymphocytes from a normal human population. 5107, (1995).

57. Hakoda, M., Akiyama, M., Kyoizumi, S. & Awa, A. A. Increased somatic cell mutant frequency in atomic bomb survivors. 201, 39–48 (1988).

58. Tates, A. D., Dam, F. J. Van, Natarajan, A. T., Zwinderman, A. H. & Osanto, S. Frequencies of HPRT mutants and micronuclei in lymphocytes of cancer patients under chemotherapy : a prospective study. 307, 293–306 (1994).

59. Glaab, W. E. & Tindall, K. R. Mutation rate at the hprt locus in human cancer cell lines with specific mismatch repair-gene defects. 18, 1–8 (1997).

60. Homey, B. *et al.* Involvement of chemokine receptors in breast cancer metastasis. *Nature*

410, 50–56 (2001).

61. Townsend, M. H. *et al.* Elevated Expression of Hypoxanthine Guanine Phosphoribosyltransferase within Malignant Tissue. *Cancer Clin. Oncol.* 6, 19 (2017).

62. Townsend, M. H. *et al.* Non-small-cell lung cancer cell lines A549 and NCI-H460 express hypoxanthine guanine phosphoribosyltransferase on the plasma membrane. *Onco. Targets. Ther.* 10, 1921–1932 (2017).

63. Pennock, N. D. *et al.* T cell responses: naive to memory and everything in between. *Adv. Physiol. Educ.* 37, 273–83 (2013).

64. Cohen, I. J. & Blasberg, R. Impact of the Tumor Microenvironment on Tumor-Infiltrating Lymphocytes: Focus on Breast Cancer. *Breast Cancer Basic Clin. Res.* 11, (2017).

65. Riberdy, J. M., Mostaghel, E. & Doyle, C. Coevolution of TCR-MHC interactions: Conserved MHC tertiary structure is not sufficient for interactions with the TCR. *Proc. Natl. Acad. Sci. U. S. A.* 95, 4493–8 (1998).

66. Gross, G., Waks, T. & Eshhar, Z. Expression of immunoglobulin-T-cell receptor chimeric molecules as functional receptors with antibody-type specificity. *Proc. Natl. Acad. Sci.* 86, 10024–10028 (1989).

67. Kloss, C., Lee, J. & June, C. 638. TGFBeta Signaling Blockade within PSMA Targeted CAR Human T Cells for the Eradication of Metastatic Prostate Cancer. *Mol. Ther.* 24, S252–S253 (2016).

68. Kochenderfer, J. N. *et al.* cytokine-associated toxicity in a clinical trial of anti-CD19 Plenary paper B-cell depletion and remissions of malignancy along with cytokine-

associated toxicity in a clinical trial of anti-CD19 chimeric-antigen-receptor – transduced T cells. 119, 2709–2720 (2012).

69. Kochenderfer, J. N. *et al.* Chemotherapy-refractory diffuse large B-cell lymphoma and indolent B-cell malignancies can be effectively treated with autologous T cells expressing an anti-CD19 chimeric antigen receptor. *J. Clin. Oncol.* 33, 540–549 (2015).

70. Hay, K. A. & Turtle, C. J. Chimeric Antigen Receptor (CAR) T Cells: Lessons Learned from Targeting of CD19 in B-Cell Malignancies. *Drugs* 77, 237–245 (2017).

71. Ruella, M. & Maus, M. V. Catch me if you can: Leukemia Escape after CD19-Directed T Cell Immunotherapies. *Comput. Struct. Biotechnol. J.* 14, 357–362 (2016).

72. Jackson, H. & Brentjens, R. Overcoming antigen escape with CART-cell therapy. 27, 138–144 (2016).

73. Lai, X. *et al.* CD19 Epitope Escape after 4SCAR19 T Cell Therapy Resulted in Re-Establishment of Chemo-Sensitivity in Adult B-Cell Acute Lymphocytic Leukemia Patients. *Blood* 128, (2016).

74. Su, W. *et al.* Immunohistochemical analysis of human CD5 positive B cells : mantle cells and mantle cell lymphoma are not equivalent in terms of CD5 expression Short reports Immunohistochemical analysis of human CD5 positive B cells : mantle cells and mantle cell lympho. 395–397 (2000). doi:10.1136/jcp.53.5.395

75. Doronin, I. I. *et al.* T-cell modulatory properties of CD5 and its role in antitumor immune responses. *Leukemia* 9, 865–877 (2007).

76. Filipovich, A. H. *et al.* T cell depletion with anti-CD5 immunotoxin in histocompatible

bone marrow transplantation. The correlation between residual CD5 negative T cells and subsequent graft-versus-host disease. *Transplantation* 50, 410–5 (1990).

77. Gasanov, S. E., Rael, E. D., Gasanov, N. E. & Vernon, L. P. In vitro evaluation of Pyrularia thionin-anti-CD5 immunotoxin. *Cancer Immunol. Immunother.* 41, 122–128 (1995).

78. Antin, J. H. *et al.* Selective depletion of bone marrow T lymphocytes with anti-CD5 monoclonal antibodies: effective prophylaxis for graft-versus-host disease in patients with hematologic malignancies. *Blood* 78, 2139–49 (1991).

79. Hertler, A. A. *et al.* An anti-CD5 immunotoxin for chronic lymphocytic leukemia: Enhancement of cytotoxicity with human serum albumin-monensin. *Int. J. Cancer* 43, 215–219 (1989).

80. Ravel, S., Colombatti, M. & Casellas, P. Internalization and intracellular fate of anti-CD5 monoclonal antibody and anti-CD5 ricin A-chain immunotoxin in human leukemic T cells. *Blood* 79, 1511–1517 (1992).

81. Manske, J. M., Buchsbaum, D. J. & Vallera, D. A. The role of ricin B chain in the intracellular trafficking of anti-CD5 immunotoxins. *J Immunol* 142, 1755–1766 (1989).

82. Vallera, D. A., Manske, J. M., Buchsbaum, J., Azemove, S. M. & Hanna, D. E. Antigenic modulation by anti-CD5 Information about subscribing to The Journal of Immunology is online at : ANTIGENIC MODULATION BY ANTI-CD5 IMMUNOTOXINS '. (2018).

83. Mamonkin, M., Rouce, R. H., Tashiro, H. & Brenner, M. K. IMMUNOBIOLOGY A T-cell – directed chimeric antigen receptor for the selective treatment of T-cell malignancies.

Blood 126, 983–993 (2015).

84. Chen, K. H. *et al.* Preclinical targeting of aggressive T-cell malignancies using anti-CD5 chimeric antigen receptor. *Leukemia* 31, 2151–2160 (2017).

85. Macdonald, K. P. a *et al.* Characterization of human blood dendritic cell subsets. *Cell* 100, 4512–4520 (2002).

86. Muñoz, L. *et al.* Interleukin-3 receptor alpha chain (CD123) is widely expressed in hematologic malignancies. *Haematologica* 86, 1261–9 (2001).

87. Shao, H. *et al.* Development and validation of diagnostic criteria. *Leuk. Res.* 37, 1–9 (2013).

88. Testa, U. *et al.* associated with enhanced blast proliferation , increased cellularity , and Elevated expression of IL-3R ␣ in acute myelogenous leukemia is associated with enhanced blast proliferation , increased cellularity , and poor prognosis. 100, 2980–2988 (2011).

89. Jordan, C. T. *et al.* The interleukin-3 receptor alpha chain is a unique marker for human acute myelogenous leukemia stem cells. *Leukemia* 14, 1777–84 (2000).

90. Testa, U., Pelosi, E. & Frankel, A. CD 123 is a membrane biomarker and a therapeutic target in hematologic malignancies. *Biomark. Res.* 2, 4 (2014).

91. Testa, U. *et al.* Expression of growth factor receptors in unilineage differentiation culture of purified hematopoietic progenitors. *Blood* 88, 3391–406 (1996).

92. Mardiros, A. & Santos, C. Dos. T cells expressing CD123-specific chimeric antigen

receptors exhibit specific cytolytic effector functions and antitumor effects against human acute myeloid leukemia. *Blood* 122, 3138–3148 (2013).

93. Kim, E. *et al.* HHS Public Access. 27, 617–630 (2016).

94. Fan, M. *et al.* Chimeric antigen receptors for adoptive T cell therapy in acute myeloid leukemia. *J. Hematol. Oncol.* 10, 151 (2017).

95. Tettamanti, S., Biondi, A., Biagi, E. & Bonnet, D. CD123 AML targeting by chimeric antigen receptors: A novel magic bullet for AML therapeutics? *Oncoimmunology* 3, (2014).

96. Luo, Y. *et al.* First-in-Man CD123-Specific Chimeric Antigen Receptor-Modified T Cells for the Treatment of Refractory Acute Myeloid Leukemia. *Blood* 126, (2015).

97. Gill, S. *et al.* Preclinical targeting of human acute myeloid leukemia and myeloablation using chimeric antigen receptor – modi fi ed T cells. *Blood* 123, 2343–2354 (2014).

98. Walter, R. B. *et al.* Brief report CD33 expression and P-glycoprotein – mediated drug efflux inversely correlate and predict clinical outcome in patients with acute myeloid leukemia treated with gemtuzumab ozogamicin monotherapy. *Response* 109, 4168–4170 (2007).

99. Griffin, J. D., Linch, D., Sabbath, K., Larcom, P. & Schlossman, S. F. A monoclonal antibody reactive with normal and leukemic human myeloid progenitor cells. *Leuk. Res.* 8, 521–34 (1984).

100. Dinndorf, P. *et al.* Expression of Normal Myeloid-Associated Antigens by Acute Leukemia Cells. 67, 1048–1053 (2016).

101. Schwonzen, M., Diehl, V., Dellanna, M. & Staib, P. Immunophenotyping of surface antigens in acute myeloid leukemia by flow cytometry after red blood cell lysis. *Leuk. Res.* 31, 113–116 (2007).

102. Hoyer, J. D., Grogg, K. L., Hanson, C. A., Gamez, J. D. & Dogan, A. CD33 detection by immunohistochemistry in paraffin-embedded tissues: A new antibody shows excellent specificity and sensitivity for cells of myelomonocytic lineage. *Am. J. Clin. Pathol.* 129, 316–323 (2008).

103. Dutta, S. & Saxena, R. The expression pattern of CD33 antigen can differentiate leukemic from normal progenitor cells in acute myeloid leukemia. *Indian J. Hematol. Blood Transfus.* 30, 130–134 (2014).

104. de Propris, M. S. *et al.* High CD33 expression levels in acute myeloid leukemia cells carrying the nucleophosmin (NPM1) mutation. *Haematologica* 96, 1548–1551 (2011).

105. Sievers, E. L. Efficacy and safety of gemtuzumab ozogamicin in patients with CD33-positive acute myeloid leukaemia in first relapse. *Expert Opin. Biol. Ther.* 1, 893–901 (2001).

106. Rafiq, S., Purdon, T. J., Schultz, L. M. & Brentjens, R. J. CD33-Directed Chimeric Antigen Receptor (CAR) T Cells for the Treatment of Acute Myeloid Leukemia (AML). *Blood* 128, (2016).

107. Shaffer, D. R. *et al.* T cells redirected against CD70 for the immunotherapy of CD70-positive malignancies. *Blood* 117, 4304–4314 (2011).

108. Bowman, M. R. *et al.* The cloning of CD70 and its identification as the ligand for CD27.

J. Immunol. 152, 1756–61 (1994).

109. Hintzen, R. Q. *et al.* Characterization of the human CD27 ligand, a novel member of the TNF gene family. *J. Immunol.* 152, 1762–73 (1994).

110. McEarchern, J. A. *et al.* Preclinical characterization of SGN-70, a humanized antibody directed against CD70. *Clin. Cancer Res.* 14, 7763–7772 (2008).

111. Baba, M. *et al.* Highly enhanced expression of CD70 on human T-lymphotropic virus type 1-carrying T-cell lines and adult T-cell leukemia cells. *J. Virol.* 82, 3843–3852 (2008).

112. Centre, A. M. Aberrant expression and reverse signalling of CD70 on malignant B cells. (1999).

113. Hunter, Z. R. *et al.* High Levels of Soluble Immunoregulatory Receptors in Patients with WaldenströM's Macroglobulinemia. *Blood* 104, (2004).

114. Agathanggelou, A. *et al.* Expression of Immune Regulatory Molecules in Epstein-Barr Virus-Associated Nasopharyngeal Carcinomas with Prominent Lymphoid Stroma Evidence for a Functional Interaction between Epithelial Tumor Cells and Infiltrating Lymphoid Cells. *Am. J. Pathol.* 147, (1995).

115. Jin, L. *et al.* CD70, a novel target of CAR T-cell therapy for gliomas. *Neuro. Oncol.* 20, 55–65 (2018).

116. Miller, J. *et al.* Soluble CD70: a novel immunotherapeutic agent for experimental glioblastoma. *J. Neurosurg.* 113, 280–285 (2010).

117. Ge, H. *et al.* Tumor associated CD70 expression is involved in promoting tumor migration and macrophage infiltration in GBM. *Int. J. Cancer* 141, 1434–1444 (2017).

118. Wischhusen, J. *et al.* Identification of CD70-mediated apoptosis of immune effector cells as a novel immune escape pathway of human glioblastoma. *Cancer Res* 62, 2592–2599 (2002).

119. Petrau, C. *et al.* CD70: A potential target in breast cancer? *J. Cancer* 5, 761–764 (2014).

120. Jacobs, J. *et al.* CD70: An emerging target in cancer immunotherapy. *Pharmacol. Ther.* 155, 1–10 (2015).

121. Adam, P. J. *et al.* CD70 (TNFSF7) is expressed at high prevalence in renal cell carcinomas and is rapidly internalised on antibody binding. *Br. J. Cancer* 95, 298–306 (2006).

122. Jilaveanu, L. B. *et al.* CD70 expression patterns in renal cell carcinoma. *Hum Pathol* 43, 1394–1399 (2012).

123. JUNKER, K. *et al.* CD70: A NEW TUMOR SPECIFIC BIOMARKER FOR RENAL CELL CARCINOMA. *J. Urol.* 173, 2150–2153 (2005).

124. Ryan, M. C. *et al.* Targeting pancreatic and ovarian carcinomas using the auristatin-based anti-CD70 antibody-drug conjugate SGN-75. *Br. J. Cancer* 103, 676–684 (2010).

125. American Association for Cancer Research., S. *et al. Cancer research : the official organ of the American Association for Cancer Research, Inc. Cancer Research* 68, (Waverly Press, 2008).

126. Aggarwal, S. *et al.* Immune modulator CD70 as a potential cisplatin resistance predictive marker in ovarian cancer. *Gynecol. Oncol.* 115, 430–437 (2009).

127. Wajant, H. Therapeutic targeting of CD70 and CD27. *Expert Opin. Ther. Targets* 20,

959–973 (2016).

128. Nolte, M. A., van Olffen, R. W., van Gisbergen, K. P. J. M. & van Lier, R. A. W. Timing and tuning of CD27-CD70 interactions: the impact of signal strength in setting the balance between adaptive responses and immunopathology. *Immunol. Rev.* 229, 216–231 (2009).

129. Hendriks, J. *et al.* CD27 is required for generation and long-term maintenance of T cell immunity. *Nat. Immunol.* 1, 433–440 (2000).

130. Mcearchern, J. A. *et al.* Engineered anti-CD70 antibody with multiple effector functions exhibits in vitro and in vivo antitumor activities Engineered anti-CD70 antibody with multiple effector functions exhibits in vitro and in vivo antitumor activities. 109, 1185–1192 (2012).

131. Israel, B. F. *et al.* Anti-CD70 antibodies: a potential treatment for EBV+ CD70-expressing lymphomas. *Mol. Cancer Ther.* 4, 2037–44 (2005).

132. Lokhorst, H. M. *et al.* Targeting CD38 with Daratumumab Monotherapy in Multiple Myeloma. *N. Engl. J. Med.* 373, 1207–1219 (2015).

133. Deaglio, S. *et al.* CD38 / CD19 : a lipid raft – dependent signaling complex in human B cells. *Blood* 109, 5390–5398 (2007).

134. Konopleva, M., Estrov, Z., Zhao, S., Andreeff, M. & Mehta, K. Ligation of cell surface CD38 protein with agonistic monoclonal antibody induces a cell growth signal in myeloid leukemia cells. *J. Immunol.* 161, 4702–8 (1998).

135. Santonocito, A. M. *et al.* Flow cytometric detection of aneuploid CD38(++) plasmacells and CD19(+) B-lymphocytes in bone marrow, peripheral blood and PBSC harvest in

multiple myeloma patients. *Leuk. Res.* 28, 469–77 (2004).

136. Vences-Catalán, F. & Santos-Argumedo, L. CD38 through the life of a murine B lymphocyte. *IUBMB Life* 63, 840–846 (2011).

137. Dimopoulos, M. A. *et al.* Daratumumab, Lenalidomide, and Dexamethasone for Multiple Myeloma. *N. Engl. J. Med.* 375, 1319–1331 (2016).

138. Mihara, K. *et al.* T cells bearing anti-CD19 and/or anti-CD38 chimeric antigen receptors effectively abrogate primary double-hit lymphoma cells. *J. Hematol. Oncol.* 10, 1–4 (2017).

139. Carpenter, R. O. *et al.* B-cell maturation antigen is a promising target for adoptive T-cell therapy of multiple myeloma. *Clin. Cancer Res.* 19, 2048–2060 (2013).

140. Tai, Y.-T. & Anderson, K. C. Targeting B-cell maturation antigen in multiple myeloma. *Immunotherapy* 7, 1187–1199 (2015).

141. Lin, L. *et al.* CD8+ Anti-BCMA mRNA CAR T-Cells Effectively Kill Human Multiple Myeloma Cells In Vitro and In Vivo. *Blood* 130, (2017).

142. Ali, S. A. *et al.* T cells expressing an anti-B-cell maturation antigen chimeric antigen receptor cause remissions of multiple myeloma. *Blood* 128, 1688–700 (2016).

143. Cohen, A. D. *et al.* B-Cell Maturation Antigen (BCMA)-Specific Chimeric Antigen Receptor T Cells (CART-BCMA) for Multiple Myeloma (MM): Initial Safety and Efficacy from a Phase I Study. *Blood* 128, (2016).

144. Hassan, R. *et al.* Mesothelin Immunotherapy for Cancer: Ready for Prime Time? *J. Clin. Oncol.* 34, 4171–4179 (2016).

145. Hassan, R., Bera, T. & Pastan, I. Mesothelin: A New Target for Immunotherapy. *Clin. Cancer Res.* 10, 3937–3942 (2004).

146. Hassan, R. *et al.* Detection and Quantitation of Serum Mesothelin, a Tumor Marker for Patients with Mesothelioma and Ovarian Cancer. *Clin. Cancer Res.* 12, 447–453 (2006).

147. Kachala, S. S. *et al.* Mesothelin overexpression is a marker of tumor aggressiveness and is associated with reduced recurrence-free and overall survival in early-stage lung adenocarcinoma. *Clin. Cancer Res.* 20, 1020–8 (2014).

148. Ho, M. *et al.* Mesothelin expression in human lung cancer. *Clin. Cancer Res.* 13, 1571–5 (2007).

149. Tchou, J. *et al.* Mesothelin, a novel immunotherapy target for triple negative breast cancer. *Breast Cancer Res. Treat.* 133, 799–804 (2012).

150. Hassan, R., Bera, T. & Pastan, I. Mesothelin: A New Target for Immunotherapy. *Clin. Cancer Res.* 10, 3937–3942 (2004).

151. Rizk, N. P. *et al.* Tissue and serum mesothelin are potential markers of neoplastic progression in Barrett's associated esophageal adenocarcinoma. *Cancer Epidemiol. Biomarkers Prev.* 21, 482–6 (2012).

152. Einama, T. *et al.* Luminal membrane expression of mesothelin is a prominent poor prognostic factor for gastric cancer. *Br. J. Cancer* 107, 137–142 (2012).

153. Argani, P. *et al.* Mesothelin is overexpressed in the vast majority of ductal adenocarcinomas of the pancreas: identification of a new pancreatic cancer marker by serial analysis of gene expression (SAGE). *Clin. Cancer Res.* 7, 3862–8 (2001).

154. Lamberts, L. E., de Groot, D. J. A., Bense, R. D., de Vries, E. G. E. & Fehrmann, R. S. N. Functional genomic mRNA profiling of a large cancer data base demonstrates mesothelin overexpression in a broad range of tumor types. *Oncotarget* 6, 28164–72 (2015).

155. Bera, T. K. & Pastan, I. Mesothelin is not required for normal mouse development or reproduction. *Mol. Cell. Biol.* 20, 2902–6 (2000).

156. Morello, A., Sadelain, M. & Adusumilli, P. S. Mesothelin-targeted CARs: Driving T cells to solid Tumors. *Cancer Discov.* 6, 133–146 (2016).

157. Hassan, R. *et al.* Mesothelin Immunotherapy for Cancer: Ready for Prime Time? *J. Clin. Oncol.* 34, 4171–4179 (2016).

158. Kachala, S. S. *et al.* Mesothelin overexpression is a marker of tumor aggressiveness and is associated with reduced recurrence-free and overall survival in early-stage lung adenocarcinoma. *Clin. Cancer Res.* 20, 1020–8 (2014).

159. Nellan, A. *et al.* Durable regression of Medulloblastoma after regional and intravenous delivery of anti-HER2 chimeric antigen receptor T cells. *J. Immunother. cancer* 6, 30 (2018).

160. Yarden, Y. & Sliwkowski, M. X. Untangling the ErbB signalling network. *Nat. Rev. Mol. Cell Biol.* 2, 127–137 (2001).

161. Yan, M. *et al.* HER2 expression status in diverse cancers: review of results from 37,992 patients. *Cancer Metastasis Rev.* 34, 157–64 (2015).

162. Zhu, X., Chi, F., Wu, R., Jin, X. & Jiang, M. HER2 induces cell proliferation and invasion of non-small-cell lung cancer by upregulating COX-2 expression via MEK/ERK signaling

pathway. *Onco. Targets. Ther.* 9, 2709 (2016).

163. Wright, C. *et al.* Relationship between c-erbB-2 protein product expression and response to endocrine therapy in advanced breast cancer. *Br. J. Cancer* 65, 118–21 (1992).

164. Kumar, R., Mandal, M., Lipton, A., Harvey, H. & Thompson, C. B. Overexpression of HER2 modulates bcl-2, bcl-XL, and tamoxifen-induced apoptosis in human MCF-7 breast cancer cells. *Clin. Cancer Res.* 2, 1215–9 (1996).

165. Omabe, M. *et al.* HER2-Specific Vaccines for HER2-Positive Breast Cancer Immunotherapy. *World J. Vaccines* 05, 106–128 (2015).

166. Al-Awadhi, A., Lee Murray, J. & Ibrahim, N. K. Developing anti-HER2 vaccines: Breast cancer experience. *Int. J. Cancer* (2018). doi:10.1002/ijc.31551

167. Perez, E. A. *et al.* Trastuzumab Plus Adjuvant Chemotherapy for Human Epidermal Growth Factor Receptor 2–Positive Breast Cancer: Planned Joint Analysis of Overall Survival From NSABP B-31 and NCCTG N9831. *J. Clin. Oncol.* 32, 3744–3752 (2014).

168. Han, Y. *et al.* Antitumor effects and persistence of a novel HER2 CAR T cells directed to gastric cancer in preclinical models. *Am. J. Cancer Res.* 8, 106–119 (2018).

169. Priceman, S. J. *et al.* Regional Delivery of Chimeric Antigen Receptor–Engineered T Cells Effectively Targets HER2 $^{+}$ Breast Cancer Metastasis to the Brain. *Clin. Cancer Res.* 24, 95–105 (2018).

170. Nellan, A. *et al.* Durable regression of Medulloblastoma after regional and intravenous delivery of anti-HER2 chimeric antigen receptor T cells. *J. Immunother. cancer* 6, 30 (2018).

171. Feng, K. *et al.* Phase I study of chimeric antigen receptor modified T cells in treating HER2-positive advanced biliary tract cancers and pancreatic cancers. *Protein Cell* (2017). doi:10.1007/s13238-017-0440-4

172. Ahmed, N. *et al.* HER2-Specific Chimeric Antigen Receptor–Modified Virus-Specific T Cells for Progressive Glioblastoma. *JAMA Oncol.* 3, 1094 (2017).

173. Ahmed, N. *et al.* Human Epidermal Growth Factor Receptor 2 (HER2) –Specific Chimeric Antigen Receptor–Modified T Cells for the Immunotherapy of HER2-Positive Sarcoma. *J. Clin. Oncol.* 33, 1688–1696 (2015).

174. Cahan, L. D., Irie, R. F., Singh, R., Cassidenti, A. & Paulson, J. C. Identification of a human neuroectodermal tumor antigen (OFA-I-2) as ganglioside GD2. *Proc. Natl. Acad. Sci.* 79, 7629–7633 (1982).

175. Tivnan, A. *et al.* Anti-GD2-ch14.18/CHO coated nanoparticles mediate glioblastoma (GBM)-specific delivery of the aromatase inhibitor, Letrozole, reducing proliferation, migration and chemoresistance in patient-derived GBM tumor cells. *Oncotarget* 8, 16605–16620 (2017).

176. Alvarez-Rueda, N. *et al.* A monoclonal antibody to O-Acetyl-GD2 ganglioside and not to GD2 shows potent anti-tumor activity without peripheral nervous system cross-reactivity. *PLoS One* 6, 1–12 (2011).

177. Yuki, N., Yamada, M., Tagawa, Y., Takahashi, H. & Handa, S. Pathogenesis of the neurotoxicity caused by anti-GD2 antibody therapy. *J. Neurol. Sci.* 149, 127–30 (1997).

178. Schulz, G. *et al.* Detection of Ganglioside G D2 in Tumor Tissues and Sera of

Neuroblastoma Patients Detection of Ganglioside GD2in Tumor Tissues and Sera of Neuroblastoma. 44, 5914–5920 (1984).

179. Newick, K., Moon, E. & Albelda, S. M. Chimeric antigen receptor T-cell therapy for solid tumors. *Mol. Ther. - Oncolytics* 3, 16006 (2016).

180. Long, A. H. *et al.* 4-1BB costimulation ameliorates T cell exhaustion induced by tonic signaling of chimeric antigen receptors. *Nat. Med.* 21, 581–90 (2015).

181. Pule, M. A. *et al.* NIH Public Access. *Nat. Med.* 14, 1264–1270 (2008).

182. Louis, C. U. *et al.* Antitumor activity and long-term fate of chimeric antigen receptor–positive T cells in patients with neuroblastoma. *Mol. Ther. J. Am. Soc. Gene Ther.* 14, 1324–1334 (2011).

183. Ploessl, C., Pan, A., Maples, K. T. & Lowe, D. K. Dinutuximab. *Ann. Pharmacother.* 50, 416–422 (2016).

184. Raffaghello, L. *et al.* Anti-GD2 monoclonal antibody immunotherapy: a promising strategy in the prevention of neuroblastoma relapse. *Cancer Lett.* 197, 205–9 (2003).

185. Ahmed, M. & Cheung, N.-K. V. Engineering anti-GD2 monoclonal antibodies for cancer immunotherapy. *FEBS Lett.* 588, 288–297 (2014).

186. Richman, S. A. *et al.* High-Affinity GD2-Specific CAR T Cells Induce Fatal Encephalitis in a Preclinical Neuroblastoma Model. *Cancer Immunol. Res.* 6, 36–46 (2018).

187. Girling, A. *et al.* A core protein epitope of the polymorphic epithelial mucin detected by the monoclonal antibody SM-3 is selectively exposed in a range of primary carcinomas. *Int. J. cancer* 43, 1072–6 (1989).

188. van Dam, P. A. *et al.* Multi-parameter flow cytometric quantitation of the expression of the tumor-associated antigen SM3 in normal and neoplastic ovarian tissues. A comparison with HMFG1 and HMFG2. *Cancer* 68, 169–77 (1991).

189. Burchell, J. *et al.* An alpha2,3 sialyltransferase (ST3Gal I) is elevated in primary breast carcinomas. *Glycobiology* 9, 1307–11 (1999).

190. Julien, S. *et al.* Sialyl-Tn vaccine induces antibody-mediated tumour protection in a relevant murine model. *Br. J. Cancer* 100, 1746–1754 (2009).

191. Brockhausen, I., Yang, J. -M, Burchell, J., Whitehouse, C. & Taylor-Papadimitriou, J. Mechanisms Underlying Aberrant Glycosylation of MUC1 Mucin in Breast Cancer Cells. *Eur. J. Biochem.* 233, 607–617 (1995).

192. Lloyd, K. O., Burchell, J., Kudryashov, V., Yin, B. W. T. & Taylor-Papadimitriou, J. Comparison of O -Linked Carbohydrate Chains in MUC-1 Mucin from Normal Breast Epithelial Cell Lines and Breast Carcinoma Cell Lines: *J. Biol. Chem.* 271, 33325–33334 (1996).

193. Hilkens, J. *et al.* Monoclonal antibodies against human milk-fat globule membranes detecting differentiation antigens of the mammary gland and its tumors. *Int. J. cancer* 34, 197–206 (1984).

194. Hayes, D. F. *et al.* Use of a murine monoclonal antibody for detection of circulating plasma DF3 antigen levels in breast cancer patients. *J. Clin. Invest.* 75, 1671–1678 (1985).

195. van de Wiel-van Kemenade, E. *et al.* Episialin (MUC1) inhibits cytotoxic lymphocyte-target cell interaction. *J. Immunol.* 151, 767–76 (1993).

196. Wilkie, S. *et al.* Retargeting of Human T Cells to Tumor-Associated MUC1: The Evolution of a Chimeric Antigen Receptor. *J. Immunol.* 180, 4901–4909 (2008).

197. Wilkie, S. *et al.* Retargeting of Human T Cells to Tumor-Associated MUC1: The Evolution of a Chimeric Antigen Receptor. *J. Immunol.* 180, 4901–4909 (2008).

198. Maher, J. *et al.* Targeting of Tumor-Associated Glycoforms of MUC1 with CAR T Cells. *Immunity* 45, 945–946 (2016).

199. You, F. *et al.* Phase 1 clinical trial demonstrated that MUC1 positive metastatic seminal vesicle cancer can be effectively eradicated by modified Anti-MUC1 chimeric antigen receptor transduced T cells. *Sci. China Life Sci.* 59, 386–397 (2016).

200. Gao, H. *et al.* Development of T cells redirected to glypican-3 for the treatment of hepatocellular carcinoma. *Clin. Cancer Res.* 20, 6418–6428 (2014).

201. Filmus, J. & Selleck, S. B. Glypicans: Proteoglycans with a surprise. *J. Clin. Invest.* 108, 497–501 (2001).

202. Dargel, C. *et al.* T Cells Engineered to Express a T-Cell Receptor Specific for Glypican-3 to Recognize and Kill Hepatoma Cells In Vitro and in Mice. *Gastroenterology* 149, 1042–1052 (2015).

203. Xue, R. *et al.* The significance of glypican-3 expression profiling in the tumor cellular origin theoretical system for hepatocellular carcinoma progression. *J. Gastroenterol. Hepatol.* 32, 1503–1511 (2017).

204. Castillo, L. *et al.* Expression of Glypican-3 (GPC3) in Malignant and Non-malignant Human Breast Tissues. *Open Cancer J.* 8, 12–23 (2015).

205. Kandil, D., Leiman, G., Allegretta, M. & Evans, M. Glypican-3 protein expression in primary and metastatic melanoma: A combined immunohistochemistry and immunocytochemistry study. *Cancer Cytopathol.* 117, 271–278 (2009).

206. Mounajjed, T., Zhang, L. & Wu, T. T. Glypican-3 expression in gastrointestinal and pancreatic epithelial neoplasms. *Hum. Pathol.* 44, 542–550 (2013).

207. Baumhoer, D. *et al.* Glypican 3 expression in human nonneoplastic, preneoplastic, and neoplastic tissues: A tissue microarray analysis of 4,387 tissue samples. *Am. J. Clin. Pathol.* 129, 899–906 (2008).

208. Jiang, Z. *et al.* Anti-GPC3-CAR T cells suppress the growth of tumor cells in patient-derived xenografts of hepatocellular carcinoma. *Front. Immunol.* 7, 1–10 (2017).

209. Zhai, B. *et al.* A phase I study of anti-GPC3 chimeric antigen receptor modified T cells (GPC3 CAR-T) in Chinese patients with refractory or relapsed GPC3+ hepatocellular carcinoma(r/r GPC3+ HCC). *J. Clin. Oncol.* 35, 3049 (2017).

210. Papageorgis, P. *et al.* Targeting IL13Ralpha2 activates STAT6-TP63 pathway to suppress breast cancer lung metastasis. *Breast Cancer Res.* 17, 1–15 (2015).

211. Krebs, S. *et al.* T cells redirected to interleukin-13Rα2 with interleukin-13 mutein--chimeric antigen receptors have anti-glioma activity but also recognize interleukin-13Rα1. *Cytotherapy* 16, 1121–31 (2014).

212. Brown, C. E. *et al.* Bioactivity and Safety of IL13R 2-Redirected Chimeric Antigen Receptor CD8+ T Cells in Patients with Recurrent Glioblastoma. *Clin. Cancer Res.* 21, 4062–4072 (2015).

213. Krenciute, G. *et al.* Characterization and functional analysis of scFv-based chimeric antigen receptors to redirect T Cells to IL13Rα2-positive glioma. *Mol. Ther.* 24, 354–363 (2016).

214. Wang, M. C. *et al.* Prostate antigen: A new potential marker for prostatic cancer. *Prostate* 2, 89–96 (1981).

215. Cunha, A. C., Weigle, B., Kiessling, A., Bachmann, M. & Rieber, E. P. Tissue-specificity of prostate specific antigens: Comparative analysis of transcript levels in prostate and non-prostatic tissues. *Cancer Lett.* 236, 229–238 (2006).

216. Ono, H., Yanagihara, K., Sakamoto, H., Yoshida, T. & Saeki, N. Prostate stem cell antigen gene is expressed in islets of pancreas. *Anat. Cell Biol.* 45, 149–154 (2012).

217. Zhigang, Z. & Wenlv, S. Prostate stem cell antigen (PSCA) expression in human prostate cancer tissues and its potential role in prostate carcinogenesis and progression of prostate cancer. *World J. Surg. Oncol.* 2, 1–7 (2004).

218. Gerdts, E. *et al.* Development and optimization of PSCA-specific CAR T cells for the treatment of bone metastatic prostate cancer. *J. Immunother. Cancer* 3, P115 (2015).

219. Gu, Z. *et al.* Prostate stem cell antigen (PSCA) expression increases with high gleason score , advanced stage and bone metastasis in prostate cancer. 1288–1296 (2000).

220. Zhigang, Z. & Wenlv, S. Prostate Stem Cell Antigen (PSCA) Expression in Human Prostate Cancer Tissues: Implications for Prostate Carcinogenesis and Progression of Prostate Cancer. *Jpn. J. Clin. Oncol.* 34, 414–419 (2004).

221. Kiesgen, S., Chicaybam, L., Chintala, N. K. & Adusumilli, P. S. Chimeric Antigen

Receptor (CAR) T-Cell Therapy for Thoracic Malignancies. *J. Thorac. Oncol.* 13, 16–26 (2018).

222. Zou, Q., Yang, L., Yang, Z., Huang, J. & Fu, X. PSCA and Oct-4 expression in the benign and malignant lesions of gallbladder: Implication for carcinogenesis, progression, and prognosis of gallbladder adenocarcinoma. *Biomed Res. Int.* 2013, (2013).

223. Zhao, X., Wang, F. & Hou, M. Expression of stem cell markers nanog and PSCA in gastric cancer and its significance. *Oncol. Lett.* 11, 442–448 (2016).

224. Wei, X. *et al.* PSCA and MUC1 in non-small-cell lung cancer as targets of chimeric antigen receptor T cells. *Oncoimmunology* 6, 1–10 (2017).

225. Abate-Daga, D. *et al.* A Novel Chimeric Antigen Receptor Against Prostate Stem Cell Antigen Mediates Tumor Destruction in a Humanized Mouse Model of Pancreatic Cancer. *Hum. Gene Ther.* 25, 1003–1012 (2014).

226. Anurathapan, U. *et al.* Kinetics of tumor destruction by chimeric antigen receptor-modified T cells. *Mol. Ther.* 22, 623–633 (2014).

227. Hillerdal, V., Ramachandran, M., Leja, J. & Essand, M. Systemic treatment with CAR-engineered T cells against PSCA delays subcutaneous tumor growth and prolongs survival of mice. *BMC Cancer* 14, 1–9 (2014).

228. Wey, J. S., Stoeltzing, O. & Ellis, L. M. Vascular endothelial growth factor receptors: expression and function in solid tumors. *Clin. Adv. Hematol. Oncol.* 2, 37–45 (2004).

229. Ellis, L. M. & Hicklin, D. J. VEGF-targeted therapy: mechanisms of anti-tumour activity. *Nat. Rev. Cancer* 8, 579–591 (2008).

230. Dagmara, K.-M., Mirosław, J., Milczek, T., Lipińska, B. & Emerich, J. *Clinical significance of VEGFR-2 and VEGFR-3 expression in ovarian cancer patients*. *Polish Journal of Pathology* 62, (Termedia).

231. Holzer, T. R. *et al.* Tumor cell expression of vascular endothelial growth factor receptor 2 is an adverse prognostic factor in patients with squamous cell carcinoma of the lung. *PLoS One* 8, (2013).

232. Prewett, M. *et al.* Antivascular Endothelial Growth Factor Receptor (Fetal Liver Kinase 1) Monoclonal Antibody Inhibits Tumor Angiogenesis and Growth of Several Mouse and Human Tumors. 5209–5218 (1999).

233. Neuchrist, C. *et al.* Vascular Endothelial Growth Factor Receptor 2 (VEGFR2) Expression in Squamous Cell Carcinomas of the Head and Neck. *Laryngoscope* 111, 1834–1841 (2001).

234. O'Byrne, K. J. *et al.* Vascular endothelial growth factor, platelet-derived endothelial cell growth factor and angiogenesis in non-small-cell lung cancer. *Br. J. Cancer* 82, 1427–1432 (2000).

235. Duff, S. E. *et al.* Vascular endothelial growth factors and receptors in colorectal cancer: Implications for anti-angiogenic therapy. *Eur. J. Cancer* 42, 112–117 (2006).

236. Price, D. J., Miralem, T., Jiang, S., Steinberg, R. & Avraham, H. Role of Vascular Endothelial Growth Factor in the Stimulation of Cellular Invasion and Signaling of Breast Cancer Cells. *Cell Growth Differ.* 12, 129–135 (2001).

237. Ryd﷽n, L. *et al.* Tumor-specific VEGF-A and VEGFR2 in postmenopausal breast cancer

patients with long-term follow-up. Implication of a link between VEGF pathway and tamoxifen response. *Breast Cancer Res. Treat.* 89, 135–143 (2005).

238. Koukourakis, M. I. *et al.* Vascular Endothelial Growth Factor / KDR Activated Microvessel Density versus CD31 Standard Microvessel Density in Non-Small Cell Lung Cancer Vascular Endothelial Growth Factor / KDR Activated Microvessel Density versus. *Cancer Res.* 60, 3088–3095 (2000).

239. Hung, C. J. *et al.* Expression of vascular endothelial growth factor-C in benign and malignant thyroid tumors. *J. Clin. Endocrinol. Metab.* 88, 3694–9 (2003).

240. Andersen, S. *et al.* Prognostic impacts of angiopoietins in NSCLC tumor cells and stroma: VEGF-A impact is strongly associated with Ang-2. *PLoS One* 6, (2011).

241. Miettinen, M., Rikala, M.-S., Rys, J., Lasota, J. & Wang, Z.-F. Vascular Endothelial Growth Factor Receptor 2 as a Marker for Malignant Vascular Tumors and Mesothelioma. *Am. J. Surg. Pathol.* 36, 629–639 (2012).

242. Bruns, C. J. *et al.* Vascular endothelial growth factor is an in vivo survival factor for tumor endothelium in a murine model of colorectal carcinoma liver metastases. *Cancer* 89, 488–99 (2000).

243. Inoue, K. *et al.* Treatment of human metastatic transitional cell carcinoma of the bladder in a murine model with the anti-vascular endothelial growth factor receptor monoclonal antibody DC101 and paclitaxel. *Clin. Cancer Res.* 6, 2635–43 (2000).

244. Camidge, D. R. *et al.* A phase II, open-label study of ramucirumab (IMC-1121B), an IgG1 fully human monoclonal antibody (MAb) targeting VEGFR-2, in combination with

paclitaxel and carboplatin as first-line therapy in patients (pts) with stage IIIb/IV non-small cell lung cancer (NSCLC). *J. Clin. Oncol.* 28, 7588–7588 (2010).

245. Carvajal, R. D. *et al.* A Phase 2 Randomized Study of Ramucirumab (IMC-1221B) with or without Dacarbazine in Patients with Metastatic Melanoma. 50, 2099–2107 (2017).

246. Zhu, A. X. *et al.* A phase II and biomarker study of ramucirumab, a human monoclonal antibody targeting the VEGF receptor-2, as first-line monotherapy in patients with advanced hepatocellular Cancer. *Clin. Cancer Res.* 19, 6614–6623 (2013).

247. Clarke, J. M. & Hurwitz, H. I. Targeted inhibition of VEGF Receptor-2: An update on Ramucirumab. *Expert Opin. Biol. Ther.* 13, 1187–1196 (2014).

248. Penson, R. *et al.* A phase II study of ramucirumab (IMC-1121B) in the treatment of persistent or recurrent epithelial ovarian, fallopian tube or primary peritoneal carcinoma. 134, 87–92 (2016).

249. Cancer Immunotherapy- Clinical Trials.gov.

250. Li, K., Lan, Y., Wang, J. & Liu, L. Chimeric antigen receptor – engineered T cells for liver cancers , progress and obstacles. 1–8 (2017). doi:10.1177/1010428317692229

251. Burga, R. A. *et al.* Liver myeloid-derived suppressor cells expand in response to liver metastases in mice and inhibit the anti-tumor efficacy of anti-CEA CAR-T. *Cancer Immunol. Immunother.* 64, 817–829 (2015).

252. Moreno Carretero, G. *et al.* Serum and tissue CEA in colorectal cancer: clinical relevance. *Rev. Esp. Enferm. Dig.* 90, 391–401 (1998).

253. Ng, I. O., Ho, J., Pritchett, C. J., Chan, E. Y. & Ho, F. C. CEA tissue staining in colorectal

cancer patients--correlation with plasma CEA, histology and staging. *Pathology* 25, 219–22 (1993).

254. Fichera, A., Michelassi, F. & Arenas, R. B. Selective expression of carcinoembryonic antigen promoter in cancer cell lines: targeting strategy for gene therapy in colorectal cancer. *Dis. Colon Rectum* 41, 747–54 (1998).

255. Wang, L. *et al.* Efficient tumor regression by adoptively transferred CEA-specific CAR-T cells associated with symptoms of mild cytokine release syndrome. *Oncoimmunology* 5, 1–13 (2016).

256. Nap, M., Mollgard, K., Burtin, P. & Fleuren, G. J. Immunohistochemistry of carcino-embryonic antigen in the embryo, fetus and adult. *Tumour Biol.* 9, 145–53 (1988).

257. Yan, Z. *et al.* Oncogenic c-Ki-ras but not oncogenic c-Ha-ras up-regulates CEA expression and disrupts basolateral polarity in colon epithelial cells. *J. Biol. Chem.* 272, 27902–27907 (1997).

258. Shao, Y., Sun, X., He, Y., Liu, C. & Liu, H. Elevated levels of serum tumor markers CEA and CA15-3 are prognostic parameters for different molecular subtypes of breast cancer. *PLoS One* 10, 1–11 (2015).

259. Nan, J. *et al.* Preoperative Serum Carcinoembryonic Antigen as a Marker for Predicting the Outcome of Three Cancers. *Biomark. Cancer* 9, 1–7 (2017).

260. Kazarian, A. *et al.* Testing breast cancer serum biomarkers for early detection and prognosis in pre-diagnosis samples. *Br. J. Cancer* 116, 501–508 (2017).

261. Latteri, S. *et al.* Carcinoembryonic antigen serum levels in nonmelanoma skin cancer.

Biomedicines 6, 1–11 (2018).

262. Dong, Y. *et al.* Serum carcinoembryonic antigen, neuron-specific enolase as biomarkers for diagnosis of nonsmall cell lung cancer. *J. Cancer Res. Ther.* 12, 34 (2016).

263. Arrieta, O. *et al.* Usefulness of serum carcinoembryonic antigen (CEA) monitoring to define response or progression to chemotherapy and its correlation with survival in patients with advanced non small-cell lung cancer: A prospective cohort study. *J. Thorac. Oncol.* 6, S1105 (2011).

264. Kataoka, Y. *et al.* Carcinoembryonic Antigen as a Predictive Biomarker of Response to Nivolumab in Non–small Cell Lung Cancer. *Anticancer Res.* 38, 559–563 (2018).

265. Jin, Z., Jiang, W. & Wang, L. Biomarkers for gastric cancer: Progression in early diagnosis and prognosis (review). *Oncol. Lett.* 9, 1502–1508 (2015).

266. Căinap, C. *et al.* Classic Tumor Markers in Gastric Cancer. Current Standards and Limitations. *Clujul Med.* 88, 111–115 (2015).

267. Shimada, H., Noie, T., Ohashi, M., Oba, K. & Takahashi, Y. Clinical significance of serum tumor markers for gastric cancer: A systematic review of literature by the Task Force of the Japanese Gastric Cancer Association. *Gastric Cancer* 17, 26–33 (2014).

268. Ahn, H. S. *et al.* Serum biomarker panels for the diagnosis of gastric adenocarcinoma. *Br. J. Cancer* 106, 733–739 (2012).

269. Meng, Q. *et al.* Diagnostic and prognostic value of carcinoembryonic antigen in pancreatic cancer: a systematic review and meta-analysis. *Onco. Targets. Ther.* 10, 4591–4598 (2017).

270. Chang, J. C. & Kundranda, M. Novel diagnostic and predictive biomarkers in pancreatic adenocarcinoma. *Int. J. Mol. Sci.* 18, 4–6 (2017).

271. Bhat, K. *et al.* Advances in Biomarker Research for Pancreatic Cancer. *Curr. Pharm. Des.* 18, 2439–2451 (2012).

272. Zeng, Z., Cohen, A. M. & Urmacher, C. Usefulness of carcinoembryonic antigen monitoring despite normal preoperative values in node-positive colon cancer patients. *Dis. Colon Rectum* 36, 1063–8 (1993).

273. Parkhurst, M. R. *et al.* T cells targeting carcinoembryonic antigen can mediate regression of metastatic colorectal cancer but induce severe transient colitis. *Mol. Ther.* 19, 620–626 (2011).

274. Schmittgen, T. D., Teske, S., Vessella, R. L., True, L. D. & Zakrajsek, B. A. Expression of prostate specific membrane antigen and three alternatively spliced variants of PSMA in prostate cancer patients. *Int. J. Cancer* 107, 323–329 (2003).

275. Pinto, J. T. *et al.* Prostate-specific membrane antigen: a novel folate hydrolase in human prostatic carcinoma cells. *Clin. Cancer Res.* 2, 1445–1451 (1996).

276. Carter, R. E., Feldman, A. R. & Coyle, J. T. Prostate-specific membrane antigen is a hydrolase with substrate and pharmacologic characteristics of a neuropeptidase. *Proc. Natl. Acad. Sci.* 93, 749–753 (1996).

277. Kiessling, A. *et al.* Tumor-associated antigens for specific immunotherapy of prostate cancer. *Cancers (Basel).* 4, 193–217 (2012).

278. Feldmann, A. *et al.* Retargeting of T lymphocytes to PSCA- or PSMA positive prostate

cancer cells using the novel modular chimeric antigen receptor platform technology “UniCAR” *Oncotarget* 8, 31368–31385 (2017).

279. Kawakami, M. & Nakayama, J. Enhanced expression of the prostate specific membrane antigen gene in prostate cancer as revealed by in situ hybridization. *Cancer Res.* 57, 231–234 (1997).

280. Mhawech-Fauceglia, P. *et al.* Prostate-specific membrane antigen (PSMA) protein expression in normal and neoplastic tissues and its sensitivity and specificity in prostate adenocarcinoma: An immunohistochemical study using mutiple tumour tissue microarray technique. *Histopathology* 50, 472–483 (2007).

281. Feldmann, A. *et al.* Retargeting of T lymphocytes to PSCA- or PSMA positive prostate cancer cells using the novel modular chimeric antigen receptor platform technology “UniCAR” *Oncotarget* 8, 31368–31385 (2017).

282. Zuccolotto, G. *et al.* PSMA-Specific CAR-Engineered T Cells Eradicate Disseminated Prostate Cancer in Preclinical Models. 9, (2014).

283. Junghans, R. P. *et al.* Phase I Trial of Anti-PSMA Designer CAR-T Cells in Prostate Cancer: Possible Role for Interacting Interleukin 2-T Cell Pharmacodynamics as a Determinant of Clinical Response. *Prostate* 76, 1257–1270 (2016).

284. Kloss, C., Lee, J. & June, C. 638. TGFBeta Signaling Blockade within PSMA Targeted CAR Human T Cells for the Eradication of Metastatic Prostate Cancer. *Mol. Ther.* 24, S252–S253 (2016).

285. Borcherding, N., Kusner, D., Liu, G. H. & Zhang, W. ROR1, an embryonic protein with

an emerging role in cancer biology. *Protein Cell* 5, 496–502 (2014).

286. Zhou, J.-K. *et al.* ROR1 expression as a biomarker for predicting prognosis in patients with colorectal cancer. *Oncotarget* 8, 32864–32872 (2017).

287. Hojjat-Farsangi, M. *et al.* The receptor tyrosine kinase ROR1 – An oncofetal antigen for targeted cancer therapy. *Semin. Cancer Biol.* 29, 21–31 (2014).

288. Balakrishnan, A. *et al.* Analysis of ROR1 protein expression in human cancer and normal tissues. *Clin. Cancer Res.* 23, 3061–3071 (2017).

289. Zhang, S. *et al.* The onco-embryonic antigen ROR1 is expressed by a variety of human cancers. *Am. J. Pathol.* 181, 1903–1910 (2012).

290. Henry, C. E. *et al.* Distinct Patterns of Stromal and Tumor Expression of ROR1 and ROR2 in Histological Subtypes of Epithelial Ovarian Cancer. *Transl. Oncol.* 10, 346–356 (2017).

291. Tan, H. *et al.* MiR 382 inhibits migration and invasion by targeting ROR1 through regulating EMT in ovarian cancer. *Int. J. Oncol.* 48, 181–190 (2016).

292. Zhang, H. *et al.* ROR1 expression correlated with poor clinical outcome in human ovarian cancer. *Sci. Rep.* 4, 1–7 (2014).

293. Galloway, D. A., Laimins, L. A., Division, B. & Hutchinson, F. A ROR1-Her3-LncRNA signaling axis modulates the Hippo-YAP pathway to regulate bone metastasis. 19, 87–92 (2016).

294. Chien, H.-P. *et al.* Expression of ROR1 has prognostic significance in triple negative breast cancer. *Virchows Arch.* 468, 589–595 (2016).

295. Zhang, S. *et al.* ROR1 Is Expressed in Human Breast Cancer and Associated with Enhanced Tumor-Cell Growth. *PLoS One* 7, e31127 (2012).

296. Zheng, Y.-Z. *et al.* ROR1 is a novel prognostic biomarker in patients with lung adenocarcinoma. *Sci. Rep.* 6, 36447 (2016).

297. Liu, Y. *et al.* Silencing of receptor tyrosine kinase ROR1 inhibits tumor-cell proliferation via PI3K/AKT/mTOR signaling pathway in lung adenocarcinoma. *PLoS One* 10, 1–14 (2015).

298. Chang, H. *et al.* Expression of ROR1, pAkt, and pCREB in gastric adenocarcinoma. *Ann. Diagn. Pathol.* 19, 330–334 (2015).

299. Zhou, J.-K. *et al.* ROR1 expression as a biomarker for predicting prognosis in patients with colorectal cancer. *Oncotarget* 8, 32864–32872 (2017).

300. Henry, C. *et al.* Targeting the ROR1 and ROR2 receptors in epithelial ovarian cancer inhibits cell migration and invasion. *Oncotarget* 6, 40310–40326 (2015).

301. Rottman, J. B. *et al.* ROR1-Directed Chimeric Antigen Receptor T Cell Recognition of Self-Antigen Is Associated with Acute Toxicity, T Cell Dysfunction, and Poor Tumor Control. *Blood* 130, (2017).

302. Gohil, S. *et al.* Preclinical development of novel humanised ROR1 targeting chimeric antigen receptor T cells and bispecific T-cell engagers. *Lancet* 389, S40 (2017).

303. Gohil, S. H. *et al.* An ROR1 bi-specific T-cell engager provides effective targeting and cytotoxicity against a range of solid tumors. *Oncoimmunology* 6, 1–11 (2017).

304. Targeting Fibroblast Activation Protein in Tumor Stroma with Chimeric Antigen Receptor

T Cells Can Inhibit Tumor Growth and Augment Host Immunity Without Severe Toxicity.pdf.crdownload.

305. Goscinski, M. A. *et al.* FAP-α and uPA Show Different Expression Patterns in Premalignant and Malignant Esophageal Lesions. *Ultrastruct. Pathol.* 32, 89–96 (2008).

306. Scanlan, M. J. *et al.* Molecular cloning of fibroblast activation protein alpha, a member of the serine protease family selectively expressed in stromal fibroblasts of epithelial cancers. *Proc. Natl. Acad. Sci.* 91, 5657–5661 (1994).

307. Cohen, S. J. *et al.* Fibroblast Activation Protein and Its Relationship to Clinical Outcome in Pancreatic Adenocarcinoma. *Pancreas* 37, 154–158 (2008).

308. Henry, L. R. *et al.* Clinical implications of fibroblast activation protein in patients with colon cancer. *Clin. Cancer Res.* 13, 1736–1741 (2007).

309. Rerrig, W. J. *et al.* Cell-surface glycoproteins of human sarcomas: Differential expression in normal and malignant tissues and cultured cells. *Pnas* 85, 3110–3114 (1988).

310. Huber, M. A. *et al.* Fibroblast Activation Protein: Differential Expression and Serine Protease Activity in Reactive Stromal Fibroblasts of Melanocytic Skin Tumors. *J. Invest. Dermatol.* 120, 182–188 (2003).

311. Aertgeerts, K. *et al.* Structural and kinetic analysis of the substrate specificity of human fibroblast activation protein alpha. *J. Biol. Chem.* 280, 19441–4 (2005).

312. Loeffler, M., Krüger, J. A., Niethammer, A. G. & Reisfeld, R. A. Targeting tumor-associated fibroblasts improves cancer chemotherapy by increasing intratumoral drug uptake. *J. Clin. Invest.* 116, 1955–1962 (2006).

313. Ostermann, E. *et al.* Effective immunoconjugate therapy in cancer models targeting a serine protease of tumor fibroblasts. *Clin. Cancer Res.* 14, 4584–4592 (2008).

314. Tran, E. *et al.* Immune targeting of fibroblast activation protein triggers recognition of multipotent bone marrow stromal cells and cachexia. *J. Exp. Med.* 210, 1125–1135 (2013).

315. Lee, P. P. *et al.* Characterization of circulating T cells specific for tumor-associated antigens in melanoma patients. *Nat. Med.* 5, 677–685 (1999).

316. Schuberth, P. C. *et al.* Treatment of malignant pleural mesothelioma by fibroblast activation protein-specific re-directed T cells. *J. Transl. Med.* 11, 1–11 (2013).

317. van der Gun, B. T. F. *et al.* EpCAM in carcinogenesis: The good, the bad or the ugly. *Carcinogenesis* 31, 1913–1921 (2010).

318. Schnell, U., Cirulli, V. & Giepmans, B. N. G. EpCAM: Structure and function in health and disease. *Biochim. Biophys. Acta - Biomembr.* 1828, 1989–2001 (2013).

319. Xia Ang, W. *et al.* Intraperitoneal immunotherapy with T cells stably and transiently expressing anti-EpCAM CAR in xenograft models of peritoneal carcinomatosis. *Oncotarget* 8, 13545–13559 (2017).

320. Patriarca, C., Macchi, R. M., Marschner, A. K. & Mellstedt, H. Epithelial cell adhesion molecule expression (CD326) in cancer: A short review. *Cancer Treat. Rev.* 38, 68–75 (2012).

321. Patriarca, C., Macchi, R. M., Marschner, A. K. & Mellstedt, H. Epithelial cell adhesion molecule expression (CD326) in cancer: A short review. *Cancer Treat. Rev.* 38, 68–75

(2012).

322. Litvinov, S. V *et al.* Expression of Ep-CAM in cervical squamous epithelia correlates with an increased proliferation and the disappearance of markers for terminal differentiation. *Am. J. Pathol.* 148, 865–75 (1996).

323. Heiss, M. M. *et al.* The trifunctional antibody catumaxomab for the treatment of malignant ascites due to epithelial cancer: Results of a prospective randomized phase II/III trial. *Int. J. Cancer* 127, 2209–2221 (2010).

324. Kowalski, M. *et al.* A phase i study of an intravesically administered immunotoxin targeting EpCAM for the treatment of nonmuscle-invasive bladder cancer in BCG-refractory and BCG-intolerant patients. *Drug Des. Devel. Ther.* 4, 313–320 (2010).

325. MacDonald, G. C. *et al.* A phase I clinical study of VB4-845: weekly intratumoral administration of an anti-EpCAM recombinant fusion protein in patients with squamous cell carcinoma of the head and neck. *Drug Des. Devel. Ther.* 2, 105–14 (2009).

326. Berek, J. S. *et al.* Catumaxomab for the Treatment of Malignant Ascites in Patients With Chemotherapy-Refractory Ovarian Cancer. *Int. J. Gynecol. Cancer* 24, 1583–1589 (2014).

327. Andersson, Y. *et al.* Phase I trial of EpCAM-targeting immunotoxin MOC31PE, alone and in combination with cyclosporin. *Br. J. Cancer* 113, 1548–1555 (2015).

328. Tavri, S. *et al.* Optical Imaging of Cellular Immunotherapy against Prostate Cancer. *Mol. Imaging* 8, 7290.2009.00002 (2009).

329. Shirasu, N., Yamada, H., Shibaguchi, H., Kuroki, M. & Kuroki, M. Molecular characterization of a fully human chimeric T-cell antigen receptor for tumor-associated

antigen EpCAM. *J. Biomed. Biotechnol.* 2012, (2012).

330. Deng, Z., Wu, Y., Ma, W., Zhang, S. & Zhang, Y. Q. Adoptive T-cell therapy of prostate cancer targeting the cancer stem cell antigen EpCAM. *BMC Immunol.* 16, 1–9 (2015).

331. Xia Ang, W. *et al.* Intraperitoneal immunotherapy with T cells stably and transiently expressing anti-EpCAM CAR in xenograft models of peritoneal carcinomatosis. *Oncotarget* 8, 13545–13559 (2017).

332. Greenall, S. A. & Johns, T. G. EGFRvIII: the promiscuous mutation. *Cell Death Discov.* 2, 16049 (2016).

333. Warren, J. J. *et al.* Targeting a glioblastoma cancer stem cell population defined by EGF receptor variant III. 44, 319–335 (2017).

334. Swartz, A. M., Li, Q.-J. & Sampson, J. H. Rindopepimut: a promising immunotherapeutic for the treatment of glioblastoma multiforme. *Immunotherapy* 6, 679–690 (2014).

335. Ohno, M. *et al.* Retrovirally engineered T-cell-based immunotherapy targeting type III variant epidermal growth factor receptor, a glioma-associated antigen. *Cancer Sci.* 101, 2518–2524 (2010).

336. Johnson, L. A. *et al.* Rational development and characterization of humanized anti-EGFR variant III chimeric antigen receptor T cells for glioblastoma. 7, 1–30 (2016).

337. Shen, C. J. *et al.* Chimeric antigen receptor containing ICOS signaling domain mediates specific and efficient antitumor effect of T cells against EGFRvIII expressing glioma. *J. Hematol. Oncol.* 6, 1–7 (2013).

338. Ohno, M. *et al.* Expression of miR-17-92 enhances anti-tumor activity of T-cells

transduced with the anti-EGFRvIII chimeric antigen receptor in mice bearing human GBM xenografts. *J. Immunother. Cancer* 1, 1–12 (2013).

339. O'Rourke, D. M. *et al.* A single dose of peripherally infused EGFRvIII-directed CAR T cells mediates antigen loss and induces adaptive resistance in patients with recurrent glioblastoma. *Sci. Transl. Med.* 9, eaaa0984 (2017).

340. Song, W. *et al.* Targeting EphA2 impairs cell cycle progression and growth of basal-like/triple-negative breast cancers. *Oncogene* 36, 5620–5630 (2017).

341. Brantley-Sieders, D. M. *et al.* The receptor tyrosine kinase EphA2 promotes mammary adenocarcinoma tumorigenesis and metastatic progression in mice by amplifying ErbB2 signaling. *J. Clin. Invest.* 118, 64–78 (2008).

342. Larsen, A. B. *et al.* Activation of the EGFR Gene Target EphA2 Inhibits Epidermal Growth Factor-Induced Cancer Cell Motility. *Mol. Cancer Res.* 5, 283–293 (2007).

343. Hafner, C. *et al.* Differential Gene Expression of Eph Receptors and Ephrins in Benign Human Tissues and Cancers. *Clin. Chem.* 50, 490–499 (2004).

344. Park, J., Son, A. & Zhou, R. Roles of EphA2 in Development and Disease. *Genes (Basel).* 4, 334–357 (2013).

345. Andres, A. C. *et al.* Expression of two novel eph-related receptor protein tyrosine kinases in mammary gland development and carcinogenesis. *Oncogene* 9, 1461–7 (1994).

346. Andres, A. C., Zuercher, G., Djonov, V., Flueck, M. & Ziemiecki, A. Protein tyrosine kinase expression during the estrous cycle and carcinogenesis of the mammary gland. *Int. J. cancer* 63, 288–96 (1995).

347. Pasquale, E. B. Eph receptors and ephrins in cancer: bidirectional signalling and beyond. *Nat. Rev. Cancer* 10, 165–180 (2010).

348. Huang, F. *et al.* Identification of candidate molecular markers predicting sensitivity in solid tumors to dasatinib: Rationale for patient selection. *Cancer Res.* 67, 2226–2238 (2007).

349. Tandon, M., Vemula, V. & Mittal, S. *Emerging strategies for EphA2 receptor targeting for cancer therapeutics*. *Expert Opn Ther Targets* 15, (2011).

350. Li, N. *et al.* Chimeric Antigen Receptor-Modified T Cells Redirected to EphA2 for the Immunotherapy of Non-Small Cell Lung Cancer. *Transl. Oncol.* 11, 11–17 (2018).

351. Yi, Z., Prinzing, B. L., Cao, F., Gottschalk, S. & Krenciute, G. Optimizing EphA2-CAR T Cells for the Adoptive Immunotherapy of Glioma. *Mol. Ther. - Methods Clin. Dev.* 9, 70–80 (2018).

352. Chow, K. K. *et al.* T cells redirected to EphA2 for the immunotherapy of glioblastoma. *Mol. Ther.* 21, 629–637 (2013).

353. Song, W. *et al.* Targeting EphA2 impairs cell cycle progression and growth of basal-like/triple-negative breast cancers. *Oncogene* 36, 5620–5630 (2017).

354. Wang, Y., Luo, F., Yang, J., Zhao, C. & Chu, Y. New Chimeric Antigen Receptor Design for Solid Tumors. *Front. Immunol.* 8, 1–9 (2017).

355. Chen, K. H. *et al.* A compound chimeric antigen receptor strategy for targeting multiple myeloma. *Leukemia* 32, 402–412 (2018).

356. Hegde, M. *et al.* Tandem CAR T cells targeting HER2 and IL13Rα2 mitigate tumor

antigen escape. *J. Clin. Invest.* 126, 3036–3052 (2016).

357. Schneider, D. *et al.* A tandem CD19/CD20 CAR lentiviral vector drives on-target and off-target antigen modulation in leukemia cell lines. *J. Immunother. Cancer* 5, 1–17 (2017).

358. Grada, Z. *et al.* TanCAR: A novel bispecific chimeric antigen receptor for cancer immunotherapy. *Mol. Ther. - Nucleic Acids* 2, (2013).

359. Sadelain, M. Antigen-specific inhibitory chimeric antigen receptors (iCARs) as a self-regulating safety switch to constrain T cell–based therapies. *Sci. Exch.* 7, 2014 (2014).

360. Zhang, E. & Xu, H. A new insight in chimeric antigen receptor-engineered T cells for cancer immunotherapy. *J. Hematol. Oncol.* 10, 1 (2017).

361. Hofmann, O. *et al.* Genome-wide analysis of cancer/testis gene expression. *Proc. Natl. Acad. Sci.* 105, 20422–20427 (2008).

362. Sahin, U. *et al.* Expression of multiple cancer/testis (CT) antigens in breast cancer and melanoma: basis for polyvalent CT vaccine strategies. *Int. J. cancer* 78, 387–9 (1998).

363. NR, dos S. *et al.* - Heterogeneous expression of the SSX cancer/testis antigens in human melanoma. *Mod Pathol* 13, 363–365 (2000).

364. Salmaninejad, A. *et al.* Cancer/Testis Antigens: Expression, Regulation, Tumor Invasion, and Use in Immunotherapy of Cancers. *Immunol. Invest.* 45, 619–640 (2016).

365. Chen, Y.-T. *et al.* Cancer/testis antigen CT45: Analysis of mRNA and protein expression in human cancer. *Int. J. Cancer* 124, 2893–2898 (2009).

366. Zendman, A. J. W. *et al.* Expression profile of genes coding for melanoma differentiation antigens and cancer/testis antigens in metastatic lesions of human cutaneous melanoma.

Melanoma Res. 11, 451–459 (2001).

367. Gjerstorff, M. F., Johansen, L. E., Nielsen, O., Kock, K. & Ditzel, H. J. Restriction of GAGE protein expression to subpopulations of cancer cells is independent of genotype and may limit the use of GAGE proteins as targets for cancer immunotherapy. *Br. J. Cancer* 94, 1864–1873 (2006).

368. Greve, K. B. V. *et al.* SSX2-4 expression in early-stage non-small cell lung cancer. *Tissue Antigens* 83, 344–349 (2014).

369. Obenaus, M. *et al.* Identification of human T-cell receptors with optimal affinity to cancer antigens using antigen-negative humanized mice. *Nat. Biotechnol.* 33, 402–407 (2015).

370. Magee, M. S. *et al.* GUCY2C-directed CAR-T cells oppose colorectal cancer metastases without autoimmunity. *Oncoimmunology* 5, 1–10 (2016).

371. Snook, A. E., Eisenlohr, L. C., Rothstein, J. L. & Waldman, S. A. Cancer Mucosa Antigens as a Novel Immunotherapeutic Class of Tumor-associated Antigen. *Clin. Pharmacol. Ther.* 82, 734–739 (2007).

372. Frick, G. S. *et al.* Guanylyl cyclase C: a molecular marker for staging and postoperative surveillance of patients with colorectal cancer. *Expert Rev. Mol. Diagn.* 5, 701–713 (2005).

373. Carrithers, S. L. *et al.* Guanylyl cyclase C is a selective marker for metastatic colorectal tumors in human extraintestinal tissues. *Proc. Natl. Acad. Sci. U. S. A.* 93, 14827–32 (1996).

374. Birbe, R. *et al.* Guanylyl cyclase C is a marker of intestinal metaplasia, dysplasia, and

adenocarcinoma of the gastrointestinal tract. *Hum. Pathol.* 36, 170–9 (2005).

375. Schulz, S. *et al.* A validated quantitative assay to detect occult micrometastases by reverse transcriptase-polymerase chain reaction of guanylyl cyclase C in patients with colorectal cancer. *Clin. Cancer Res.* 12, 4545–4552 (2006).

376. Snook, A. E., Magee, M. S., Schulz, S. & Waldman, S. A. Self-Tolerance eliminates CD4+ T, but not CD8+ T or B, cells corrupting cancer corrupting immunotherapy. 44, 1956–1966 (2015).

377. Snook, A. E. *et al.* Lineage-specific T-cell responses to Cancer mucosa antigen oppose systemic metastases without mucosal inflammatory disease. *Cancer Res.* 69, 3537–3544 (2009).

378. Ponnusamy, M. P. *et al.* Expression of TAG-72 in ovarian cancer and its correlation with tumor stage and patient prognosis. *Cancer Lett.* 251, 247–57 (2007).

379. Xu, M. *et al.* Expression of TAG-72 in normal colon, transitional mucosa, and colon cancer. *Int. J. cancer* 44, 985–9 (1989).

380. Pizzi, C. *et al.* TAG-72 expression and clinical outcome in primary breast cancer. *Oncol. Rep.* 6, 1399–403

381. Lottich, S. C. *et al.* Tumor-associated antigen TAG-72: correlation of expression in primary and metastatic breast carcinoma lesions. *Breast Cancer Res. Treat.* 6, 49–56 (1985).

382. Murray, J. L. *et al.* Enhanced TAG-72 expression and tumor uptake of radiolabeled monoclonal antibody CC49 in metastatic breast cancer patients following alpha-interferon

treatment. *Cancer Res.* 55, 5925s–5928s (1995).

383. Brenner, P. C. *et al.* TAG-72 expression in primary, metastatic and hormonally treated prostate cancer as defined by monoclonal antibody CC49. *J. Urol.* 153, 1575–9 (1995).

384. Karan, D., Johansson, S. L., Lin, M. F. & Batra, S. K. Expression of tumor-associated glycoprotein-72 (TAG-72) antigen in human prostatic adenocarcinomas. *Oncol. Rep.* 8, 1123–6

385. Osteen, K. G., Anderson, T. L., Schwartz, K., Hargrove, J. T. & Gorstein, F. Distribution of tumor-associated glycoprotein-72 (TAG-72) expression throughout the normal female reproductive tract. *Int. J. Gynecol. Pathol.* 11, 216–20 (1992).

386. Soisson, A. P. *et al.* Immunohistochemical expression of TAG-72 in normal and malignant endometrium: correlation of antigen expression with estrogen receptor and progesterone receptor levels. *Am. J. Obstet. Gynecol.* 161, 1258–63 (1989).

387. Townsend, M. H., Robison, R. A. & O'Neill, K. L. A review of HPRT and its emerging role in cancer. *Med. Oncol.* 35, 89 (2018).

388. Weagel, E. G. *et al.* Abstract 2149: Unusual expression of HPRT on the surface of the colorectal cancer cell lines HT29 and SW620. *Cancer Res.* 77, 2149–2149 (2017).

389. Weagel, E. G. *et al.* Biomarker analysis and clinical relevance of thymidine kinase 1 on the cell membrane of Burkitt's lymphoma and acute lymphoblastic leukemia. *Onco. Targets. Ther.* 10, 1–13 (2017).

390. Aktar, M. W., Sengupta, D. & Chowdhury, A. Impact of pesticides use in agriculture: their benefits and hazards. *Interdiscip. Toxicol.* 2, 1–12 (2009).

391. Fernandez-Cornejo, J. & Nehring, R. Pesticide Use in US Agriculture: 21 Selected Crops, 1960-2008. 1960–2008 (2014). at <http://farmpolicy.com/wp-content/uploads/2014/05/eib124.pdf>

392. Woodburn, A. T. Glyphosate : production , pricing and use. 312, 309–312 (2000).

393. Knutson, R. D. Economic impacts of reduced pesticide use in the United States: measurement of costs and benefits. *Agric. Econ.* 21 (1999).

394. Amrhein, N., Deus, B., Gehrke, P. & Steinrucken, H. C. The Site of the Inhibition of the Shikimate Pathway by Glyphosate. 830–834 (2015).

395. Padgette, S. R., Fraley, R. T. & Press, A. History of Herbicide-Tolerant Crops , Methods of Development and Current State of the Art - Emphasis on Glyphosate Tolerance. 6, 626–634 (2015).

396. Schönbrunn, E. *et al.* Interaction of the herbicide glyphosate with its target enzyme 5-enolpyruvylshikimate 3-phosphate synthase in atomic detail. *Proc. Natl. Acad. Sci. U. S. A.* 98, 1376–1380 (2001).

397. Delaplane, K. Pesticide usage in the United States: history, benefits, risks, and trends. *Athens, GA Coop. Ext. Serv. ...* (2000). at <http://scholar.google.com/scholar?hl=en&btnG=Search&q=intitle:Pesticide+Usage+in+the+United+States+:+History+,+Benefits+,+Risks+,+and+Trends#0>

398. Horowitz, A. & Amore, M. D. and Environmental Costs of Pesticide Use An assessment based on currently available US data , although. 42, 750–760 (2015).

399. Gasnier, C. *et al.* Glyphosate-based herbicides are toxic and endocrine disruptors in

human cell lines. *Toxicology* 262, 184–191 (2009).

400. Mañas, F. *et al.* Genotoxicity of glyphosate assessed by the comet assay and cytogenetic tests. *Environ. Toxicol. Pharmacol.* 28, 37–41 (2009).

401. Peruzzo, P. J., Porta, A. a. & Ronco, A. E. Levels of glyphosate in surface waters, sediments and soils associated with direct sowing soybean cultivation in north pampasic region of Argentina. *Environ. Pollut.* 156, 61–66 (2008).

402. Battaglin, W. a., Rice, K. C., Focazio, M. J., Salmons, S. & Barry, R. X. The occurrence of glyphosate, atrazine, and other pesticides in vernal pools and adjacent streams in Washington, DC, Maryland, Iowa, and Wyoming, 2005-2006. *Environ. Monit. Assess.* 155, 281–307 (2009).

403. Ito, M. *et al.* Emergence and Spread of Neisseria gonorrhoeae Clinical Isolates Harboring Mosaic-Like Structure of Penicillin-Binding Protein 2 in Central Japan. 49, 137–143 (2005).

404. Koller, V. J. *et al.* Cytotoxic and DNA-damaging properties of glyphosate and Roundup in human-derived buccal epithelial cells. *Arch. Toxicol.* 86, 805–813 (2012).

405. Li, Q. *et al.* Glyphosate and AMPA inhibit cancer cell growth through inhibiting intracellular glycine synthesis. *Drug Des. Devel. Ther.* 7, 635–643 (2013).

406. Brusick, D., Aardema, M., Kier, L., Kirkland, D. & Williams, G. Genotoxicity Expert Panel review: weight of evidence evaluation of the genotoxicity of glyphosate, glyphosate-based formulations, and aminomethylphosphonic acid. *Crit. Rev. Toxicol.* 46, 56–74 (2016).

407. De Roos, A. J. *et al.* Cancer incidence among glyphosate-exposed pesticide applicators in the Agricultural Health Study. *Environ. Health Perspect.* 113, 49–54 (2005).

408. Eriksson, M. & Ph, D. A Case – Control Study of Non-Hodgkin Lymphoma and Exposure to Pesticides. (1992).

409. Braafladt, S., Reipa, V. & Atha, D. H. The Comet Assay: Automated Imaging Methods for Improved Analysis and Reproducibility. *Sci. Rep.* 6, 32162 (2016).

410. Collins, A. R. The Comet Assay for DNA Damage and Repair: Principles, Applications, and Limitations. *Mol. Biotechnol.* 26, 249–261 (2004).

411. Duty, S. M. *et al.* The relationship between environmental exposures to phthalates and DNA damage in human sperm using the neutral comet assay. *Environ. Health Perspect.* 111, 1164–9 (2003).

412. Olive, P. L., Banáth, J. P. & Durand, R. E. Heterogeneity in radiation-induced DNA damage and repair in tumor and normal cells measured using the 'comet' assay. *Radiat. Res.* 122, 86–94 (1990).

413. Xiao, M. *et al.* DNA damage caused by inorganic particulate matter on Raji and HepG2 cell lines exposed to ultraviolet radiation. *Mutat. Res. - Genet. Toxicol. Environ. Mutagen.* 771, 6–14 (2014).

414. Solomon, K. R., Marshall, E. J. P. & Carrasquilla, G. Human health and environmental risks from the use of glyphosate formulations to control the production of coca in Colombia overview and conclusions.pdf. *J. Toxicol. Environ. Heal. Part A* 72, 914–920 (2009).

415. Plewka, D. *et al.* Colorectal Cancer Epidemiology : Incidence , Mortality , Survival , and Risk Factors. *Res. Vet. Sci.* 52, 191–197 (2006).

416. Society, A. C. Colorectal Cancer Facts & Figures 2014-2016. *Color. Cancer Facts Fig.* 1–32 (2014). doi:10.1101/gad.1593107

417. Siegel, R. L., Miller, K. D. & Jemal, A. Cancer statistics. *CA Cancer J Clin* 66, 7–30 (2016).

418. Nowell, P. C. Linked references are available on JSTOR for this article : The Clonal Evolution of Tumor Cell Populations. *Science (80-.).* 194, 23–28 (1976).

419. Dunn, G. P., Old, L. J. & Schreiber, R. D. The immunobiology of cancer immunosurveillance and immunoediting. *Immunity* 21, 137–148 (2004).

420. Landskron, G., Fuente, M. De, Thuwajit, P., Thuwajit, C. & Hermoso, M. A. Review Article Chronic Inflammation and Cytokines in the Tumor Microenvironment. *J Immunol Res* 2014:14918, (2014).

421. Kryczek, I. *et al.* Cutting edge: Th17 and regulatory T cell dynamics and the regulation by IL-2 in the tumor microenvironment. *J. Immunol.* 178, 6730–6733 (2007).

422. Coussens, L. M. & Werb, Z. Inflammation and cancer. *Nature* 420, 860–867 (2002).

423. Whiteside, T. L. The tumor microenvironment and its role in promoting tumor growth. *Oncogene* 27, 5904–12 (2008).

424. Klampfer, L. Cytokines, inflammation and colon cancer. *Curr. Cancer Drug Targets* 11, 451–64 (2011).

425. Lewis, A. M., Varghese, S., Xu, H. & Alexander, H. R. Interleukin-1 and cancer

progression: the emerging role of interleukin-1 receptor antagonist as a novel therapeutic agent in cancer treatment. *J. Transl. Med.* 4, 48 (2006).

426. Balkwill, F. TNF-?? in promotion and progression of cancer. *Cancer Metastasis Rev.* 25, 409–416 (2006).

427. Lundholm, K. *et al.* Anti-inflammatory treatment may prolong survival in undernourished patients with metastatic solid tumors. *Cancer Res.* 54, 5602–5606 (1994).

428. Lebrun, J.-J. The Dual Role of TGFβ in Human Cancer: From Tumor Suppression to Cancer Metastasis. *ISRN Mol. Biol.* 2012, 381428 (2012).

429. Calon, A., Tauriello, D. V. F. & Batlle, E. TGF-beta in CAF-mediated tumor growth and metastasis. *Semin. Cancer Biol.* 25, 15–22 (2014).

430. Mantovani, A. Cancer: Inflaming metastasis. *Nature* 457, 36–37 (2009).

431. Rosenblum, I. Y. & Dayan, a D. Carcinogenicity testing of IL-10: principles and practicalities. *Hum. Exp. Toxicol.* 21, 347–58 (2002).

432. Kawamura, K., Bahar, R., Natsume, W., Sakiyama, S. & Tagawa, M. Secretion of interleukin-10 from murine colon carcinoma cells suppresses systemic antitumor immunity and impairs protective immunity induced against the tumors. *Cancer Gene Ther.* 9, 109–115 (2002).

433. Kundu, N. & Fulton, A. M. Interleukin-10 Inhibits Tumor Metastasis , Downregulates MHC Class I , and Enhances NK Lysis. 61, 55–61 (1997).

434. Dennis, K. L., Blatner, N. R., Gounari, F. & Khazaie, K. Current status of interleukin-10 and regulatory T-cells in cancer. *Curr. Opin. Oncol.* 25, 637–45 (2013).

435. Buer, J. *et al.* Interleukin 10 secretion and impaired effector function of major histocompatibility complex class II-restricted T cells anergized in vivo. *J Exp Med* 187, 177–183 (1998).

436. Moore, K. W., de Waal Malefyt, R., Coffman, R. L. & O'Garra, A. Interleukin -10 and the I Nterleukin -10 R Eceptor. *Annu. Rev. Immunol.* 19, 683–765 (2001).

437. Muto, G. *et al.* TRAF6 Is Essential for Maintenance of Regulatory T Cells That Suppress Th2 Type Autoimmunity. *PLoS One* 8, 1–12 (2013).

438. Badalà, F., Nouri-mahdavi, K. & Raoof, D. A. NIH Public Access. *Computer (Long. Beach. Calif).* 144, 724–732 (2008).

439. Baglaenko, Y. *et al.* IL-10 production is critical for sustaining the expansion of CD5+ B and NKT cells and restraining autoantibody production in congenic lupus-prone mice. *PLoS One* 11, 1–16 (2016).

440. Chen, W. & Zlotnik, A. IL-10 : a novel cytotoxic T cell differentiation W F Chen and A Zlotnik Information about subscribing to The Journal of Immunology is online at : T CELL DIFFERENTIATION FACTOR '. (2017).

441. Rutenberg, B. D. Quick Stats Fact Sheet Quick Stats Fact Sheet. *Natl. High Sch. Cent.* 1–6 (2009).

442. National Education Association. Rankings 2013 & Estimates 2014. 129 (2013).

443. Costa, M. L., Rensburg, L. Van & Rushton, N. teaching style Does teaching style matter ? A randomised trial of group discussion versus lectures in orthopaedic undergraduate teaching. 214–217 (2007). doi:10.1111/j.1365-2929.2006.02677.x

444. Frederickson, N., Reed, P. & Clifford, V. I. V. Evaluating web-supported learning versus lecture-based teaching : Quantitative and qualitative perspectives. 645–664 (2005). doi:10.1007/s10734-004-6370-0

445. Wilson, K., Korn, J. H., Wilson, K. & Korn, J. H. Attention During Lectures : Beyond Ten Minutes Attention During Lectures : Beyond Ten Minutes. 6283, (2017).

446. Adams, D. Wireless Laptops in the Classroom (and the Sesame Street Syndrome). 49, 25–27 (2006).

447. Coates, H. & Coates, H. The value of student engagement for higher education quality assurance The Value of Student Engagement for Higher Education Quality Assurance. 8322, (2017).

448. Kahu, E. R. Studies in Higher Education Framing student engagement in higher education. 5079, (2017).

449. Robinson, C. C. New Benchmarks in Higher Education : Student Engagement in Online Learning New Benchmarks in Higher Education : Student Engagement in Online Learning. 2323, (2017).

450. Deslauriers, L., Schelew, E. & Wieman, C. Physics Class Improved Learning in a Large-Enrollment. 332, 862–864 (2017).

451. Fleming, M. A Comparison of In-Class and Online Quizzes on Student Exam Performance. 14, 121–134 (2003).

452. Fitzgerald, D. Employing think-pair-share in associate degree nursing curriculum. *Teach. Learn. Nurs.* 8, 88–90 (2013).

453. Siburian, T. A. & Medan, U. N. Improving Students ' Achievement on Writing Descriptive Text Through Think Pair. 3, 30–43 (2013).

454. Educational, M. Think Pair Share : A teaching Learning Strategy to Enhance Students ' Critical Thinking. (2013).

455. Wiener, H. Collaborative learning in the classroom: A guide to evaluation. *Coll. English* 48, 52–61 (1986).

456. Crouch, C. H. & Mazur, E. Peer Instruction: Ten years of experience and results. *Am. J. Phys.* 69, 970–977 (2001).

457. Lasry, N., Mazur, E. & Watkins, J. Peer instruction: From Harvard to the two-year college. *Am. J. Phys.* 76, 1066–1069 (2008).

458. Mazur, E. Peer instruction: getting students to think in class. *AIP Conf. Proc.* 399, 981–988 (1997).

459. Watkins jessica.e.watkins@gmail.com, J. & Mazur, E. Retaining Students in Science, Technology, Engineering, and Mathematics (STEM) Majors. *J. Coll. Sci. Teach.* 42, 36–41 (2013).

460. Fagen, A. P., Crouch, C. H. & Mazur, E. Peer Instruction: Results from a Range of Classrooms. *Phys. Teach.* 40, 206–209 (2002).

461. International Technology Education Association., A. & Council on Technology Teacher Education (U.S.), A. A. *Journal of technology education. Journal of Technology Education* 7, (Council of Technology Teacher Education and the International Technology Education Association, 1989).

462. American Cancer Society. Cancer Facts & Figures 2015. *Cancer Facts Fig. 2015* 1–9 (2015). doi:10.1097/01.NNR.0000289503.22414.79

463. Molina, J. R., Yang, P., Cassivi, S. D., Schild, S. E. & Adjei, A. A. Non-small cell lung cancer: epidemiology, risk factors, treatment, and survivorship. *Mayo Clin. Proc.* 83, 584–94 (2008).

464. Planque, C. *et al.* Identification of five candidate lung cancer biomarkers by proteomics analysis of conditioned media of four lung cancer cell lines. *Mol. Cell. Proteomics* 8, 2746–2758 (2009).

465. Hanash, S. M., Pitteri, S. J. & Faca, V. M. Mining the plasma proteome for cancer biomarkers. *Nature* 452, 571–579 (2008).

466. Singhal, S., Vachani, A., Antin-ozerkis, D., Kaiser, L. R. & Albelda, S. M. Prognostic Implications of Cell Cycle , Apoptosis , and Angiogenesis Biomarkers in Non ^ Small Cell Lung Cancer : A Review. 11, 3974–3987 (2005).

467. Tan, S. *et al.* Quantitative assessment of lung cancer associated with genes methylation in the peripheral blood. *Exp. Lung Res.* 39, 182–90 (2013).

468. Palmisano, W. A. *et al.* Predicting Lung Cancer by Detecting Aberrant Promoter Methylation in Sputum Advances in Brief Predicting Lung Cancer by Detecting Aberrant Promoter Methylation in Sputum 1. *Cancer* 5954–5958 (2000).

469. Hua, F. *et al.* A meta-analysis of the relationship between RARβ gene promoter methylation and non-small cell lung cancer. *PLoS One* 9, 1–8 (2014).

470. Esteller, M., Rosell, R., Sidransky, D., Baylin, S. B. & Herman, J. G. Detection of

Aberrant Promoter Hypermethylation of Tumor Suppressor Genes in Serum DNA from Non-Small Cell Lung Cancer Patients Advances in Brief Detection of Aberrant Promoter Hypermethylation of Tumor Suppressor Genes in. 67–70 (1999).

471. An, Q. *et al.* Detection of p16 hypermethylation in circulating plasma DNA of non-small cell lung cancer patients. *Cancer Lett.* 188, 109–114 (2002).

472. Zochbauer-Muller, S. *et al.* Aberrant promoter methylation of multiple genes in non-small cell lung cancers. *Cancer Res.* 61, 249–255 (2001).

473. Belinsky, S. A. *et al.* Aberrant methylation of p16(INK4a) is an early event in lung cancer and a potential biomarker for early diagnosis. *Proc. Natl. Acad. Sci. U. S. A.* 95, 11891–6 (1998).

474. Phillips, M. *et al.* Detection of lung cancer using weighted digital analysis of breath biomarkers. *Clin. Chim. Acta* 393, 76–84 (2008).

475. Phillips, M. *et al.* Prediction of lung cancer using volatile biomarkers in breath. *Cancer Biomark.* 3, 95–109 (2007).

476. Belani, C. P. *et al.* Comparison of four chemotherapy regimens for advanced non–small-cell lung cancer. *N. Engl. J. Med.* 346, 92 (2002).

477. Kim, E. S. *et al.* The BATTLE trial: Personalizing Therapy for Lung Cancer. *Cancer Discov.* 1, 44–53 (2011).

478. Kim, B. *et al.* Clinical validity of the lung cancer biomarkers identified by bioinformatics analysis of public expression data. *Cancer Res.* 67, 7431–8 (2007).

479. Midha, A., Dearden, S. & McCormack, R. EGFR mutation incidence in non-small-cell

lung cancer of adenocarcinoma histology: a systematic review and global map by ethnicity (mutMapII). *Am. J. Cancer Res.* 5, 2892–911 (2015).

480. Rich, J. N., Rasheed, B. K. A. & Yan, H. EGFR mutations and sensitivity to gefitinib. *N. Engl. J. Med.* 351, 1260-1261261; author reply 1260-1261261 (2004).

481. Shepherd, F. a. *et al.* Erlotinib in previously treated non-small-cell lung cancer. *N. Engl. J. Med.* 353, 123–132 (2005).

482. Paez, J. G. EGFR Mutations in Lung Cancer : Correlation with Clinical Response to Gefitinib Therapy. 1497, 1–5 (2006).

483. Gogali, A. *et al.* Soluble adhesion molecules E-cadherin, intercellular adhesion molecule-1, and E-selectin as lung cancer biomarkers. *Chest* 138, 1173–1179 (2010).

484. Linehan, D. C. & Goedegebuure, P. S. CD25 + CD4 + Regulatory T-Cells in Cancer. 155–168 (2005).

485. Kessenbrock, K., Plaks, V. & Werb, Z. Matrix Metalloproteinases: Regulators of the Tumor Microenvironment. *Cell* 141, 52–67 (2010).

486. Bertelli, M. *et al.* Study of the adenosinergic system in the brain of HPRT knockout mouse (Lesch–Nyhan disease). *Clin. Chim. Acta* 373, 104–107 (2006).

487. Gomez-Casal, R. *et al.* Non-small cell lung cancer cells survived ionizing radiation treatment display cancer stem cell and epithelial-mesenchymal transition phenotypes. *Mol. Cancer* 12, 94 (2013).

488. Manley, E., Waxman, D. J. & Waxman, D. J. H460 non-small cell lung cancer stem-like holoclones yield tumors with increased vascularity. *Cancer Lett.* 346, 63–73 (2014).

489. Wang, C. *et al.* Evaluation of CD44 and CD133 as cancer stem cell markers for colorectal cancer. *Oncol. Rep.* 28, 1301–1308 (2012).

490. Fong, Y., Fortner, J., Sun, R. L., Brennan, M. F. & Blumgart, L. H. Clinical score for predicting recurrence after hepatic resection for metastatic colorectal cancer: analysis of 1001 consecutive cases. *Ann. Surg.* 230, 309-318; discussion 318-321 (1999).

491. Lynch, H. T. 030306 Hereditary Colorectal Cancer. *Color. Cancer* 348, 919–932 (2003).

492. Finkelstein, S. D., Sayegh, R., Christensen, S. & Swalsky, P. a. Genotypic classification of colorectal adenocarcinoma. Biologic behavior correlates with K-ras-2 mutation type. *Cancer* 71, 3827–3838 (1993).

493. Leibovitz, A. *et al.* Classification of human colorectal adenocarcinoma cell lines. *Cancer Res.* 36, 4562–4569 (1976).

494. Vasen, H. F. a, Watson, P., Mecklin, J. P. & Lynch, H. T. New Clinical Criteria for Hereditary Nonpolyposis Colorectal Definition (HNPCC, Lynch Syndrome) Proposed by the International Collaborative Group on HNPCC. *Gastroenterology* 116, 1453–1456 (1999).

495. Schneider, M. *et al.* Characterization of colon cancer cells: a functional approach characterizing CD133 as a potential stem cell marker. *BMC Cancer* 12, 96 (2012).

496. Mummaneni, P., Yates, P., Simpson, J., Rose, J. & Turker, M. S. The primary function of a redundant Sp1 binding site in the mouse aprt gene promoter is to block epigenetic gene inactivation. *Nucleic Acids Res* 26, 5163–5169 (1998).

497. Sabini, E., Ort, S., Monnerjahn, C., Konrad, M. & Lavie, A. Structure of human dCK

suggests strategies to improve anticancer and antiviral therapy. *Nat. Struct. Biol.* 10, 513–519 (2003).

498. Torres, R. J. & Puig, J. G. Hypoxanthine-guanine phosophoribosyltransferase (HPRT) deficiency: Lesch-Nyhan syndrome. *Orphanet J. Rare Dis.* 2, 48 (2007).

499. Jones, P. A., Taylort, S. M., Mohandas, T. & Shapiro, L. J. Cell cycle-specific reactivation of an inactive X-chromosome locus by 5-azadeoxycytidine (X-chromosome inactivation/DNA methylation/differentiation/cytidine analogs/hypoxanthine phosphoribosyltransferase). *Genetics* 79, 1215–1219 (1982).

500. Maddika, S. *et al.* Cell survival, cell death and cell cycle pathways are interconnected: Implications for cancer therapy. *Drug Resist. Updat.* 10, 13–29 (2007).

501. Meller, M., Vadachkoira, S., Luthy, D. A. & Williams, M. A. Evaluation of housekeeping genes in placental comparative expression studies. *Placenta* 26, 601–607 (2005).

502. Carver, B. S. *et al.* Aberrant ERG expression cooperates with loss of PTEN to promote cancer progression in the prostate. *Nat. Genet.* 41, 619–24 (2009).

503. Liu, D. W., Chen, S. T. & Liu, H. P. Choice of endogenous control for gene expression in nonsmall cell lung cancer. *Eur. Respir. J. Off. J. Eur. Soc. Clin. Respir. Physiol.* 26, 1002–1008 (2005).

504. Reijm, E. A. *et al.* Decreased expression of EZH2 is associated with upregulation of ER and favorable outcome to tamoxifen in advanced breast cancer. *Breast Cancer Res. Treat.* 125, 387–394 (2011).

505. Boonstra, R. *et al.* Mitoxantrone resistance in a small cell lung cancer cell line is

associated with ABCA2 upregulation. *Br. J. Cancer* 90, 2411–2417 (2004).

506. Lukasiak, S. *et al.* Proinflammatory cytokines cause FAT10 upregulation in cancers of liver and colon. *Oncogene* 27, 6068–6074 (2008).

507. Morimoto-Tomita, M. *et al.* Sulf-2, a proangiogenic heparan sulfate endosulfatase, is upregulated in breast cancer. *Neoplasia* 7, 1001–1010 (2005).

508. Shabahang, M. *et al.* 1,25-Dihydroxyvitamin D3 receptor as a marker of human colon carcinoma cell line differentiation and growth inhibition. *Cancer Res.* 53, 3712–3718 (1993).

509. Alegre, M. M., Robison, R. A. & Neill, K. L. O. Thymidine Kinase 1 Upregulation Is an Early Event in Breast Tumor Formation. 2012, (2012).

510. Alegre, M. M., Robison, R. A. & Neill, K. L. O. Thymidine Kinase 1 : A Universal Marker for Cancer. 2, 159–167 (2013).

511. Worldwide cancer statistics | Cancer Research UK. at <http://www.cancerresearchuk.org/health-professional/cancer-statistics/worldwide-cancer>

512. Siegel, R., Miller, K. & Jemal, A. Cancer statistics , 2015 . *CA Cancer J Clin* 65, 29 (2015).

513. American Cancer Society. Cancer Facts & Figures 2016. *Cancer Facts Fig. 2016* 1–9 (2016). doi:10.1097/01.NNR.0000289503.22414.79

514. Monnat, R. J., Chiaverotti, T. a, Hackmann, a F. & Maresh, G. a. Molecular structure and genetic stability of human hypoxanthine phosphoribosyltransferase (HPRT) gene

duplications. *Genomics* 13, 788–96 (1992).

515. O'Neill, J. P. *et al.* The effect of T-lymphocyte 'clonality' on the calculated hprt mutation frequency occurring in vivo in humans. *Mutat. Res. Mutagen. Relat. Subj.* 313, 215–225 (1994).

516. Hou, S. M. *et al.* Hprt mutant frequency and aromatic DNA adduct level in non-smoking and smoking lung cancer patients and population controls. *Carcinogenesis* 20, 437–444 (1999).

517. Duthie, S. J., Ross, M. & Collins, A. R. The influence of smoking and diet on the hypoxanthine phosphoribosyltransferase (hprt) mutant frequency in circulating T lymphocytes from a normal human population. *Mutat. Res. - Fundam. Mol. Mech. Mutagen.* 331, 55–64 (1995).

518. He, Q. *et al.* Thymidine kinase 1 in serum predicts increased risk of distant or loco-regional recurrence following surgery in patients with early breast cancer. *Anticancer Res.* 26, 4753–4759 (2006).

519. Alegre, M. M., Robison, R. a & O'Neill, K. L. Thymidine Kinase 1: A Universal Marker for Cancer. *Cancer Clin. Oncol.* 2, 159–167 (2013).

520. Welcome to Python.org. at <https://www.python.org/>

521. Glaab, W. & Tindall, K. Mutation rate at the hprt locus in human cancer cell lines with specific mismatch repair-gene defects. *Carcinogenesis* 18, 1–8 (1997).

522. Hillion, J. *et al.* Upregulation of MMP-2 by HMGA1 promotes transformation in undifferentiated, large-cell lung cancer. *Mol. Cancer Res.* 7, 1803–1812 (2009).

523. de Kok, J. B. *et al.* Normalization of gene expression measurements in tumor tissues: comparison of 13 endogenous control genes. *Lab. Invest.* 85, 154–159 (2005).

524. Kheirelseid, E. A. H., Chang, K. H., Newell, J., Kerin, M. J. & Miller, N. Identification of endogenous control genes for normalisation of real-time quantitative PCR data in colorectal cancer. *BMC Mol. Biol.* 11, 12 (2010).

525. Murphy, C. L. & Polak, J. M. Differentiating embryonic stem cells: GAPDH, but neither HPRT nor beta-tubulin is suitable as an internal standard for measuring RNA levels. *Tissue Eng.* 8, 551–559 (2002).

526. Stathopoulou, A. *et al.* A highly specific real-time RT-PCR method for the quantitative determination of CK-19 mRNA positive cells in peripheral blood of patients with operable breast cancer. *Int. J. Cancer* 119, 1654–1659 (2006).

527. Dolezalova, H., Shankar, G., Huang, M. C., Bikle, D. D. & Goetzl, E. J. Biochemical regulation of breast cancer cell expression of S1P2 (Edg-5) and S1P3 (Edg-3) G protein-coupled receptors for sphingosine 1-phosphate. *J. Cell. Biochem.* 88, 732–743 (2003).

528. Maas, S. *et al.* Decreased Fas expression in advanced-stage bladder cancer is not related to p53 status. *Urology* 63, 392–397 (2004).

529. Bachmeier, B. *et al.* Development of resistance towards artesunate in MDA-MB-231 human breast cancer cells. *PLoS One* 6, 1–14 (2011).

530. Abal, M. *et al.* Enhanced sensitivity to irinotecan by Cdk1 inhibition in the p53-deficient HT29 human colon cancer cell line. *Oncogene* 23, 1737–1744 (2004).

531. Fiorentino, D. F. *et al.* IL-10 inhibits cytokine production by activated macrophages . Why

The JI ? Submit online . • No Triage ! Every submission reviewed by practicing scientists • Fast Publication ! 4 weeks from acceptance to publication Information about subscribing to The Jo. (2018).

532. Carver, B. S. *et al.* Reciprocal Feedback Regulation of PI3K and Androgen Receptor Signaling in PTEN-Deficient Prostate Cancer. *Cancer Cell* 19, 575–586 (2011).

533. Saatli, B., Kizildag, S., Cagliyan, E., Dogan, E. & Saygili, U. Alteration of apoptosis-related genes in postmenopausal women with uterine prolapse. *Int. Urogynecol. J. Pelvic Floor Dysfunct.* 25, 971–977 (2014).

534. Ahmed, E. M., Bandopadhyay, G., Coyle, B. & Grabowska, A. A HIF-independent , CD133-mediated mechanism of cisplatin resistance in glioblastoma cells. (2018). doi:10.1007/s13402-018-0374-8

535. Sellner, L. N. & Turbett, G. R. The presence of a pseudogene may affect the use of HPRT as an endogenous mRNA control in RT-PCR. *Mol. Cell. Probes* 10, 481–483 (1996).

536. Tatlow, P. & Piccolo, S. R. A cloud-based workflow to quantify transcript-expression levels in public cancer compendia. *Sci. Rep.* 6, 39259 (2016).

537. Barretina, J. *et al.* The Cancer Cell Line Encyclopedia enables predictive modelling of anticancer drug sensitivity. *Nature* 483, 603–607 (2012).

538. Bray, N. L., Pimentel, H., Melsted, P. & Pachter, L. Near-optimal probabilistic RNA-seq quantification. *Nat. Biotechnol.* 34, 525–527 (2016).

539. McLendon, R. *et al.* Comprehensive genomic characterization defines human glioblastoma genes and core pathways. *Nature* 455, 1061–1068 (2008).

540. Rahman, M. *et al.* Alternative preprocessing of RNA-Sequencing data in the Cancer Genome Atlas leads to improved analysis results. *Bioinformatics* 31, 3666–3672 (2015).

541. Liao, Y., Smyth, G. K. & Shi, W. The Subread aligner: Fast, accurate and scalable read mapping by seed-and-vote. *Nucleic Acids Res.* 41, (2013).

542. Liao, Y., Smyth, G. K. & Shi, W. FeatureCounts: An efficient general purpose program for assigning sequence reads to genomic features. *Bioinformatics* 30, 923–930 (2014).

543. Barter, R. L. & Yu, B. Superheat: An R package for creating beautiful and extendable heatmaps for visualizing complex data. (2015). doi:10.1111/mec.12230

544. Wickham, H. *Ggplot2 : elegant graphics for data analysis*. (Springer, 2009).

545. R: The R Foundation. at <https://www.r-project.org/foundation/>

546. Epidemiology in B-Cell Malignancies. at <http://www.targetedonc.com/publications/special-reports/2014/hematologic-malignancies-issue1/epidemiology-in-b-cell-malignancies>

547. Non-Hodgkin Lymphoma - Cancer Stat Facts. at <https://seer.cancer.gov/statfacts/html/nhl.html>

548. Key Statistics for Non-Hodgkin Lymphoma in Children. at <https://www.cancer.org/cancer/childhood-non-hodgkin-lymphoma/about/key-statistics.html>

549. Cancers that Develop in Children. at <https://www.cancer.org/cancer/cancer-in-children/types-of-childhood-cancers.html>

550. Due, H. *et al.* miR-155 as a Biomarker in B-Cell Malignancies. *Biomed Res. Int.* 2016, 1–

14 (2016).

551. Aggen, D. H. & Drake, C. G. Biomarkers for immunotherapy in bladder cancer: a moving target. *J. Immunother. Cancer* 5, 94 (2017).

552. Rodriguez-Vida, A., Strijbos, M. & Hutson, T. Predictive and prognostic biomarkers of targeted agents and modern immunotherapy in renal cell carcinoma. *ESMO open* 1, e000013 (2016).

553. Gulley, J. L. *et al.* Immunotherapy biomarkers 2016: overcoming the barriers. *J. Immunother. Cancer* 5, 29 (2017).

554. Yuan, J. *et al.* Novel technologies and emerging biomarkers for personalized cancer immunotherapy. *J. Immunother. cancer* 4, 3 (2016).

555. Schumacher, T. N., Kesmir, C. & van Buuren, M. M. Biomarkers in cancer immunotherapy. *Cancer Cell* 27, 12–14 (2015).

556. Tasian, S. K. & Gardner, R. A. CD19-redirected chimeric antigen receptor-modified T cells : a promising immunotherapy for children and adults with B-cell acute lymphoblastic leukemia (ALL). 228–241 (2015). doi:10.1177/2040620715588916

557. Lorentzen, C. L. & Straten, P. T. CD19-Chimeric Antigen Receptor T Cells for Treatment of Chronic Lymphocytic Leukemia and Acute Lymphoblastic Leukemia. *Scand. J. Immunol.* n/a-n/a (2015). doi:10.1111/sji.12331

558. Maude, S. L., Teachey, D. T., Porter, D. L. & Grupp, S. A. CD19-targeted chimeric antigen receptor T-cell therapy for acute lymphoblastic leukemia. *Blood* 125, 4017–4024 (2016).

559. Davila, M. L. & Brentjens, R. J. CD19-Targeted CAR T cells as novel cancer immunotherapy for relapsed or refractory B-cell acute lymphoblastic leukemia. *Clin. Adv. Hematol. Oncol.* 14, 802–808 (2016).

560. Wang, K., Wei, G. & Liu, D. CD19: a biomarker for B cell development, lymphoma diagnosis and therapy. *Exp. Hematol. Oncol.* 1, 36 (2012).

561. Maude, S. L. *et al.* Tisagenlecleucel in Children and Young Adults with B-Cell Lymphoblastic Leukemia. *N. Engl. J. Med.* 378, 439–448 (2018).

562. Fischer, J. *et al.* CD19 Isoforms Enabling Resistance to CART-19 Immunotherapy Are Expressed in B-ALL Patients at Initial Diagnosis. *J. Immunother.* 40, 187–195 (2017).

563. Sharma, P., Hu-Lieskovan, S., Wargo, J. A. & Ribas, A. Leading Edge Review Primary, Adaptive, and Acquired Resistance to Cancer Immunotherapy. (2017). doi:10.1016/j.cell.2017.01.017

564. Fry, T. J. *et al.* CD22-targeted CAR T cells induce remission in B-ALL that is naive or resistant to CD19-targeted CAR immunotherapy. *Nat. Med.* 24, 20–28 (2017).

565. Haso, W. *et al.* Anti-CD22-chimeric antigen receptors targeting B-cell precursor acute lymphoblastic leukemia. *Blood* 121, 1165–74 (2013).

566. Till, B. G. *et al.* CD20-specific adoptive immunotherapy for lymphoma using a chimeric antigen receptor with both CD28 and 4-1BB domains: pilot clinical trial results. *Blood* 119, 3940–50 (2012).

567. Hudecek, M. *et al.* The B-cell tumor-associated antigen ROR1 can be targeted with T cells modified to express a ROR1-specific chimeric antigen receptor. *Blood* 116, 4532–41

(2010).

568. Optimized CRISPR Design. at <http://crispr.mit.edu/>

569. TEAM, R. D. C. Statutes of " The R Foundation for Statistical Computing " Means to Meet the Objectives. 1–5 (2005).

570. Evan, G. I. & Vousden, K. H. Proliferation, cell cycle and apoptosis in cancer. *Nature* 411, (2001).

571. Fader, A. N., Arriba, L. N., Frasure, H. E. & von Gruenigen, V. E. Endometrial cancer and obesity: Epidemiology, biomarkers, prevention and survivorship. *Gynecol. Oncol.* 114, 121–127 (2009).

572. Kaaks, R., Lukanova, A. & Kurzer, M. S. Obesity, endogenous hormones, and endometrial cancer risk. *Cancer Epidemiol. Prev. Biomarkers* 11, 1531–1543 (2002).

573. Townsend, M. H., Robison, R. A. & O'Neill, K. L. A review of HPRT and its emerging role in cancer. *Med. Oncol.* 35, 89 (2018).

574. Goos, J. A. C. M. *et al.* Aurora kinase A (AURKA) expression in colorectal cancer liver metastasis is associated with poor prognosis. *Br. J. Cancer* 109, 2445–2452 (2013).

575. Baba, Y. *et al.* Aurora-A Expression Is Independently Associated with Chromosomal Instability in Colorectal Cancer. *Neoplasia* 11, 418–425 (2009).

576. Vaish, V., Kim, J. & Shim, M. Jagged-2 (JAG2) enhances tumorigenicity and chemoresistance of colorectal cancer cells. *Oncotarget* 8, 53262–53275 (2017).

577. Ai, J. *et al.* FLNA and PGK1 are two potential markers for progression in hepatocellular carcinoma. *Cell. Physiol. Biochem.* 27, 207–216 (2011).

578. Sasnauskiene, A. *et al.* NOTCH1, NOTCH3, NOTCH4, and JAG2 protein levels in human endometrial cancer. *Med.* 50, 14–18 (2014).

579. Yuan, X. *et al.* Notch signaling: An emerging therapeutic target for cancer treatment. *Cancer Lett.* 369, 20–27 (2015).

580. Zou, J. *et al.* Notch1 is required for hypoxia-induced proliferation, invasion and chemoresistance of T-cell acute lymphoblastic leukemia cells. *J. Hematol. Oncol.* 6, 1–13 (2013).

581. Pietras, A., Stedingk, K. von, Lindgren, D., Påhlman, S. & Axelson, H. JAG2 Induction in Hypoxic Tumor Cells Alters Notch Signaling and Enhances Endothelial Cell Tube Formation. *Mol. Cancer Res.* 9, 626–636 (2011).

582. Jonusiene, V. *et al.* Down-regulated expression of Notch signaling molecules in human endometrial cancer. *Med. Oncol.* 30, (2013).

583. Sagert, J. *et al.* Abstract 2665: Transforming Notch ligands into tumor-antigen targets: A Probody-Drug Conjugate (PDC) targeting Jagged 1 and Jagged 2. *Cancer Res.* 74, 2665–2665 (2014).

584. Furukawa, T. *et al.* AURKA is one of the downstream targets of MAPK1/ERK2 in pancreatic cancer. *Oncogene* 25, 4831–4839 (2006).

585. He, W. *et al.* AURKA suppression induces DU145 apoptosis and sensitizes DU145 to docetaxel treatment. *Am. J. Transl. Res.* 5, 359–367 (2013).

586. Hata, T. *et al.* RNA interference targeting aurora kinase A suppresses tumor growth and enhances the taxane chemosensitivity in human pancreatic cancer cells. *Cancer Res.* 65,

2899–2905 (2005).

587. Goos, J. A. C. M. *et al.* Aurora kinase A (AURKA) expression in colorectal cancer liver metastasis is associated with poor prognosis. *Br. J. Cancer* 109, 2445–2452 (2013).

588. Reis-Filho, J. S. & Pusztai, L. Gene expression profiling in breast cancer: classification, prognostication, and prediction. *Lancet* 378, 1812–1823 (2011).

589. Lassmann, S. *et al.* Predictive Value of Aurora-A/STK15 Expression for Late Stage Epithelial Ovarian Cancer Patients Treated by Adjuvant Chemotherapy. *Clin. Cancer Res.* 13, 4083–4091 (2007).

590. van de Vijver, M. J. *et al.* A Gene-Expression Signature as a Predictor of Survival in Breast Cancer. *N. Engl. J. Med.* 347, 1999–2009 (2002).

591. Sun, S. *et al.* Phosphoglycerate kinase-1 is a predictor of poor survival and a novel prognostic biomarker of chemoresistance to paclitaxel treatment in breast cancer. *Br. J. Cancer* 112, 1332–1339 (2015).

592. Wang, J. *et al.* A glycolytic mechanism regulating an angiogenic switch in prostate cancer. *Cancer Res.* 67, 149–159 (2007).

593. Hwang, T.-L., Liang, Y., Chien, K.-Y. & Yu, J.-S. Overexpression and elevated serum levels of phosphoglycerate kinase 1 in pancreatic ductal adenocarcinoma. *Proteomics* 6, 2259–2272 (2006).

594. Zieker, D. *et al.* Phosphoglycerate kinase 1 promoting tumor progression and metastasis in gastric cancer - detected in a tumor mouse model using positron emission tomography/magnetic resonance imaging. *Cell. Physiol. Biochem.* 26, 147–154 (2010).

595. Lay, A. J. *et al.* Phosphoglycerate kinase acts in tumour angiogenesis as a disulphide reductase. *Nature* 408, 869–873 (2000).

596. Chouchane, L. *et al.* Protein alterations in infiltrating ductal carcinomas of the breast as detected by nonequilibrium pH gradient electrophoresis and mass spectrometry. *J. Biomed. Biotechnol.* 2008, (2008).

597. Vishwanatha, J. K., Jindal, H. K. & Davis, R. G. The role of primer recognition proteins in DNA replication: association with nuclear matrix in HeLa cells. *J. Cell Sci.* 101 (Pt 1, 25–34 (1992).

598. Popanda, O., Fox, G. & Thielmann, H. W. Modulation of DNA polymerases α, δ and ε by lactate dehydrogenase and 3-phosphoglycerate kinase. *Biochim. Biophys. Acta - Gene Struct. Expr.* 1397, 102–117 (1998).

599. Zieker, D. *et al.* Dissemination in Gastric Cancer. 126, 1513–1520 (2011).

600. Wang, J. *et al.* Characterization of phosphoglycerate kinase-1 expression of stromal cells derived from tumor microenvironment in prostate cancer progression. *Cancer Res.* 70, 471–480 (2010).

601. Bando, H., Toi, M., Kitada, K. & Koike, M. Genes commonly upregulated by hypoxia in human breast cancer cells MCF-7 and MDA-MB-231. *Biomed. Pharmacother.* 57, 333–340 (2003).

602. Schindelin, J., Rueden, C. T., Hiner, M. C. & Eliceiri, K. W. The ImageJ ecosystem: An open platform for biomedical image analysis. *Mol. Reprod. Dev.* 82, 518–529 (2015).

603. Li, T. *et al.* TIMER: A web server for comprehensive analysis of tumor-infiltrating

immune cells. *Cancer Res.* 77, e108–e110 (2017).

604. Jang, I. S., Neto, E. C., Guinney, J., Friend, S. H. & Margolin, A. A. Systematic assessment of analytical methods for drug sensitivity prediction from cancer cell line data. *Pac. Symp. Biocomput.* 63–74 (2014). at <http://www.ncbi.nlm.nih.gov/pubmed/24297534>

605. Subramanian, A. *et al.* A Next Generation Connectivity Map: L1000 Platform and the First 1,000,000 Profiles. *Cell* 171, 1437–1452.e17 (2017).

606. Read Rectangular Text Data [R package readr version 1.1.1]. at <https://cran.r-project.org/web/packages/readr/index.html>

607. A Grammar of Data Manipulation [R package dplyr version 0.7.5]. at <https://cran.r-project.org/web/packages/dplyr/index.html>

608. Wickham, H. Reshaping data with the reshape package. (2006). at <http://had.co.nz/reshape>

609. Daley-Brown, D., Oprea-Ilies, G., Quarshie, A. & Gonzalez-Perez, R. R. in *Role of Biomarkers in Medicine* (InTech, 2016). doi:10.5772/62772

610. Banno, K. *et al.* Biomarkers in endometrial cancer: Possible clinical applications (Review). *Oncol. Lett.* 3, 1175–1180 (2012).

611. Perez, I. *et al.* Cross-Talk between AURKA and Plk1 in Mitotic entry and Spindle Assembly. *Mini Rev.* 5, (2015).

612. Prostate Cancer - Cancer Stat Facts. at <https://seer.cancer.gov/statfacts/html/prost.html>

613. Alinezhad, S. *et al.* Validation of Novel Biomarkers for Prostate Cancer Progression by

the Combination of Bioinformatics, Clinical and Functional Studies. *PLoS One* 11, e0155901 (2016).

614. Thompson, I. M. *et al.* Operating Characteristics of Prostate-Specific Antigen in Men With an Initial PSA Level of 3 . 0 ng / mL or Lower. 78229, (2014).

615. Hendriks, R. J. *et al.* Comparative analysis of prostate cancer specific biomarkers PCA3 and ERG in whole urine, urinary sediments and exosomes. *Clin. Chem. Lab. Med.* 54, 483–492 (2016).

616. Etzioni, R., Kooperberg, C., Pepe, M., Smith, R. & Gann, P. H. Combining biomarkers to detect disease with application to prostate cancer. *Biostatistics* 4, 523–38 (2003).

617. Velonas, V. M., Woo, H. H., dos Remedios, C. G. & Assinder, S. J. Current status of biomarkers for prostate cancer. *Int. J. Mol. Sci.* 14, 11034–11060 (2013).

618. Sanda, M. G. *et al.* Autoantibody Signatures in Prostate Cancer. 1224–1235 (2005).

619. Parekh, D. J., Ankerst, D. P., Troyer, D., Srivastava, S. & Thompson, I. M. Biomarkers for Prostate Cancer Detection. *J. Urol.* 178, 2252–2259 (2007).

620. Nilsson, B. O., Carlsson, L., Larsson, A. & Ronquist, G. Autoantibodies to Prostasomes as New Markers for Prostate Cancer. *Ups. J. Med. Sci.* 106, 43–50 (2001).

621. Bradley, S. V. *et al.* Serum antibodies to Huntingtin interacting protein-1: A new blood test for prostate cancer. *Cancer Res.* 65, 4126–4133 (2005).

622. Sardana, G., Dowell, B. & Diamandis, E. P. Emerging biomarkers for the diagnosis and prognosis of prostate cancer. *Clin. Chem.* 54, 1951–1960 (2008).

623. Bussemakers, M. J. G. *et al.* DD3: A new prostate-specific gene, highly overexpressed in

prostate cancer. *Cancer Res.* 59, 5975–5979 (1999).

624. Filella, X. & Foj, L. Emerging biomarkers in the detection and prognosis of prostate cancer. *Clin. Chem. Lab. Med.* 53, 963–973 (2015).

625. Tomlins, S. a *et al.* Recurrent Fusion of TMPRSS2 and. *Science (80-.).* 310, 644–648 (2005).

626. Smit, F. P., Salagierski, M., Jannink, S. & Schalken, J. A. High-resolution ERG-expression profiling on GeneChip exon 1.0 ST arrays in primary and castration-resistant prostate cancer. *BJU Int.* 111, 836–842 (2013).

627. Ghosh, A. & Heston, W. D. W. Tumor target prostate specific membrane antigen (PSMA) and its regulation in prostate cancer. *J. Cell. Biochem.* 91, 528–539 (2004).

628. Landers, K. A. *et al.* Use of multiple biomarkers for a molecular diagnosis of prostate cancer. *Int. J. Cancer* 114, 950–956 (2005).

629. Xin, L., Lawson, D. A. & Witte, O. N. The Sca-1 cell surface marker enriches for a prostate-regenerating cell subpopulation that can initiate prostate tumorigenesis. *Proc. Natl. Acad. Sci. U. S. A.* 102, 6942–7 (2005).

630. Miki, J. *et al.* Identification of putative stem cell markers, CD133 and CXCR4, in hTERT-immortalized primary nonmalignant and malignant tumor-derived human prostate epithelial cell lines and in prostate cancer specimens. *Cancer Res.* 67, 3153–3161 (2007).

631. Townsend, M. H. *et al.* Abstract 1949: Salvage pathway enzyme HPRT as a molecular marker for Burkitt's Lymphoma. *Cancer Res.* 77, 1949–1949 (2017).

632. Stout, J. T. & Caskey, C. T. HPRT: gene structure, expression, and mutation. *Annu. Rev.*

Genet. 19, 127–148 (1985).

633. Becerra, A. & Lazcano, A. The role of gene duplication in the evolution of purine nucleotide salvage pathways. *Orig. Life Evol. Biosph.* 28, 539–553 (1998).

634. Sewda, K. *et al.* Cell-surface markers for colon adenoma and adenocarcinoma. *Oncotarget* 7, 17773–89 (2016).

635. Cronstein, B. N., Levin, R., Belanoff, J., Weissmann, G. & Hirschhorn, R. Adenosine: an Endogenous Inhibitor of Neutrophil-mediated Injury. 78, 760–770 (1986).

636. Haskó, G. & Cronstein, B. Regulation of inflammation by adenosine. *Front. Immunol.* 4, 85 (2013).

637. Haskó, G. *et al.* Adenosine receptor agonists differentially regulate IL-10, TNF-alpha, and nitric oxide production in RAW 264.7 macrophages and in endotoxemic mice. *J. Immunol.* 157, 4634–40 (1996).

638. Szabó, C. *et al.* Suppression of macrophage inflammatory protein (MIP)-1alpha production and collagen-induced arthritis by adenosine receptor agonists. *Br. J. Pharmacol.* 125, 379–87 (1998).

639. Koscso, B. *et al.* Adenosine Augments IL-10 Production by Microglial Cells through an A2B Adenosine Receptor-Mediated Process. *J. Immunol.* 188, 445–453 (2012).

640. Adair, T. H. Growth regulation of the vascular system: an emerging role for adenosine. *Am. J. Physiol. Integr. Comp. Physiol.* 289, R283–R296 (2005).

641. Deaglio, S. *et al.* Adenosine generation catalyzed by CD39 and CD73 expressed on regulatory T cells mediates immune suppression. *J. Exp. Med.* 204, 1257–1265 (2007).

642. Tabas, I. & Glass, C. K. Anti-inflammatory therapy in chronic disease: challenges and opportunities. *Science* 339, 166–72 (2013).

643. Cronstein, B. N. Adenosine, an endogenous anti-inflammatory agent. at <https://www.physiology.org/doi/pdf/10.1152/jappl.1994.76.1.5>

644. Haskó, G., Linden, J., Cronstein, B. & Pacher, P. Adenosine receptors: therapeutic aspects for inflammatory and immune diseases. *Nat. Rev. Drug Discov.* 7, 759–770 (2008).

645. Rodbell, M., Birnbaumer, L., Pohl, S. L. & Krans, H. M. The glucagon-sensitive adenyl cyclase system in plasma membranes of rat liver. V. An obligatory role of guanylnucleotides in glucagon action. *J. Biol. Chem.* 246, 1877–82 (1971).

646. Lanznaster, D., Dal-Cim, T., Piermartiri, T. C. B. & Tasca, C. I. Guanosine: a Neuromodulator with Therapeutic Potential in Brain Disorders. *Aging Dis.* 7, 657–679 (2016).

647. Hepler, J. R. & Gilman, A. G. G proteins. *Trends Biochem. Sci.* 17, 383–7 (1992).

648. Bellaver, B. *et al.* Guanosine inhibits LPS-induced pro-inflammatory response and oxidative stress in hippocampal astrocytes through the heme oxygenase-1 pathway. doi:10.1007/s11302-015-9475-2

649. Zizzo, M. G. *et al.* P100 Guanosine prevents nuclear factor-κB nuclear translocation ameliorating experimental colitis in rats. *J. Crohn's Colitis* 12, S144–S144 (2018).

650. Su, C. *et al.* Guanosine improves motor behavior, reduces apoptosis, and stimulates neurogenesis in rats with parkinsonism. *J. Neurosci. Res.* 87, 617–625 (2009).

651. Di Iorio, P. *et al.* The antiapoptotic effect of guanosine is mediated by the activation of the

PI 3-kinase/AKT/PKB pathway in cultured rat astrocytes. *Glia* 46, 356–368 (2004).

652. Dal-Cim, T. *et al.* Guanosine protects human neuroblastoma SH-SY5Y cells against mitochondrial oxidative stress by inducing heme oxigenase-1 via PI3K/Akt/GSK-3β pathway. *Neurochem. Int.* 61, 397–404 (2012).

653. Oleskovicz, S. P. B., Martins, W. C., Leal, R. B. & Tasca, C. I. Mechanism of guanosine-induced neuroprotection in rat hippocampal slices submitted to oxygen–glucose deprivation. *Neurochem. Int.* 52, 411–418 (2008).

654. Jackson, E. K. & Mi, Z. The Guanosine-Adenosine Interaction Exists In Vivo. *J. Pharmacol. Exp. Ther.* 350, 719–726 (2014).

655. Jackson, E. K., Cheng, D., Jackson, T. C., Verrier, J. D. & Gillespie, D. G. Extracellular guanosine regulates extracellular adenosine levels. *Am. J. Physiol. Physiol.* 304, C406–C421 (2013).

656. Bartrons, R. & Caro, J. Hypoxia, glucose metabolism and the Warburg's effect. *J. Bioenerg. Biomembr.* 39, 223–229 (2007).

657. Weljie, A. M. & Jirik, F. R. Hypoxia-induced metabolic shifts in cancer cells: Moving beyond the Warburg effect. *Int. J. Biochem. Cell Biol.* 43, 981–989 (2011).

658. Kim, J. & Dang, C. V. Cancer's molecular sweet tooth and the Warburg effect. *Cancer Res.* 66, 8927–30 (2006).

659. Vander Heiden, M. G., Cantley, L. C. & Thompson, C. B. Understanding the Warburg effect: the metabolic requirements of cell proliferation. *Science* 324, 1029–33 (2009).

660. Lu, H., Forbes, R. A. & Verma, A. Hypoxia-inducible factor 1 activation by aerobic

glycolysis implicates the Warburg effect in carcinogenesis. *J. Biol. Chem.* 277, 23111–5 (2002).